SCUOLA DI DOTTORATO
UNIVERSITÀ DEGLI STUDI DI MILANO-BICOCCA

School of Medicine and Surgery

PhD program in Neuroscience
Cycle XXIX

CHROMOSOMAL INSTABILITY IN GLIOMA STEM CELL LINES FROM GLIOBLASTOMA MULTIFORME: IMPLICATIONS FOR NEW THERAPEUTIC STRATEGIES

Surname: CILIBRASI Name: CHIARA

Registration number: 709467

Tutor: Dr. ANGELA BENTIVEGNA

Coordinator: Prof. GUIDO ANGELO CAVALETTI

Academic Year 2015/2016

TABLE OF CONTENT

SUMMARY

Glioblastoma is the most common primary malignant brain tumour in the adult population. Despite multimodality treatment with surgery, radiotherapy and chemotherapy, outcomes are very poor, with less than 15% of patients alive after two years. Increasing evidence suggests that Glioma stem cells (GSCs) are likely to play an important role in the biology of this disease and are involved in treatment resistance and tumour recurrence following standard therapy.

GSCs are characterized by enhanced self-renewal, highlighted by the expression of stem cell markers, such as CD133 and Nestin, elevated invasive behaviour, chemo and radiotherapy resistance, and the ability to generate multi-lineage progenities. A typical feature of GSCs is also the elevated chromosomal instability (CIN): they are characterized by various numerical and structural aberrations, deletions, amplification and loss of heterozygosity. A variety of alterations have been proposed as being responsible for CIN, including defects in genes involved in the regulation of the mitotic machinery, such as the Aurora Kinases, making them a promising therapeutic target for GSCs depletion.

My thesis address two main aspects of this research area, aiming at the identification of new GSCs-targeted therapeutic strategies for GBM complete eradication.

In the first part of my project I investigated the effect of Danusertib, a pan-Aurora kinases inhibitor on 5 GSC lines isolated from glioblastoma patients, previously characterized in our laboratory from a cytogenomic and epigenomic point of view. Results showed that response to Danusertib exposure was heterogeneous among GSC lines. Some of them were more sensitive to subtle changes in Aurora kinases activity, which result in huge morphological alterations, a rapid increase in polyploidy and subsequently in senescence, with a consistent reduction in clonogenic survival and proliferation. Interestingly I also observed that the more resistant cell lines showed an increase in ploidy and senescence after repeated rounds of Danusertib exposure, suggesting that there could be the presence of an intolerable ploidy threshold that leads cells to senescence.

In the second part of my thesis I presented some preliminary results I achieved in Dr Hochegger's lab (Genome Damage and Stability Center, University of Sussex, Brighton, UK), where I took part in a project aimed on setting up CrispR/Cas9 mediated GFP or RFP-tagged CD133 (*PROM1* gene) and Nestin (*NES* gene)

glioma stem cell lines in order to look, with live cell imaging techniques, for signs for asymmetric cell division, by which a single GSC would be able to both maintain a pool of self-renewing stem cells and produce differential progeny, using live cell imaging.

The biological significance of asymmetric or symmetric division modes is not yet fully understood, but improved understanding of this phenomenon may lead to the development of preventative treatments or improved therapeutic options for brain tumour patients through the identification of novel targets that are involved in the control of asymmetric cell division in human brain tissue.

ABBREVIATIONS

2DG	2-deoxyglucose
ACD	asymmetric cell division
aCGH	array comparative genomic hybridization
AJ	adherent junction
AML	acute myeloid leukemia
ATM	ataxia telangiectasia mutated
AurkA	Aurora kinase A
AurkB	Aurora kinase B
AurkC	Aurora kinase C
BER	base excision repair
BMPs	bone morphogenetic proteins
BP	basal progenitors
BSA	bovine serum albumin
CDK	cyclin dependent kinase
CENP-F	centromere protein F
CPC	chromosomal passenger complex
CIN	chromosomal instability
CML	chronic myeloid leukaemia
CNS	central nervous system
CSCs	cancer stem cells
CT	computerized tomography
DAPI	4',6-diamidino-2-phenylindole
DIN	DNA integrity number
DMSO	dimethyl sulfoxide
DSB	double strand breaks
EBRT	fractionated external beam radiotherapy
ECM	extracellular matrix
EDTA	ethilenediaminetetraacetic acid
EdU	5-ethynyl-2'-deoxyuridine
EGF	epidermal growth factor
EGFR	epidermal growth factor receptor
EGFRvIII	EGFR variant III
EMEA	European Medicines Agency
FDA	Food and Drug Administration
FGF	fibroblast growth factor
FGFR	fibroblast growth factor receptor
FISH	fluorescence in situ hybridization
γH2AX	phosphorylated histone 2A
GBM	glioblastoma multiforme
GMC	ganglion mother cell

GSCs	glioma stem cells
HATs	histone acetyltransferases
HGF	hepatocyte growth factor
HIF	hypoxia inducible factor
HNPCC	hereditary nonpolyposis colorectal cancer
HRP	horseradish peroxidase
ICGC	International Cancer Genome Consortium
IF	immunofluorescence
IR	ionizing radiation
KPS	Karnofsky performance status
LOH	loss of heterozygosity
MDR	multidrug resistance
MGMT	O6-methylguanine–DNA methyltransferase
MIN	microsatellite instability
MMR	mismatch repair
MRI	magnetic resonance imaging
MT	microtubules
MTT	3-(4,5-dimethyltiazol-2-il)-2,5-difeniltetrazolium
NB	neuroblast
NSTC	nonstem tumor cells
PBS	phosphate-buffered saline
PDGF	platelet-derived growth factor
PFA	paraformaldehyde
PP1	protein phosphatase 1
PS	performance status
PTEN	phosphatase and tensin homolog
PVN	perivascular niche
RG	radial glia
RTOG	Radiation Therapy Oncology Group
SAC	spindle assembly checkpoint
SCID	severe combined immunodeficiency
SHH	sonic hedgehog
SKY	spectral karyotyping
SNP	single nucleotide polymorphism
SOP	sensory organ precursor
STLC	S-Trityl-L-Cysteine, Tocris
STR	short tandem repeats
SVZ	subventricular zone
TMZ	temozolomide
TCGA	The Cancer Genome Atlas
TSC	tumour stem cells
TTF	tumour treating fields
VEGF	vascular endothelial growth factor
VEGFRs	VEGF receptors

VZ	ventricular zone
WB	western blot

FIGURES

Page

TABLES

Page

Chapter 1
Introduction

Chromosomal instability in Glioma Stem Cell lines from Glioblastoma multiforme: implications for new therapeutic strategies

1.1 GLIOMAS

Primary malignant central nervous system (CNS) tumours represent about 2% of all cancers but account for a disproportionate rate of morbidity and mortality. Malignant CNS tumours are the leading cause of death from solid tumours in children and the third leading cause of cancer-related death for adolescents and adults aged 15 to 34 years. [1]

According to the European Cancer Observatory (http://eco.iarc.fr/), 57099 new cases of primary brain and central nervous system tumours were diagnosed by the end of 2012. The incidence of brain tumours is 6.6 per 100,000 person-years, with approximately half being histologically benign. However, even benign tumours, if not amenable to excision or radiation therapy, can be fatal as a result of progressive growth in the closed space of the skull.

Primary CNS tumours comprise a diverse range of pathological entities, each with a distinct natural history. They may be classified as nonglioma and glioma neoplasia. The first ones are not so frequent and consist of typically benign tumours, such as meningiomas and pituitary adenomas, as well as malignant tumuors, such as primitive neuroectodermal tumours (medulloblastomas), primary CNS lymphomas, and the rarely occurring CNS germ cell tumours.

Glioma account for approximately 70% of all brain tumours. The annual incidence of malignant gliomas is approximately 5 cases per 100,000 people. [2]

No underlying cause has been identified for the majority of malignant gliomas. The only established risk factor is exposure to ionizing radiation. Evidence for an association with head injury, foods containing N-nitroso compounds, occupational risk factors, and exposure to electromagnetic fields is inconclusive. [3]

Genetic predisposition to CNS tumours appears relatively uncommon, although gliomas may be inherited as a part of several familial diseases. Specifically, germline mutation of some known tumour-suppressor genes characterizes several genetic syndromes that carry an increased incidence of developing brain tumours: type 1 neurofibromatosis (mutation of *NF1*), Turcot syndrome (mutation of *APC*), basal cell nevus (or Gorlin) syndrome (mutation of *PTCH*), and LiFraumeni syndrome (mutation of *TP53* or *CHEK2*) are associated with the greatest risk of brain tumours. [4]

Malignant gliomas are heterogeneous and they have been for long time classified histologically, immunohistochemically, and/or ultrastructurally as astrocytomas, oligodendrogliomas and ependymomas, exclusively based on the type of glial cells they are most similar to. They have been further graded on a WHO consensus-derived scale of I to IV, with higher grades corresponding to more aggressive tumors, according to their degree of malignancy as judged by various histological features, such as nuclear atypia, cells density, vascular proliferation degree and necrosis, accompanied by genetic alterations [5]. Tumour grade is a key factor in the clinical setting influencing the choice of therapies, particularly determining the use of adjuvant radiation and specific chemotherapy protocols.

Astrocytomas are the most frequent type of brain tumours accounting for 80% of gliomas. They develop from astrocytes and are characterised by heterogeneous morphology, biologic behaviour and clinical course. [6]

According to the WHO classification system, grade 1 astrocytomas such as pilocytic astrocytoma are typically benign lesions with low proliferative potential and generally does not tend to evolve into higher-grade tumours. Diffuse astrocytoma (WHO grade II) is a well-differentiated, slowly growing tumour, but it is also generally infiltrative and may tend to progress to higher grade of malignancy, such as anaplastic astrocytoma (grade III). Anaplastic astrocytoma is characterized by focal or diffuse anaplasia, increased cellularity, nuclear atypia and mitotic activity. Grade 4 astrocytomas (Glioblastoma multiforme) have also evidence of endothelial proliferation and/ or tumour necrosis. [5]

For the past century, the classification of brain tumours has been based largely on concepts of histogenesis that tumours can be classified according to their microscopic similarities with different putative cells of origin and their presumed levels of differentiation. However, the 2016 World Health Organization Classification of Tumours of the Central Nervous System used “integrated” [7] phenotypic and genotypic parameters for CNS tumour classification adding a level of objectivity that has been missing from some aspects of the diagnostic process in the past. This additional objectivity may yield more biologically homogeneous and narrowly defined diagnostic entities than in prior classifications, which in turn should lead to greater diagnostic accuracy as well as improved patient management and more accurate determination of prognosis and treatment response.

Indeed, glial tumours can now be in diffuse and circubscribed lesions based not only

on their growth pattern and behaviours, but also more pointedly on the shared genetic driver mutations in the *IDH1* and *IDH2* genes. From a pathogenetic point of view, this provides a dynamic classification that is based on phenotype and genotype; from a prognostic point of view, it groups tumours that share similar prognostic markers; and from the patient management point of view, it guides the use of therapies (conventional or targeted) for biologically and genetically similar entities. In this new classification, the diffuse gliomas include the WHO grade II and grade III astrocytic tumours, the grade II and III oligodendrogliomas, the grade IV glioblastomas, as well as the related diffuse gliomas of childhood (see below). This approach leaves those astrocytomas that have a more circumscribed growth pattern, lack *IDH* gene family alterations and frequently have *BRAF* alterations (pilocytic astrocytoma, pleomorphic xanthastrocytoma) or *TSC1/TSC2* mutations (subependymal giant cell astrocytoma) distinct from the diffuse gliomas. In other words, diffuse astrocytoma and oligodendrogliomas are now nosologically more similar than are diffuse astrocytoma and pilocytic astrocytoma; the family trees have been redrawn (Fig. 1.1). [7]

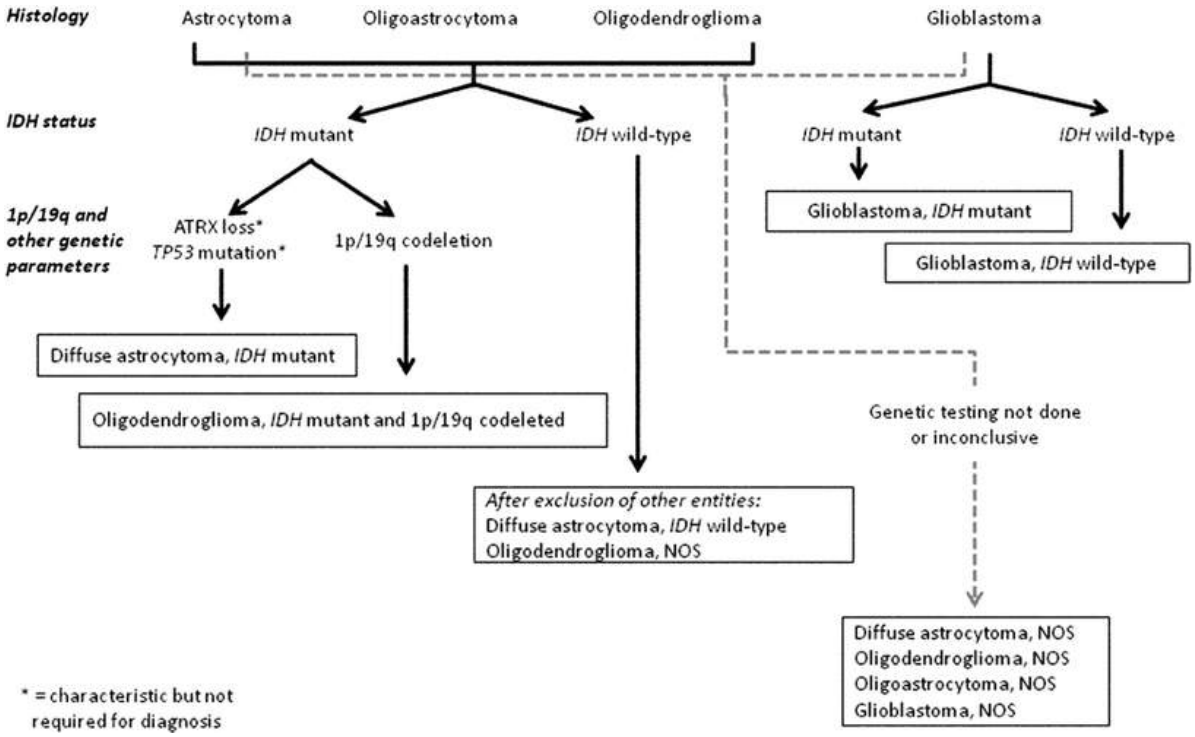

Figure 1.1 A simplified algorithm for the classification of the diffuse gliomas based on histological and genetic features. A caveat to this diagram is that the diagnostic "flow" does not necessarily always proceed from histology first to molecular genetic features next, since molecular signatures can sometimes outweigh histological characteristics in achieving an "integrated" diagnosis. [7]

1.2 GLIOBLASTOMA MULTIFORME

Glioblastoma multiforme (GBM) is a grade IV astrocytoma (WHO grade) and the most common and malignant of the primary brain tumours. It accounts for 12-15% of all brain tumours and 50- 60% of astrocytomas. Although GBM incidence is less than 10 to 100000, the median survival of a little over 1 year from diagnosis makes it a considerable public health issue [8, 9]. GBM may present itself at any age, but typically affects adults, with increasing incidence until aged 85 and above. The median age at diagnosis is 64 years, with more than 80 % of diagnosed glioblastoma patients being older than 55 years and only 1 % younger than 20 years. Males are more commonly affected, with an incidence rate almost 1.6 times higher than in females [10]. GBM usually appears as an irregular mass in the subcortical white matter of the cerebral hemispheres and frequently extend across the border of the frontal lobe into the temporal lobe. Typically, it is a unilateral tumour but, sometimes, its infiltration progresses into the adjacent cortex and, through the corpus callosum, crosses the midline into the contralateral hemisphere producing the typical “butterfly” shape. The tumour mass is poorly delineated and heterogeneous. Highly proliferating cancer cells are usually found in the peripheral, hypercellular zone of the tumour, whereas the central tumour area mainly consists of necrotic tissue, comprising up to 80% of the total tumour mass. Histopathologically, the lesions typically exhibit cellular hyperplasia in the peripheral zones harboring cancer cells with atypical nuclei, increased mitotic activity, cellular pleomorphism and poor stages of differentiation. A diagnostic feature of glioblastoma multiforme is the presence of areas with vascular hyperplasia, necrosis or both in the tumour tissue [11, 12]. (Fig. 1.2)

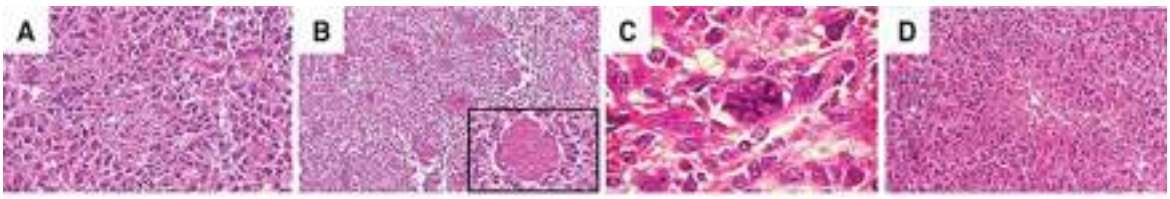

Figure 1.2 Histopathological features of GBM. **A.** Atypical cells displaying pleomorphic, irregular, and hypercromatic nuclei. **B.** Multiple neoplastic vessels with endothelial hyperplasia. **C.** Atypical mitotic figure. **D.** Necrotic focus (pseudopalisades).

Another hallmark of glioblastoma multiforme is rapid invasion of the surrounding brain tissue, especially along myelinated brain structures such as the corpus callosum or within perivascular spaces. Infiltrating tumour cells are dispersed within the normal brain tissue surrounding the contrast enhancing tumour border at high-resolution scans. These satellite cancer cells are thought to be the origin of local tumour recurrence after therapy, since the infiltrating cells escape surgical resection and high-dose radiotherapy of the primary tumour mass. Despite the highly infiltrative nature of glioblastoma multiforme, it tends to invade neither the subarachnoidal space nor the vessel lumen, and therefore distant metastases are rarely found, both within and outside the CNS.[13]

Etiologically, there are some known risk factors linked to GBM development. Environmental risk factors include primarily exposure to therapeutic ionizing radiations. An inverse association between GBM incidence and allergies, atopic diseases and systemic infections has been reported by several groups.[3]

The onset of symptoms is often abrupt and is most commonly related to mass effect and focal neurologic symptoms. Patients develop headache, nausea, vomiting, drowsiness and visual abnormalities. Moreover, they usually have partial or generalized seizures and vasogenic oedema due to the raised intracranial pressure that produces leakage of the blood-tumour barrier.[14] The duration of symptoms before diagnosis is usually short, ranging from a few days to a few weeks. Magnetic resonance imaging (MRI) and computerized tomography (CT) are the first steps for a GBM diagnosis. T1-weighted MRI scans using gadolinium as contrast agent typically show a ring-enhanced mass lesion, with low signal intensity at its centre and surrounding the ring-enhanced component (Fig. 1.3). Definitive diagnosis of a suspected GBM on CT or MRI requires a stereotactic biopsy or a craniotomy with tumour resection and pathologic confirmation. Imaging of tumour blood flow using perfusion MRI and measuring tumour metabolite concentration with MR spectroscopy may add value to standard MRI in selected cases by showing increased relative cerebral blood volume and increased choline peak respectively, but pathology remains the gold standard for diagnosis and molecular characterization.

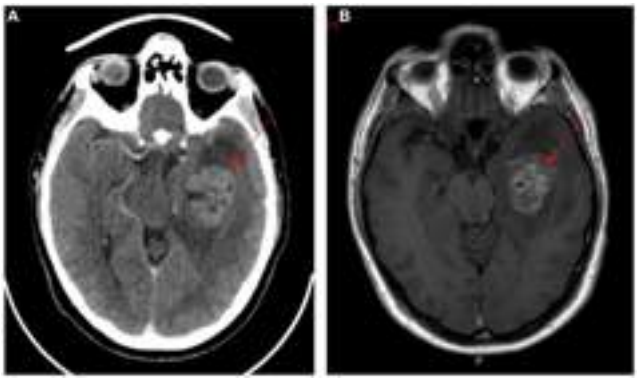

Figure 1.3 CT (A) and T1 weighted MRI (B) scans with contrast of a patient with GBM. Lesion indicated by red arrows.

Traditionally, GBM has been separated into 2 major classes as primary and secondary GBM. Primary GBM was suggested as generally presenting without a known clinical precursor, accounting for the vast majority of cases (95%) and tending to occur in older patients (mean age 55 years). On the contrary, secondary GBM typically occurred in younger adults (45 years of age or less) and arose through malignant progression from less malignant astrocytoma. [15]

Current WHO brain tumour classification relies on traditional methods using morphology to classify diffuse gliomas into histologic categories and later to assign a grade based on presence of mitoses, vascular endothelial proliferation, and necrosis. Although this method provides considerable information regarding outcome, significant variation exists within given grades and histologies. Recent advances in molecular diagnostic techniques provide alternative methods for tumour classification using molecular abnormalities and signalling pathways involved in gliomagenesis. These molecular subtypes have distinct prognoses and treatment responses. [16-18] While there is significant correlation between traditional pathologic groupings and newer molecular subtypes, overlap is incomplete.

Glioblastoma was the first cancer to be systematically studied by The Cancer Genome Atlas Research Network, which revealed recurrent alterations in 3 core pathways [19]:

- *Rb signalling*. Rb pathway has a central role in regulating G1/S transition. Unphosphorylated Rb normally sequesters e2f, a transcription factor that controls the transcription of genes required for S phase initiation. Under proliferative signals, Rb is serially phosphorylated by cyclin dependent kinases Cdk4/6 and Cdk2:

hyperphosphorylated Rb releases e2f, activating genes involved in G1/S transition. Cyclins, such as cyclin D or cyclin E, positively regulate Cdk activity, promoting cell cycle progression. Instead, cyclin dependent kinase inhibitors (Ckis) negatively regulate Rb pathway. The INK4 family, a member of CKIs, is composed by INK4A (p16), INK4B (p15), INK4C (p18) and INK4D (p19) and blocks the activation of cyclin D-cdk4/6 complex [20]. Rb signalling is disrupted through several genetic alterations. Loss of Rb in 13q14 was identified in 14-33% of GBMs [21], whereas amplification of *CDK4* gene, in 12q13-15, accounts for 14% of GBM cases [22]. Rb activity might be influenced by some negative regulators, such as $p16^{INK4A}$ and $p14^{ARF}$, both mapping at *CDKN2A* locus and resulting deleted in 40-57% of GBMs [23]. In addition *CDK6* and *CCND1* are amplified in a small number of GBMs [24].

- *p53 signalling*. The p53 pathway prevents the uncontrolled growth of cells, blocking the cell cycle in G1 phase or inducing apoptosis, primarily regulating the transcription of several genes. Functional loss of *TP53* occurs in 30-40% of GBMs by mutations of *TP53* gene or loss of chromosome 17p [6]. 10% of GBMs show amplification of 12q14-15 region, containing *MDM2* gene, a negative regulator of p53 [25]. MDM4 gene (1q32), a homologue of *MDM2*, encodes for a protein that inhibits p53 transcription and is amplified in 4% of malignant gliomas [26]. The second protein encoded by *CDKN2A*, $p14^{ARF}$, controls the activity of Mdm2 and is also involved in the inhibition of progenitor cell renewal in the subventricular zone of aging mice [27]. 9p21 region includes *CDKN2A* and *CDKN2B* loci. The latter gene encodes for $p15^{INK4B}$, a CKI involved in Rb pathway. The chromosomal region 9p21 is homozygously deleted in at least 30-40% of GBMs. This deletion has a critical role in GBM pathogenesis as it guides the simultaneous disruption both of Rb and p53 pathways [28].

- *Receptor tyrosine kinase signalling*. The first genetic abnormality detected in GBM was amplification of the epidermal growth-factor receptor (*EGFR*) gene, which maps in 7p11-12, in 40% of cases [29]. Gain of chromosome 7 is one of the most common chromosomal alterations in approximately 60% of GBMs, with or without *EGFR* amplification [30]. Nevertheless, all GBMs with *EGFR* amplification show *EGFR* overexpression [31]. *EGFR* amplification is often associated with rearranged transcripts and *EGFR* variant III (*EGFRvIII* or delta *EGFR*) is the most common

rearrangement, found in 50-60% of GBMs with *EGFR* amplification [32]. The rearrangement results in an in-frame deletion of 801 bp of exons 2-7 of *EGFR* gene, leading to the expression of an aberrant protein, which does not bind ligand and is constitutively activated [33]. *EGFR* overexpression, or its constitutive activation, enhances tumorigenic potential of GBM cells by reducing apoptosis and increasing proliferation [34]. In addition, another receptor-mediated signalling, altered both in lower-grade glioma and GBM, is platelet-derived growth-factor receptor (*PDGFR*) signalling, through amplification of 4q12, involving *PDGFRA* gene (13% of GBMs) [35] and/or its mutation or ligand overexpression [36]. Co-expression of the receptor and its ligand suggests a possible autocrine-paracrine loop sustaining oncogenic signalling [37].

Functional loss of the tumour suppressor phosphatase and tensin homolog (*PTEN*) occurs in more than 80% of GBMs by deletions, mutation or epigenetic mechanisms [19]. Loss of the long arm of chromosome 10 was detected in 70-90% of GBMs [30]. PTEN is an important negative regulator of the PI3K-AKT-mTOR signalling, which is a well established anti-apoptotic and pro-survival pathway. In addition, recent studies highlighted other possible roles of *PTEN* in suppressing tumour progression. *PTEN* is expressed at high level in differentiated cells and is believed to possess a role in the maintenance of genomic integrity, promoting DNA repair [38]. The presence of three commonly deleted regions at 10q suggested the existence of several tumour suppressor genes: *PTEN* in 10q23; *MTXI1* located at 10q25.2, a negative regulator of Myc oncoprotein [39]; and *DMBT1*, deleted in malignant brain tumour, in 10q26.13 [40].

Recently large-scale molecular profiling of diffuse gliomas performed in individual laboratories, at the national level in the US by TCGA network, and the International Cancer Genome Consortium (ICGC) demonstrated that GBM is potentially sub-classifiable into distinct biologic entities based on molecular pathogenesis and “driver” lesions especially in *PDGFRA, EGFR, NF1* and *IDH1* genes. In general, there are four subtypes that have been determined through extensive genomic analysis [18, 41-43], characterized by distinct survival times and response to therapies.

• *Classical*. These tumours subtype is characterized by higher expression of neural precursor and stem cell marker *NES*, as well as Notch (*NOTCH3*, *JAG1*, and *LFNG*) and Sonic hedgehog (*SMO*, *GAS1*, and *GLI2*) signalling pathways. Chromosome 7 amplification paired with chromosome 10 loss is a highly frequent event in GBM and was seen in 100% of the Classical subtype. Although chromosome 7 amplification is seen in tumours of other classes, high-level *EGFR* amplification is observed in 97% of the Classical subtype and infrequently in other subtypes. In tandem with high rates of *EGFR* alteration, there is also a distinct lack of *TP53* mutations, even though *TP53* is the most frequently mutated gene in GBM. Focal 9p21.3 homozygous deletion, targeting *CDKN2A* (encoding for both $p16^{INK4A}$ and $p14^{ARF}$), is a frequent and significantly associated event, co-occurring with *EGFR* amplification in 94% of the classical subtype. Homozygous 9p21.3 deletion is almost mutually exclusive with aberrations of other RB pathway components, such as *RB1*, *CDK4* and *CCDN2*. This finding suggests that, in samples with focal *EGFR* amplification, the Rb pathway is almost exclusively affected through *CDKN2A* deletion.

• *Mesenchymal*. This subtype displays expression of mesenchymal markers, such as *CHI3L1* (also known as *YKL40*) and *MET*. The combination of higher activity of mesenchymal and astrocytic markers (*CD44* and *MERTK*) is reminiscent of a epithelial-to-mesenchymal transition that has been linked to dedifferentiated and transdifferentiated tumours [44]. Genes in the tumour necrosis factor super family pathway and NF-kB pathway, such as *TRADD*, *RELB*, and *TNFRSF1A*, are highly expressed in this subtype, potentially as a consequence of higher overall necrosis and associated inflammatory infiltrates in the mesenchymal class. Focal hemizygous deletions of a region at 17q11.2, containing the gene *NF1*, and lower *NF1* expression levels are also present.

• *Proneural.* This subgroup shows high expression of oligodendrocytic development genes, such as *PDGFRA*, *NKX2-2*, and *OLIG2*, underlining its status as an atypical GBM subtype. High expression of *OLIG2* has shown to be able to down-regulate the tumour suppressor p21 (*CDKN1A*), thereby increasing proliferation, and *CDKN1A* expression is indeed lower in this class. The proneural signature further contains several proneural development genes, such as *SOX*,

DCX, *DLL3*, *ASCL1*, and *TCF4*. Gene ontology (GO) categories identified for the proneural subtype involves developmental processes and a previously identified cell cycle/proliferation signature. Two major features of the proneural class are alterations of *PDGFRA* and point mutations in *IDH1*. Focal amplifications of the locus at 4q12 harboring *PDGFRA* are seen in all subtypes of GBM but at a much higher rate in proneural. The characteristic signature of *PDGFRA* in proneural samples, however, is best described as the concomitant focal amplification in conjunction with high levels of *PDGFRA* gene expression, which is seen almost exclusively in this tumour type. *TP53* mutations and loss of heterozygosity are frequent events in this subtype. All these characteristics have also been associated with secondary glioblastomas.

- *Neural*. This subtype is typified by the expression of neuron markers, such as *NEFL*, *GABRA1*, *SYT1*, and *SLC12A5*. GO categories associated with the neural subtype includes neuron projection and axon and synaptic transmission.

The most recent glioblastoma publication from The Cancer Genome Atlas showed that the only subgroup with improved survival was proneural tumours with *IDH1* mutations and hypermethylation across the genome. Concomitant loss of chromosomes 1p and 19q is one of the best studied molecular alterations in gliomas and is strongly associated with oligodendroglial morphology and improved survival [45]. In fact, the vast majority of these tumours with 1p/19q codeletion have *IDH* mutations and frequently carry gene mutations in the far upstream element binding protein 1 (*FUBP1*, on chromosome 1p) and capicua transcriptional repressor (*CIC*, on chromosome 19q) [16, 46, 47]. These tumours rarely possess *EGFR* amplifications common to primary glioblastomas and also lack *TP53* and alpha thalassemia/mental retardation syndrome X-linked (*ATRX*) mutations, which are common in secondary glioblastomas and lower-grade astrocytomas [48, 49].
Other established markers of favorable prognosis are mutations in *IDH1* and *IDH2*, present in 70%–80% of lower-grade gliomas and secondary glioblastomas and only a small proportion of primary glioblastomas (~5%–10%) [50-52]. Subsequent studies have found a strong link between *IDH* mutations and a genome-wide glioma cytosine–phosphate–guanine island methylator phenotype (G-CIMP) across all

glioma subtypes [17, 53]. G-CIMP is more prevalent among lower-grade gliomas, is strongly associated with proneural glioblastomas, and has better patient outcomes [53]. Methylation of the O^6-methylguanine-DNA methyltransferase (*MGMT*) gene promoter is a positive prognostic factor for glioblastomas, especially in the setting of chemotherapy with alkylating agents (i.e. temozolomide) [54-56]. The impact of *MGMT* methylation on survival in patients with WHO grades II–III gliomas is less clear [57, 58]. The significant overlap among 1p/19q codeletion, *IDH* mutation, G-CIMP phenotype, and *MGMT* methylation complicates assessment of the independent prognostic role of these alterations. Recent studies indicate that gliomas can additionally be classified based on their telomere maintenance mechanisms [59]. Point mutations in the telomerase reverse transcriptase (*TERT*) gene promoter, leading to increased telomerase activity, are found in ~75% of oligodendrogliomas and primary glioblastomas [60]. Gliomas that do not carry *TERT* promoter mutations frequently harbor mutations of the telomere binding protein *ATRX*, activating the pathway of alternative lengthening of telomeres (*ALT*). Nearly 75% of WHO grades II–III astrocytomas and secondary glioblastomas activate this telomerase-independent telomere maintenance pathway [61]. More recently in the 2016 CNS WHO glioblastomas have been classified into (1) glioblastoma, *IDH*-wildtype (about 90 % of cases), which corresponds most frequently with the clinically defined primary or de novo glioblastoma and predominates in patients over 55 years of age; (2) glioblastoma, *IDH*-mutant (about 10 % of cases), which corresponds closely to so-called secondary glioblastoma with a history of prior lower grade diffuse glioma and preferentially arises in younger patients; and (3) glioblastoma, NOS, a diagnosis that is reserved for those tumours for which full *IDH* evaluation cannot be performed. [7]

1.2.1 Glioblastoma standard of care

Current standard treatment primarily involves neurosurgical evaluation to assess feasibility of maximal safe resection. When appropriate, this procedure should always be performed, given that extent of surgery is associated with increased survival [62, 63]. In fact, surgical resection of the lesion is fundamental to reduce the increased pressure as well as to have a histologic confirmation of the diagnosis made; recent advances in surgical imaging techniques, as intraoperative magnetic

resonance imaging or fluorescent-guided resection, allow a better delineation of tumour borders [64]. In order to improve patients' survival and response to radiotherapy and chemotherapy, it is necessary a maximal cytoreduction of 98%. Approximately 20- 30% of patients are not eligible for surgery at all and simply undergo a diagnostic biopsy [65]. After surgery or biopsy, patients are evaluated based on their performance status (PS) and age:

- ✓ Karnofsky PS (KPS) ≥70 and age ≤70 years, fractionated external beam radiotherapy (EBRT) with concurrent and adjuvant temozolomide (TMZ) [66];
- ✓ KPS ≥70 and age >70 years: fractionated external beam radiotherapy (EBRT) with concurrent and adjuvant TMZ (not licensed in all countries), fractionated EBRT or TMZ [67];
- ✓ KPS <70: fractionated EBRT or TMZ or best supportive care [68, 69].

TMZ is a small lipophilic alkylating agent administered orally that causes DNA damages and triggers a series of events leading to cell death by apoptosis or autophagy. As an alkylating agent, TMZ exerts its action through the addition of a methyl group to the purine bases of the DNA, leading to DNA damages and triggering a cascade of events that culminates in programmed cell death. However, this methyl group added to guanine may be removed by O6-methylguanine methyltransferase (*MGMT*), a DNA repair protein that confers resistance both to TMZ and to other alkylating agents (such as chloroethylnitrosureas) by protecting the cells from their DNA-damaging effects.TMZ is a prodrug which is activated by neutral or alkaline pH, is able to cross the BBB and has little toxicity; its addition to radiotherapy increased the median survival from 12.1 to 14.6 months and improved 2-year median survival from 10.4 to 26.5%. All these findings support the therapeutic benefit of TMZ in combination with RT, the so called "Stupp regimen", which is the current standard of care for GBM treatment [8]. Although this combined treatment slows tumour growth, it's typical to find tumour recurrence after surgery, indicating the presence of a TMZ-resistant subpopulation of cells within the tumour [70].
Following approval of the current standard regimen with TMZ, other new therapeutic approaches have been shown to be active in patients with relapsed glioblastoma. Amongst these, three received approval by the US Food and Drug Administration (FDA), but not by the European Medicines Agency (EMEA).

Gliadel wafers are biodegradable wafers soaked with carmustine, a small lipophilic alkylating and interstrand crosslinking nitrosurea (1,3-bis (2-chloriethyl)-1-nitrosurea (BCNU) wafers) [71]. Gliadel is positioned in the cavity left by tumour resection in order to release carmustine in the surrounding brain tissue and its effects last for several weeks; its use in clinical trials in combination with radiation therapy and TMZ administration showed to modestly prolong survival in a subset of patients [72].

Bevacizumab is a monoclonal antibody directed against the vascular endothelial grow factor (VEGF), as adjuvant therapy with TMZ and radiation therapy after surgical resection of the tumour [73]. This approach has a strong theoretical rationale in glioblastomas, given that these tumours have a very high vasculature density and express *VEGF* [74, 75]. The FDA licensed the use of bevacizumab for recurrent glioblastoma, based on the results of two phase II clinical trials, which showed objective responses in pre-treated patients, with a median survival of around 9 months [76, 77]. The EMEA refused approval because “validity of objective response rates as a surrogate endpoint for clinical benefit has not been established” and “due to the lack of a randomised concurrent control”. Following the initial enthusiasm towards anti-angiogenic drugs, a phase III trial, evaluating the use of bevacizumab as first line therapy in combination with current standard treatment, was conducted by the Radiation Therapy Oncology Group (RTOG). No overall survival improvement from the addition of bevacizumab was reported. Several clinical trials are ongoing and will likely address some of the controversies regarding the use of bevacizumab in glioblastomas, such as the optimal treatment schedule and dose, the most appropriate therapeutic agent for combination, the most reliable way to evaluate radiographic response [78].

Tumour Treating Fields (TTF), consisting in low intensity, intermediate frequency, alternating electric fields, are emitted by a portable device and administered via transducer arrays applied onto the scalp [79]. The anticancer effect is due to cell death of the proliferating tumour population, which some investigators interpret as a consequence of mitotic spindle disruption during the metaphase to anaphase transition and aggregation of macromolecules and organelles during telophase [80, 81]. The FDA approved the use of TTF for recurrent glioblastoma based on the results of a phase III clinical trial comparing TTF alone to physician’s choice chemotherapy: overall survival did not differ in the two arms; responses were more frequent in the experimental arm, though not significantly; toxicity and quality of life

were more favourable in patients treated with TTF [82]. Currently, a randomised phase III clinical trial is enrolling newly diagnosed patients who have undergone standard radiochemotherapy: TTF in combination with adjuvant temozolomide will be compared to temozolomide alone. This trial will give an indication of whether this new treatment modality can be beneficial as first line therapy in glioblastoma patients.

However, despite of multimodal treatments, nearly all malignant gliomas recur generally after 6.9 months, making GBM one of the most malignant and hard to treat tumours [8].

Patients outcome remains dismal as the median survival rate is about 9-12 months after diagnosis and only 2-5% of all patients survives longer than 5 years [83].

The cause of this dismal outcome lies in the high infiltrative nature of GBM, as emphasized by Bramwell in 1888, who stated that tumour tissue is not surrounded by a capsule and it is therefore impossible to say, without microscopic examination, where the lesion ends and where normal brain tissue begins [84].

As a matter of fact, even though tumour cells are mainly in the tumour core, they may extend as far as 4 to 5 cm away from it; moreover, the localization of the tumour is important to guide surgical resection as it's affected by the location and size of the area involved. In order to define the tumour area, tumour cells have been quantified in the peripheral region of the tumour, away from the core; starting from 0-2 cm from the tumour epicentre, the percentage of tumour cells found is about 6%, 2-4 cm from the core this percentage decreases to 1.8% while more than 4 cm away from the epicentre (e.g. in the contralateral emisphere) it becomes 0.2% [11].

Another factor underlying tumour recurrence and poor long-term survival is the marked intratumoral heterogeneity, due to the presence of different cell populations with distinct genetic mutations, differentiation status and responses to external stimuli. These include populations characterized by greater tumorigenic potential called Glioma stem cells (GSCs), characterized by self-renewal, highlighted by the expression of stem cell markers, such as CD133 and Nestin, elevated invasive behaviour, chemo and radiotherapy resistance, and the ability to generate multi-lineage progenities.

1.3 CANCER STEM CELLS THEORY

It has long been known that tumours exhibit significant heterogeneity with respect to cell morphology, surface marker, cell proliferation potential and response to therapy [85].

There are two current concepts about the origin of cancer and its continued propagation as a heterogeneous mass: (1) the clonal evolution (or stochastic) model (16, 17), and (2) the hierarchical cancer stem cells (CSCs) model. (Fig. 1.4)

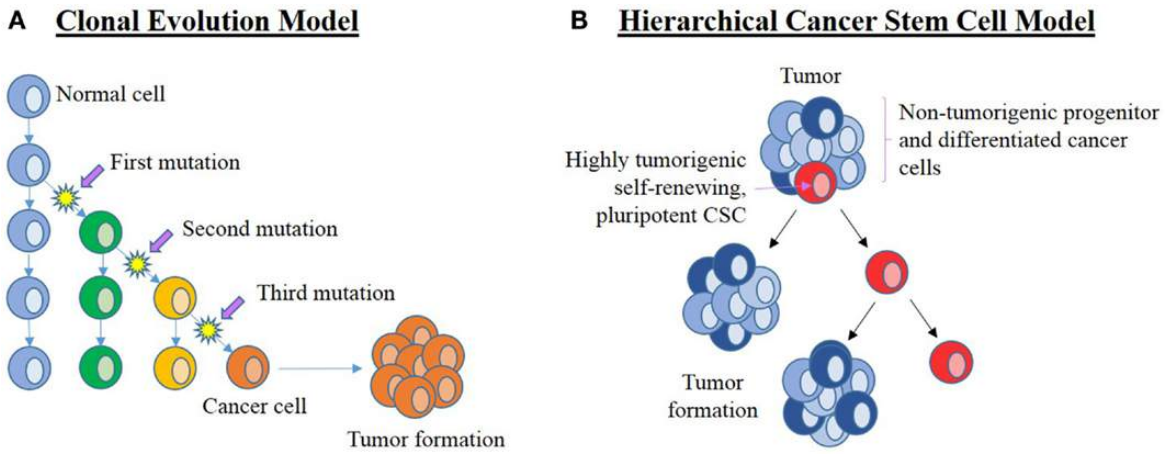

Figure 1.4 Current leading models of carcinogenesis. A. The clonal evolution model hypothesizes that a normal cell (blue) within the organism undergoes a series of mutations to form a cancer cell (orange) that clonally expands and form the bulk of the tumour. Successful treatment must, therefore, eliminate all cancer cells. **B.** The cancer stem cell (CSC) hierarchical model proposes that the origin of cancer being CSCs (red) that are pluripotent and self-renewing. They are highly tumorigenic with the ability to establish new tumours. CSCs divide asymmetrically to form new CSCs and progenitor (dark blue) cells that in turn give rise to differentiated cancer cells (light blue) that form the bulk of the tumour. [86]

The stochastic model suggests that every tumour cell is biologically homogeneous and the behaviour of the tumour cell is determined by stimuli which arise either intrinsically (e.g. transcription factors, hormones, etc.) or extrinsically (e.g. microenvironment, mutagens, etc.). If these changes confer a selective advantage to a particular cell, then this allows the selected “clone” to outcompete other potential tumour forming clones. According to this model, the stimulations which randomly or stochastically affect the tumour cells induce tumour heterogeneity [85].

The hierarchical model or CSC hypothesis asserts that the organisation of cell lineage in tumours is hierarchical and only a subpopulation of cells termed "cancer stem cells", which is at the top of this hierarchy, is responsible for tumour expansion. According to this hypothesis, stem cells or cells that acquired the ability to self-

renew, accumulate genetic changes over long periods of time, escape from the control of their environment, and give rise to cancerous growth. One of the postulations of the cancer stem cell hypothesis is that a population of cells with stem cell-like features exists in tumours and this population gives rise to the bulk of the tumour cells with more differentiated phenotypes.

However, the stochastic and cancer stem cell models need not be mutually exclusive because theoretically, a new clone of cancer stem cells might also be generated stochastically by intrinsic or extrinsic carcinogenic factors. The essential difference between these two models is that, in the stochastic model, cancer stem cells arise randomly and every tumour cell has the potential to give rise to progeny cells, although the chance for generating novel stem cell clones is low because this would require the mutagenic stimulus to affect specifically genes which are crucial for acquiring stem cell properties. For the cancer stem cell model, there is only one distinct subpopulation of cells that plays the role of cancer stem cells essential for sustaining the cancer [87].

CSCs are indeed defined as a fraction of slowly proliferating cells within a tumour that possess the ability to: I) self-renew and expand the CSCs pool; II) initiate, maintain or expand the tumour; and 3) differentiate into a heterogeneous mix of non-tumour-initiating cells that make up the tumour bulk. The actual cell of origin of CSCs has not yet been determined. There are three main theories: III) de-differentiation of mature cells; II) restricted progenitors acquire mutations that endow them with stem-like properties; III) adult tissue stem cells are hit by mutations that influence their division and proliferation properties, achieving a tumorigenic potential [88, 89].

The hypothesis of the existence of this subpopulation of cells was first made in the 1960s when a series of ethically questionable experiments were carried out, in which tumour cells were harvested from cancer patients and injected sub-cutaneously into the same or different patients; the results demonstrated that tumours only formed in recipients when more than $1x10^6$ cells were implanted and suggested that tumour-initiating ability was the property of a small subset of the tumour cells [90]. Around the same time, Bruce and van der Gaag, based on injection of colony-forming lymphoma cells into mice, concluded that only a minority of cancer cells had the capability of initiating and maintaining the tumour population [91].

The CSC hypothesis was firmly established in 1990s when John Dick and colleagues described the identification of an AML (acute myeloid leukemia)-initiating cell based on cell surface antigen expression ($CD34^+/CD38^-$) and its ability to establish human leukaemia in SCID mice. Like SCs, the leukaemia-initiating cell was present at a low frequency, shared the $CD34^+/CD38^-$ phenotype with haematopoietic stem cells and exhibited in vivo self-renewal as assessed by serial transplantation. It has also been shown that a second type of leukaemia (chronic myeloid leukaemia (CML)) is driven by a stem-like cell [92, 93]. Hence, for at least two types of leukaemia (AML and CML), the concept of a CSC seems to be well established in that a cell with the defining functional characteristics of stem cells (long-term self-renewal and slow cycling, which are also associated with a specific immunophenotype) is responsible for driving tumour initiation and growth and also plays a role in resistance to therapy.
These were only the firsts of a series of studies that led to the identification of CSC populations also in solid tumours, including breast [94], glioma [95], prostate [96], lung [97], liver [98] and colon [99] cancers.

1.3.1 Glioma stem cells

The first *in vitro* evidence for the existence of CSCs in brain tumours was published in 2002, when Ignatova and colleagues reported the isolation from high grade gliomas of cells that could form clones under culture conditions used in neural stem cell research, i.e. these cells could grow as neurospheres in serum free medium supplemented with epidermal growth factor (EGF), fibroblast growth factor (FGF) and insulin [95] (Fig. 1.5). These “neural stem-like cells” were also shown to differentiate and express astroglial and neuronal markers following serum stimulation. Soon after, Singh et al. confirmed these findings *in vitro* and developed an intracranial xenograft assay, showing that a subpopulation of cells isolated from glioblastoma specimens was capable of inducing tumours phenotypically resembling the patient’s original specimen [100]. These cells, selected for CD133 expression, gave tumours at a very high frequency (100 cells were sufficient) and could be serially transplanted, while the rest of the population, i.e. CD133 negative cells, was not tumorigenic, following the injection of up to 10^5 cells.
GSCs are indeed defined by three different properties: I) the capacity to generate

cluster of clonally derived-cells, called neurosphere, a clue of self-renewal; II) multipotency, that is the ability to differentiate into cells with neural phenotype; III) tumour initiation and propagation upon serial orthotopic implantation in immunocompromised mice [100, 101].

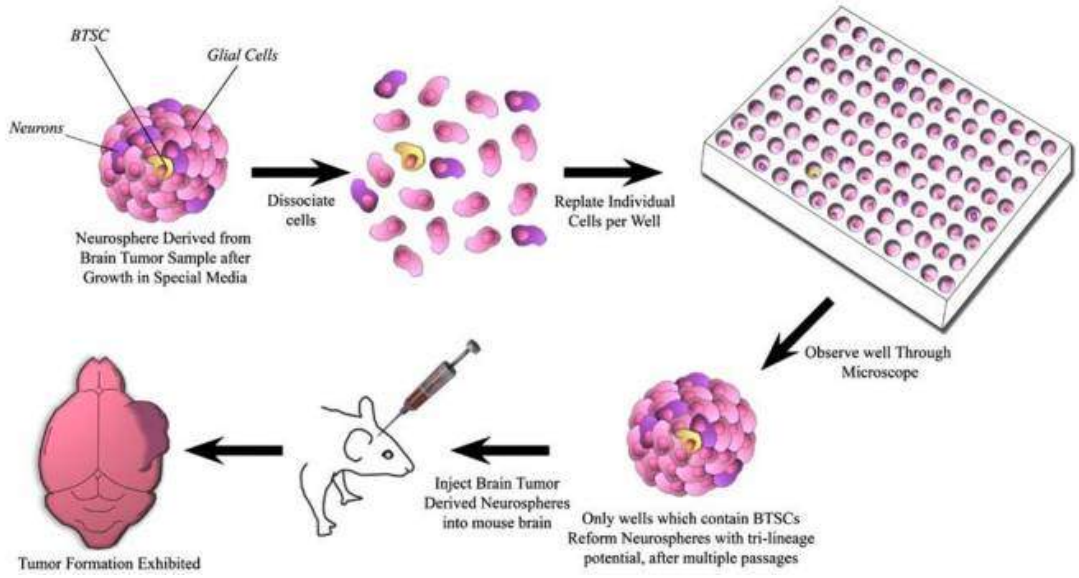

Figure 1.5 Isolation and perpetuation of brain tumour stem cells in culture. Neurosphere assay was originally developed in 1992 to help isolate and identify normal NSCs from neural tissue. This assay was subsequently utilized 13 years later to identify GSCs from human tumour samples. [89]

1.3.1.1 Glioma stem cells markers

Great energy and passion have been devoted to the discovery, validation, and use of CSC enrichment methods. The identification of specific surface markers is necessary in order to isolate GSCs and subsequently characterize them for future GSC-targeted therapies. Ideally, an enrichment method would be based on a property that defines an essential CSC feature (self-renewal, tumour initiation, etc.) that is immediately lost upon differentiation (i.e., a digital readout) and is usable with live cells. Currently, no such system exists for any cell type (normal or neoplastic) because biologic systems rarely exhibit “all or none” phenomena.

Most glioma CSC markers have been appropriated from normal stem cells, but the linkage between glioma CSCs and normal stem cells remains controversial. Many of the transcription factors or structural proteins essential for normal stem cells function also mark glioma CSCs, including Sox2 [102], Nanog [103, 104], Olig2 [105], Myc [106], Musashi1 [102], Bmi1 [102], Nestin [107], and inhibitor of differentiation protein 1 (ID1) [108]. Among this, Oct4, Sox2, and Nanog are thought to be key players in the transcriptional regulation of CSCs.

Sox2 is a member of the family of transcriptional co-factors that are associated with various developmental milestones and is over-expressed in tumours [109, 110]. It plays a role in maintaining pluripotency in several types of cancer, including rectal [111], breast [112], and lung [113] cancers. *SOX2* has also found overexpressed in GBM and little detected in normal brain tissue [114]. Additionally, GBM demonstrated greater *SOX2* mRNA expression than lower grade tumours [115]. Furthermore, Sox2 inhibition using shRNA halted tumour growth when GBM cells were transplanted into immunodeficient mice [116].

Nanog is an embrional stem cell (ESC) transcription factor and its expression has been associated with multiple types of cancer, including those affecting the lung [117], oral cavity [118], breast [119, 120], and prostate [121]. It has also been implicated in the regulation of GBM and has been found to be highly expressed in stem cells extracted from the cerebellum and medulloblastoma [122]. Nanog has been demonstrated to modulate GBM stem cell tumorigenicity, clonogenicity, and proliferation [123]. Moreover inhibition of Nanog in GBM prevented tumour proliferation and invasion [124].

Together with Nanog, the transcription factor, Oct4, is required for propagation of ESCs and they both work synergistically with Sox2 to achieve this regulation [125]. It has also been associated with cancer, functioning as a driver for the self-renewal of CSCs [115, 126]. Oct4 is expressed by glioma cells, but not by normal brain tissue, and is implicated in the pathogenesis of GBM [127], correlating with tumour aggressiveness with GBM cells showing greater nuclear staining for Oct4 and Sox2 [115].

Nestin is another well known GSC markers. It is a cytoskeletal protein expressed during the development of the central nervous system. It is expressed in several types of cancer [128-130] and it is strongly associated with GBM [100, 131, 132]. In fact increased Nestin expression has been associated with higher grade gliomas and lower patient survival rates [133]. Additionally, induced differentiation of GBM cells has been associated to Nestin downregulation.

Because of the limited utility of intracellular proteins for enriching CSCs from nonstem tumour cells (NSTCs) using traditional methods such as flow cytometry, a multitude of potential cell surface markers have been also suggested.

The first proposed marker, CD133 (*PROM1*), a cell surface glycoprotein expressed on neural stem cells, enriches for cells with higher rates of self-renewal and

proliferation and increased differentiation ability [100]. However, CD133 expression, rather than the AC133 surface epitope, should be used with care to enrich for any cells: Surface CD133 marks stem cells and decreases with differentiation, but the expression of Prominin-1 mRNA is not regulated with stemness [134], suggesting that only the glycosylated surface protein CD133 is CSC-specific. Moreover, accumulated results in GBM molecular research led to several CD133 related controversies. For example, GSCs display a variation in the levels of CD133 expression that did not directly correlate with the tumorigenic potential [135]. Most importantly, different studies suggested that $CD133^-$ tumour cells isolated from GBMs can also be stably cultured under stem cell conditions. Similar to the $CD133^+$ cells, these cells also showed stem cell properties such as self-renewal, differentiation *in vitro*, and formed transplantable tumours in a xenograft model [136, 137]. Further phenotypic analysis showed that unlike the $CD133^+$ cells, which can form floating spheroids in culture, the $CD133^-$ cells tend to grow as adherent spheres. This observation led to the assumption that $CD133^+$ and $CD133^-$ cells may originate from different pools of self-renewing GSCs [138]. It has recently been reported that a small population of $CD133^-$ cells can give rise to $CD133^+$ cells, suggesting a possible stem cell hierarchy in the spheroid culture system that may or may not have *in vivo* relevance [139]. These results, however, have been brought into discussion in 2013 by Brescia et al., who argued that the CD133 status depends, in fact, on the protein subcellular localization between the cytoplasm and the plasma membrane [140]. Additionally, the use of CD133 as a stem marker is complicated by the observation that expression of CD133 can be regulated at the level of the cell cycle, with potentially slow-cycling NSTCs lacking CD133 expression during G_0/G_1 cell cycle phase but still maintaining multipotency [141]. However data continues to accumulate on CD133 biology, as it has been repeatedly demonstrated to be essential for GSC maintenance and neurosphere formation [142] and it is a good indicator of resistance to conventional therapies [70]. Although CD133 continues to be the most commonly used cell surface marker, other markers, such as integrin α6, have been proposed to segregate CSCs and NSTCs [143]. CD15/SSEA-1 [144], CD44 [70], L1CAM [145], and A2B5 [146] have also been proposed as possible markers.

CD44 is a transmembrane glycoprotein commonly expressed in numerous malignancies [147]. In GBM xenograft models, knockdown of CD44 inhibited cell

growth and improved response to chemotherapy [148].

L1CAM is another cell surface marker related to CD133 expression and GSCs. It is a neuronal cell adhesion molecule regulating neural cell growth, survival and migration during central nervous system development [149]. L1CAM is overexpressed in gliomas and other solid malignancies [150]. Bao et al. demonstrated that most $CD133^+$ glioma cells were also positive for L1CAM, and in contrast, $CD133^-$ cells were $L1CAM^-$ [145]. Interestingly, inhibiting L1CAM by lentiviral-mediated short hairpin RNA interference reduced the growth and survival of $CD133^+$ cells in murine xenografts of human glioma [145]. These findings suggest a L1CAM-mediated interplay between different cell subpopulations within a tumour. However, the use of L1CAM to identify GSCs or glioma grade has not yet been validated, meriting further investigation.

1.3.1.2 Glioma stem cells implicated signalling pathways

Compared to NSCs, GSCs exhibit enhanced self-renewal capacity and compromised differentiation [151]. GSCs upregulate a number of signalling pathways required for maintaining NSC stemness, which enables them to enhance their stemness and aberrant cell survival, consequently leading to tumorigenesis [101, 102]. Therefore, further understanding the signalling pathways in normal neural development including Notch, bone morphogenic proteins (BMPs), NF-kB, Wnt, EGF, and Shh will give significant insight into the cellular features of GSCs and will aid in designing better treatment strategies for GBM.

Notch signalling is important for mediating various cellular and developmental processes including the regulation of proliferation, differentiation, apoptosis, and cell lineage decisions in NSCs [152, 153]. Recent studies have implicated Notch signalling to be highly active in GSCs to suppress differentiation and maintain stem-like properties. Downregulation of Notch and its ligands such as Delta-like-1 and Jagged-1 leads to decrease in oncogenic potential of GSCs, which indicates n important role of Notch signalling in GSC survival and proliferation [153, 154].

BMPs regulate proliferation, differentiation, and apoptosis in NSCs. BMP signalling pathways are activated in different developmental processes depending on their interaction with various signalling molecules including Wnt/β-catenin, basic helix-loop-helix (bHLH), and hypoxia-inducible factor-1α (HIF-1α) [155]. Wnt signalling

induces BMP expression, which predisposes NSCs toward an astroglial lineage [156]. Similarly, BMPs in GSCs are shown to play an important role in directing astroglial differentiation to inhibit the tumorigenic potential of GSCs [157]. Specifically, BMP-2 decreases GSC proliferation by directing astroglial differentiation and sensitizes GSCs to TMZ through destabilization of HIF-1α [158]. *In vivo* delivery of BMP-4 inhibits brain tumour growth with a resultant decrease in mortality [157]. A BMP antagonist, Gremlin1, inhibits differentiation of GSCs by its regulation of endogenous BMP levels to maintain GSC self- renewal and tumorigenic potential [159].

Wnt/β-catenin signalling is also important for regulating NSC expansion and promoting astroglial lineage differentiation in normal neural development [160]. β-catenin is a critical factor for proliferation and differentiation of GSCs [161, 162]. Aberrant activation of Wnt signalling in GSCs leads to tumour growth through nuclear localization of stabilized β-catenin. FoxM1/β-catenin interaction regulates the transcription of c-Myc and other Wnt target genes inducing glioma formation [163]. In addition, Wnt/β-catenin signaling regulates the expression of *PLAGL2* to suppress the differentiation of GSCs, maintaining their stemness [164].

The EGFR signalling pathway mediates proliferation, migration, differentiation, and survival in NSCs [165]. Levels of *EGFR* expression vary with specific stages of development, which suggests a requirement for precise modulation of *EGFR* expression by balancing extrinsic signals such as BMP and FGF during normal neuronal development [166]. Egfr activation promotes GSC proliferation and tumorigenesis by transactivation of β-catenin [167]. Furthermore, overexpression of *EGFR* increases the self-renewal capacity of GSCs resulting in induction of their tumorigenic potential [168].

Sonic hedgehog (Shh) signalling is pivotal in ventral patterning, proliferation, differentiation, and survival of NSCs [169]. In the adult brain, persistent Shh pathway signalling in the SVZ is critical for the regional specification and maintenance of NSCs [170]. Recent studies demonstrate that the Shh pathway is highly active in GSCs to maintain self-renewal and induce tumorigenesis by regulating stemness genes. Suppression of Shh signalling reduces self-renewal and *in vivo* tumorigenicity, which indicates the dependency of GSCs on Shh signalling for their survival [122].

1.3.1.3 Glioma stem cells microenvironment

In physiological context neural stem cells are located in specific regions of the brain called neurogenic niches, a microenvironment comprising somatic cells and the extracellular matrix. The relationship between stem cells and these niches is not passive. Rather stem cells actively influence their microenvironment and they are regulated by signalling from that same microenvironment. Similarly, GSCs also exist in specific niches that play a role in enhancing the stem-cell features of GSCs, promote invasion and metastasis and even affect response to therapy.

Perivascular niche. Neovascularization in malignant glioma is well documented, being characterized as hypervascular tumours associated with aberrant vascular morphology [171, 172]. Vasculature appears to be critical for providing trophic support and maintaining the undifferentiated state of GSCs, giving rises to the so-called perivascular niche (PVN) [173]. In fact, the vascularization degree significantly correlates with aggressiveness and poor prognosis in GBM [174], setting itself as a characteristic feature of these tumours [173]. The PVN is composed of a heterogeneous group of cell types, all of them engaged in crosstalk phenomena that eventually lead to tumour initiation, maintenance and progression [175]. In perivascular regions, GSCs appear to be enriched, where a great deal of regional signals have been found to promote their phenotypes [176]. GSCs are generally located near the endothelial cells (ECs) that line capillaries, especially in the subventricular zone and the hippocampus [177].

It has been reported that GSCs release high levels of proangiogenic factors, such as vascular endothelial growth factor (VEGF) that drives the migration of newly endothelial cells into the mass and promotes angiogenesis. ECs overexpress VEGF receptors (*VEGFR2*); thus, an environment of high VEGF increased endothelial cells proliferation, migration, and blood vessel permeability. Permeability alterations are associated with increased oedema usually observed in GBM [177]. GSCs also secrete hepatoma-derived growth factor that promotes endothelial cell migration *in vitro* and angiogenesis *in vivo* [178].

Several studies indicated also that GSCs also differentiate into endothelial cells in the tumour. Ricci-Vitiani et al. reported that some $CD31^+$ endothelial cells in human glioblastoma specimens carried the same chromosomal aberrations as tumour cells. $CD133^+$ GSCs cultured in endothelial conditions generated $CD31^+$ and $Tie2^+$

endothelial cells, and vessels in tumours formed by GSCs in immunocompromised mice were mainly composed of human $CD31^+$ endothelial cells [179]. Wang et al. reported that glioblastoma-derived $CD133^+$ cells included a $CD144^+$ population. These CD133/CD144 double positive cells showed an increase in expression of *CD31, CD105, CD34*, and *VEGFR-2* and decrease in *CD144* expression under endothelial culture conditions and were capable of forming a tubular network in Matrigel [180]. Finally, Soda et al. demonstrated that glioma tumour-initiating cells produced endothelial cells expressing CD31, CD34, CD144, and von Willebrand factor in a genetically engineered mouse brain tumour model [181]. CSCs may even be capable of differentiating into cells that functionally resemble pericytes, supplying the raw material necessary to continue supporting the perivascular niche [182].

The interaction between GSCs and ECs promotes activity in critical stem pathways, such as Notch signalling. GSCs Nestin-positive cells express the Notch receptors Notch-1 and Notch-2 and show elevated level of Notch activity [183]. ECs express the Notch ligands Delta-like 4 (*DLL4*) and Jagged-1. Knockdown of these ligands in brain microvascular endothelial cells (BMECs) reduced tumour growth upon co-transplantation of GSCs with BMECs [183]. GSCs may directly stimulate the expression of Notch ligands on ECs suggested by the findings that GSCs secrete elevated levels of VEGF, which induces *DLL4* expression in ECs [184].

The perivascular region is also enriched for extracellular matrix proteins (e.g., laminin) that madiate GSC maintenance induced by endothelial cells. It has been showed that, in glioblastoma patient specimens, laminin α2 is expressed by tumour associated endothelial cells in integrin $\alpha6^+$ areas and that tumour formation *in vivo* is delayed when GSCs are injected with endothelial cells with laminin α2 knockdown [185].

The interaction between vascular niche and GSCs also involves chemokines and their receptors. CXCR4 works as a biomarker of CSCs in several types of cancer, including glioma [186]. CXCR4-positive tumour cells can self-renew in a serum-free medium and display potent tumour-initiating capability. The ligand for CXCR4, namely, CXCL12, is secreted by ECs and the immune cells in tumour microenvironment [187], which highlights the importance of CXCL12/CXCR4 axis in the maintenance of GSCs in vascular niches. By using a three-dimensional culture system, Infanger et al. proved that ECs promoted GSC-like properties by secreting enhanced levels of the chemokine CXCL8/IL-8 and upregulating its cognate

receptors CXCR1 and CXCR2 [188].

Perinecrotic niche. In addition to aberrant vasculature, GBM is histologically known to contain areas of intratumour necrosis that are surrounded by a rim of densely packed tumour cells, known as pseudopalisading necrosis. These areas are believed to be another niche for CSCs to demonstrate increased self-renewal and differentiation that result from the hypoxia in the environment. Hypoxia promotes tumour angiogenesis, cancer aggression, and therapeutic resistance to various therapies [172, 189]. It also supports GSC self-renewal, proliferation, and tumorigenicity and can induce non-GSCs to acquire GSC features and increased tumorigenic potential [190]. Hypoxia stimulates the expression of the transcription factor, hypoxia-inducible factor (HIF) family. The HIF factors exert their transcriptional roles by acting on hypoxia-responsive elements as heterodimers, composed of a constitutively expressed HIFβ subunit and an oxygen-labile HIFα subunit. Two homologous isoforms of HIFα have been identified [191]: while HIF1α has a dominant role in controlling responses to acute hypoxia, HIF2α activity is favored on a chronic hypoxic state. Li et al. were the first to report the involvement of the HIF pathway in GSCs. Using xenograft glioma-initiating, *in vitro* neurosphere formation assays and CD133 expression, they observed significant enhancement of stem cell activity under a hypoxic environment [192].

GSCs are enriched in perinecrotic regions of human glioblastoma biopsies. They are characterized by reduced oxygen tension and activation of HIF1α and HIF2α [193]. In culture, hypoxia upregulates HIF1α and HIF2α in GSCs. HIF2α is directly involved in promoting the GSC phenotype, whereas HIF1α appears to play a more general, permissive role in GSC maintenance, possibly by enabling cell survival. Furthermore, HIF1α is expressed in both GSCs and non-GSC cells, whereas HIF2α is specifically expressed in GSCs [192, 193]. HIF2α upregulates key genes involved in the induction of a pluripotent state [148], including Klf4 and the direct HIF2 targets Sox2 and Oct4. Besides, HIF2 activates c-Myc, another fundamental stem cell regulator. [194, 195]

Hypoxia is also responsible for metabolic reprogramming, leading to acidification of the tumour microenvironment. Under conditions of limit nutrients, such as glucose and oxygen, cancer cells, including GSCs, exhibit the “Warburg” effect, a metabolic shift toward aerobic glycolysis and the accumulation of lactate in exchange for sustained ATP production and metabolite generation for macromolecule synthesis.

GSCs demonstrate plasticity in the metabolic pathways used in response to metabolic restrictions and may shift toward the use of the pentose phosphate shunt [196, 197]. In conditions of nutrient deprivation such as low glucose, GSCs outcompete neighboring NSTCs for glucose uptake through preferential up-regulation of the high-affinity GLUT3 transporter [198]. A consequence of altered metabolic state is the production of reactive oxygen species. GSCs not only are dependent on NOS2 activity for promoting tumour growth but also synthesize nitric oxide through the specific up-regulation of NOS2 protein [199]. Importantly, in GBM, cellular metabolic characteristics are often genetically hardwired, such as recurrent *IDH1* mutations, which are commonly observed in proneural GBM. Mutant *IDH1* leads to a gain-of-function enzymatic activity, causing accumulation of 2-hydroxyglutarate, an oncometabolite that inhibits the TET1 and TET2 demethylases to cause aberrant hypermethylation of DNA and histones [200].

Immune niche. The immune system appears to have a central role in the control of tumour progression [201]. Recent studies show a direct interaction of GSCs with immune cells, highlighting the major role of these components in the GSCs niche. Furthermore, GSCs and inflammatory cells are involved in a dynamic cross talk involving GSC-mediated induction of immune cell infiltration, generation of a pro-tumorigenic inflammatory environment, and inflammation-driven cancer promotion [202].

Tumour-associated macrophages (TAMs) represent prevalent tumour-infiltrating inflammatory cells in GBM [203, 204]. The great number of TAMs in GSCs niche suggests their key role in GBM tumour progression, also positively correlated with the malignancy grade [205]. TAMs are mainly located near $CD133^+$ GSCs, around microvessels and in hypoxic areas, suggesting a direct interaction between GSCs and TAMs [206, 207]. Enhanced expression of proinflammatory genes like RAGE, COX2, and NF-kB was recently found in hypoxic niche of GSCs [208]. When compared to differentiated tumour cells, the GSCs show an increased capacity in active chemoattraction and recruitment of TAMs, processes mediated by chemokines and growth factors, secreted by GSCs, including VEGF, neurotensin, SDF1, and soluble colony-stimulating factor 1 (sCSF-1) [207, 209]. Other CSC-secreted factors include IL-10 and TGF-β, which also suppresses tumour-associated microglia/macrophage function and generates a more immunosuppressive (M2) phenotype [210]. Immune suppression is another

hallmark of brain cancer [211]; while the brain possesses a unique series of immune surveillance mechanisms that become active during pathogenic states, brain tumours have been characterized as immuno-suppressive [212, 213]. *In vitro* experiments demonstrated that GSC populations produced more immunosuppressive cytokines when cultured in hypoxic conditions; exposure to GSC-conditioned medium resulted in reduction of T cell proliferation, interferon γ production by $CD3^+$ T cells and phagocytosis in monocytes; these effects were augmented if GSCs were grown at low oxygen levels. In co-culture studies, CSCs induced regulatory T cells while inhibiting proliferation and cytotoxic T-cell activation with a concomitant induction of cytotoxic T-cell apoptosis, mediated via PD1 and soluble galectin-3 [214, 215]. There is increasing enthusiasm for immunotherapy strategies which include cellular (adoptive T-cell transfer and chimeric antigen receptor engineered T cells), vaccination, and immunomodulatory therapies targeting immune checkpoints [216]. Reversing tumour-induced immune suppression by increasing cytotoxic cell function and reducing suppressor cell function may unleash the endogenous immune response. Immunologic therapies may offer an additional benefit, as most strategies do not require intracranial delivery, a major restriction point for many oncologic treatments.

1.3.1.4 Glioma stem cell-dependent therapeutic resistance

The common cause for treatment failure in many malignancies, including glioblastoma, is tumour resistance to radiotherapy and chemotherapy [216] (Fig. 1.6). Collective data have established that CSCs, such as GSCs, are more resistant to conventional radiotherapy and chemotherapy than non-CSCs [217]. The exact mechanisms of GSC chemo- and radio-resistance are unknown, but probably include a combination of slow cell cycle kinetics, resistance to DNA and oxidative damage, avoiding cell death, hypoxia and multidrug resistance [70, 218]. CSCs probably exist in a quiescent state and may be more treatment resistant compared to rapidly dividing cells. Ionizing radiation represents an effective therapeutic option for glioblastoma by inducing DNA damage [219]. Thus, DNA damage responses play crucial roles in cellular radiosensitivity and radioresistance. To date, the underlying mechanism of radioresistance in glioblastoma remains elusive. Bao et al. observed that $CD133^+$ GSCs were enriched after radiation, while $CD133^-$ cells

were more sensitive to ionizing radiation [218]. Mechanistically, they found that $CD133^+$ cells preferentially activated the DNA damage checkpoint in response to radiation and thus repaired DNA damage more efficiently. The higher levels of phosphorylated, activated ATM, Rad17, Chk1 and Chk2 present in $CD133^+$ cells are consistent with the enhanced capacity of these cells to sense and repair DNA damage. Upon inhibition of these checkpoint kinases, $CD133^+$ cells are sensitized to ionizing radiation both *in vitro* and *in vivo*. TMZ is a commonly used alkylating agent, which causes DNA damage by methylating the O6-position or N7-position of guanine, used in treatment of GBM. The methyl adducts lead to a continuous cycle of DNA base mismatch repair (MMR), resulting in double strand breaks and eventual apoptosis. Increasing evidence demonstrates that the O6-methylguanine methyltransferase (*MGMT*), whose function is repairing the mutagenic DNA lesion O6- methylguanine back to guanine, is expressed in 80% of glioblastoma patients [55]. MGMT plays an important role in resistance to TMZ, and glioblastoma patients carrying a methylated *MGMT* promoter exhibit improved progression-free and overall survival after treatment with alkylating agents [220]. Expression profiling of $CD133^+$ GSCs demonstrates a 32-fold increase in the level of *MGMT* transcripts relative to $CD133^-$ tumour cells and indicates that this resistance mechanism is highly active in the glioma TSC population [70].

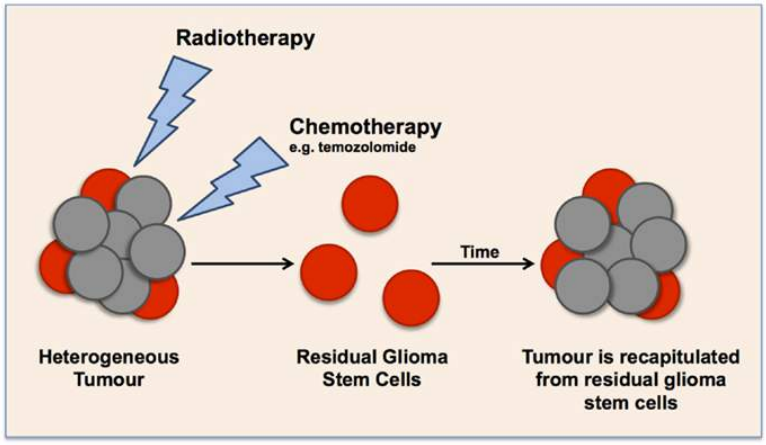

Figure 1.6 Cancer stem cell-mediated therapeutic resistance.

Moreover, recurrent glioblastoma exhibits resistance to multiple therapeutic drugs, leading to the hypothesis that GSCs are naturally resistant to chemotherapy. One potential explanation is that GSCs can reduce drug uptake or expel cytotoxic drugs by increasing the expression of ATP-binding cassette (*ABC*) transporter [221]. A

recent study suggested that the PTEN/PI3K/Akt pathway could regulate ABCG2 activity in glioma cancer stem-like cells [222]. Another possibility for chemo and radio resistance of GSCs is that GSCs exhibit abnormalities of cell death pathways, such as overexpression of antiapoptotic proteins or downregulation of proapoptotic factors [223]. The differentiation of TSC with all-trans-retinoic acid increases apoptotic sensitivity. Immature $CD133^{+}$ U87 MG cells are more resistant to Fas-mediated apoptosis than their mature $CD133^{-}$ counterparts and glioma TSC are poor responders to TRAIL-induced apoptosis [224]. One contributing mechanism to decreased apoptotic sensitivity may be the low or absent caspase-8 levels present in glioma TSC induced by hypermethylation of the procaspase-8 gene promoter [225]. Further efforts need to be devoted to understanding the molecular mechanisms of chemoresistance in GSCs and developing novel and effective therapeutic approaches against GSCs (Fig. 1.7).

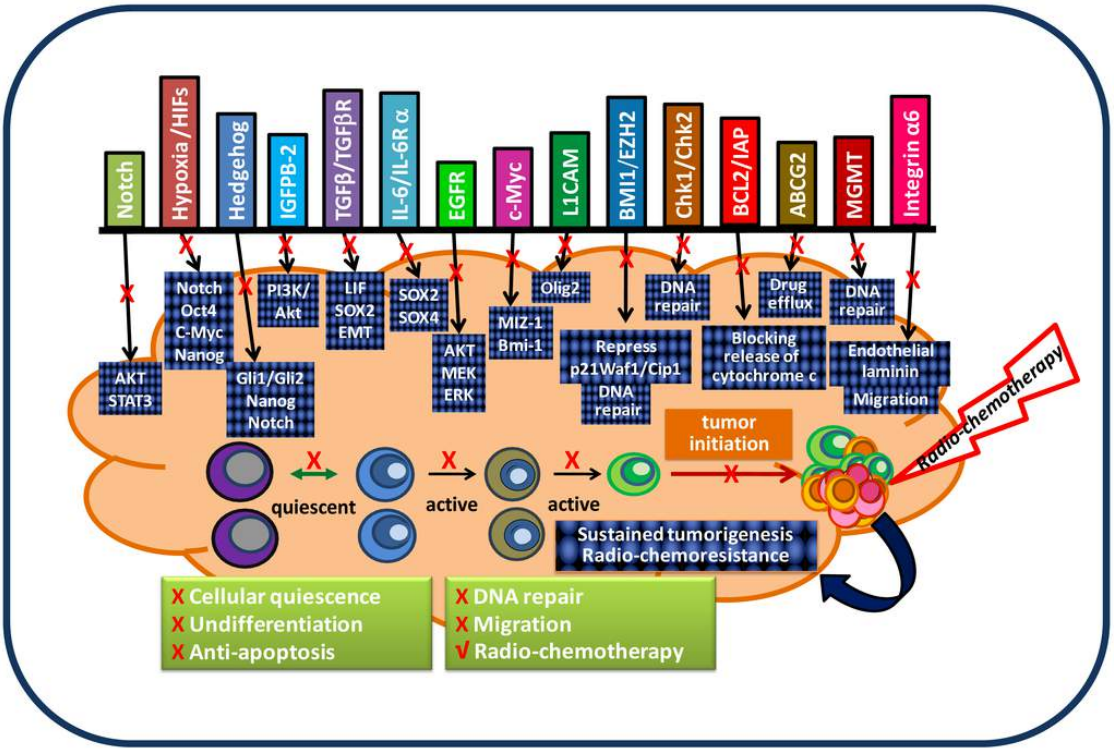

Figure 1.7 A model of GSC-targeted therapy. Several gene pathways have been determined to be required for maintaining tumorigenic capacity and a radio-chemoresistant phenotype of GSC. These signalling pathways work collaboratively and cooperatively to generate a quiescent, undifferentiated, and anti-apoptotic phenotype as well as to constitutively activate the DNA damage checkpoint response in GSC. In order to eradicate a tumour, a therapeutic strategy that disrupts GSC signalling pathways must be developed to be fully integrated into radio-chemotherapy in order to target both GSC and non-GSC populations. [226]

1.4 SYMMETRIC AND ASYMMETRIC CELL DIVISION

Glioblastoma is a highly heterogeneous tumour constituted by cells with different grade of differentiation. The mechanism by which GSCs are maintained and generate cellular diversity of the bulk tumour is still elusive. Additionally, it is unclear which modes of cell division (symmetric and/or asymmetric) GSCs utilize for tumour maintenance and the generation of differentiated progeny.

1.4.1 Symmetric and asymmetric cell division in *D.Melanogaster* stem-like cells

Symmetric divisions are defined as the generation of daughter cells that are destined to acquire the same fate. Although the idea that stem cells can divide symmetrically may seem counterintuitive, stem cells are defined by their potential to generate more stem cells and differentiated daughters, rather than by their production of a stem cell and a differentiated daughter at each division. When viewed as a population, a pool of stem cells with equivalent developmental potential may produce only stem-cell daughters in some divisions and only differentiated daughters in others. In principle, stem cells can rely either completely on symmetric divisions or on a combination of symmetric and asymmetric. Asymmetric cell division (ACD) is a fundamental process whereby the asymmetric inheritance of cellular components (e.g. proteins, RNAs) during mitosis defines distinct fates for each daughter cell. This evolutionarily conserved division mode is used by stem and progenitor cells in different tissues. In a typical outcome of an asymmetric division, the stem or progenitor cell generates a copy of itself, which retains self-renewal ability and differentiation potential, and one daughter that enters the path of differentiation. Thus, by balancing self-renewal with differentiation, asymmetric divisions maintain the stem and progenitor cell pool while allowing the generation of diverse functional cells.[227]

Much of what we know about the regulation of ACD is gleaned from studies of two stem-like cells from *Drosophila*: sensory organ precursor (SOP) cells, in the peripheral nervous system, and neuroblasts (NBs) in the CNS (Fig. 1.8 A, B, C). SOP cells undergo three rounds of asymmetric cell divisions to form the four different cell type of the bristle sensory organ. The SOP cell divides asymmetrically

along the anteroposterior axis to originate an anterior pIIb cell and a posterior pIIa cell. The pIIb and pIIa cells give rise, through a further three ACDs, to five cells. The first ACD of pIIb produces a glial cell, which later undergoes apoptosis, and a pIIIb cell that in turn divides asymmetrically to produce the sheath cell and neuron. The ACD of the pIIa cell produces the socket and hair cells (Fig. 1.8 C).

NBs form by delamination of the ventral neuroectoderm. They divide asymmetrically along the apical-basal axis, producing two daughter cells of distinct size and identity. The smaller basal daughter, called a ganglion mother cell (GMC), undergoes a single terminal division to produce two neurons/glial cells, whereas the larger apical daughter retains NB identity and undergoes multiple rounds of asymmetric divisions to, in effect, bud off a series of basal GMC daughters (Fig. 1.8 A,B).[228]

Asymmetric cell division of both SOP and NB cells is mainly regulated by the uneven segregation of cell fate determinants in the two daughter cells. In order for this to occur, the orientation of the mitotic spindle, determining the cell polarity (apical-basal or antero-posterior axis) needs to be co-ordinated with the site of localization of the cell fate determinants.

In both cell types Bazooka (Baz)/Par6/aPKC complex, which localizes apically in neuroblasts and posteriorly in SOP cells set up polarity for asymmetric cell division. Moreover a complex consisting of a heterotrimeric G-protein α subunit (called Gαi), a GoLoco domain protein (either Pins or Loco), and a NuMA-related Dynein-binding protein (called Mud) controls the position of the mitotic spindle during mitosis [229]. During late interphase/early prophase Baz assembles a polarity complex through the binding and the activation of the Rho GTPase family Cdc42, which in turn recruit atypical protein kinase C (aPKC) and the aPKC inhibitory subunit Par6. Subsequently a second complex consisting of partner of Insc (Pins) and the heterotrimeric G protein coupled subunits Gαi and Gβγ is assembled. In NB cells, both complexes are apical, because of the binding of the adaptor protein Inscuteable (Insc), and the spindle is displaced to generate a smaller basal daughter cell. In SOP cells, the Par-3/6/aPKC complex localizes to the posterior cell cortex, whereas Pins and Gαi are on the anterior side. Taken together, these results suggest that both Pins/Gαi and Par-3/6/aPKC can exert pulling forces in Drosophila: When the two complexes are on the opposite side, this results in equal daughter cells, but when they are combined by the expression of Insc, their concerted action displaces the spindle, resulting in unequal daughter cell size. [230-232]

The Baz/Par6/aPKC complex directs the distribution of the cell-fate determinant Numb, an evolutionary conserved protein primarily known for its ability to inhibit the Notch signalling pathway, and the adaptor protein Miranda (Mira). This process depends on an intact actin cytoskeleton and two myosin motors, MyoII and MyovI, which operate downstream of the complex [233, 234].

In interphase, aPKC and Par6 form a complex with the wD40 protein lethal giant larvae (Lgl). Mitotic phosphorylation of Par6 by AurkA stimulates aPKC to phosphorylate Lgl, which is then released from aPKC, allowing Baz to enter the Par complex [235]. Assembly of Baz/ Par6/aPKC changes aPKC substrate specificity, allowing it to phosphorylate Numb which is uniformly distributed around the plasma membrane of NB and SOP during interphase. Phosphorylated Numb then concentrate at one of the two spindle poles during mitotic division assisted by the adaptor protein Partner of Numb (PON) [236, 237], whose activity is largely dependent on its phosphorylation by Polo kinase. Once in the GMC, Numb prevents self-renewal, predominantly by antagonizing Notch signalling [238]. This event also ensures that the SOP daughter cell which inherits Numb, the pIIb cell, acquires a different fate from the pIIa cell. At the molecular level, it subsequently became clear that Numb acts by counteracting the function of Notch. In the SOP system, gain-of-function *NOTCH* mutations phenocopied *NUMB* loss-of-function.

In addition, Numb and Notch were shown to interact genetically with an epistatic relationship compatible with Numb functioning as an inhibitor of Notch activity. Finally, Numb and Notch were shown to interact physically. [239]

Similar to Numb, Mira polarization has been proposed to occur as a consequence of direct aPKC phosphorylation. However, in *AURKA* mutant NBs, which display delocalized aPKC, Mira distribution is unaltered, implying the existence of alternative mechanisms acting upstream of or in parallel to aPKC [240]. Mira binds to and directs the asymmetric localization of distinct cell-fate determinants, including the transcriptional regulator Prospero [241], the double-stranded RNA-binding protein Staufen (Stau) [242] and the NHL-domain protein Brain tumour (Brat) [243]. In the GMC, Prospero activates a neurogenic program and represses expression of genes associated with stem cell fate and cell-cycle progression [244]. Brat, on the other hand, promotes cell-cycle exit, represses NB fate, and inhibits cell growth, at least in part, by inhibiting the expression of the transcription factor dMyc at a post-transcriptional level [243].

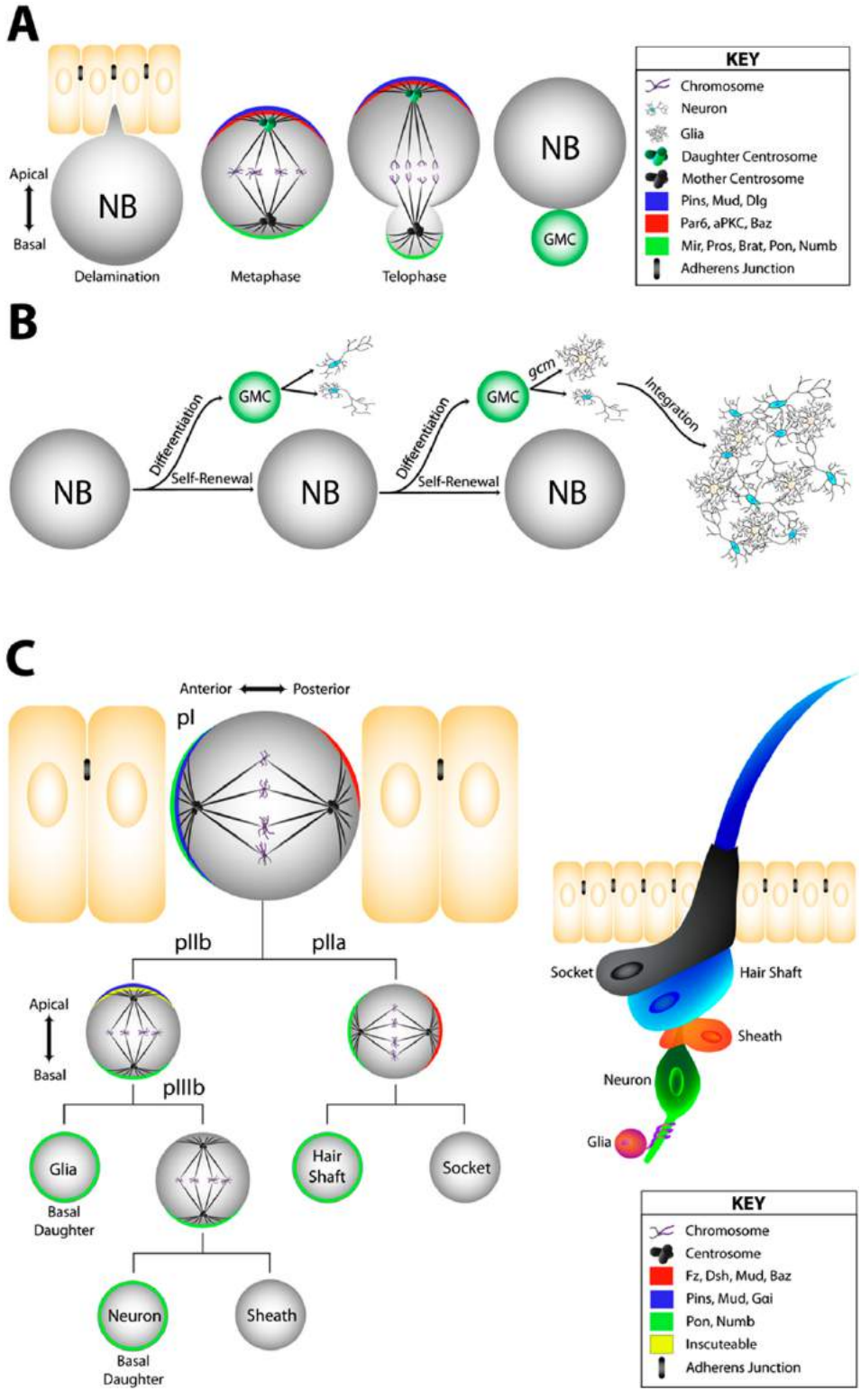

Figure 1.8 Oriented cell division in *Drosophila*. A. Neuroblasts asymmetric cell division. **B.** Neuroblast divisions must properly balance self-renewal with differentiation: GMC daughters generate neurons and glial cells that integrate into the functioning central nervous system, whereas the neuroblast pool remains relatively constant throughout development. *GMC* (glial cells missing) is a gene that is known to regulate glial cell fate in *Drosophila*. If *GMC* is upregulated in a GMC daughter cell, it will differentiate into a glial cell. **C.** Sensory organ precursors (SOPs) produce mechanosensory organs within the developing wing through asymmetric cell divisions. [245]

1.4.2 Cell division mode in mammalian neural stem cells

The production of the different cell types in the mammalian central nervous system (CNS) occurs in temporally defined, though overlapping, developmental phases. Generally, neurons arise first, followed by astrocytes and oligodendrocytes. This process is largely determined by cell intrinsic changes that alter the differentiation potential of CNS progenitors as development proceeds [246].

Mammalian embryonic neural stem cells, or radial glia (RG) cells, arise from neuroepithelial cells, with which they share pronounced apico-basal polarization. RG cells divide in the ventricular zone (vZ) and they contact the ventricular and pial surfaces of the neural tube through an apical process and a long basal fiber, respectively. At its apical endfoot, each RG cell forms close contacts with its neighboring cells via adherens junctions (AJs) [247, 248].

During the peak of neurogenesis, RG cells execute mainly asymmetric self-renewing divisions to produce either neurons or basal progenitors (BPs) [249]. The newly born neurons and BPs lose both ventricular and pial attachments and migrate basally. BPs then divide symmetrically in the subventricular zone (SvZ) to give rise to either two BPs, or, as in most cases, to two neurons that migrate further basally [250]. Another type of neurogenic progenitor with a short basal fiber has been reported to divide adjacent to RG cells, which has led to the proposal that multiple types of neural progenitors co-exist in the vZ [251]. (Fig. 1.9)

Recently, a new class of RG residing in the outer SvZ of the human, ferret, and mouse embryonic brain has been identified. Murine outer RG (oRG) arise from asymmetrically dividing RG cells and, in contrast to BPs and neurons, oRG inherit the basal fiber, but lose their apical attachment and migrate to the SvZ, where they undergo asymmetric self-renewing divisions to produce neurons [252]. (Fig. 1.9)

The molecular mechanisms that establish polarity in RG and oRG cells are only partially delineated. The mammalian homologs of the polarity regulators Par3, Par6, and aPKC, as well as of Cdc42, localize to RG apical endfeet and appear to serve two main functions: 1) they maintain apical AJs integrity, thereby preserving RG polarity and vZ organization; 2) they participate in the control of RG cell fate [227]. Gain- and loss-of-function studies are conclusive in showing that unequal segregation of Par3/aPKC is responsible for differential cell-fate determination. Forced expression of *PAR3* increases symmetric RG divisions at the expense of BP

generation. In contrast, conditional *PAR3* depletion increases neurogenesis [253]. The effects of Par3 on RG cell fate depend on Numb and its close relative Numb-like (Numbl). Par3 seems to directly interact with Numb and thereby to modulate its antagonistic effect on Notch signalling. Since Notch activity is involved in the maintenance of RG identity, this provides a mechanism by which Par3 promotes RG fate. Interestingly, Numb and Numbl have also been implicated in the maintenance of RG AJs and polarity [254]. Thus, Par3 and Numb/Numbl maintain polarity and balance self-renewal and differentiation of RG cells. Also CD133, a cell surface marker, has been shown to segregate asymmetrically. In fact an apical region enriched for Par3 and aPKC, together with the most apical part of the plasma membrane, which shows localized expression of Prominin-1, have been found to be consistently distributed to only one daughter cell in neurogenic divisions [255].

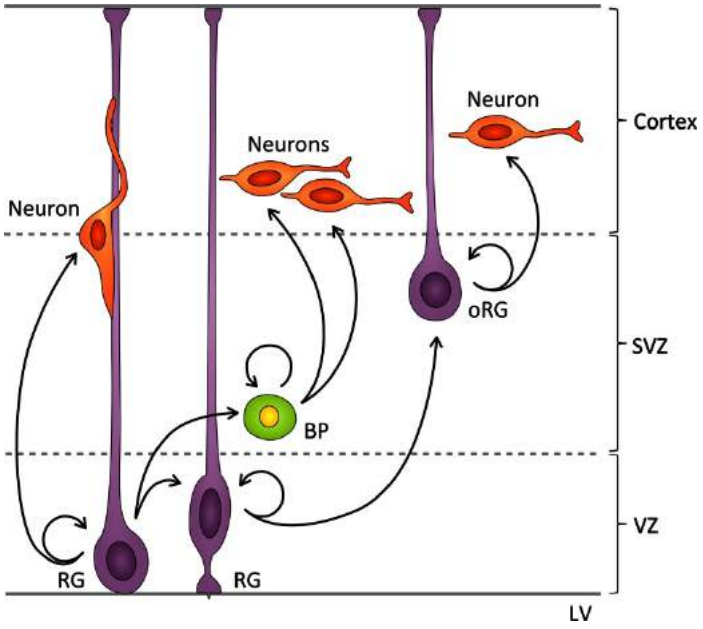

Figure 1.9 Patterns of cell division during mammalian embryonic neurogenesis. During the peak period of murine neurogenesis radial glia (RG) cells divide in the ventricular zone (VZ) mainly asymmetrically, generating one RG cell and one neuron, or one RG cell and one basal progenitor (BP), which migrates to the subventricular zone (SVZ). Asymmetric RG divisions also produce outer RG (oRG) cells, which lose their ventricular attachment and translocate to the SvZ, where they divide asymmetrically to produce neurons. [227]

1.4.3 Evidence of GSCs division mode

Single-cell-based studies from the *Drosophila* NB and SOP system and developing mammalian brain have demonstrated that the generation of differentiated progeny from stem/progenitor cells is tightly controlled. This process is regulated by cell polarity and the segregation of cellular components indicative of cell fate determination, such as Numb [256]. Interestingly, studies in the mammalian brain have shown that CD133, which marks neural stem and progenitor cells, is asymmetrically distributed during the generation of differentiated progeny in the developing neuroepithelium [255].

It is still poorly investigated how GSCs self-renew or generate cellular diversity at the single-cell level. In a pilot study Lathia and colleagues evaluated the cell division behaviour of GSCs using single-cell analyses [257].

They found that GSCs utilize two cell division modes to generate GSCs. The first method is to generate two GSCs through a symmetric cell division, and the other is to generate one GSC and one non-GSC through an asymmetric cell division. Lineage-tracing analysis revealed that the majority of GSCs were mainly generated through expansive symmetric cell division in the presence of growth factors suggesting that growth factor signalling contributes to the expansion of the stem cell population in the tumour (Fig. 1.10). The majority of differentiated progeny was generated through symmetric pro-commitment divisions under expansion conditions and in the absence of growth factors, occurred mainly through asymmetric cell divisions (Fig. 1.10). This division mode would contribute to increased cellular heterogeneity of the tumour, while still maintaining a GSC pool.

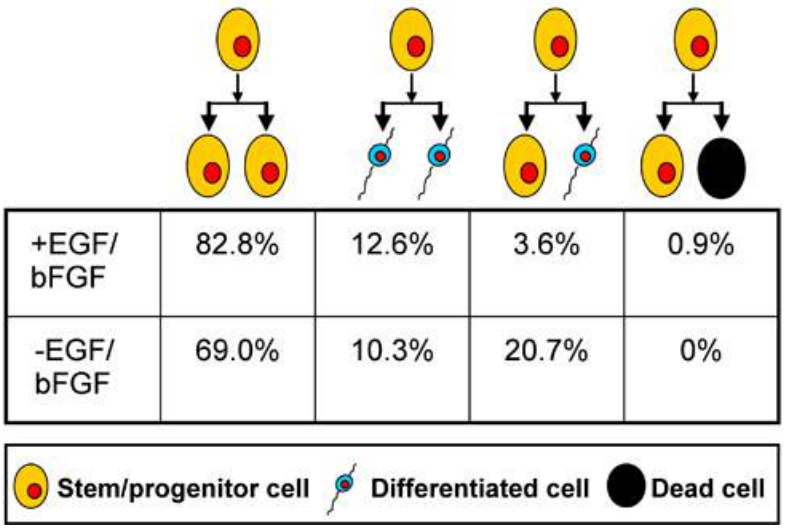

Figure 1.10 Analysis of time-lapse video microscopy detected four types of cell divisions in GSCs. Single-cell lineage-tracing time-lapse microscopy movies demonstrated that growth factor withdrawal (n = 111 cell divisions for EGF and basic FGF conditions, n = 29 cell divisions for growth factor withdrawal conditions) decreased the number of symmetric stem/progenitor cell divisions and increased the generation of differentiated progeny and cell death. Proportional comparison of cell division types between conditions indicated a statistically significant difference. [257]

Mitotic pair analysis detected asymmetric CD133 segregation and not any other GSC marker in a fraction of mitoses (Fig. 1.11 A). The fact that other stem cell markers were not co-segregated with CD133 suggests that there are multiple factors contributing to GSC maintenance. In support of this notion, CD15 serves as a GSC marker in CD133-negative glioma cells [144]. In fact, CD15-positive cells, similar to CD133 positive cells, survive better and proliferate faster as compared with their negative counterparts, indicating its potential to complement some part of CD133 function. A correlation between CD133 and Numb was observed during cell divisions with Numb asymmetry (Fig. 1.11 B). The daughter cells receiving less Numb and CD133 can potentially give rise to CD133-negative GSCs due to attenuated Numb function. Such complex combinations of stem cell markers and Numb inheritance would contribute to multiple states of GSCs as proposed [139]. Under growth factor withdrawal conditions, the proportion of asymmetric CD133 divisions increased, congruent with the increase in asymmetric cell divisions observed in the lineage-tracing studies. The biological significance of these two division modes is not yet fully understood, but it is expected that therapies that increase asymmetric division would generate decreased numbers of resistant GSCs and be favorable for patient outcome. Hence more detailed studies are needed.

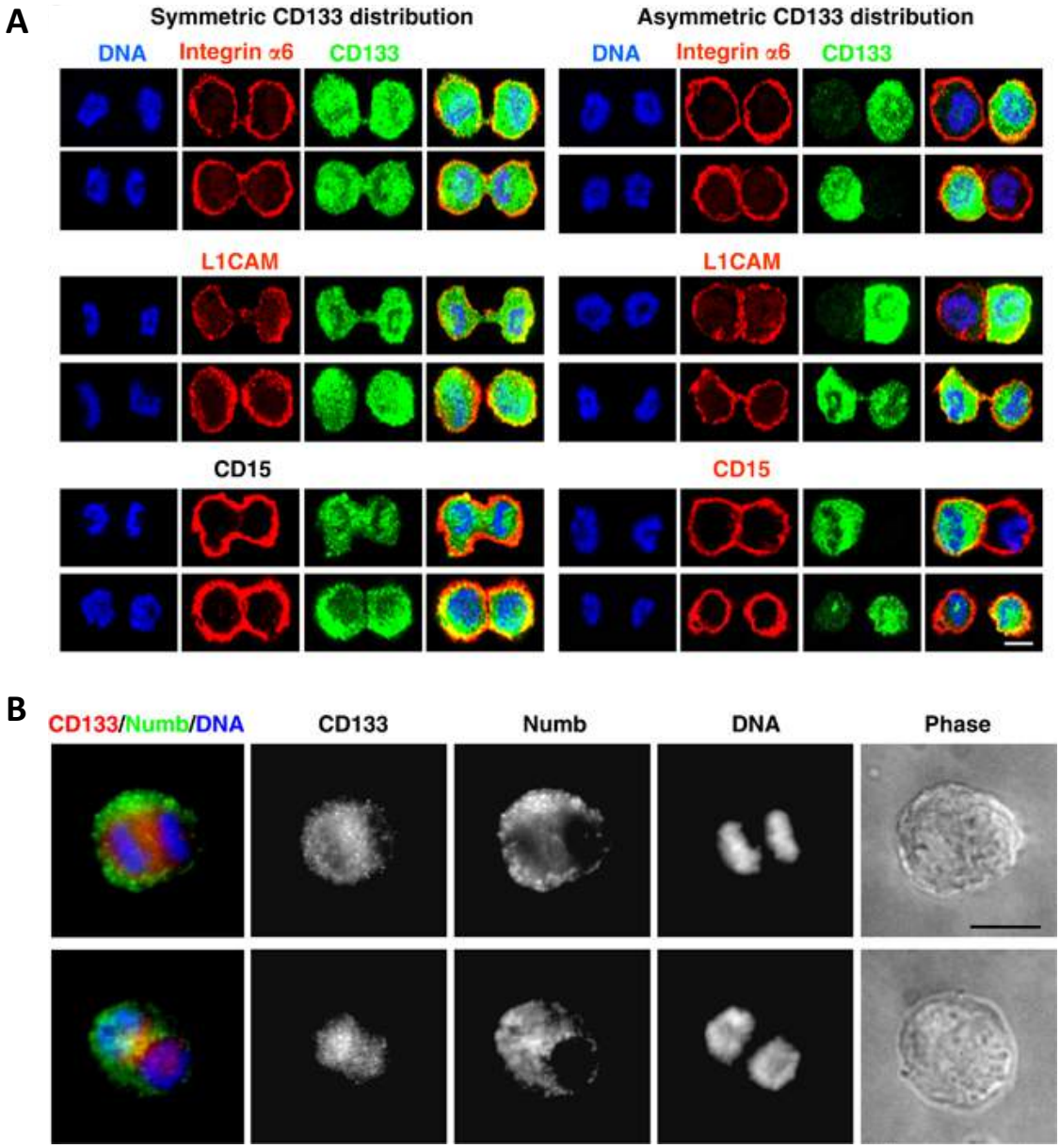

Figure 1.11 Equal and unequal distribution of CD133 irrespective of other GSC markers, but Numb. A. Confocal micrographs of mitotic GSCs grown in expansion conditions demonstrated constant uniform expression patterns for integrin-a6, L1CAM, and CD15 (red). In contrast, symmetric or asymmetric CD133 distribution was detected (green). **B.** Fluorescent micrographs of mitotic GSCs grown in expansion conditions demonstrated consistent asymmetric distribution of CD133 and Numb. Nuclei were counterstained with Hoechst 33342 (blue). [257]

1.5 CHROMOSOMAL INSTABILITY (CIN)

Genomic instability or genetic aberrations are commonly observed in solid tumours and some haematological malignancies. It broadly covers alterations from the single nucleotide level to the chromosomal level. Some of these alterations result in a stable form of aneuploidy and others lead to a continuous reshuffling of genomic material; both can lead to tumorigenesis. [258]

Genomic instability can be further characterised into at least two major subtypes, one is microsatellite instability (MIN) and the other is chromosomal instability (CIN) [259].

Microsatellites are simple repeated nucleotide sequences which remain stable during the whole life span. The MIN phenotype occurs in ~15% of all tumours and is often not associated with chromosomal changes. A third of these cases (~5% of all colorectal cancers) are associated with a family history of colorectal cancers and are often caused by mutations in mismatch repair genes (i.e. *hMSH2*, *hMLH1*, *hMSH6*, and *hPMS2*), resulting in hereditary nonpolyposis colorectal cancer (HNPCC) [260].

MIN in cancer is often associated with good prognosis regardless of tumour stage. MIN tumours are less prone to metastasis and associated with increased patient survival [261].

Chromosomal instability is defined as a failure of cells to maintain stable chromosome number and integrity. CIN is primarily characterized in two types, numerical CIN and structural CIN. Structural CIN refers to high rate of sub-chromosomal alterations via translocations, insertion, deletions and amplification of DNA. In many cancers, translocation is the most effective way of producing the formation or over expression of oncogenes by the fusion or duplication of genes or to knockout of tumour suppressor genes [262]. Mutations in the double-strand DNA damage repair machinery can lead to translocations and structural CIN. Non homologous end joining (NHEJ) is an error prone DNA damage repair pathway, which contributes to structural CIN by joining two non-specific broken ends of DNA. Double strand breaks (DSB) can thus generate non-specific chromosomal fusions especially at dysfunctional telomeres. Fusion at telomeres leads to the formation of di-centric chromosomes or ring chromosomes, which leads to the formation of chromatin bridges at anaphase because of improper attachment of microtubules to

these dicentric chromosomes. These unresolved chromosomal bridges result in breakage at cytokinesis and fusion again in the subsequent cell cycle. [263]
Numerical CIN is a prominent type of CIN in which the gain or loss of whole chromosome occurs with higher rates as compared to normal cells.

1.5.1 Methods for the analysis of CIN

It is challenging to obtain true scores of CIN, especially in vivo, as it requires the measurement of rate of change of whole chromosome number or structure across a cell population.
The key strength of single cell approaches is their ability to perform analysis on a cell per cell basis, whereas the molecular or multiple cell methods are performed on a merged population of cells in which chromosomal instability is often masked. Interphase fluorescence *in situ* hybridization (FISH) enables the rapid screening of hundreds of cells and provides cellular chromosomal copy numbers for the regions included in the respective probe set [264]. Especially popular are chromosome-specific centromere probes, because their use usually results in signals with high fluorescence intensities, thus facilitating evaluation. Additional or missing chromosome-specific centromere signals are usually interpreted as evidence for whole chromosome aneuploidy. By contrast, region-specific probes are used to assess the presence of selected regions on chromosome arms. A missing signal might indicate either segmental aneuploidy or whole chromosome aneuploidy; probe sets can be tailored to distinguish between them [264]. For example, if probes for both the long and short chromosome arms (p- and q arms) are applied and both probes simultaneously have a reduced or an increased signal, loss or gain of the entire respective chromosome is likely. The disadvantage of interphase FISH is that only a limited number of probes can be used simultaneously. Thus, chromosomal copy number changes could be missed.
Karyotyping, either by traditional banding analysis or by 24-color FISH (i.e. multiplex FISH or spectral karyotyping (SKY)), yields information about chromosomal copy numbers, chromosomal structural changes and cell-to-cell variability [264]. However, the preparation of metaphase spreads from solid tumours is labour intensive and requires skilled multidisciplinary teams including surgeons, pathologists and cytogeneticists. Furthermore, metaphase spreads from even short-

term cultures might acquire culturing artifacts, which can mask characteristics of the tumour.

Lagging chromosomes or chromosome fragments can be excluded from the main daughter nuclei during cell division and form small nuclei within the cytoplasm; these are termed micronuclei. Thus, the presence of micronuclei is a surrogate marker for CIN; unlike other approaches, this detection method is based on cell morphology without direct visualization of chromosomes or genomic regions. Micronuclei counting is a very popular method of CIN analysis because it enables the rapid evaluation of hundreds of cells. However, it cannot distinguish whole chromosome aneuploidy from segmental aneuploidy. [259]

By contrast, array comparative genomic hybridization (aCGH) easily identifies both whole chromosome and segmental aneuploidies [264]. Recently developed protocols for the isolation of individual cells and unbiased whole genome amplification enable these analyses to be performed using DNA derived from as little as a single cell [265]. Therefore, single cell array-CGH currently offers the best resolution for the assessment of CIN and the presence of whole chromosome or segmental aneuploidies. However, single cell array-CGH is not amenable to automation and therefore does not represent a high-throughput approach.

Most proxy methods of scoring CIN are static measures that take a snapshot at a certain point in time that measure the number of chromosomes, chromosome complexity and genetic diversity in a supposedly clonal population. Flow cytometry is commonly used to measure the DNA content of cancer cells and by extension, estimate the ploidy [266]. Vast amounts of aCGH and Single Nucleotide Polymorphism (SNP) microarray data are available on various platforms, which can be used to derive surrogate measures of aneuploidy or CIN. Recently developed algorithms for the analysis of biallelic SNP arrays allow for the estimation of ploidy levels, loss of heterozygosity (LOH) events and the degree of chromosomal structural instability and the location of aberrant chromosomal regions [267, 268]. Digital polymerase chain reaction (PCR) or digital single nucleotide polymorphism (SNP) analysis is a PCR-based approach in which the alleles within a tumour sample are individually counted [269]. Digital PCR identifies allelic imbalances, which reflect gains and losses of particular chromosomal regions. The presence of allelic imbalances has been used as a marker for CIN in early-stage tumours [270].

1.5.2 Causes of CIN

Different causes that have been postulated to be responsible for these genomic aberrations are outlined below i.e. defects in sister chromatid cohesion [271], merotelic attachments [272], improper attachment of kinetochore to the mitotic spindle [273], centrosome amplification [274] and an aberrant spindle assembly checkpoint [275], which is the best characterized cause of chromosomal instability. (Fig. 1.12)

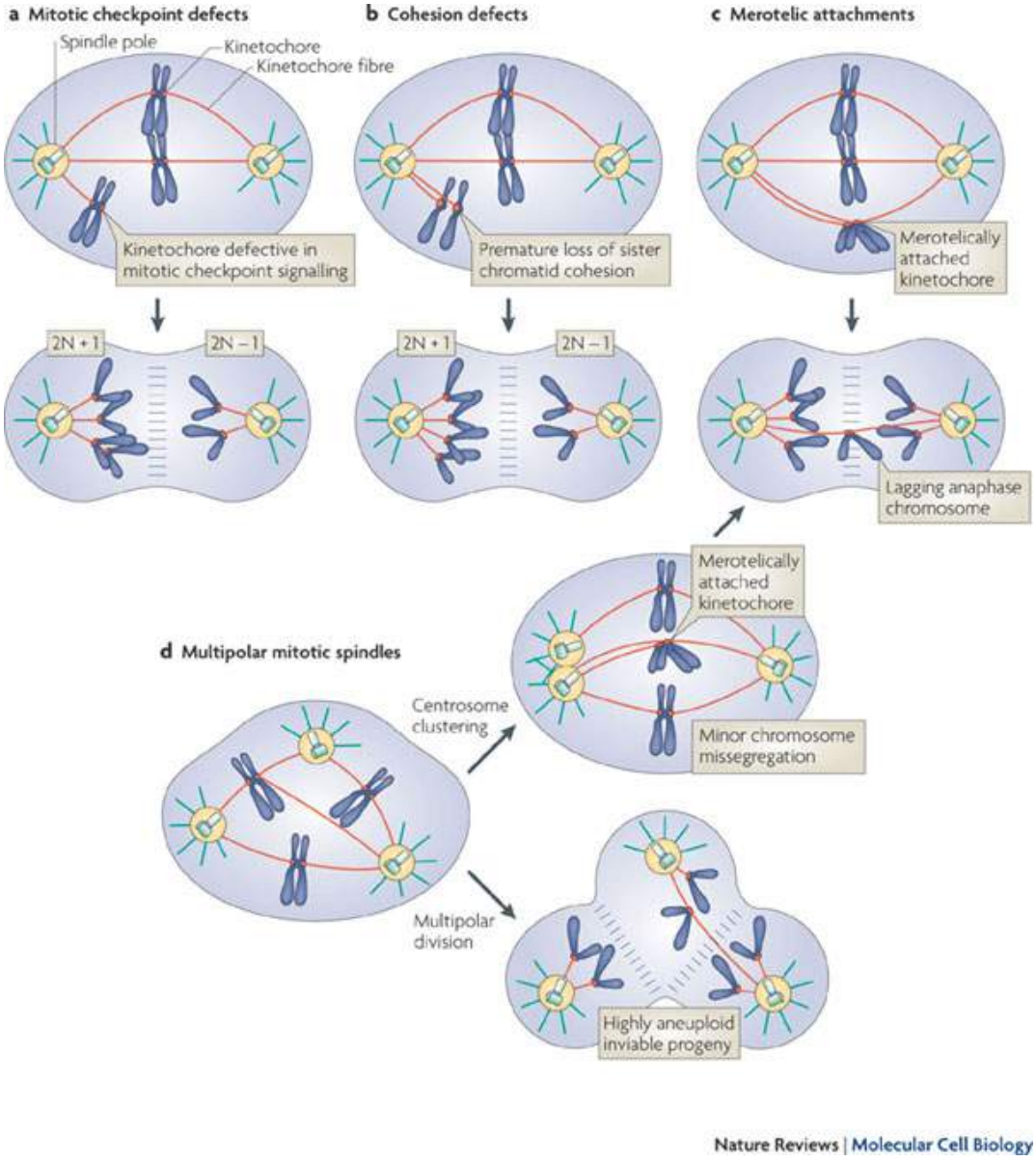

Figure 1.12 Pathways to the generation of aneuploidy. There are several pathways by which cells might gain or lose chromosomes during mitosis. [275]

Merotelic attachment

For proper chromosome segregation, kinetochores on every sister chromatid pair must attach to microtubules from different spindle poles; this is called bipolar or amphitelic attachment. There are three types of erroneous attachments: 1) monotelic attachment, in which only one of the sister kinetochores attaches to microtubules, 2) syntelic attachment, in which both sister kinetochores attach to microtubules from the same spindle pole, and 3) merotelic attachment, in which one kinetochore attaches to microtubule from both spindle poles (Fig. 1.13). Monotelic attachments trigger the spindle assembly checkpoint (SAC), which senses the lack of microtubule attachment onto kinetochores. Syntelic attachment indirectly activates the SAC, as lack of proper tension generates unattached kinetochores [276]. The SAC halts chromosome segregation until these errors are corrected. In contrast, merotelic attachment is not sensed by the SAC, because kinetochores are, in principle, occupied by microtubules and the presence of tension stabilizes microtubule attachments [272]. Although the mitotic kinase Aurora B plays a role in correcting merotelic attachment, cells may enter anaphase before completing the correction [277]. Chromosomes forming merotelic attachments are often left behind in the middle of the spindle when the other chromosomes are segregated to spindle poles; such missegregating chromosomes are termed lagging chromosomes. In consequence, merotelic attachment is considered to be a major cause of CIN [278]. The incidence of lagging chromosomes in cancer cells exhibiting CIN is 10–60%. Most lagging chromosomes eventually segregate properly, but sometimes they may be segregated to the wrong pole, giving rise to aneuploidy. If the nuclear envelope is reformed before a lagging chromosome joins the other chromosomes, it will be isolated as a micronucleus [279].

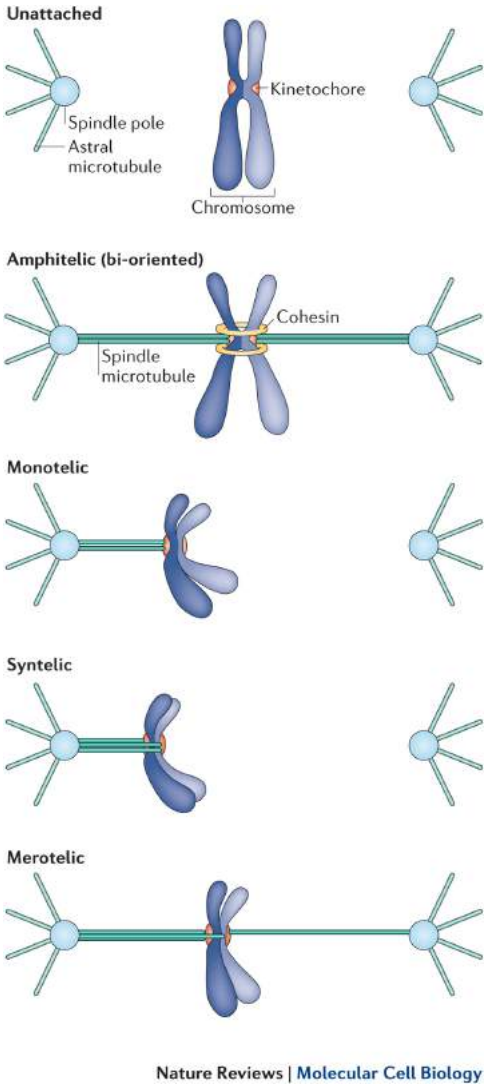

Figure 1.13 Kinetochore–microtubule attachment states on the mitotic spindle. [280]

Centrosome amplification

Centrosome amplification has been closely correlated with CIN, and is frequently found in cancer cells. Supernumerary centrosomes lead to the formation of multipolar spindles and subsequently multiple nuclei, as a result of multipolar mitoses, which are deleterious to cell survival [281]. To avoid this situation, cells have a mechanism to arrange multiple spindle poles into two clusters (centrosome clustering) allowing the formation of a bipolar spindle [282]. In multipolar spindles, kinetochores can be attached to microtubules emanating from multiple directions, and such loss of geometric constraints results in an increased rate of merotelic attachment in the pseudo-bipolar spindle after centrosome clustering. It has been reported that kinetochore and spindle components, including dynein and Hset/KifC1, a kinesin-14 family member, are involved in centrosome clustering [283].

Defects in sister chromatid cohesion

Cohesion holds the sister chromatids together during mitosis until the SAC is satisfied [284]. Cohesion is essential for the faithful segregation of replicated chromosomes during mitosis. Aberrant cohesion leads to loosely attached or unattached sister chromatids floating around in the cell and generates difficulties in the equal distribution of chromatids between the two daughter cells. Similarly, alteration in cohesion release from chromosomes causes the failure of sister chromatid separation and results in numerical CIN [262].

Premature separation or partial failure of segregation leads to chromosomal instability or aneuploidy and the complete failure of chromatid separation leads to tetraploidy) [262]. Genes involved in the cohesion of sister chromatids are often mutated in CIN cancers. Furthermore, members of the core cohesion complex (i.e. Scc1 and Smc3) and cohesion regulators (i.e. separase) are overexpressed in some CIN cancers [285].

Defects in the spindle assembly checkpoint (SAC)

The SAC is a mechanism by which eukaryotic cells arrest cell division at metaphase until all sister kinetochores are attached to microtubules from opposite spindle poles (Fig. 1.14). Kinetochores mediate chromosome attachment to microtubules. They are complex multi-subunit structures with an inner layer interfacing with the unique centromeric chromatin present on each chromosome, and an outer layer involved in microtubule binding and SAC control. Within the outer layer, the Knl1 complex–Mis12 complex–Ndc80 complex (abbreviated as KMN network) promotes microtubule binding through a calponin-homology (CH) domain on the Ndc80/Hec1 subunit of the Ndc80 complex.[286]

In prometaphase, sister chromatids are topologically linked by the ring-like cohesin complexes [287]. In addition, the activity of cyclin-dependent kinase 1 (Cdk1, also known as cell division cycle 2; Cdc2), the main mitotic kinase, is high and maintains the mitotic state. As mammalian cells proceed from prometaphase to metaphase, a signalling complex that contains mitotic arrest deficient 1 (Mad1), Mad2, MpS1 (also known as TTK), Bub1, Bub3 and BubR1 assembles at unoccupied kinetochores in order to verify if proper attachments between microtubules and kinetochores are established. In addition to microtubule-kinetochore attachment, tension is important for SAC activation [288]. Stretching of centromeric chromatin on bi-orientation increases kinetochore to kinetochore distance and kinetochore tension.

Microtubule-kinetochore attachment is normally destabilized at low kinetochore tension and stabilized by high tension between bi-orientated sister kinetochores. Tension might therefore provide a fundamental criterion to discriminate against incorrect attachments. For example, kinetochores lacking tension because both sisters are attached to microtubules from the same pole (syntelic attachment) activate the checkpoint even though kinetochore-microtubule attachments are made, indicating that lack of tension can be sufficient for checkpoint activation. Chemical inhibition of spindle dynamics, which relieves tension but does not destroy kinetochore-microtubule attachments, also activates the checkpoint [288].

One clear difference between the checkpoint response to lack of tension and that to lack of attachment is the recruitment of the Mad and Bub proteins. Mad1 and Mad2 localise to unattached kinetochores but not to attached kinetochores that lack tension, but Bub1 and BubR1/Mad3 localise to kinetochores lacking either tension or microtubule attachment. However, because Mad1 and Mad2 are required for checkpoint activation in response to tension, these differences are unlikely to reflect distinct checkpoint signalling pathways [289].

A key role is played by the protein kinase Aurora B, a component of the chromosomal passenger complex, which is thought to promote bipolar attachment by destabilising kinetochore microtubule interactions that are not under tension. This may explain the requirement of Aurora B kinase for the checkpoint response to lack of tension, because by breaking inappropriate attachments Aurora B kinase produces unattached kinetochores that could then be sensed by the Mad/Bub machinery.

However, Aurora B is critical for correcting merotelic attachments, which are not sensed by the SAC. Merotelic attachment occurs when one sister kinetochore becomes attached to microtubules from opposite poles. Bi-orientation of chromosomes with merotelic kinetochores produces sufficient occupancy and tension to turn off SAC activity. As a result, merotelic kinetochores, if left uncorrected, can produce lagging chromatids and potential chromosome missegregation in anaphase. The recruitment of the mitotic checkpoint complex at kinetochores generate a diffusible signal that is dependent on Mad2 and BubR1, which prevents the e3 ubiquitin ligase complex anaphase promoting complex/cyclosome (ApC/C) from degrading its mitotic targets cyclin B1 and securin (also known as pituitary tumour-transforming 1; pTTG1). In this state, exit from

mitosis and the separation of sister chromatids are inhibited. As soon as the last kinetochore pair is attached to the microtubules at opposite spindle poles, the inhibitory diffusible signal is extinguished and the ApC/C is fully activated through the release of inhibition of its cofactor, Cdc20. This leads to the ubiquitylation of cyclin B1 and securin, the two crucial partners of Cdk1 and the cysteine protease separase (also known as eSpl1), respectively. Degradation of cyclin B1 by the 26S proteasome leads to a rapid decline in Cdk1 activity, allowing exit from mitosis. Securin is a small inhibitory chaperone of separase, the activity of which is essential for the dissolution of cohesin complexes at and near sister chromatid kinetochores. Degradation of securin by the 26S proteasome and release from inhibition by Cdk1-cyclin B1 phosphorylation owing to cyclin B1 degradation leads conjunctly to activation of separase and cleavage of the Scc1 (also known as Rad21) component of cohesin; the net effect of this is the separation of sister chromatids. Both of these events, inhibition of Cdk1 and activation of separase, are necessary for a correct metaphase-to-anaphase transition and faithful segregation of chromosomes. Although it is clear that a diffusible inhibitory signal is generated at kinetochores and prevents ApC/C acting on cyclin B1 and securin, the nature of this event remains unclear. Musacchio and others have proposed a prion-like model based on two structural conformations adopted by Mad2: open and closed. At this point the evidence for this model is biochemical but it accounts for the role of Mad2 at kinetochores, its interaction with Cdc20 and the signal amplification required for the inhibition of the cell cycle by a single unoccupied kinetochore. Unoccupied kinetochores are known to recruit Mad1, which in turn binds with high affinity to Mad2 in its closed conformation. This Mad1-Mad2 complex is then thought to catalyse the conversion of open Mad2 monomers (the predominant form in the cytosol) to closed Mad2 forms that then bind to Cdc20. This interaction serves a dual purpose: it inhibits the activity of ApC/C (at least with regard to cyclin B1 and securin) and catalyses the further conversion of Mad2 open monomers to closed Mad2-Cdc20 complexes, accounting for the required signal amplification. [290]

Although the SAC components are essential for cell survival and embryonic development, mouse models with reduced expression of SAC genes are viable, and show CIN and high rates of spontaneous cancer formation or acceleration of carcinogen-induced oncogenesis in most cases, supporting the idea that CIN promotes oncogenesis [291]. The *BUB1B* gene encoding BubR1 is one of the genes

mutated in a rare congenital human disorder, mosaic variegated aneuploidy (MVA), and MVA patients show aneuploidy as well as increased rates of cancer formation [292]. In addition to a weakened SAC, sustained activity of SAC can also be the cause of chromosome missegregation leading to CIN. Artificial targeting of the mitotic kinase Plk1 on metaphase kinetochores was reported to cause prolonged mitotic arrest due to the sustained SAC activity in response to reduced microtubule dynamics, and cells exhibited increased rates of merotelic attachment and lagging chromosomes [293].

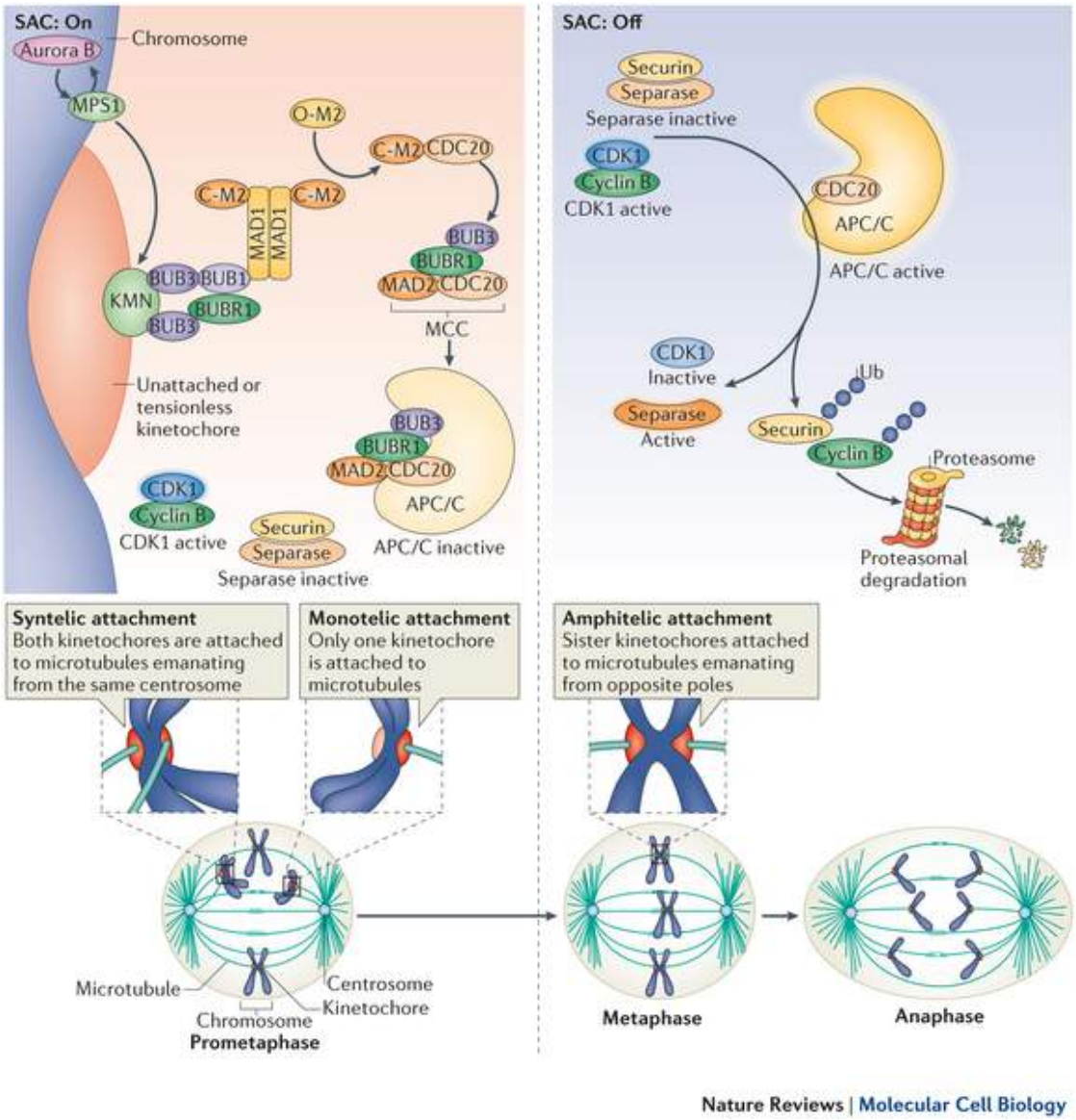

Figure 1.14 Spindle assembly checkpoint mechanism of function. [294]

1.5.3 CIN and tumorigenesis

The link between chromosomal instability and tumorigenesis has been in discussion since 1914 when Theodore Boveri first observed the high number of aneuploid cells in cancer and now CIN is one of the hallmarks of cancer [275]. CIN is the major cause of chromosomal alterations or aneuploidy. Almost 90% of solid tumours and 50% of haematopoietic tumours exhibit aneuploidy [295]. CIN is linked with tumour progression and poor clinical outcomes such as metastasis and adaptability to environmental and chemical stresses. Drug resistance and relapse is also common in cancers with CIN as they evolve rapidly, making them difficult to target with regular therapies [296, 297]. Although some arguments can still be made for aneuploidy as simply a passenger event in tumours, three lines of observation argue otherwise. First, *in vitro* transformation of cell lines through various genetic alterations that lead to CIN suggests aneuploidy has a direct causal role in tumorigenesis. Transformation of cells in culture has been a standard assay to determine the oncogenic or tumour suppressive nature of a gene for more than two decades [298]. Although the genetic events that must occur for a primary cell to become transformed may differ substantially from those that occur in human tumours, several now-established oncogenes and tumour suppressors were identified by transformation assays [299]. Among the mitotic check- point genes with roles that have been explored in *in vitro* transformation, securin overexpression in primary cells leads to marked aneuploidy and is sufficient for transformation. Overexpression of aurora kinase A (*AURKA*), the function of which is required for centrosome maturation, bipolar spindle assembly and mitotic entry, similarly leads to aneuploidy and transformation in human and rodent cells as a result of abnormal mitoses. [300, 301]

Second, perhaps the most robust causative data linking CIN to tumorigenesis comes from the study of mouse models of aneuploidy. Several CIN mouse models have been generated with deletions or hypomorphic alleles of genes important for mitotic fidelity. Homozygous deletion of genes required for faithful mitotic progression leads to embryonic lethality [302]. Haploinsufficiency of mitotic genes, however, is tolerated in all cases and is therefore used extensively to investigate in the effects of CIN in tumorigenesis. Following recent findings that mitotic genes are more frequently upregulated than downregulated in CIN tumours, various mouse

models have been generated that overexpress genes involved in mitotic progression, such as the mitotic checkpoint genes *BUB1* and *MAD2* and the E2 enzyme *UBCH10* [302]. Several laboratories have generated mouse models of aneuploidy based on mutations or transcriptional changes of mitotic checkpoint genes observed in tumours. An obvious caveat of all these individual studies is that these genes have non-mitotic functions that might explain their tumorigenic potential. In addition to their accepted mitotic functions, Mad2 and RanBp2, a RAN GTpase binding protein that localizes to kinetochores during mitosis, have been implicated in nuclear trafficking. Securin has also been linked to modification of p53 function, and BuB1 and BuBR1 have been shown to play a part in the response to DNA damage. [291]

Third, a large amount of data collected from human tumours suggests that aneuploidy has a causative role in tumorigenesis by showing that CIN and chromosomal aberrations correlate with tumour grade and prognosis [297]. Transcriptional expression profiles of aneuploid tumours have revealed a CIN signature that can be used to stratify lesions according to prognosis in an unbiased manner. The fact that this CIN signature, which contains genes that are involved in a wide range of pathways, can predict clinical outcome even if genes that are regulated by the cell cycle are omitted provides further evidence that CIN plays a contributory part in the progression of these human tumours [297].

1.5.3.1 Aurora kinases and cancer

The progression and execution of mitosis is under heavy control by several protein kinases. Among these Aurora kinases play an essential role as they are involved in centrosome separation and maturation, spindle assembly and stability, chromosome condensation, congression and segregation, and cytokinesis [300]. In mammalian cells three Aurora kinases have been identified, named Aurora A, B and C. They present a similar domain organization: a N-terminal domain of 39-129 residues in length, a protein kinase domain and a short C-terminal domain of 15-20 residues. The N-terminal domain shares low sequence conservation, which determines selectivity during protein-protein interactions, while the catalytic C-terminal domain is more conserved. They are serin-threonin protein kinases and

their functions are highly regulated by means of activation and localization. [303] (Fig. 1.15)

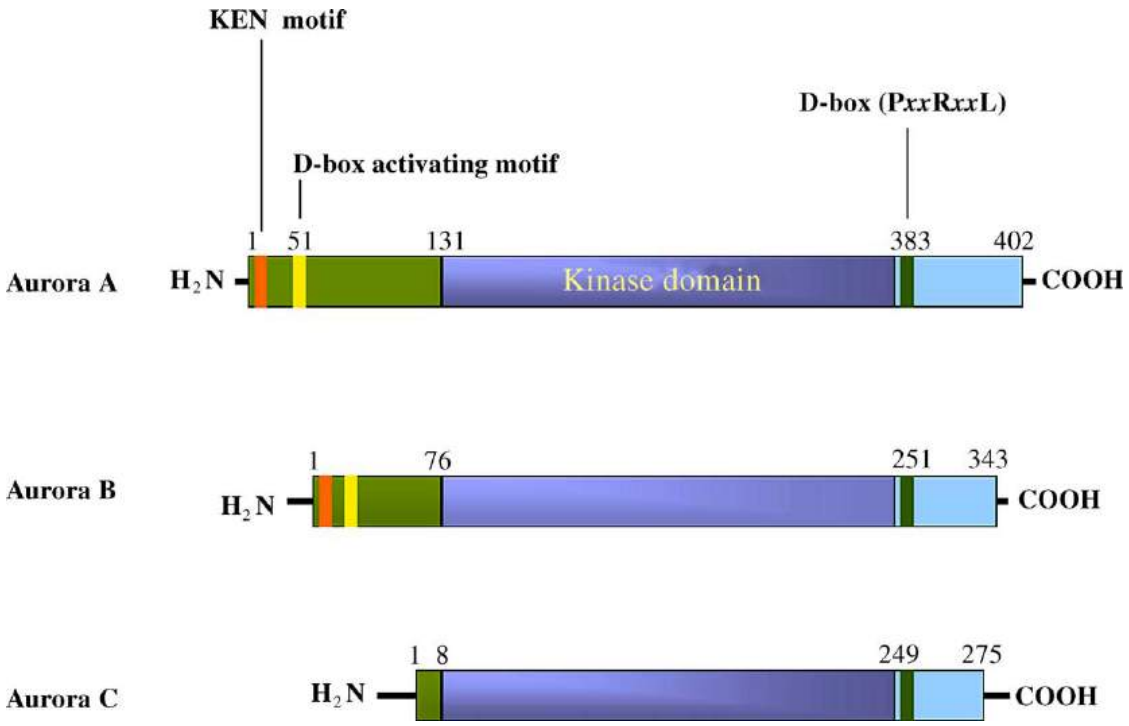

Figure 1.15 Schematic representation of human Aurora A, B, C. As shown here, Aurora kinases present three domains: The N-terminal and the C-terminal domains contain most of the Aurora's regulatory motifs, while the central region contains the catalytic domain. In addition to the kinase activity, this central domain also presents regulatory motifs, as the crystal structure of the Aurora A-TPX2 complex has shown. [304]

Aurora kinase A

Aurora A has well-established but perhaps not yet fully understood roles in centrosome function and duplication, mitotic entry, and bipolar spindle assembly. By the G_2 phase of the cell cycle through anaphase, it can be detected in the pericentriolar material. Additionally, it spreads to mitotic spindle poles and midzone microtubules during metaphase. Aurora A activation requires auto phosphorylation of the activation loop (T288), which is facilitated by forming a complex with other protein. To date the microtubule binding protein Tpx2 is the best understood protein that activates Aurora A. In addition, a variety of other proteins, such as Ajuba, Bora and Pak1 bind to and activate Aurora A at the centrosome. Aurora A T-loop phosphorylation is reversed by the activity of the protein phosphatase PP1, at least *in vitro*. Aurora A levels in cells are regulated by proteasome-mediated degradation. Inhibition of proteasomes in HeLa cells leads to increased levels of poly-ubiquitinated Aurora A and a simultaneous accumulation of Aurora A

phosphorylated at T288, suggesting that this form of Aurora A is targeted for degradation. Aurora A is degraded as cells exit mitosis and is ubiquitinated by the anaphase-promoting complex (APC) *in vitro*. [305]

The human Aurora A gene, *STK15*, resides in a region of the genome (20q13.2) often amplified in certain cancers [306].

Aurora A overexpression occurs in a high proportion of breast, colorectal and gastric cancers [307]. Similarly, the Aurora A gene has been found to be amplified in human gliomas [308]. Using Northern and Southern blotting, Zhou et al. observed 2.5 to 8-fold amplification of Aurora A in many tumour cell lines [309]. Aurora A overexpression can occur because of gene amplification, transcriptional induction or post-translational stabilization [307]. Furthermore, Aurora A has been characterized as a potential low-penetrance tumour susceptibility gene, since the Phe31Ile functional polymorphism is strongly associated with familial breast cancer [310]. Recently, an Aurora A-p53 connection has been revealed. Previously, parallels had been noticed between phenotypes associated with Aurora A gain-of-function mutations (or its overexpression) and those caused by p53 loss of function [311]. The activity and stability of p53 is governed by many post-translational modifications, most importantly, multisite phosphorylation. In an intriguing new development, Aurora A has been shown to phosphorylate Ser315 of p53, leading to its Mdm2-mediated destabilization. Aurora A RNAi led to a loss of Ser315 phosphorylation, p53 stabilization and a G_2/M cell cycle arrest. In a separate study, phosphorylation of Ser215 of p53 abrogated p53's DNA-binding and transactivation function. To complicate matters further, p53 has been shown to block Aurora A activity, an effect overcome by TPX2. How this web of interactions plays out in cells remains to be dissected. Aurora A may regulate p53 *in vitro*, but it is still unclear whether this occurs *in vivo*. [307]

Aurora kinase B

Aurora B is partnered with Incenp, Survivin and Borealin in the chromosomal passenger complex (CPC), named after its transient localization to the chromosomes and inner centromere from prometaphase to metaphase, the central spindle in anaphase and the cleavage furrow during cytokinesis. A critical function of Aurora B and the CPC is the control of chromosome biorientation. The kinase destabilizes incorrectly attached MT–kinetochore connections via the MT

depolymerase mitotic centromere-associated kinesin (MCAK), and by targeting kinetochore components in the KNL1/Mis12/Ndc80 network and the Ska complex. Auto phosphorylation of Aurora B within its activation segment occurs on threonin 232.These phosphorylations are removed by PP1, once tension is established and the outer kinetochore is separated from the centromeric Aurora B. By generating unattached kinetochores during error correction, Aurora B intrinsically impacts on the spindle assembly checkpoint (SAC), but a more direct involvement of Aurora B in the SAC has also been proposed. Thus, Aurora B inhibition does affect SAC maintenance in response to loss of attachment or when the SAC is caused by constitutive tethering of Mad1 to the kinetochore. This could be explained by a possible role for Aurora B to recruit SAC components such as Mad2 and BubR1 to the kinetochore. Furthermore, Aurora B plays a role in sister chromatid cohesion, spindle disassembly and cytokinesis, and has meiosis-specific functions in regulating the synaptonemal complex. These various roles reflect the differential localization of Aurora B at the chromosome arms, centromeres, central spindle and midbody during mitotic progression. Cell division in the absence of Aurora B activity results in chromosome missegregation. However, the major consequence of Aurora B inhibition in mammalian cells is a cytokinesis failure resulting in binucleate daughter cells. [312]

The role of Aurora B in tumorigenesis is not so clear. Aurora B gene is located on chromosome 17p13.1, a chromosomal region that has not been associated with amplification in tumours. There have been reports that Aurora B is overexpressed in certain tumour types, but it is not clear whether the observed overexpression of Aurora B is a mere reflection of the high proliferative index of cancerous cells or whether it is indeed causally related to tumorigenesis [300]. Katayama et al. reported a correlation between overexpression of Aurora B and tumour progression in surgically resected colon tumour specimens [313]. The malignant progression of thyroid anaplastic carcinoma has also been shown to correlate with the overexpression of Aurora B [314]. The silent functional polymorphism, Ser295Ser (885 A > G) in the C-terminal end of Aurora B has been associated with an elevated risk of familial breast cancer [310], and overexpression of Aurora B has been correlated with decreased survival in glioblastoma patients [315].

Some studies have also shown that forced expression of Aurora B can enhance cellular transformation. For example, expression of Aurora B in CHO cells was

reported to promote aneuploidy and increase invasiveness in xenograft experiments. Furthermore, Aurora B overexpression strongly enhances cellular transformation in cells expressing oncogenic Ras-V12. [300]

Aurora kinase C

The gene encoding Aurora kinase C was first isolated from testis cDNA library and the gene localized to Chr19q13. Subsequent analysis reported high transcript levels in testes and oocytes [316]. Several recent studies demonstrated that Aurora C, like Aurora B, interacts with the inner centromere protein (INCENP) at the carboxyl terminal end spanning the conserved IN box domain. Competition binding assays and transfection experiments revealed that, compared with Aurora B, Aurora C has a lower binding affinity to INCENP. It has also been shown that an Aurora C kinase-dead mutant induces multinucleation in a dose-dependent manner and that siRNA mediated silencing of both Auroras B and C give rise to multinucleated cells. Interestingly, Aurora C is able to rescue the Aurora B silenced multinucleation phenotype, demonstrating that Aurora C kinase function overlaps with and complements Aurora B kinase function in mitosis. Thus, Aurora C is a chromosomal passenger protein localizing first to centromeres and then to the midzone of mitotic cells that cooperates with Aurora B to regulate mitotic chromosome segregation and cytokinesis in mammalian cells. [304]

AurkC is believed to be oncogenic because its overexpression transforms NIH 3T3 cells into tumours. *AURKC* is overexpressed in many cancer cell lines, including NB1RGB, MDA-MB-453, HEPG2, HeLa, and HuH7, and in cancer of the reproductive tract. Overexpression increases cellular proliferation and migration and enhances xenograft tumour growth. Kinase-dead AurkC decreases proliferation of HeLa cells while expression of the constitutively active AurkC leads to more aggressive tumours. Other carcinogenic genes are also located in the telomeric region of human chromosome 19, a genomic region susceptible to translocations and deletions. The functional significance of *AURKC* expression in cancer cells is unknown but may relate to centrosome regulation. Overexpression of AURKC in mitotic cells leads to centrosome amplification and multinucleation, a hallmark of cancer. Extra centrosomes are associated with the formation of multipolar spindles. Multipolar spindle formation usually leads to cell death however centrosome clustering appears to support cancer cell survival and frequently leads to

chromosome segregation defects. AurkC localizes to centrosomes with AurkA during interphase and may play a role in centrosome clustering. Many new cancer therapies are aimed at declustering centrosomes which forces cancer cells to form a multipolar spindle and induces cell death. AurkC inhibition may alter this clustering pathway. AurkC interactions with other proteins linked to cancer may also explain its oncogenic role. AurkC, as well as AurkA and AurkB, phosphorylate the transforming acidic coiled-coil 1 protein (*TACC1*). Overexpression of *TACC1* drives cell transformation and serves as a prognostic marker of endocrine therapy resistance in breast cancer. AurkC also phosphorylates TRF2, a protein involved in telomere length regulation. Decreased telomere length predisposes individuals to cancer and negatively impacts fertility. In addition, tumor necrosis factor alpha induces increased *AURKC* expression through the inflammation response factor CEBPD in HeLa cells. Ongoing studies of normal AurkC functions in meiotic cells are critical to improving our understanding of the role of aberrant expression in cancer. [316]

1.6 CIN AS A THERAPEUTIC TARGET

Drug resistance and poor prognosis associated with CIN tumours renders their treatment a considerable challenge. However, the frequency and clinical significance of CIN and its restriction to neoplastic tissue suggests the CIN phenotype could be an attractive therapeutic target. In this regard, the direct targeting of CIN by anti-cancer therapeutics is a subject of active research.

Given the plethora of mechanisms that have been attributed to CIN, several possible strategies have been suggested, such as the use of microtubules-targeting agents. However, the interesting observation that extreme CIN might be detrimental for cancer growth suggest new potential therapeutic approaches.

Hence there is increasing support for the concept that increasing the level of chromosomal instability may be lethal towards cancer cells (Fig. 1.16). Weaver and colleagues have postulated in their animal models that excessive chromosomal instability leads to tumour lethality as the karyotype that generated the tumour is lost following further chromosomal missegregation and this was likened to mutational meltdown. In this case, CIN was acting both as a tumour initiator but excessive CIN acted as a tumour suppressor, supporting the idea that an optimal level of CIN is required to initiate and propagate cancer. In line with such a possible negative impact of CIN on tumour cell viability, various mouse models of enhanced CIN have also revealed a possible tumour suppressive role for CIN. For example, while reducing levels of CENP-E leads to an increase in spleen and lung tumour formation, crossing these mice with p19 knockout mice or treating them with carcinogens resulted in decreased tumour formation [317]. Similar results were found in Bub1-insufficient mice; increased tumorigenesis has been observed when crossing these mice with p53 or Rb heterozygous mice, but a reduction in tumour formation in the prostate was observed when Bub1 insufficiency was combined with a reduction in PTEN [318]. Importantly, this latter reduction correlated with increased cell death. These results all argue in favour of the hypothesis that the level of CIN needs to be tightly regulated in tumours: mild CIN can facilitate tumorigenesis, but severe CIN is incompatible with tumour cell viability.

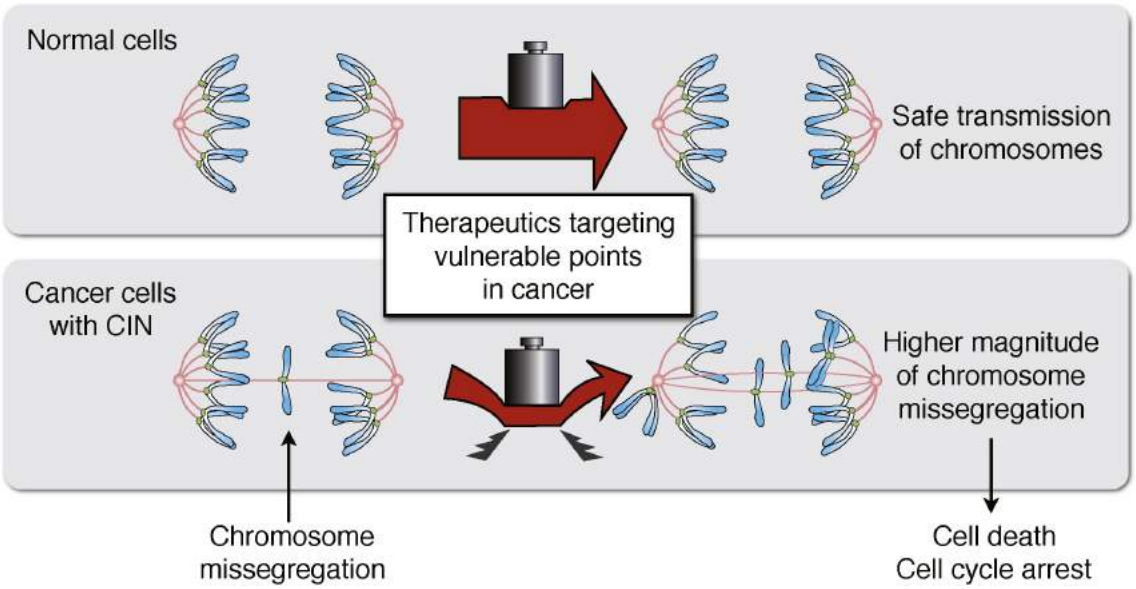

Figure 1.16 Increasing the level of chromosomal instability may be lethal towards cancer cells. [319]

1.6.1 Aurora kinases inhibitors

Aurora kinase family members generated great interest after their overexpression and amplification was reported in a number of tumours. Their overexpression and association with genetic instability in tumours have made them the focus of drug discovery. Due to their involvement in a wide range of cell cycle events (e.g., centrosome function, mitotic entry, kinetochore function, spindle assembly, chromosome segregation, microtubule dynamics, spindle checkpoint function, and cytokinesis), they attracted a lot of attention from pharmaceutical companies to develop potential inhibitors against them.

Depletion of Aurora kinase activity using techniques such as siRNA or expression of kinase inactive protein has helped to predict the biological profile for Aurora inhibitors (AKI). However, these techniques do not readily differentiate between inhibition of catalytic kinase activity and any scaffold function that the proteins may have. For this, selective small molecule inhibitors are required [320].

The discoveries of small molecule AKIs have been fuelled by the use of a variety of experimental and theoretical approaches. Examples include also structure-based drug design, especially in a fragment-based setup, structure-based virtual screening, FRET-based biochemical cell proliferation assay, and rational design followed by combinatorial expansion [321].

Currently, more than 30 AKIs are in various stages of preclinical and clinical studies. Most compounds compete with the ATP substrate and as such bind in a ATP binding site. A series of Aurora inhibitors had been identified from the combinatorial expansion of the 1,4,5,6-tetrahydropyrrol o[3,4-c] pyrazole bi-cycle, a versatile scaffold designed to target the ATP pocket of protein kinases. In particular the SAR (structure activity relationship) analysis of several pyrrolopyrazole subclasses performed by Nerviano Medical Science Srl, resulted in the synthesis of PHA-680632 which showed high anti-cancer activity *in vitro* and *in vivo* and have thus become a preclinical candidate [322]. The X-ray crystallographic structure of PHA-680632 in complex with Aurora A guided further design. Through combinatorial expansion of a related 1,4,5,6-tetrahydropyrrolo [3,4-c] pyrazole core and SAR refinements of the 5-amido-pyrrolopyrazole series a potent Aurora kinase inhibitor PHA-739358 (Danusertib) was identified [321].

1.6.1.1 Danusertib

Danusertib is a potent small-molecule 3-aminopyrazole derivative developed by Nerviano Medical Science Srl (Milan, Italy) (Fig. 1.17 A). It inhibits the ATP site of all three members of the Aurora kinase family. The major route of metabolism of Danusertib involves the formation of the N-oxide derivative, mainly through the enzyme flavin containing monooxigenase 3. The N-oxide metabolite has less than 1% potency of the parent compound [323].

A

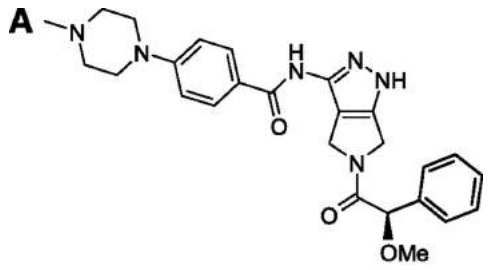

B

Kinase	IC_{50}(nmol/L)
Aurora -A	13
Aurora -B	79
Aurora -C	61
FGFR1	47
Abl	25
Ret	31
Trka	31

Figure 1.17 PHA-739358 structure and biochemical activity. A. chemical structure of PHA-739358. N-[5-(2-Methoxy-2-phenyl-acetyl)-1,4,5,6-tetrahydro-pyrrolo [3,4-c] pyrazol-3-yl]-4-(4-methyl-piperazin-1-yl)-benzamide. **B.** kinase inhibition profile of PHA-739358. Twenty-eight other kinases displayed at least 10-fold selectivity compared with Aurora A (LCK, VEGFR3, C-KIT, VEGFR2, CDK2/cyA, STLK2, FLT3, PLK1, LYN, IR, GSK3, NIM-1, PAK4, p38, PDK1, CK2, CHK1, Cdc7, ZAP70, PKA, IKK2, MET, EGFR, ERK2, AKT1, IKK1, PKC, and SULU; ref. 21). IC_{50}, the concentration of PHA-739358 that causes 50% inhibition of kinase activity. [324]

In vitro studies

PHA-739358 shows a low nanomolar activity towards the Aurora kinase family members inhibiting Aurora A, B and C at 13 nM, 79 nM and 61 nM, respectively (Fig. 1.17 B). When tested against a panel of 32 additional kinases, four kinases scored <10 fold relative to the IC_{50} for Aurora A kinase; PHA-739358 shows cross-reactivity with Ret, TrkA and FGFR (Fig 1.16 B). These cross-reactivities might increase the usability of the compound by increasing antitumor activity or extending the indications since, for example, Abl is the major driver in the majority of CML and a subset of ALL patients[325]. Anti-proliferative activity of Danusertib has been observed in a variety of tumour cell lines in the low nano-molar to sub-micromolar range and treated cells usually show an accumulation in the number of cells with a 4N DNA content and often sub-population of >4N are observed. These different effects of Danusertib may be due to the genetic background of the tumour cells tested, reflecting different requirements for Aurora kinase activity. Most probably they depend on the status of p53-dependent mitotic checkpoint, since treatment with Danusertib of cells with wild-type p53 resulted in a growth arrest with 4N DNA content, whereas cells with defective p53 were more prone to progress through the cell cycle after failed cytokinesis and accumulated with >4N DNA content [323].

Inhibition of Aurora A or B can be followed at the cellular level by determination of Aurora A auto phosphorylation or by inhibition of phosphorylation of histone H3. Histone H3, a protein implicated in chromosome condensation, is phosphorylated at serine 10 by Aurora B during mitosis. Treatment of Hela cells with PHA-739358 led to a decrease in histone H3 phosphorylation and Aurora A auto-phosphorylation that correlates well with the IC_{5O} for Aurora A and B in biochemical assays, suggesting a potent inhibition of both kinases at nano-molar concentrations in cells [325].

The Ret kinase inhibitory activity of PHA-739358 was evaluated in cells which contain a Ret allele with a constitutively activating mutation in the extracellular domain and which can be used to determine receptor auto phosphorylation. Trk-A kinase inhibitory activity was evaluated in cells that allow the inhibition of NGF-dependent Trk-A phosphorylation to be determined. Both kinases were inhibited at low

micromolar concentrations, although sensitivity was lower compared to Aurora inhibition. PHA-739358 has an effect on MAPK activation induced by FGF, but not by EGF demonstrating selectivity for inhibition of the FGFR pathway, but not the EGFR pathway.

The activity on wild-type and mutant *ABL* has been investigated in more detail. PHA 739358 binds wild-type Abl with high affinity as well as several mutants, including the T315I mutant for which at present no treatment option exists if allogenic bone marrow transplantation is excluded. This mutation is predicted to play a critical role in the future, since there will be a growing medical need for new treatments for this group of patients. Indeed, in CML patients increased resistance to treatments is observed at a rate of 4 percent per treatment year. As seen in the crystal structure of Abl (T315I) in complex with Danusertib the compound associates with the catalytic domain of an active and phosphorylated conformation of Abl (T315I) and lacks the steric hindrance imposed by the substitution of threonine by isoleucine which is, for example, seen with Imatinib. Although second generation inhibitors have recently been registered for the treatment of patients resistant to Imatinib (Dasatinib, Nilotinib), none of them inhibits the Abl (T315I) mutant. The potent inhibition of Abl kinase activity seen in biochemical and cellular assays is also seen in primary CD34+ tumour cells taken from CML patients bearing the Abl T315I mutation, and promising clinical responses were also observed in patients. [325]

In vivo studies

The pharmacokinetics properties of PHA-739358 have been investigated in the mouse, rat, dog and monkey. In all the species the compound showed moderate to high systemic clearance and a high volume of distribution, suggesting extensive tissue distribution. Following both I.V. bolus and infusion administration, PHA-739358 plasma levels increased largely in proportion to dose and data from repeated dose studies indicating that the pharmacokinetics of PHA-739358 were not time-dependent and did not show important differences when different schedules of treatment (i.e., duration of infusion) were applied. Single dose I.V. administration of PHA-739358 to mice resulted in a time-dependent inhibition of histone H3 phosphorylation measured in bone marrow. Strong inhibition at one hour post-administration was still

apparent at three hours and returned to baseline levels by eight hours.[325]
Similar observations for the inhibition of histone H3 phosphorylation were obtained after single I.V. administration of the compound both in tumour and skin tissue lysates. A PK/PD model relating the time-concentration profiles of PHA-739358 with the tumour growth was developed for A2780 xenografts. In this model it is assumed that the cells, after being exposed to the drug, are damaged and the severity of the damage (potency) and the rate at which the cells die (cell death distribution) are the critical parameters of the model and are calculated after fitting to experimental data. The model successfully predicted the response of tumours exposed to different treatment schedules with PHA-739358. Based on this PK/PD approach, the efficacy of PHA-739358 was essentially found to be related to the total amount of the compound administered in the exponential phase of the tumour growth. [325]
The antitumor activity of PHA-739358 *in vivo* was evaluated in several solid human tumour xenograft models in nude mice and a significant activity was observed. Efficacy experiments were performed in models including syngenic, transgenic and carcinogen induced tumour models in different species to monitor species-related effects on efficacy or toxicity. Usually the compound was administered intravenously twice a day at the maximally efficacious dose of 30 mg/kg for dosing periods ranging from five to ten days. A dose-finding study was performed in HL60 leukemia cells implanted sub-cutaneously in SCID mice. After intravenous administration, at doses between 7.5 and 30 mg/kg I.V. BID for five days, a significant tumour growth inhibition was observed showing dose-dependency and a tumour growth inhibition (TGI) of up to 98 percent at the highest dose. There was also evidence of tumour regression and occasional cures [326]. Having observed similar activity on ovarian and colon tumour xenograft, PHA-739358 activity was also tested on two breast tumour models represented by a DMBA carcinogen-induced mammary carcinoma in rats and an activated Ras-driven mammary tumours in transgenic mice (MMTV-v-Ha-Ras). In both models good activity in terms of TGI was observed demonstrating the effectiveness of PHA-739358 against syngenic models of mammary cancers arising from either oncogene activation or genetic insult by carcinogen exposure in rodents. The transgenic mouse prostate (TRAMP) model was used to evaluate the efficacy of PHA-739358 against a prostate cancer model [327].

After detection of tumour onset, which was monitored by MRI, mice were treated for five days BID with 30 mg/kg of the compound. As in the human disease, prostate tumours in TRAMP mice manifest as islands of low MRI signal intensity surrounded by high MRI signals from neighboring benign tissue, and after detection the tumour grows very fast and doubles its volume in about five days. The treatment induced tumour regression in some animals with long-term stabilizations was observed in the majority of treated animals. In a study by Benten et al., the efficacy and toxicity of Danusertib was evaluated in a subcutaneous hepatocellular carcinoma (HCC) xenograft models showing high antiproliferative activity at well tolerated doses [328]. Inhibition of tumour growth in rapidly proliferating Huh-7 tumours was highly significant although tumours continued to grow at a very slow rate. Antiproliferative efficacy was even more pronounced in moderately growing HepG2 tumours, although no significant tumour regression was observed. Based on the results from preclinical testing, Danusertib was progressed to Phase I clinical investigation.

Phase I clinical trials

Two parallel Phase I dose escalation studies were performed [323]. The first study evaluated Danusertib administered i.v. on days 1, 8, 15 every 4 weeks in 6 and 3 h infusion schedules at dose ranges 45-400 mg/m^2 in 50 patients with solid tumours. The main dose-limiting toxicity (DLT) observed was grade 3/4 neutropenia. The most frequent non-hematologic adverse events were mainly grade 1 and 2 fatigue, nausea, diarrhea and anorexia. Stable disease was observed in 24% of the evaluable patients, in five of whom the disease stabilization lasted more than 6 months. The second study tested 24 h infusion in a 2-week cycle in patients with advanced solid tumours. In the first part of the study, 40 patients were treated without granulocyte colony-stimulating factor (G-CSF) and 7 dose levels were explored (45-650 mg/m^2). Again, principal DLTs were grade 3/4 neutropenia, diarrhea, nausea, vomiting and fatigue. 11 of the 40 patients showed disease stabilization. One patient with refractory small lung cancer had an objective response lasting 23 weeks. Post-therapy skin biopsies showed decreased level of histone H3 phosphorylation starting at 500 mg/m^2. In the second part of the study, further dose escalation (580-1000 mg/m^2) was performed with co-administration of G-CSF in 16

patients. Renal toxicity became dose limiting and the maximum tolerated dose (MTD) was set at 750 mg/m^2 i.v. over 24 h every 14 days. In an exploratory study on patients of a Phase I trial and subsets of two Phase II trials no significant association between polymorphism in genes coding for drug metabolizing enzymes, transporter proteins and clearance of Danusertib, between target receptor polymorphisms and toxicity of Danusertib and between polymorphisms in the Aurora kinases B receptor and the extent histone H3 phosphorylation were observed [329]. Danusertib was also explored in combination with bevacizumab in a Phase I trial [323].
All the studies reported above were performed in patients with solid tumours. In addition, 23 patients with CML and Philadelphia chromosome positive ALL were enrolled in a Phase I study of Danusertib administered via 3 h infusion daily for 7 consecutive days every 14 days. 14 out of 24 patients carried a confirmed T315I BCR-Abl mutation, 2 patients demonstrated hematologic response and 9 patients demonstrated a haematological improvement. [323]

Phase II clinical trials

A Phase II clinical trial was performed in patients with CML relapsing on Imatinib or other c-ABL therapy, and explored Danusertib at two dose levels, 250 or 330 mg/ m^2/day, given as a weekly 6 h infusion for three consecutive weeks, every 4 weeks. In a preliminary abstract reported on the first seven CML patients enrolled, six out of seven patients had the T315I BCR-Abl mutation [323]. 2 patients with T315I BCR-Abl mutation achieved a complete hematologic response associated with a complete cytogenetic response and a minor cytogenetic response (one case each). In another Phase II trial evaluating 4 months progression free rate, 42 patients with breast cancer and 34 patients with ovarian cancer, progressing after two prior chemotherapy lines for advanced/metastatic disease were enrolled [323]. Danusertib was administered i.v. over 24 h every 14 days at 500 mg/m^2. In breast cancer 7 out of 38 evaluable patients were progression free at 4 months. In ovarian cancer, 4 patients out of 34 were free from progression at 4 months. There were 10 patients with stable disease. The most frequent side effects from all phase II trials were grade 3/4 haematological toxicity consisted of neutropenia (86%).

In a phase II study by Laffranchi et al. [323] patients with advanced/metastatic pancreatic and colorectal cancers (CRC) Danusertib was administered every 14 days, over 24 h i.v. infusion at 500 mg/m^2. 33 patients with CRC and two prior lines of chemotherapy were included. No patient was progression free at 4 months. 35 patients with pancreatic cancer, relapsing after one prior chemotherapy line for advanced/metastatic disease were enrolled. 3 of the 31 patients were progression free at 4 months and had a stable disease for 6-8.5 months. In a randomized phase II study in patients with metastatic castration-resistant prostate cancer (CRPC) progressing after first-line docetaxel based chemotherapy, Danusertib was administered using two different schedules with equivalent dose intensity. Clinically relevant disease stabilization lasting > 6 months was reported in 12 patients.[323]

Chapter 2
Aim of the work

Chromosomal instability in Glioma Stem Cell lines from Glioblastoma multiforme: implications for new therapeutic strategies

Glioblastoma multiforme (GBM) is the most aggressive brain tumour; despite the current standard of care, the majority of the patients presents a relapse of the lesion, probably due to the presence, within the tumour, of a subpopulation of cells with stem-like properties, such as self-renewal capacity, multilineages differentiation potential and tumorigenicity *in vivo*. These cells were named Glioma stem cells (GSCs) and are characterized by high tumorigenic potential and resistance to current therapies.

As GSCs are believed to play a key role in tumour initiation and progression, great efforts have been making in order to better characterize this subpopulation of cells and to find new therapeutic strategies GSC-targeted. This research project aims to address two main aspects of this research area, with the purpose of finding new therapeutic approaches.

The first one, which will be discussed in chapter 3, is to better characterize the effect of a pan Aurora kinases inhibitor (Danusertib) in five glioma stem cell lines. As a matter of fact, a feature of GSCs is the elevated chromosomal instability, which can be due to different alterations, including defects in genes involved in the regulation of the mitotic machinery. Among these, different studies have demonstrated an impaired expression of Aurora kinases A and B in glioblastoma and suggested them to be promising therapeutic targets for GSCs eradication.

The second one aimed at studying the division mode of GSCs in order to better characterize the mechanisms by which GSC are able to both maintain a pool of self-renewing and highly invasive stem cells and produce differential progeny. In 2011 Lathia and colleagues, using single-cell based time-lapse microscopy and quantitative immunofluorescence, found that GSCs utilize both symmetric and asymmetric cell division. Intriguingly they also demonstrated that only CD133 and Numb could be asymmetrically segregated. The biological significance of these two division modes is not yet fully understood, but improved understanding of this phenomenon may lead to the development of preventative treatments or improved therapeutic options for brain tumour patients through the identification of novel targets that are involved in the control of asymmetric cell division in human brain tissue. Hence in chapter 4 I will present some preliminary data about the setting up of CrispR/Cas9 mediated GFP-tagged CD133 (*PROM1* gene) and Nestin (*NES* gene) glioma stem cell lines that could be used to look for signs for asymmetric cell division using live cell imaging.

Chapter 3

Effect of Aurora kinases inhibition on GSCs

MATERIALS AND METHODS

3.1 MATERIALS

3.1.1 Cell lines

All the Glioma stem cell (GSC) lines used in this work (GBM2, G179, G144, G166, GliNS2) were isolated from patients affected by glioblastoma and extensively characterized for their stem cell properties. GBM2, G144, G166, GliNS2 derived from classic glioblastoma multiforme, while G179 derived from a giant cell variant glioblastoma. GBM2 cell line was kindly provided by the National Institute for Cancer Research, Department of Haematology-Oncology, Genova, while G179, G144, G166 and GliNS2 cell lines were kindly provided by Professor A. Smith of the Wellcome Trust Medical Research Council Stem Cell Institute, University of Cambridge, Cambridge (UK). All the GSC lines have been already characterized for their cytogenomic and epigenomic profiles and already expanded in vitro as stable cell lines and used as powerful model for studying their biology and testing drug susceptibility [330-332].
CB660 are human foetal neural stem cell lines derived from the forebrain. They were stored by BioRep Srl.

3.1.2 Drugs

Danusertib (PHA-739358, Selleckem) was dissolved in DMSO to a stock concentration of 10 mM and stored at -80° C. It was then further diluted to the required concentrations using complete medium and the aliquotes were stored at -20° C.
EgV inhibitor STLC (S-Trityl-L-Cysteine, Tocris) was dissolved in DMSO at a stock concentration of 50 mM. It was used at a final concentration of 5 μM in order to synchronize cells in M phase.
DMSO had no effect on the cell survival.

3.1.3 Solutions and buffers

- Fixative solution: 3:1 methanol:acetic acid
- Hypotonic solution 0.56% KCl in H_2O
- HRP Solution: 100 mM Tris-phosphate, 1.25 mM Luminol, 0.2 mM p-Coumaric acid and 6.5% H_2O_2
- Western blot lysis buffer: 50 mM Tris pH 7.5, 120 mM NaCl, 0.5% NP40, 1 mM EDTA, 1 mM DTT, Protease and Phosphatase inhibitors (Complete and PhosStop; Roche Diagnostics, West Sussex, U.K)
- Western blot running buffer: 100 mM Tris, 750 mM glycine, 0.04% SDS
- Western blot sample buffer: 0.01% bromophenol blue, 62.5mM Tris-HCl pH 6.8, 7% SDS, 20% sucrose and β-mercaptoethanol
- Western blot transfer anode 1 buffer: 300 mM Tris, 20% methanol, pH 10.4
- Western blot transfer anode 2 buffer: 25 mM Tris, 20% methanol, pH 10.4
- Western blot transfer cathode buffer: 25 mM Tris, 40 mM 6-aminohexanoic acid, 20% methanol, pH 9.6

3.1.4 Other reagents

- AmpliTaq Gold DNA Polymerase, Applied Biosystems
- B-27 supplement without vitamin A, Invitrogen
- BigDye terminator v.3.1 kit, Applied Biosystem
- Bovine serum albumin (BSA), Sigma
- Cellular Senescence Assay Kit, Cell biolabs
- Click-iT® EdU Alexa Fluor® 647 Imaging kit, Life Technologies
- Colcemid, Roche
- Direct-zol™ RNA MiniPrep, Zymo Research
- DMEM F-12, Euroclone
- DNeasy® Blood & Tissue Kit, Qiagen
- Euromed-N, Euroclone
- EuroSap enzymatic Kit, Euroclone
- Giemsa, Gibco
- human bFGF, Miltenyi Biotec

- human EGF, Miltenyi Biotec
- L-glutamine, Euroclone
- Laminin, Invitrogen
- M-MLV reverse transcriptase, Invitrogen
- Matrigel®, Corning, 354230
- MTT, Sigma
- N2 supplement, Invitrogen, 17502-048
- Neurobasal, Invitrogen, 21203049
- Paraformaldehyde (PFA), Sigma
- Pen/Strep, Gibco
- ProLong Diamond mounting solution, Life technologies
- Quinacrine mustard, Roche
- TaqMan® gene expression assay, Applied Biosystems
- Trypan blue dye, Sigma
- Trypsin 0.05%, Gibco

Table 3.1 List of TaqMan® probes

Gene	Code	Dye
AURKA	Hs01582072_m1	FAM-MGB
AURKB	Hs00945855_g1	FAM-MGB
AURKC	Hs00152930_m1	FAM-MGB
GAPDH	Hs99999905_m1	FAM-MGB

Table 3.2 List of primary antibodies

Antigen	Source	Species	Dilution
AurkA	Abcam (ab1287)	rabbit	1:500 (WB)
AurkB	Abcam (ab2254)	rabbit	1:500 (WB)
Cyclin A2	Abcam (ab32386)	rabbit	1:500 (WB)
Cyclin B1	Abcam (ab72)	mouse	1:500 (WB)
Phospho-histone H3	Millipore (06-570)	rabbit	1:250 (WB)
CDK1	Abcam (ab18) [a17]	mouse	1:500 (WB)
CDK1 substrates	Cell signaling (9477s)	rabbit	1:1000 (WB)
α tubulin	Abcam (ab7291) [DM1A]	mouse	1:10000 (WB)
Pospho-Aurora A,B,C	Cell signal (2914)	rabbit	1:100 (IF)
γ tubulin	Abcam (ab27074)	mouse	1:100 (IF)
Centromere (Crest)	Antibodies incorporated (15-234)	human	1:100 (IF)
CenpF	Abcam (ab5)	rabbit	1:100 (IF)

WB, Western Blot; IF, immunofluorescence

Table 3.3 List of secondary antibodies

Antigen	Source	Species	Dilution
488-anti-mouse	Life technologies (A21202)	donkey	1:2000 (IF)
594-anti-rabbit	Life technologies (A31632)	goat	1:2000 (IF)
488-anti-rabbit	Life technologies (A11034)	goat	1:2000 (IF)
670-anti-human	abcam	goat	1:2000 (IF)
Polyclonal anti-mouse HPR	DAKO (P0448)	goat	1:5000 (WB)
polyclonal anti-rabbit HPR	DAKO (P0447)	goat	1:5000 (WB)

WB, Western Blot; IF, immunofluorescence

Table 3.4 List of *TP53* primers

Name	Code	Sequence 5'->3'
Exon5-6-FW	Hs00346579_CE	GAGAAAGCCCCCCTACTGCTCA
Exon5-6-RV	Hs00346579_CE	CACTTGTGCCCTGACTTTCAACTCT
Exon7-FW	Hs00346578_CE	AAAGAGAAGCAAGAGGCAGTAAGG
Exon7-RV	Hs00346578_CE	CTTGCCACAGGTCTCCCCAAG
Exon8-FW	Hs00346577_CE	TGTTGTTGGGCAGTGCTAGGA
Exon8-RV	Hs00346577_CE	CATACTACTACCCATCCACCTCTC

Table 3.5 List of STR markers

STR Marker	Position	Sequence 5'->3'	PCR product size (bp)
D17S906	17p13.1	Left primer: AGCAAGATTCTGTCAAAAGAG Right primer: TTCTAGCAGAGTGAAACTGTCT	335
D17S1159	17p13.1	Left primer: GACAGAAGCACTACACTCAA Right primer: GTTCCCTGTTTCTGCCTAG	285
D17S785	17q25.1	Left primer: ATCCCTGGAGAGTGAAAATG Right primer: AAGGCCAACCTGAAAACTAA	181-207
D17S787	17q22	Left primer: TGGGCTCAACTATATGAACC Right primer: TTGATACCTTTTTGAAGGGG	138-166

3.2 METHODS

3.2.1 Cell culture conditions

GSCs expansion was carried out in a proliferation permissive medium composed by DMEM F-12 (Euroclone) and Neurobasal 1:1 (Invitrogen), 2% B-27 supplement without vitamin A (Invitrogen), 2 mM L-glutamine (Euroclone), 10 ng/ml recombinant human bFGF (Miltenyi Biotec) and 20 ng/ml recombinant human EGF (Miltenyi Biotec), 20 UI/ml penicillin and 20 µg/ml streptomycin (Euroclone). Human foetal NSCs expansion was carried out in Euromed-N (Euroclone) enriched with 2mM L-glutamine (Euroclone), 2% B27 supplement without vitamin A (Invitrogen), 1% N2 supplement (Invitrogen), 10 ng/ml EGF, 10 ng/ml bFGF (Miltenyi Biotec).
GSCs and human foetal NSCs were cultured in adherent culture condition in T-25 or T-75 cm^2 flasks coated with 10 µg/ml laminin (Invitrogen) or Matrigel® (Corning), in 5% CO_2/95% O_2 atmosphere.
The medium was replaced every 3-5 days in order to remove cell catabolic products and cellular debris and to supply fresh nutrients. Cells were routinely grown to confluence, dissociated using trypsin 0.05% (Gibco) and then split 1:2 or more depending on cellular concentration.

3.2.2 RNA extraction

RNA was extracted from GSC lines using the Direct-zol™ RNA MiniPrep (Zymo Research) according to the manufacturer's protocol. RNA quantity and quality were then analysed using a Nanodrop® ND-1000 spectrophotometer (Thermo Scientific).

3.2.3 TaqMan gene expression assay

Quantitative PCR using the TaqMan® gene expression assay (Applied Biosystems) were performed in order to evaluate the expression levels of Aurora kinase A, B and C in GSCs. *GAPDH* was used as a housekeeping gene while foetal neural stem cells CB660 were used as controls. Probes for real-time PCR, purchased from Applied Biosystems, are listed in table 3.1.

Firstly, RNA samples were converted into first-strand cDNA using the M-MLV reverse transcriptase (Invitrogen). cDNA was then quantified using a Nanodrop® ND-1000 spectrophotometer (Thermo Scientific).
Quantitative PCR were carried out using the ABI StepOne of Applied Biosystems, according to the manufacturer's instructions. The cycle conditions were: 2 min 50°C; 10 min 95°C; 40 cycles: 15 s 95°C, 1 min 60°C. Relative gene expression was determined using data from the real-time cycler and the $\Delta\Delta C_t$ method. The gene expression data were obtained as mean values derived from two independent experiments.

3.2.4 MTT assay

Cell metabolic activity was assessed by the MTT (3-[4,5dimethylthiazol-2-yl]-2,5-diphenyl tetrazolium bromide) assay in order to evaluate the Danusertib cytotoxic/cytostatic effect. Cells were seeded in 96 well-plates at a density of $4x10^4$ cells/well in 100 μl of culture medium and incubated at 37°C. After 24 hs, Danusertib at various concentrations (5-50-200-500-1000-5000 nM) was added to cell culture medium. After the drug incubation time (24, 48 or 72 hs) MTT solution (1 mg/ml, Sigma) was added to each well and cells were incubated for 3 hs at 37°C. Therefore, formazan granules were solubilized in absolute ethanol and the absorbance of the dye was measured spectrophotometrically with the FLUOstar Omega microplate reader (BMG Labtech) at a 570 nm wavelength. The percentage of inhibition was determined by comparing the absorbance values of drug-treated cells with that of untreated controls: [(treated-cell absorbance/untreated cell absorbance) × 100]. The results reported are the mean values of two different experiments performed at least in triplicate.

3.2.5 Trypan blue dye exclusion assay

Trypan blue dye exclusion assay was performed in order to assess GSC viability after 48 hs and 72 hs of exposure to different concentrations of Danusertib (50-500 nM). In GBM2 and G166 cell lines this assay was performed also after two round of 48 hs treatment with Danusertib 500 nM.

Cells were plated in 60 mm Petri dishes at a density of $1,2x10^6$ cells/dish, cultured overnight and treated with different concentrations of Danusertib (50-500 nM) for the desired times. Thereafter cells were stained using trypan blue dye (Sigma) to count cell numbers and determine the drug cytotoxic/antiproliferative effects. The treated samples were compared with the untreated controls. The results reported are the mean values of two different experiments.

3.2.6 Conventional cytogenetics

Conventional cytogenetics techniques were performed in order to determine the Danusertib effect on the mitotic index, used as a marker of cell proliferation, and cell ploidy.

$2x10^6$ cells were seeded in T-25 cm^2 in 5 ml of medium. Subsequently, cells in exponential growth phase were treated with 500 nM Danusertib for 48 hs. Then metaphase chromosome spreads were obtained using standard procedures. Briefly, cell cultures were treated with 0.2 µg/ml Colcemid (Roche) and then harvested and incubated with a hypotonic solution of 0.56% w/v KCl for 15 minutes at RT. Then, cells were fixed with fixative solution composed of 3∶1 methanol:acetic acid. Chromosomes were QFQ-banded using quinacrine mustard (Roche) and slides were mounted in McIlvaine buffer. Slides were analysed using Nikon Eclipse 80i fluorescence microscope (Nikon) equipped with a COHU High Performance CCD camera.

The mitotic index was evaluated counting the percentage of mitosis scoring at last 1000 nuclei, while ploidy was investigated by evaluating the number of chromosome/metaphase on 30-50 metaphases. Chromosome spreads were analysed using the Genikon software. Data were obtained as mean values derived from two independent experiments.

3.2.7 Fluorescence *in situ* hybridization

For preparation of metaphase chromosomes and interphase nuclei, standard procedures previously described were applied (view section 3.2.6). Cell suspension was dropped onto glass slides. Fluorescence *in situ* hybridization (FISH) analysis was performed using a commercial probe set targeting chromosomes X, Y, 13, 18,

21 (CytoCell, FAST FISH Prenatal Enumeration Probe kit). Signals were counted using in at least 50 interphase nuclei per sample and the number of signal was used in order to assess the cell ploidy. All digital images were captured using a Leitz microscope (Leica DM 5000B, Leica Microsystems GmbH, Wetzlar, Germany) equipped with a charge coupled device (CCD) camera (Leica Microsystems) and analysed by means of Chromowin software (Tesi Imaging, Milano, Italy).

3.2.8 Neurosphere formation assay

Cells treated with Danusertib 50 nM and 500 nM for 48 hs were retrieved from flasks to obtain a single cell suspension and counted. $4x10^3$ cells for each condition were plated in a well of a six-well plate and let grow for a week. Spheres were then counted through the observation at a phase contrast microscopy.

3.2.9 Cell morphology analysis

To evaluate cell morphology cells were seeded in 6-well plates in proliferative permissive medium at $3x10^3$-10^4 cells/ml, depending on cell growth rate, specific for each GSC line. After 24 hs, cells were treated with Danusertib (5-50-200-500-1000 nM) for different times of exposure (24-48-72 hs). Cell morphology was evaluated through the observation at a phase contrast microscopy, comparing Danusertib treated and untreated cells. Representative images were taken for each cell line and for each treatment.

3.2.10 Giemsa staining

Giemsa staining was performed in order to evaluate Danusertib effect on nuclei morphology.

Cells were grown on coverslips and treated with Danusertib 500 nM for 48 hs. Cells were then fixed with 70% methanol, stained with 10% Giemsa solution (Gibco) in distilled water for 15 minutes and rinsed off in tap water. Coverslips were let to dry and mounted using Polyvinyl alcohol mounting medium (Fulka Analytical). Nuclei morphology was evaluated through the observation at phase contrast microscopy, comparing Danusertib treated and untreated cells. Based on nuclei morphology cells were divided in four classes: normal nuclei, polymorphic nuclei, multinucleated

cells and micronucleated cells. Representative images were taken for each cell line using 100x oil lens.

3.2.11 Western blot

Western blots were generally performed on asynchronous cells. However, Aurora kinases protein levels were investigated also in cells synchronized by treatment with 5 μM STLC for 24 hs. Mitotic cells were collected by mitotic shake off.
Cells were retrieved from flasks to obtain a single cell suspension, counted, washed once with PBS and re-suspended in lysis buffer at a concentration of 10^4/μl. 5x sample buffer was subsequently added. Samples were sonicated and then boiled at 95°C for 5 min. Cell lysates were loaded to electrophoresis in SDS polyacrylamide gel (Bio-Rad Mini-PROTEAN® Tetra Cell system). Gels were then transferred with a semi-dry technique to PVDF membranes (GE Healthcare) (Bio-Rad Trans-Blot® Turbo Transfer system), which were blocked for 30 minutes with 5% milk/PBS/0.1% NP-40. Membranes were then incubated overnight at 4°C with primary antibodies (Table 3.2) diluted in blocking buffer, washed three times for 5 minutes with PBS and incubated with the appropriate horseradish peroxidase (HRP) conjugated secondary antibody (Table 3.3) for 1 hour at room temperature. Three washing steps with PBS were done before chemiluminescent detection was performed using a HRP Solution. α-tubulin was used as an internal standard. Emission was captured with radiograph films (Amersham Hyperfilm™ GE Healthcare) using an automatic Ecomax X-ray Film Processor (Photon Imaging Systems). Aurora kinases bands were then quantified with ImageJ (https://imagej.nih.gov/ij). The results are expressed as means of two independent experiments.

3.2.12 Cell cycle profile analysis

GSCs were grown to semi-confluence on coverslip and incubated with EdU solution (20 μM) for 20 minutes at 37°C. Cells were then fixed with 3.7% PFA for 10 minutes, rinsed with PBS and permeabilized with 0.1% NP40 for 15 minutes. After other two rinsing steps, cells were incubated with the Click-iT® reaction cocktail (Click-iT® EdU Alexa Fluor 647 Imaging kit, Life Technologies) for 30 minutes at room temperature in the dark. Cells were rinsed once, blocked with PBS/BSA 3% (Sigma)

for 30 minutes at room temperature in the dark, incubated with the primary antibody (anti-CENPF, see table 3.2 for details) for 1 hour, washed three times and incubated with the secondary antibody for 1 hour (Table 3.3). Coverslips were then incubated with DAPI for 10 minutes and mounted using the ProLong Diamond mounting solution (Life technologies).
Random images were acquired using the Delta Vision Olympus IX70 microscope, with 40X oil lens, equipped with a CCD camera using the Micromanager software.

3.2.13 Immunofluorescence

Phosphorylated aurora kinases levels were evaluated after Danusertib 500 nM exposure for 48 hs.
Cells were grown on coverslips, synchronized using STLC 5 μM, and fixed with 3.7% paraformaldehyde (PFA) (Sigma) and 70% methanol, for 10 minutes and 1 minutes respectively.
Cells were permeabilized in PBS 0.1% NP40 for 15 minutes, blocked in 3% BSA (Sigma) for 30 minutes and incubated with primary antibodies (Table 3.2) for one hour at 37°C. Slides were then washed and probed with the appropriate secondary antibody (Table 3.3) for one hour at room temperature. Coverslips were incubated with DAPI for 10 minutes and mounted using the ProLong Diamond mounting solution (Life technologies).
Images were acquired through a 60x oil immersion lens on a Delta Vision Olympus IX70 microscope equipped with a CCD camera using Micromanager software. Images deconvolution was performed using SVI Huygens Professional Deconvolution Software (Version 3.5). For quantitative analysis of phosphorylated Aurora kinases levels images were imported into Omero software and analysed with ImageJ software.

3.2.14 Live cell imaging

Live cell imaging analysis were performed on GBM2 and G166 cell lines in order to evaluate cell fate when Danusertib 500 nM was added to cell culture.
GSCs were plated in 4 wells chambered slides (Ibis) coated with Matrigel®.
To evaluate drug effect on GSCs, cells were incubated on the Olympus IX71 or IX73

microscopes, equipped with a CCD camera, temperature controller (37°C) and CO_2 (5%) incubation chamber, soon after the addiction of Danusertib 500 nM and monitored overnight.
Images of multiple fields per well were collected every 5 min overnight using a dry 20x objective lens. Images were acquired using the MicroManager software and analysed by means of ImageJ software.

3.2.15 DNA extraction

Genomic DNA was extracted from GSC lines, treated or untreated with Danusertib 500 nM for 48 hs, using the DNeasy® Blood & Tissue Kit (Qiagen) according to the manufacturer's protocol. DNA quantity and quality were then analysed using a Nanodrop® ND-1000 spectrophotometer (Thermo Scientific).

3.2.16 *TP53* Sanger sequencing

To assess the *TP53* mutational status in untreated GSCs, exons 5, 6, 7 and 8, representing the mutational hot spot of this gene, were sequenced. The set of primers used to amplify the target DNA and to sequence the DNA was purchased from Life technologies and is reported in table 3.4.
First, an End-Point PCR was performed in order to amplify the *TP53* target loci (exons 5-6, 7 and 8). The following thermal cycling conditions were used: 95° C for 3 minutes; 35 cycles composed of: 95° C for 30 seconds, 60° C for 30 seconds, 72° C for 30 seconds; 72° C for 7 minutes; 4° C ∞. DNA quality was examined using an agarose gel electrophoresis. PCR products were then purified before sequencing by means of the EuroSap enzymatic Kit (Euroclone). Briefly, 1.5 μl of PCR products were mixed with 0.1 μl ExoI, 0.1 μl SAP and 4.3 μl H_2O. Samples were kept at 37°C for 15 minutes and then at 80°C for further 10 minutes. Next, the sequencing reaction was performed using the BigDye terminator v.3.1 kit (Applied Biosystem) according to the manufacturer's protocol. The following thermal cycling conditions were used: 96° C for 40 seconds; 25 cycles composed of: 96° C for 10 seconds, 50° C for 5 seconds, 60° C for 4 minutes; 4° C ∞.
The reaction products were then purified using EDTA 125 mM pH8 and EtOH. DNA sequencing was performed through a capillary electrophoresis using an ABI-3130

sequencer (Applied Biosystems), with 4 capillaries of 36 cm of length each, loaded with POP-7 polymer. Samples were allowed to run for about 1 h. Data were analysed using FinchTV software.

3.2.17 Microsatellite analysis

Loss of heterozygosity (LOH) analysis of chromosomes 17 was assessed in untreated GSCs by means of PCR-based assays. STS markers used are listed in table 3.5. Specific information about primer sequence, melting and annealing temperature can be obtained referring to the UCSC Genome Browser (http://genome.ucsc.edu/). Amplification of each microsatellite was done in 20 µl volumes with 20 ng/ml of genomic DNA, 1x PCR Buffer, 1 µM primers, 200 µM dNTPs, 1.5 mM $MgCl_2$ and 1 unit of AmpliTaq Gold DNA Polymerase (Applied Biosystems). Amplification products were resolved on 6% polyacrylamide gels and electrophoresed for 5 hs at 160V. Gels were stained with 0.1% ethidium bromide and LOH was determined by visual observation.

3.2.18 DNA integrity evaluation

DNA integrity analysis was performed after treatment with Danusertib 500 nM according to the instructions using an automated tape based electrophoresis (Agilent 2200 TapeStation). Briefly, 1 µL of genomic DNA (1-100 ng/ml) was mixed with 10 µL of Genomic DNA Sample buffer and loaded into the Agilent 2200 TapeStation. A ladder and a negative control (1 µL of TE + 10 µL of Genomic DNA Sample buffer) were loaded as well.
The Agilent 2200 TapeStation Analysis Software (revision A01.05) automatically calculated the DNA concentration and provided the DNA Integrity Number (DIN). This numerical assessment of the genomic DNA integrity can range from 1–10, and was displayed directly under the gel image as well as in the sample table. A high DIN (>7) indicates highly intact genomic DNA, and a low DIN (<7) a degraded genomic DNA.

3.2.19 β Galactosidase staining

GBM2 and G166 were grown on coverslips in 6-well plates and treated with 500 nM Danusertib. After one and two round of 48 hs drug exposure they were stained using the Cellular Senescence Assay Kit (Cell biolabs) according to the manufacturer's protocol. The medium was aspirated and the cells were washed twice with PBS and incubated with the fixative solution for 5 minutes at room temperature. Cells were then washed three times with PBS and incubated with the staining solution mix overnight at 37°C protected from light. The day after the stained cells were washed twice with PBS and coverslips were mounted using the ProLong Diamond mounting solution (Life technologies).
Random images were acquired on microscope Axio Lb A1 (Zeiss) equipped with an AxioCam ERc 5s and a 40x objective. β galactosidase positive and negative cells were counted on a computer monitor and percentages of β galactosidase positive cells were calculated. The results are expressed as means of two independent experiments.

3.2.20 Statistics

Statistical analysis was carried out performing Yates' chi-square test or t-test on raw data, by means of Excel spreadsheet (Microsoft Office 2013, Microsoft Corporation). p value $\leq$ 0,05 were considered statistically significant.

RESULTS

In this chapter I will present several data about the main research area I investigated during my PhD program, performed in the Medical Genetics laboratory of the University of Milano-Bicocca, under the supervision of Dr Angela Bentivegna. This study is aimed on evaluating the effect of an Aurora kinases inhibitor on few GSC lines.

3.3 PRELIMINARY RESULTS: GSCs ARE CHARACTERIZED BY ENHANCED CIN AND *AURK* CNAs

In previous works the cytogenomic and epigenomic landscapes of the GSC lines used in this study were deeply characterized using conventional and molecular cytogenetic analysis [330]. Cytogenetic analysis are an essential tool to identify chromosomal abnormalities in tumours and to unmask specific genomic regions involved in tumorigenesis, as sequentially acquired chromosomal abnormalities are pathogenetically fundamental in the development of malignancy. Specifically, the karyotype of each GSC line (GBM2, G179, G166, G144, GliNS2) was assessed in our laboratory, through QFQ-banding, in order to determine the major chromosomal abnormalities. GBM, as many other solid tumours, is characterized by great cytogenetic heterogeneity within the tumour. Accordingly, all the GSC lines showed clonally occurring numerical and structural aberrations.

Array CGH on genomic DNA was assessed in order to screen for additional genomic alterations and copy number alterations, which were not previously identified. aCGH of G144 was already carried out by Pollard and colleagues in 2009 [331]. Data comprised both homozygous and heterozygous deletions and both gains and amplifications. aCGH revealed complex genomic changes in these cell lines: no single chromosome was free from aberrations in the GSC lines analysed, suggesting that they are characterized by enhanced chromosomal instability [330]

We focused our attention on copy number alteration of genes encoding for Aurora kinases, which have found altered in GBM. 4 out of 5 GSC lines are characterized by copy number alteration of *AURK* genes (Table 3.6). These aberrations are generally heterogeneous losses or gains of chromosome regions including *AURK* genes. Only in G166 we observed a complete gain of *AURKA*.

Table 3.6 CNAs in *AURK* genes. List of *AURK* genes CNAs detected in five GSCs by means of a-CGH.

		GBM2	G179	G144	G166	GliNS2
***AURKA* 20q13.2**	**Alteration**				GAIN	
	Cytoband				chr20 p13-q13.33	
	Size (Mb)				62,35	
	Mosaic level				100%	
***AURKB* 17p13.1**	**Alteration**	LOSS				
	Cytoband	chr17 p13.2-p13.1				
	Size (Mb)	3,81				
	Mosaic level	62%				
***AURKC* 19q13.43**	**Alteration**	LOSS	LOSS	GAIN	GAIN	
	Cytoband	chr19 q13.43	chr19 q12-q13.43	chr19 q12-q13.43	chr19 p13.11-q13.43	
	Size (Mb)	0,25	29,26	30,69	45,25	
	Mosaic level	79%	73%	74%	73%	

3.4 AURORA KINASES A AND B ARE OVEREXPRESSED IN GSC LINES

Real time PCR was performed in order to evaluate expression level of *AURK* genes in GSC lines. *GAPDH* was used as a housekeeping gene while foetal neural stem cells CB660 were used as controls. Relative gene expression was determined using data from the real-time cycler and the $\Delta\Delta C_t$ method. Results are reported in Figure 3.1 and are mean values derived from two independent experiments.

According to previous published data, which reported an overexpression of AurkA and AurkB in GBM, *AURKA* and *AURKB* are upregulated in all our GSCs compared to CB660 cell. On the contrary *AURKC* is generally downregulated. Only in G144 cell lines *AURKC* showed a slight upregulation. Interestingly in most of the cases there is not a direct correlation between copy number alterations and expression levels suggesting that different post-translational mechanisms might be involved.

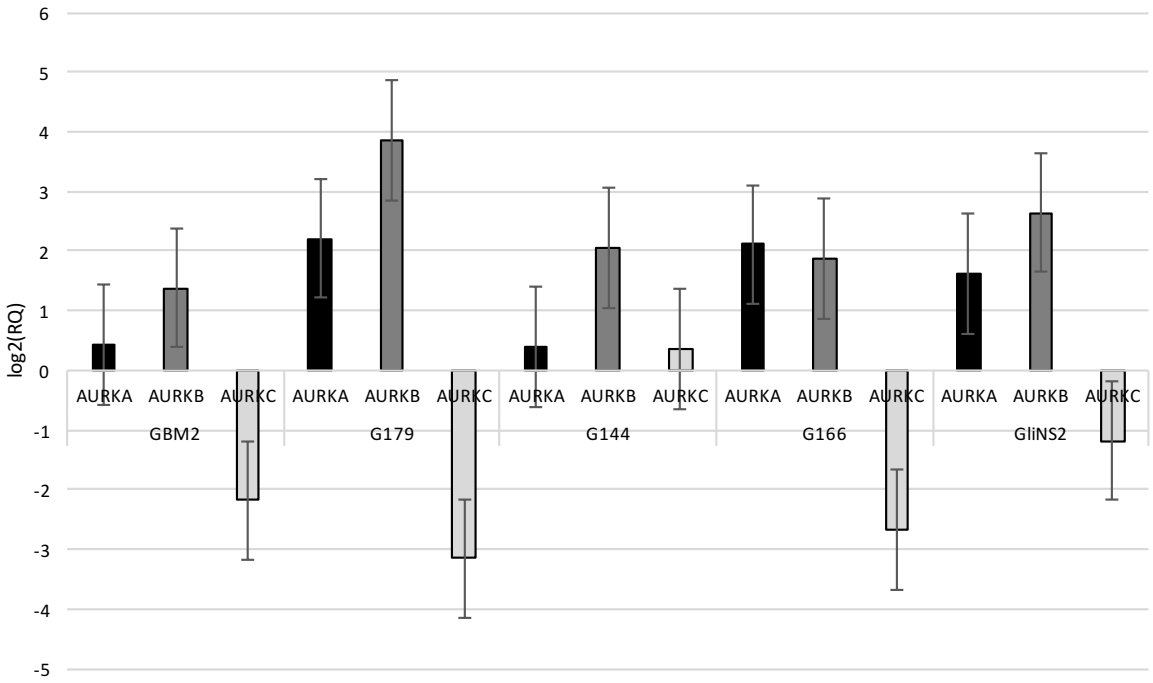

Figure 3.1 Expression levels of *AURK* genes evaluated by means of RT-PCR. Bars represent SEM.

3.5 AURORA KINASES PROTEIN LEVELS

I analysed AurkA and AurkB protein levels by Western blot in mitotic GSCs, as these two kinases are highly expresses and activated by the G_2 phase of the cell cycle through metaphase. GSCs were synchronized using STLC and mitotic cells were collected by mitotic shake off. The aim was to investigate if the GSC lines were characterized by different Aurora kinases expression levels. Protein levels were quantified using Image J software and results are reported in Figure 3.2 B. Generally, all GSC lines showed comparable levels of Aurora kinases. The only exception was GBM2 cell line which presented higher protein levels of both AurkA and AurkB. (Fig. 3.2 A/B).

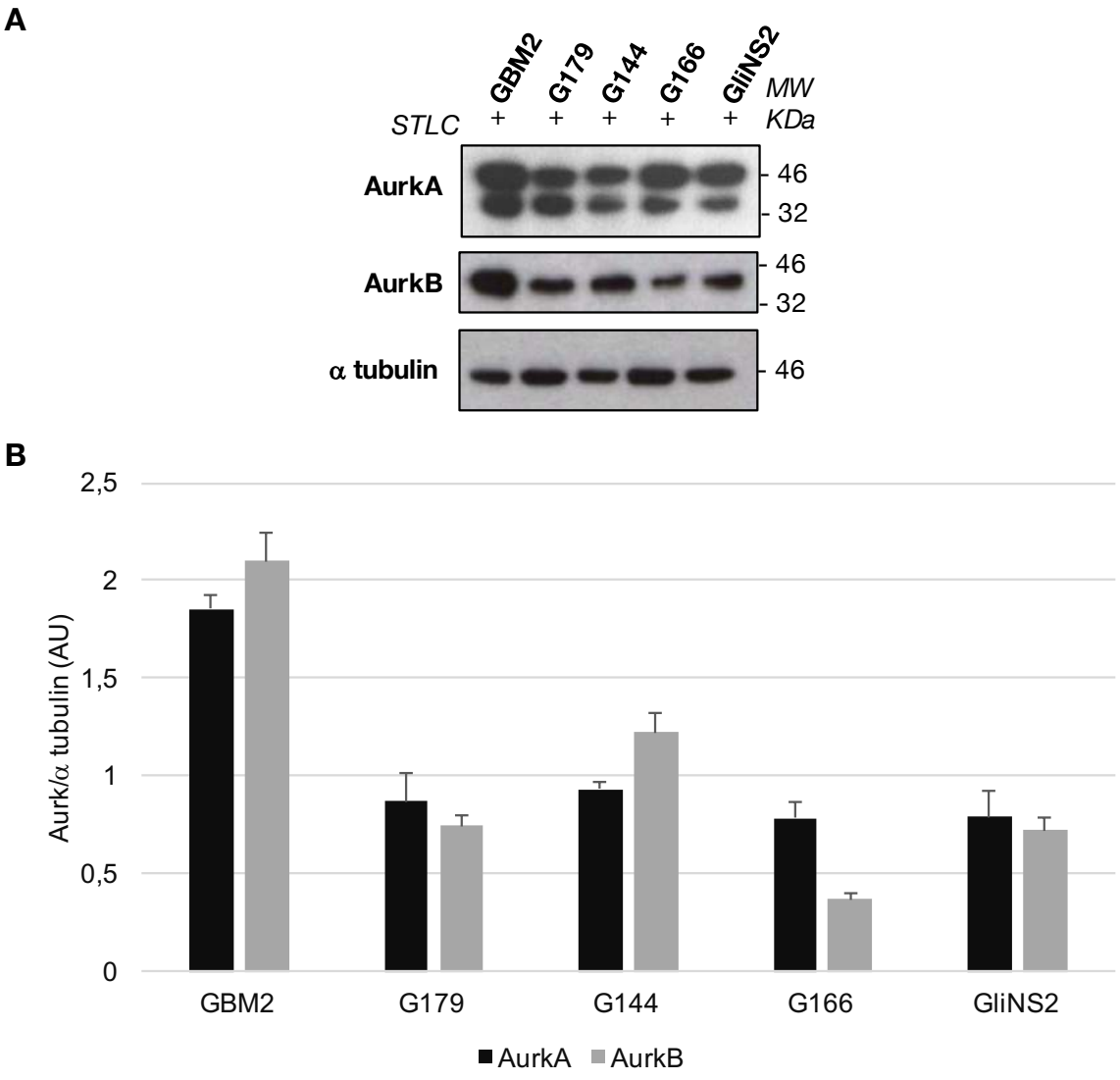

Figure 3.2 Aurora kinases A and B protein levels in synchronized GSCs. A. Representative images of Western blot analysis of AurkA and AurkB in GSCs. **B.** Quantitative densitometry analysis of at least two independent experiments. α tubulin was used as loading controls. AurkA and AurkB protein levels were normalized on α tubulin and then expressed in Arbitrary Units (AU). Bars represent SEM. * p<0,05

3.6 SENSITIVITY AND RESISTANCE TO DANUSERTIB MEASURED BY METABOLIC ACTIVITY

The effect of Danusertib on the metabolic activity was determined by means of MTT assay. Dose-response curves are shown in Figure 3.3 and individual p-value obtained by t-test on raw data are reported in the supplemental Table S1. The metabolic activity of GSCs treated with Danusertib at increasing concentration (5-50-200-500-1000-5000 nM) was compared to untreated cells at different time points (24, 48 and 72 hs). The Danusertib inhibitory effect varied between cell lines. After

24 hs of treatment there was a slight decrease of the metabolic activity in all the GSC lines which was mainly dose-dependent.

After 48 and 72 hs, this reduction was more evident in GBM2 and G179 cell lines, showing a decrease of around 50% at the highest doses of Danusertib compared to untreated cells. Otherwise G166, G144 and GliNS2 cell lines showed a faint decrease of the metabolic activity also after the longer treatment. In all the GSCs tested the reduction of the metabolic values seemed not to be affected by the prolongation of the treatment, remaining almost the same after 48 hs and 72 hs of treatment.

GBM2 and G179 cell lines, whose metabolic activity was significantly affected by the exposure to Danusertib, were pointed out as sensitive, while G144, GliNS2 and G166 were considered resistant to the treatment.

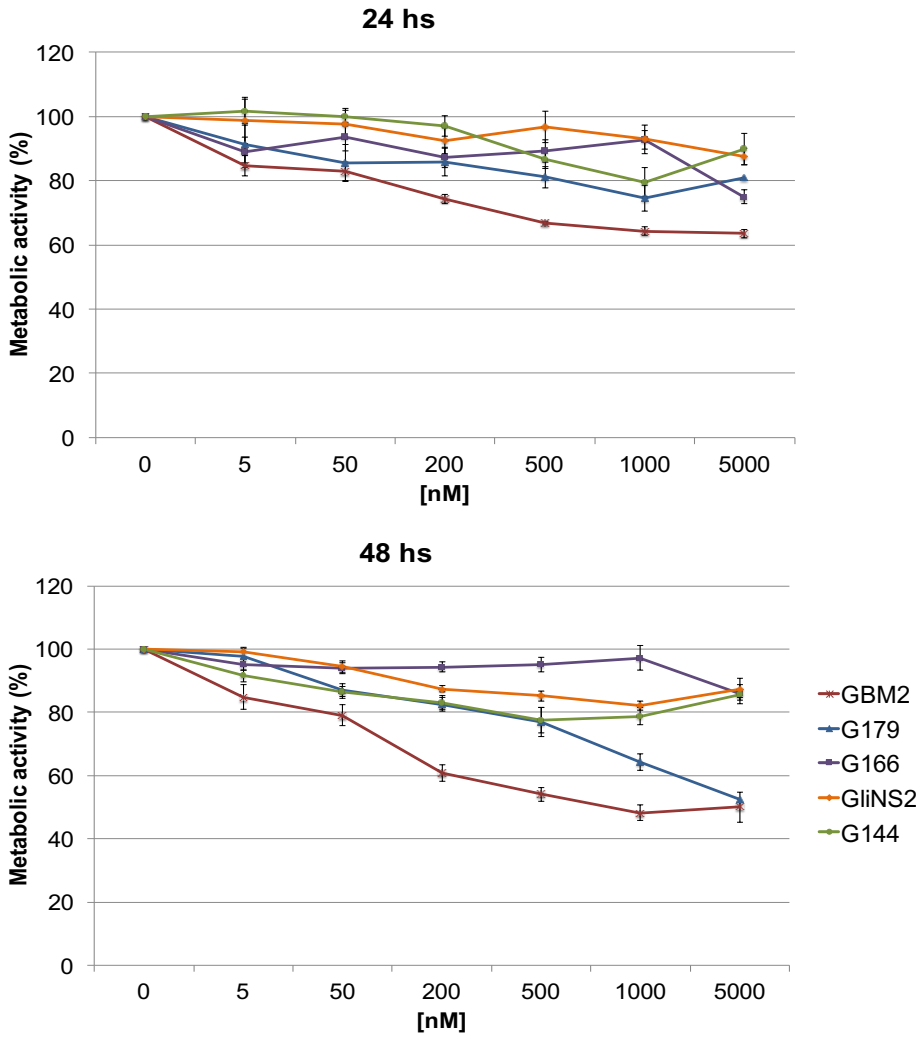

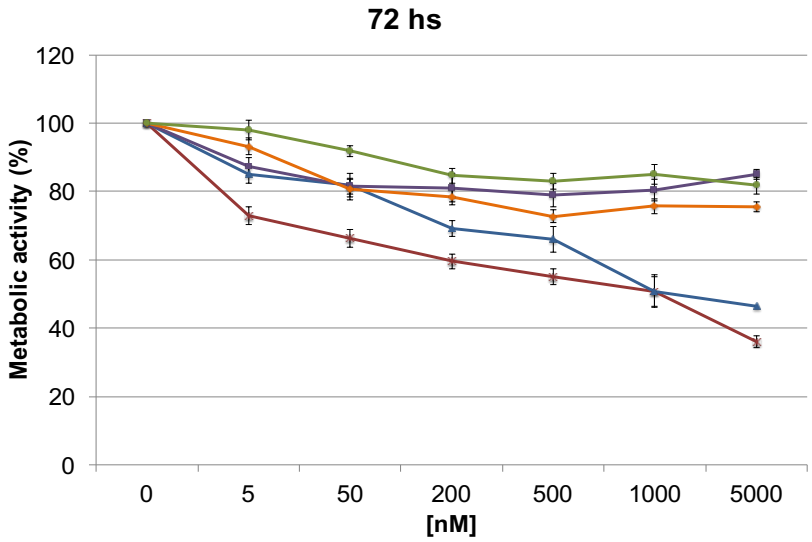

Figure 3.3 Danusertib effect on GSC metabolic activity. Metabolic activity was analyzed by MTT assay after exposure to increasing concentration of Danusertib for 24, 48, 72 hs. Results represent the means from three different experiments performed at least in triplicate and are reported as percentage of drug-treated cells relative to untreated cells. Bars represent SEM.

3.7 DANUSERTIB EFFECT ON GSCs VIABILITY

GSCs viability was evaluated by means of the Trypan blue dye exclusion assay. The administration of 50 nM Danusertib didn't induce any statistical significant changes in GSCs viability after 48 and 72 hs in both sensitive and resistant cell lines. Again, GBM2 and G179 were the most sensitive cell lines after 48 hs of treatment with 500 nM Danusertib, showing a significant increase in the percentage of cell mortality (Fig. 3.4). 72 hs of exposure resulted in a progressive significant increase in cell death in GBM2 and G179 cell lines. All the other cell lines showed lower cell mortality after both 48 hs and 72 hs of 500 nM Danusertib treatment. These data suggested that in responsive GSCs, Danusertib had mainly a cytotoxic effect, which was definitely more evident at the highest drug concentration.

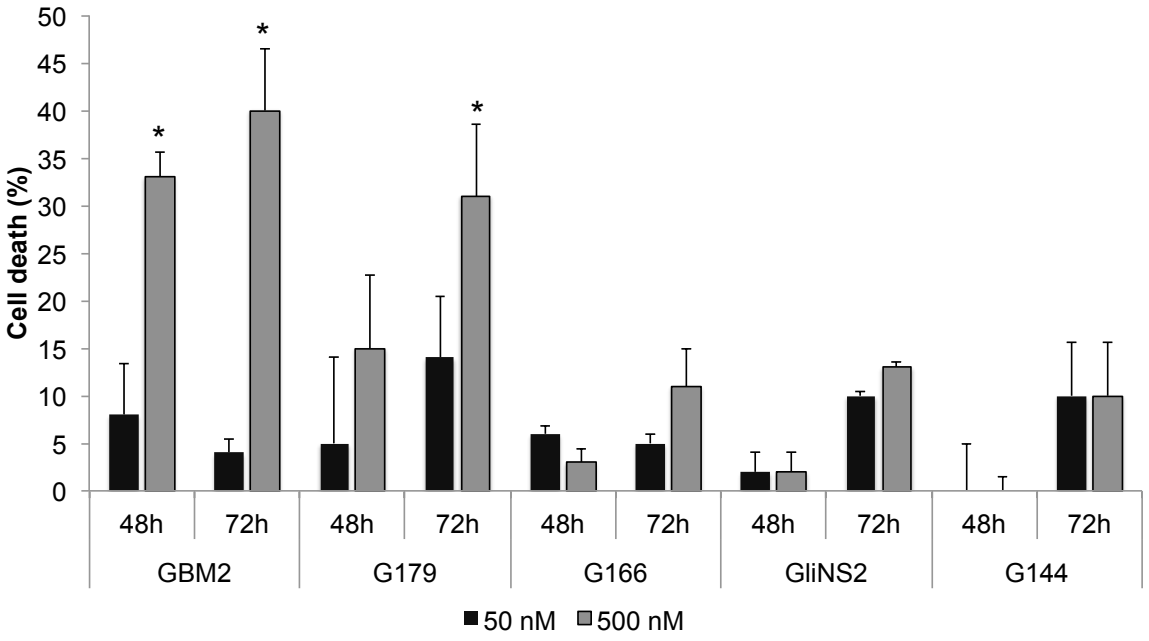

Figure 3.4 Danusertib effect on GSC viability. Cell viability was analysed by Trypan blue dye exclusion assay after exposure to two different concentrations of Danusertib (50-500 nM) for 48 and 72 hs. Results are reported as percentage of cell mortality in drug-treated cells relative to untreated cells and are the means of three different experiments ±SEM. t-test on raw data: * p<0,05.

3.8 DANUSERTIB INDUCES STRONG CHANGES IN CELL AND NUCLEI MORPHOLOGY IN SENSITIVE GSCs

GSC lines were treated with increasing concentrations of Danusertib (5-50-200-500-1000 nM) for 24, 48 and 72 hs of exposure. Matching untreated control cultures were also assessed. At each time point cell morphology was evaluated through phase contrast microscopy and representative images were taken (Fig. 3.5 and Fig. S1). Danusertib treatment determined evident morphological changes in GBM2 and G179 cell lines, which were defined accordingly to the previous assays as sensitive cell lines, showing a significant reduction in cell metabolic activity, viability and proliferation. In particular, as reported in Figure 3.5, cells showed a dramatic increase in their size starting from 48 hs of exposure to Danusertib 500 nM. At the higher concentration the Danusertib cytotoxic effect was prevailing, as demonstrated by the presence of cell debris and dead cells. Hence, 500 nM and 48 hs of exposure were the parameters used for further experiments. In the resistant cell lines Danusertib did not induce any relevant modification in cellular shape (Fig. S1).

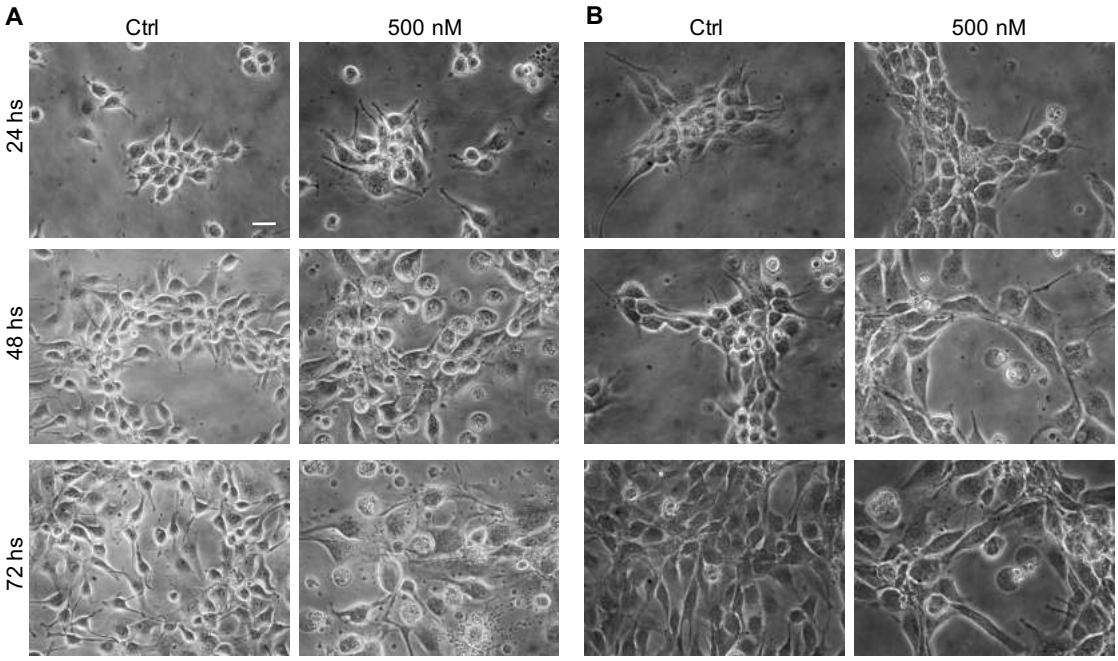

Figure 3.5 Danusertib induces morphology alterations in sensitive GSC lines. Representative images taken by phase contrast microscopy of GBM2 **(A)** and G179 **(B)** cell lines treated with Danusertib 500 nM for 24, 48 and 72 hs. Drug treatment induces a significant increase in cell size. Scale bar = 100 μm

Subsequently nuclei morphology was better investigated by means of a Giemsa staining.

A total of at least 300 nuclei were counted in each sample, distinguishing between normally shaped nuclei and abnormal ones, multinucleated and micronucleated cells. Atypical nuclei, which is a hallmark of cancer and is a peculiar feature of malignant cells, were present in all the GSC lines analysed. The nucleus shapes were irregular and various, donut-shaped, ring-shaped, polylobate nuclei and nuclei with multiple blebs are only some examples (Figure 3.6). The results are displayed in Table 3.7. Chi-square test was assessed to identify any statistically significant difference between untreated and drug treated cells.

In GBM2 and G179 treated cells there was a significant increase in the percentages of polymorphic nuclei and multinucleated cells compared to matching untreated controls. Moreover, Danusertib exposure induced in these two cell lines the appearance of micronucleated cells. All these features could mirror the increased cell size previously reported. Interestingly the same variations were found also in G144 cell line, even if they didn't show any significant variations in cell morphology. Interestingly in G166 cell line the different morphology subclasses were found also in the control, while in GliNS2 there was only a slight increase in the percentages of polymorphic nuclei and multinucleated cells, but no micronuclei were observed.

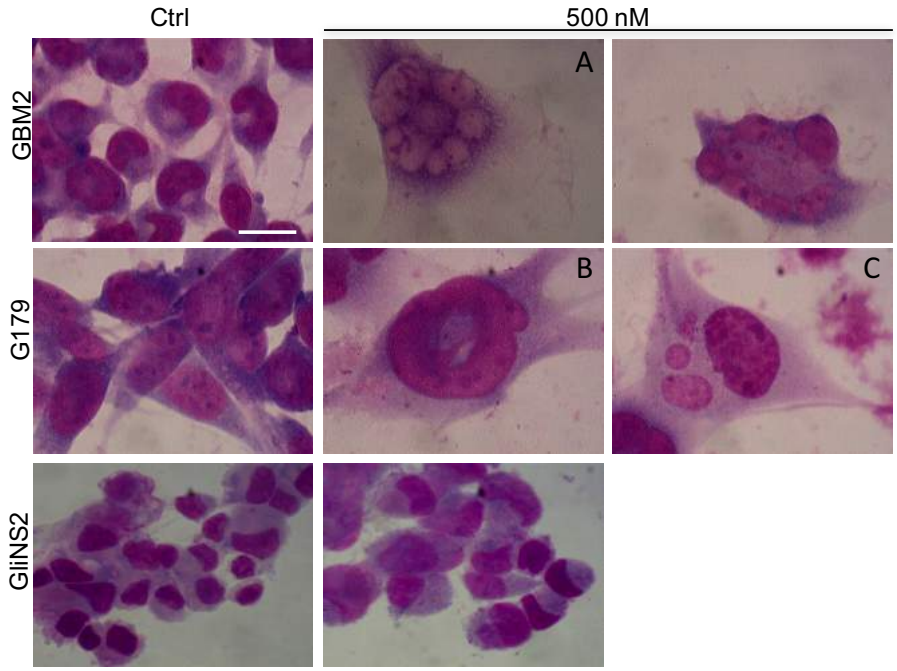

Figure 3.6 Danusertib induces relevant alterations in nuclei morphology in several GSC lines. Representative images of GBM2, G179 and GliNS2 nuclei morphology after Danusertib 500 nM treatment for 48 hs. GBM2 and G179 cell lines highlighted the presence of a huge number of large multinucleated **(C)** and micronucleated cells **(A)** and polymorphic nuclei **(B)**. GliNS2 cell line didn't show any significant variations in nuclear shape. Scale bar = 100 μm

Table 3.7 Percentages of normal shaped, polymorphic nuclei and multinucleated and micronucleated GSCs.

		GBM2		G179		G166		GliNS2		G144	
		CTRL	500nM	CTRL	500nM	CTRL	500nM	CTRL	500nM	CTRL	500nM
%	NORMAL	93,6	23,6***	87,9	6,5***	34,9	8,2***	98,5	83,9***	95,3	18***
	POLYMORPHIC	3,8	12,5*	5,8	10,4	48	38,2	1,5	9,7*	3,3	13,3*
	MULTINUCLEATED	2,6	45,3***	6,4	79,7***	10,9	27,6**	0	6,4*	1,3	28,7*
	MICRONUCLEATED	0	18,7***	0	3,4	6,1	26***	0	0	0	0

Chi square test (treated vs untreated) *p<0,05; **p<0,01; ***p<0,001

3.9 DANUSERTIB INDUCES PLOIDY INCREASE IN GSC LINES

Ploidy was evaluated through the count of the number of chromosomes in at least 50 metaphases from each treatment. Several class of ploidy were identified (listed in Table 3.8) and results were grouped according to this classification. Chi square test was performed on raw data in order to identify any variation in ploidy after drug treatment. Generally, Danusertib induced an increase in the chromosomes number both in sensitive and resistant cell lines. Only in GliNS2 cell lines the ploidy remained almost stable after Danusertib exposure.

Table 3.8 Evaluation of ploidy after Danusertib treatment.

		Class of ploidy (number chromosomes/metaphase)												
		near haploid	hypo diploid	hyper diploid	hypo triploid	hyper triploid	hypo tetraploid	hyper tetraploid	near pentaploid	near exaploid	near eptaploid	near octoploid	near nonaploid	near decaploid
Cell line	**Treatment**	**<34**	**35-46**	**47-57**	**58-69**	**70-80**	**81-92**	**93-103**	**104-126**	**127-149**	**150-172**	**173-195**	**196-218**	**219-241**
GBM2	Ctrl	0,0	0,0	0,0	0,0	10,0	0,0	0,0	16,7	73,3	0,0	0,0	0,0	0,0
	500 nM	0,0	0,0	0,0	0,0	0,0*	6*	3,0	12,0	36,4***	39,4***	0,0	0,0	3,0
G179	Ctrl	0,0	0,0	0,0	0,0	10,0	20,0	36,7	33,3	0,0	0,0	0,0	0,0	0,0
	500 nM	0,0	0,0	0,0	0,0	3,3	0,0***	6,7***	3,3***	16,7***	13,3***	30***	6,7*	20***
G166	Ctrl	0,0	0,0	66,7	33,3	0,0	0,0	0,0	0,0	0,0	0,0	0,0	0,0	0,0
	500 nM	0,0	0,0	0***	6,7***	0,0	0,0	26,7***	63,3***	0,0	0,0	3,3*	0,0	0,0
GliNS2	Ctrl	0,0	50,0	33,3	0,0	0,0	16,7	0,0	0,0	0,0	0,0	0,0	0,0	0,0
	500 nM	0,0	46,7	40,0	0,0	0,0	13,3	0,0	0,0	0,0	0,0	0,0	0,0	0,0
G144	Ctrl	0,0	0,0	0,0	2,0	23,5	56,8	15,7	2,0	0,0	0,0	0,0	0,0	0,0
	500 nM	0,0	0,0	0,0	16,7***	33,3	33,3***	0***	0,0	3,3	6,6**	3,3	0,0	0,0

Chi square test (treated vs untreated) *p<0,05; **p<0,01; ***p<0,001

3.10 DANUSERTIB EFFECT ON GSCs PROLIFERATION

In order to study the effect of Danusertib exposure on cell proliferation, we evaluated the Mitotic index (MI). This parameter has very important clinical implications because the mitotic activity is a crucial property related to the tumour aggressiveness. MI analysis was performed by counting the number of metaphases per 1000 nuclei. The MI was assessed on untreated and 500 nM Danusertib treated cells for 48 hs. Results are expressed as percentages and are displayed in Figure 3.7. Statistically significant differences were evaluated by chi-square test on raw data. Danusertib administration induced a decrease of MI in all the cell lines analysed. In particular, in GBM2 and G179 cell lines, which had already been shown to be very sensitive to the drug treatment, the reduction of the MI was statistically significant. In the remaining cell lines the alteration of the MI was faint and not statistically significant.

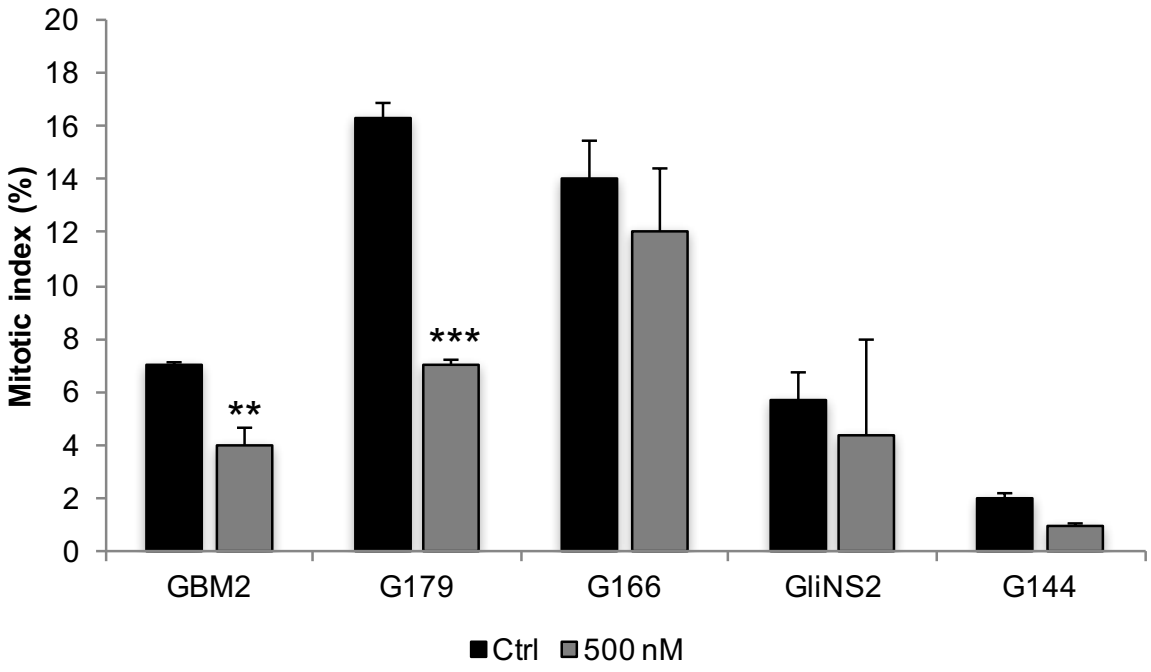

Figure 3.7 Danusertib effect on GSC proliferation. Cell proliferation was evaluated through the determination of the Mitotic index. Results are reported as percentages from the means of two independent experiments ±SEM. Yates' Chi-square test on raw data: ** p<0,01; *** p<0,001.

3.11 DANUSERTIB EFFECT ON GSCs CLONOGENIC POTENTIAL

The clonogenic potential of GSCs was evaluated after treatment with Danusertib 50 and 500 nM. In sensitive GSCs (GBM2 and G179) I observed a significant dose-dependent reduction of the number of clones, as shown in the representative pictures in Figure 3.8 A. Quantitative data are reported also in Figure 3.8 B as percentages of cell forming colonies in the treated samples over matching control values. As regards the resistant cell lines generally there was no significant decrease of the number of colonies after Danusertib treatment. Only in G144 Danusertib 500 nM induced a decrease of this parameter.

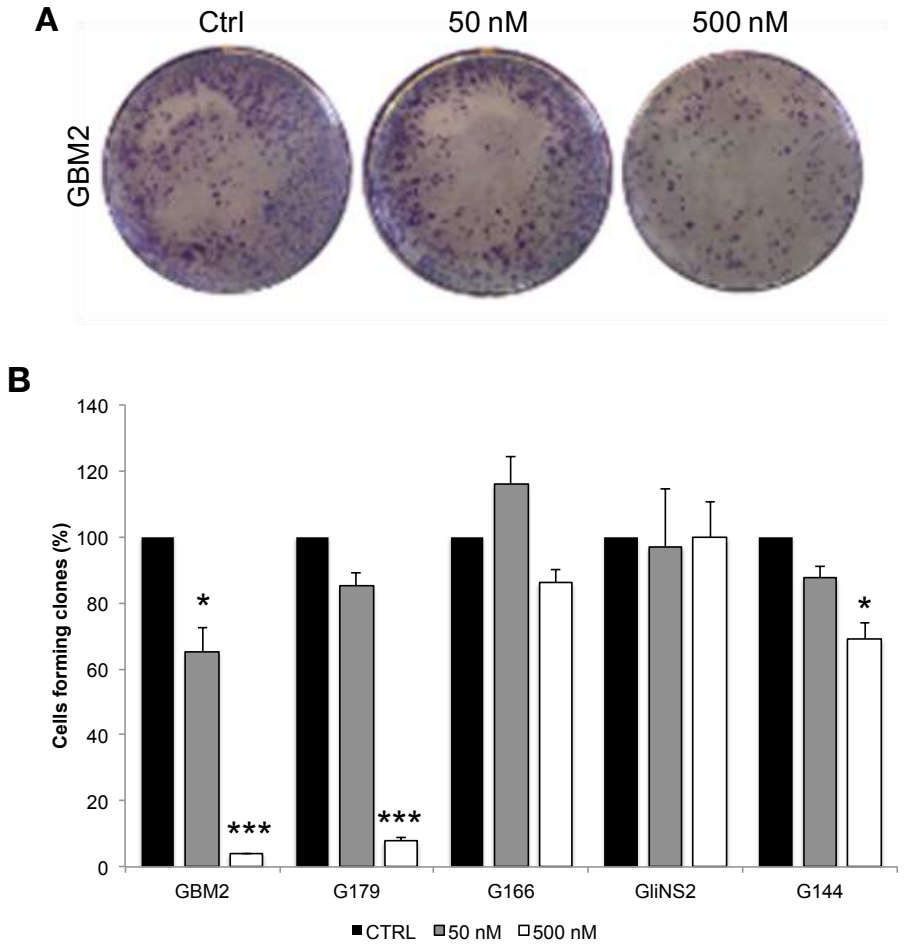

Figure 3.8 Danusertib effect on GSCs clonogenic potenitial. GSCs clonogenic potential was evaluated after treatment for 48 hs to Danusertib 50 nM and 500 nM. **A.** Representative images of the dose-dependent clones decrease highlighted in GBM2 cell line. **B**. Results are reported in a bar graph as percentages of cell forming colonies in the treated samples over matching control values. Results reported are the means of two independent experiments ±SEM. t-test on raw data: * $p<0,05$; *** $p<0,001$.

3.12 DANUSERTIB INDUCES A DECREASE IN PHOSPHO-AURORA KINASES LEVELS IN GSC LINES

Danusertib activity was evaluated by means of immunofluorescence assays aimed at detecting the expression of phosphorylated Aurora kinases in the nuclei of mitotic cells, untreated or treated with 500 nM Danusertib for 48 hs. Cells were synchronized using STLC in order to have a proper number of mitotic cells in both controls and treated samples. As a matter of fact, inhibition of Aurora kinases can be followed at the cellular level by determination of Aurora auto phosphorylation. The level of phosphorylated Aurora kinases was quantified using Image J in at least 50 cells and results are reported as mean values of two independent experiments. Quantification data are reported in Figure 3.9 A, while representative images are shown in Figure 3.9 B and Figure S2. In all the GSC lines Danusertib induced a significant reduction of the level of phosphorylated Aurora kinases demonstrating that Danusertib inhibitory activity was effective in both sensitive and resistant cell lines. Interestingly the inhibitory effect of Danusertib was even more evident in the more resistant cell lines: G166 and G144 cell lines showed a 87% reduction of the expression of phosphorylated-Aurora kinases.

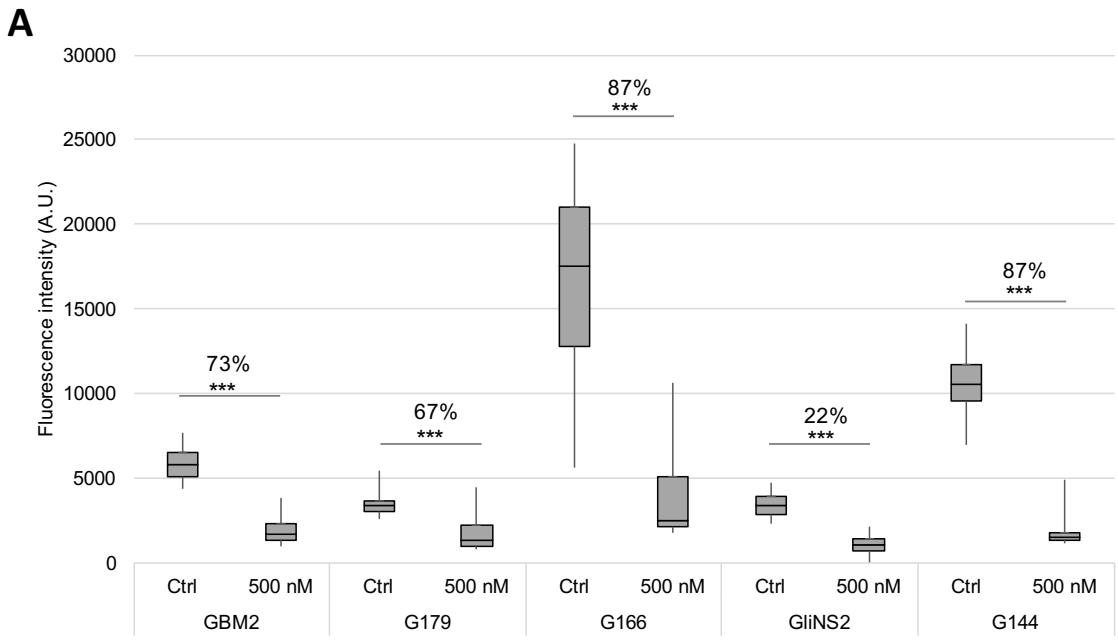

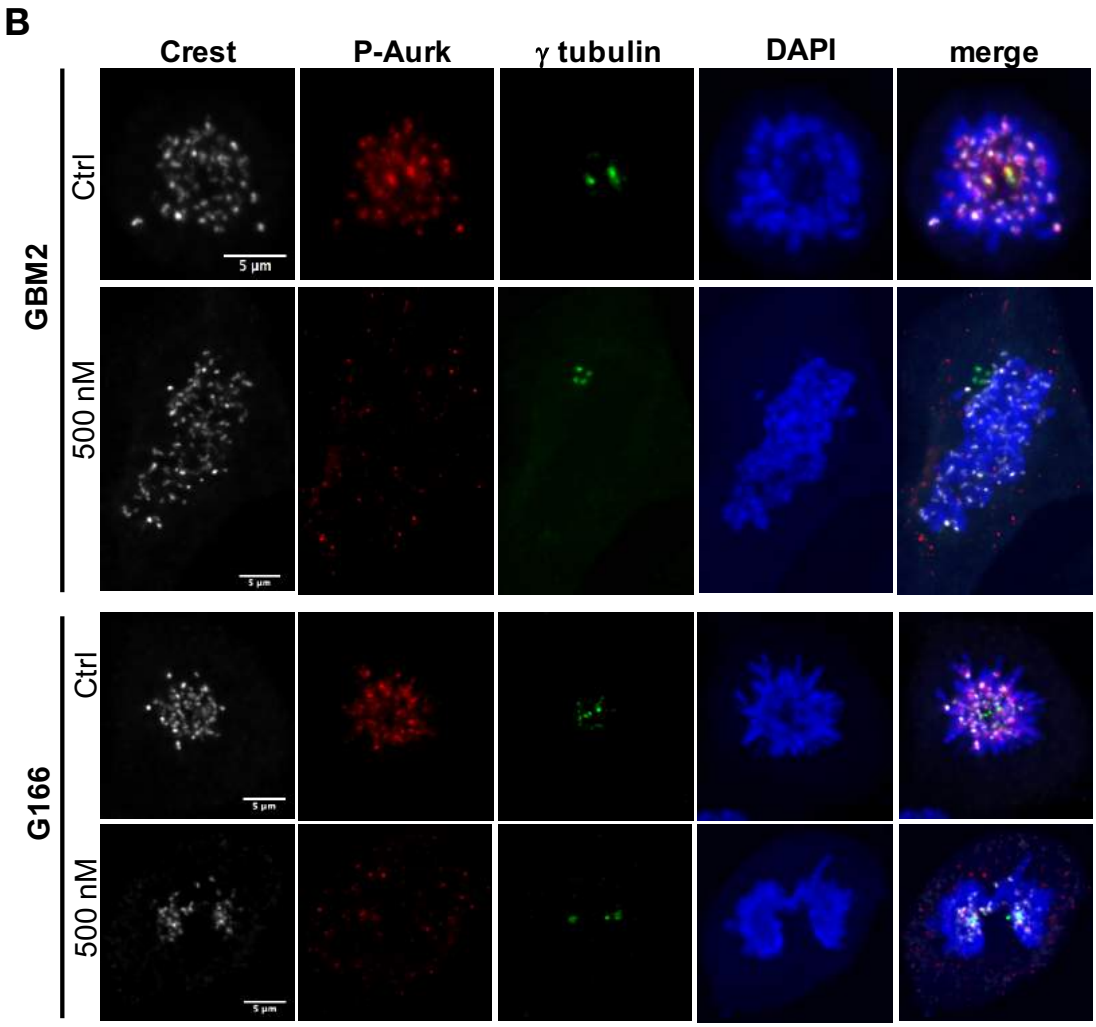

Figure 3.9 Danusertib induces a reduction of phosphorylated Aurora kinases in GSCs. A. Quantification of the pospho-Aurora kinases fluorescent signal in the nuclei of mitotic cells was performed by ImageJ software. Results are expressed as mean of two independent experiments ± SEM. t- test on raw data: *** p<0,001. **B.** Representative images of two GSCs lines (GBM2 and G166) untreated or treated with Danusertib 500 nM for 48 hs, synchronized with STLC and stained for Crest (white), phospho-Aurora kinases (red), γ tubulin (green) and DAPI (blue).

3.13 LIVE IMAGING ANALYSIS OF GSCs FATE AFTER DANUSERTIB EXPOSURE

In order to better characterize the phenotype induced by Danusertib exposure and the mechanism leading to polyploidy, I evaluated the feasibility of cell fate using live cell imaging. Live cell imaging analysis were performed on two GSC lines, which have previously showed a different sensitivity to Aurora inhibition (GBM2 and G166). Images of multiple fields per well were collected every 5 min for approximately 16 hs soon after the addition of Danusertib 500 nM. Matching untreated controls were also assessed.

In both the cell lines the main mechanism by which Danusertib induced an increase in cell ploidy was the inhibition of the cytokinesis leading to endoreduplication. In the presence of Danusertib I observed a significant decrease in the number of cells which underwent a proper cell division, and, on the other hand, an evident increase in the percentage of non cytokinetic cells (Fig. 3.10). The other parameters taken into account, such as the number of cell which did not properly divide (i.e. from one cell I observed more than two daughter cells) or the number of dead cells, did not show any relevant modification in both the cell lines.

The live cell imaging analysis highlighted also a significant increase in the mitotic length, from around 90 minutes to around 150 minutes both in GBM2 and G166 cell lines. This variation might probably due to an elongation of the S phase (Fig. 3.11). Indeed, cells might take more time to duplicate an increase DNA content.

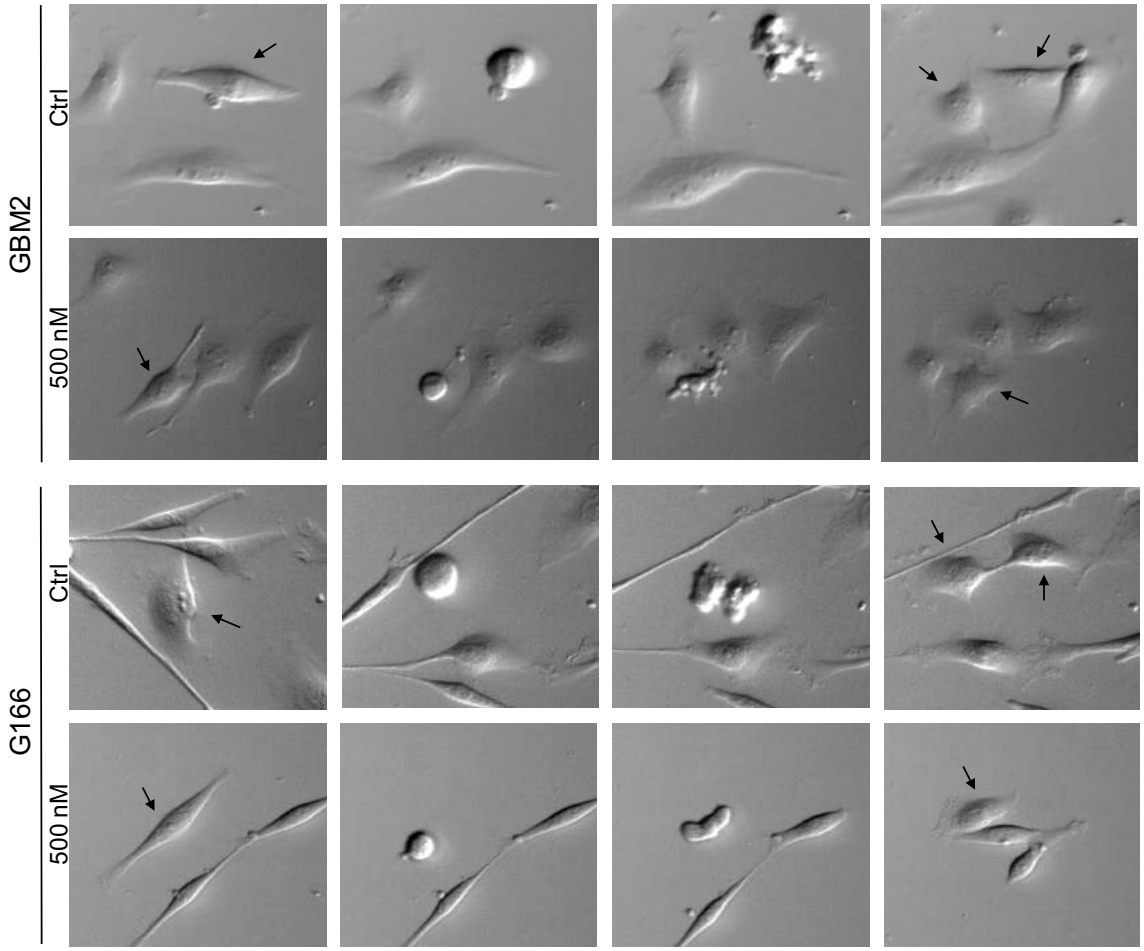

Figure 3.10 Danusertib inhibits cytokinesis in GSCs. Representative images of dividing cells (indicated by black arrows) detected by means of live cell imaging analysis. Danusertib 500 nM inhibited cytokinesis in GSCs.

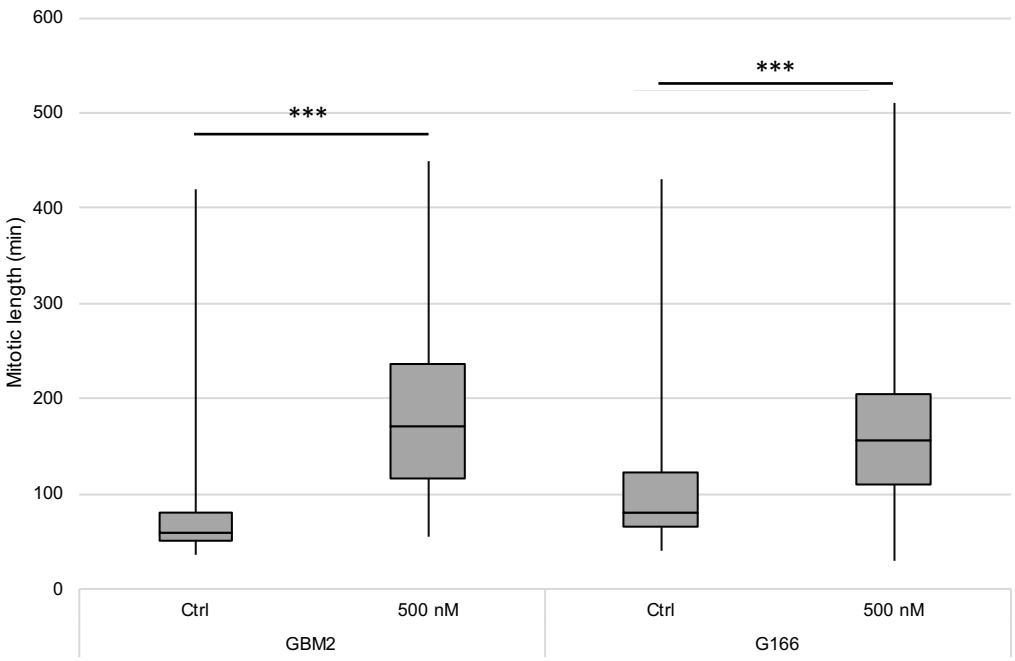

Figure 3.11 Danusertib induces a significant increase in the mitotic length. The mitotic length was determined analysing the live cell movie by means of Image J. t-test ***p<0,001

3.14 DIFFERENT SENSITIVITY OF GSCs TO AURORA INHIBITION IS NOT DEPENDENT ON *TP53* STATUS

Given the pivotal role of p53 in regulating fate of cancer cells following cytotoxic treatment, several studies analysed whether its status influences response to Aurora inhibition, yielding conflicting results [333, 334]. In order to verify if the different response of GSCs to Danusertib might be due to a different *TP53* mutational status we performed a Sanger sequencing of *TP53* exons 5,6,7 and 8 considered the mutational hot spot regions [335, 336]. Results are reported in Figure 3.12 A/B/C and all the alterations detected are listed in Table 3.9. All the cell lines sequenced carry missense mutations in the DNA-binding region of the protein, except for GliNS2 cell line which isn't affected by any mutation in *TP53*; G166 and GBM2 carry the same alterations. G144 cell line proved to be the most affected by mutations in *TP53* locus; as a matter of fact, we found two mutations, in exons 5 and 8, along with two SNPs in intron 7, 71 and 91 nucleotides downstream of exon 7 respectively, with population allele frequencies of 16% and 10%. In all the cell lines analysed, except for G144, the mutations were homozygous suggesting a loss of heterozygosity (LOH) of whole or part of chromosome 17. The presence of the

same mutations in highly polyploid cells is really unlikely. On the other hand, is much more likely that malignant cells, which loose the wild-type *TP53*, have been preferentially selected. The fact that all the cell lines, excluded GliNS2, are characterized by *TP53* mutations, does not support a role of *TP53* status in determining the observed differential sensitivity of GSCs to Aurora kinases inhibition.

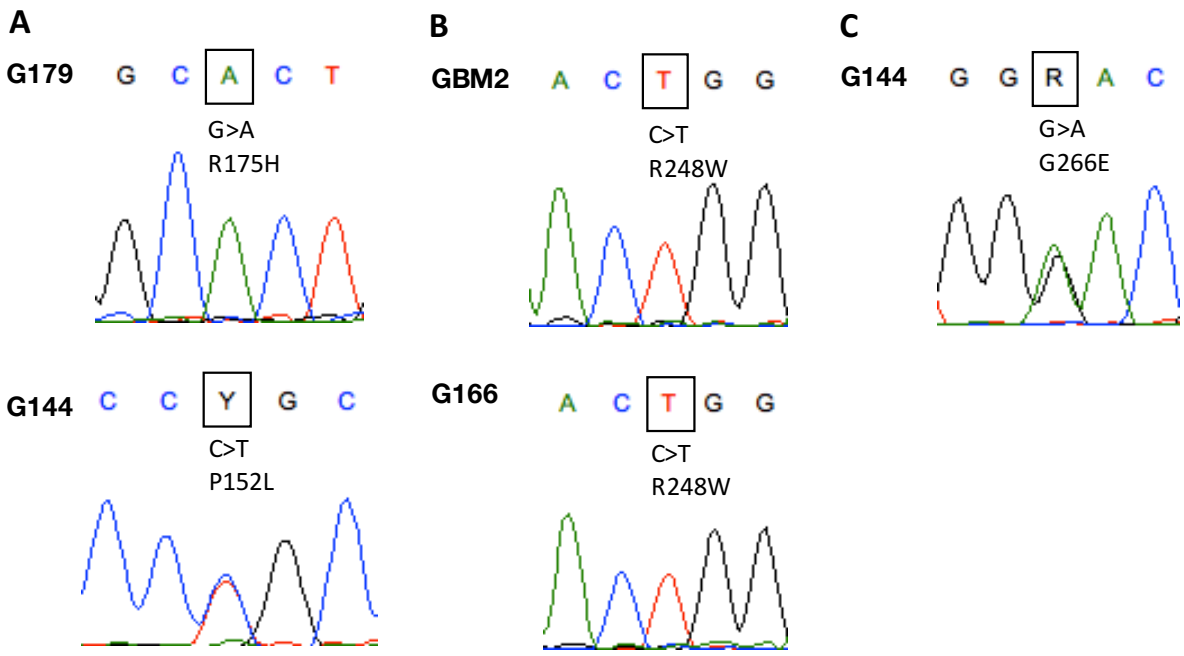

Figure 3.12 Different sensitivity of GSCs to Aurora inhibition is not dependent on *TP53* status. Electropherograms of *TP53* mutational hot spot region. All the GSC lines carry missense mutations in the DNA-binding region of the protein, except for GliNS2 line which isn't affected by any mutation in *TP53*.

Table 3.9 List of the *TP53* alterations found in the cell lines analysed.

	MUTATIONAL HOT SPOTS			
Cell lines	**Exon 5**	**Exon 6**	**Exon 7**	**Exon 8**
GBM2	no alteration	no alteration	**R248W** **Variation:**rs121912651 **Position**17:7674221 **Alleles**G/A **Protein position**248 **Amino acids**R/W Missense variant	no alteration
G179	**R175H** **Variation:**TP53_g.12512G>A **Position**17:7675088 **Alleles**C/T **Protein position**175 **Amino acids**R/H Missense variant	no alteration	no alteration	no alteration
G166	no alteration	no alteration	**R248W** **Variation:**rs121912651 **Position**17:7674221 **Alleles**G/A **Protein position**248 **Amino acids**R/W Missense variant	no alteration
GliNS2	no alteration	no alteration	no alteration	no alteration
G144	**P152L** **Variation:**rs587782705 **Position 17**7675157 **Alleles**G/A **Protein position**152 **Amino acids**P/L Missense variant	no alteration	**Nucleotide Position: 14181** SNP Location: Intron-7 SNP Alleles: C/T **Nucleotide Position: 14201** SNP Location: Intron-7 SNP Alleles: T/G	**G266E** **Variation:**rs193920774 **Position**17:7673823 **Alleles**C/T **Protein position**266 **Amino acids**G/E Missense variant

3.15 *TP53* LOSS OF HETEROZIGOSITY (LOH) ANALYSIS

In order to verify if the LOH hypothesized starting from sequencing data was present in our GSCs and if it was restricted to *TP53* locus (17p13.1) or spread to a bigger region or even to the whole chromosome 17, an LOH analysis was performed using a panel of 4 microsatellite markers for chromosome 17 p and q. This approach allowed the distinction of the homologous chromosomes, as microsatellite markers with a high rate of heterozygosity were selected. Results are reported in Figure 3.13. In particular, G144 cell lines showed a retained heterozygosity of the whole chromosome 17 as expected from sequencing data. Interestingly G166 cell line presented a whole chromosome 17 LOH as all the microsatellites were homozygous. GBM2 and G179 cell lines revealed a more restricted LOH. In GBM2 the LOH involved only the distal portion of chromosome 17 p arm, while in G179 it was probably extended to the whole p arm.

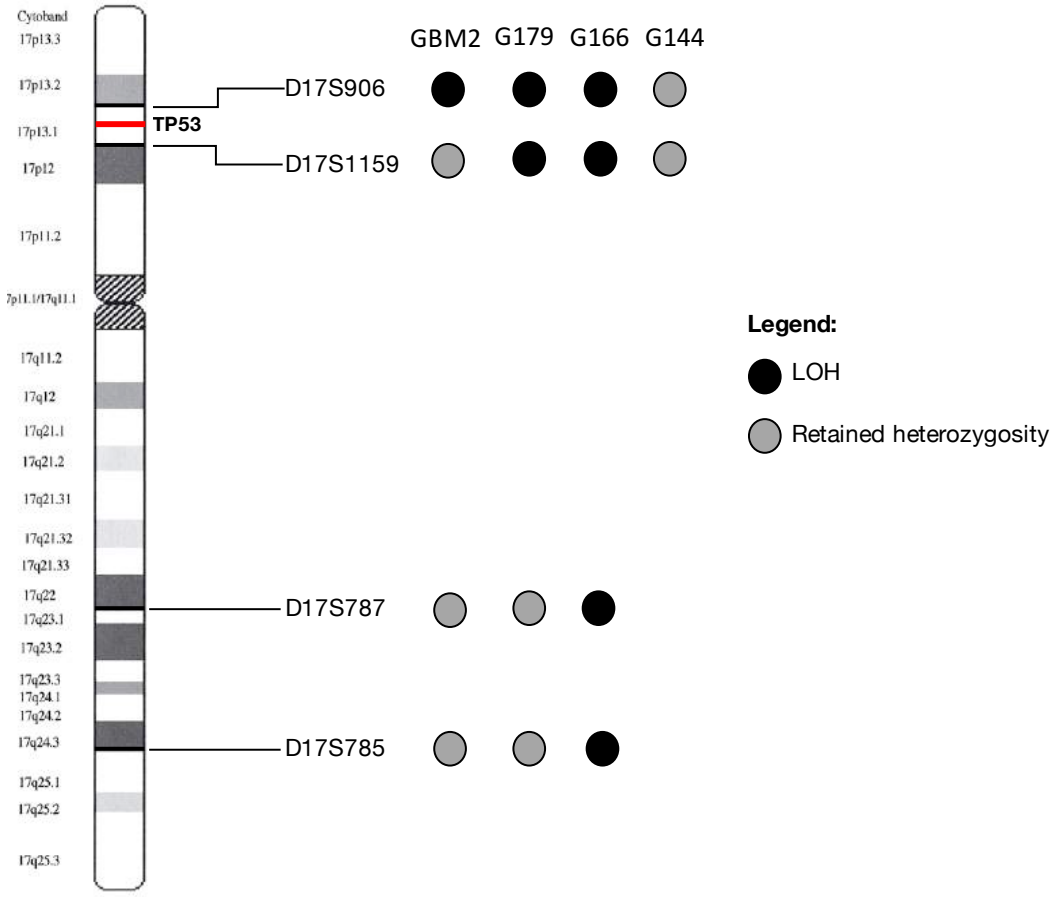

Figure 3.13 Detailed chromosome 17 LOH mapping of GSC lines. LOH analysis was performed using a panel of 4 microsatellite markers.

3.16 SENSITIVE AND RESISTANT GSCs HAVE A DIFFERENT CELL CYCLE DISTRIBUTION

In order to evaluate any difference in the cell cycle distribution between sensitive and resistant GSC lines a Western blot evaluation of mitotic markers levels was performed on asynchronous GSC lines. Moreover, I identified and quantified the percentage of cells in G1, G2, S and M phases by immunofluorescence detecting EdU, CENP-F and α-tubulin in conjunction with DAPI staining.

Sensitive and resistant GSCs revealed a completely different cell cycle distribution. As regards the Western blot data, GBM2 and G179 cell lines showed a G1 phase profile with low levels of mitotic markers. G166, G144 and GliNS2 displayed a surprisingly high levels of Cyclins A and B, Aurora kinases and pS10 histone H3 but did not have an elevated Mitotic index (as reported in section 3.10) or elevated Cdk1 activity, suggesting that these cells might accumulate in late S and G2 with

premature Aurora kinase activation. (Fig. 3.14). However, immunofluorescence assays on asynchronous cells highlighted that GBM2 and G179 cell lines seemed to be mainly in S and G2 phase, with few mitotic cells, mirroring the quiescent phenotype of these cells. On the contrary G166, G144 and GliNS2 cells presented a G1 phase profile. (Fig. 3.15 A/B)

The results collected from western blot and immunofluorescence analysis seems to be at odds, but, actually they can suggest the involvement of other mitotic proteins, such as a no functional APC/C, which can cause the weird cell cycle distribution determined by the mitotic markers levels

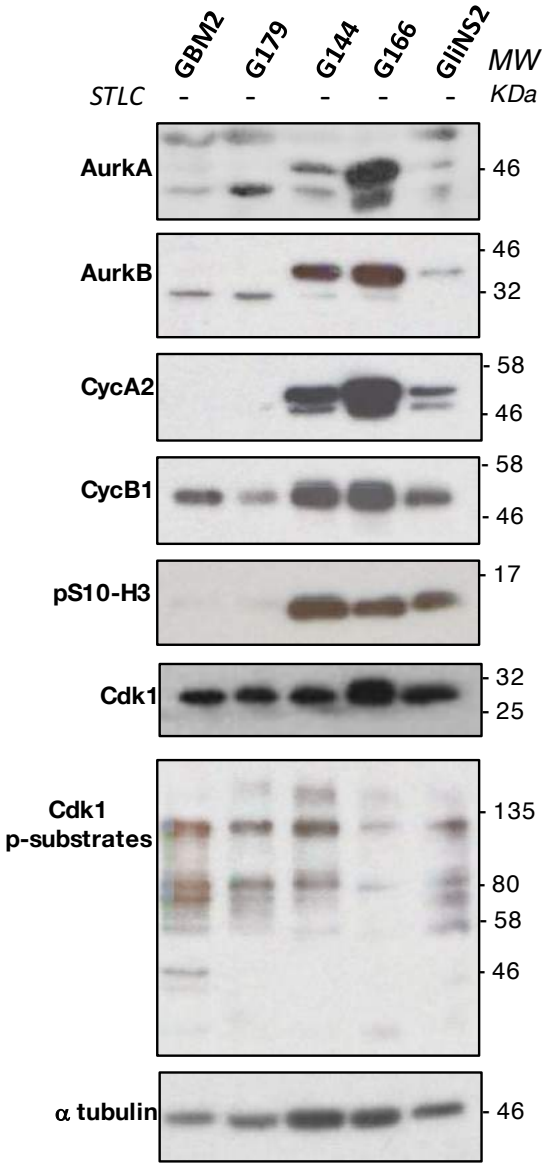

Figure 3.14 Mitotic markers expression levels. Representative images of western blot analysis of mitotic markers levels. α tubulin was used as loading controls.

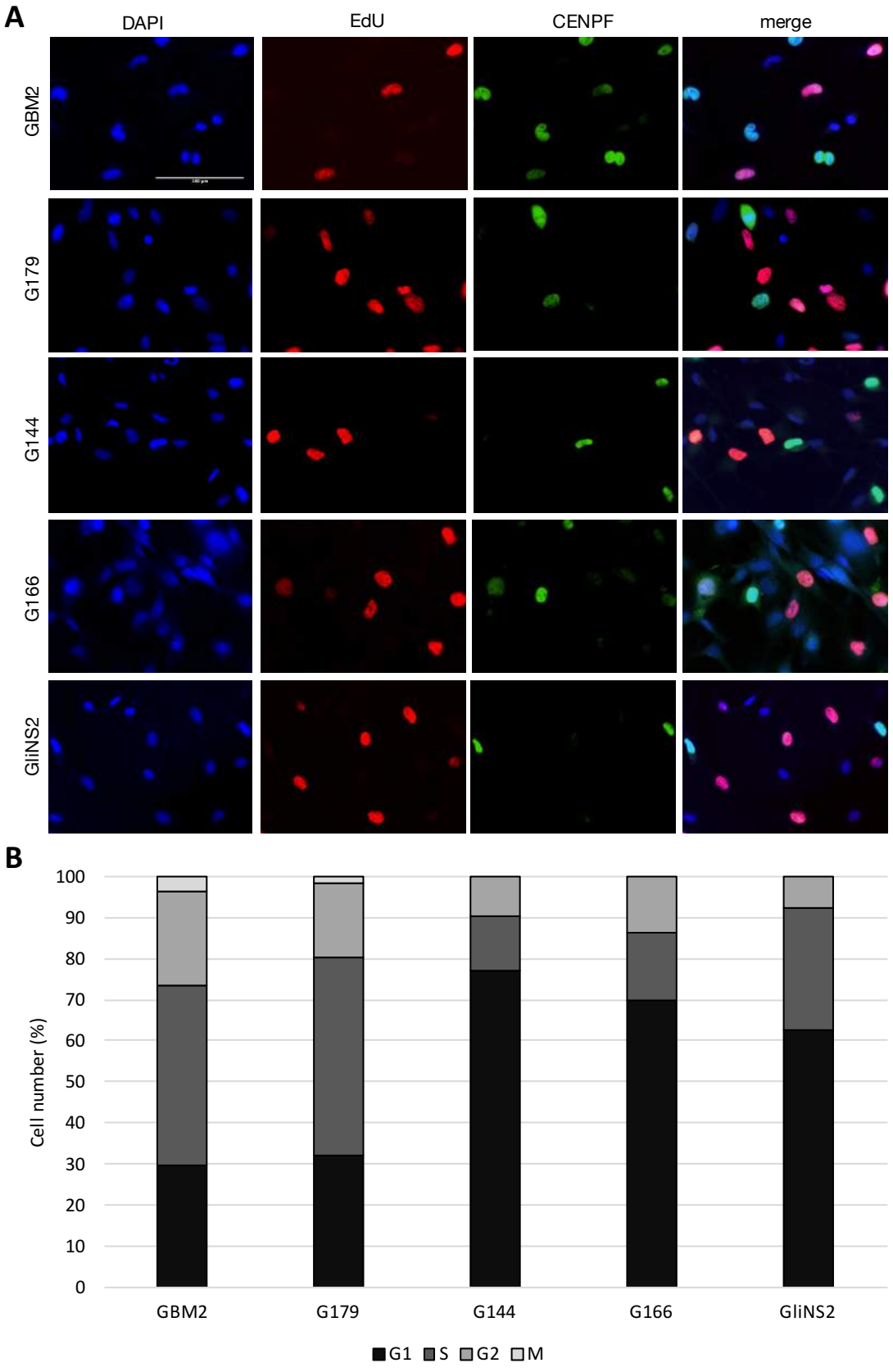

Figure 3.15 GSCs cell cycle distribution. A. Immunofluorescence representative images. Semi-confluent asynchronous GSCs were fixed and stained for CENP-F (green), EdU (red) and DAPI (blue), to visualize and quantify G1, S, G2 and M cells. **B.** A graph shows the percentages of cells in the different cycle phases G2 and M phase in the two subpopulations at the various dose levels. At least 100 cells were randomly imaged and scored.

3.17 DANUSERTIB DOES NOT INDUCE ANY DNA FRAGMENTATION

In order to better characterize the cell fate after 48 hs exposure to Danusertib 500 nM the DNA integrity status was evaluated by means of a tape based electrophoresis which automatically provided the DNA Integrity Number (DIN) reported in Figure 3.16. All the value both in untreated and treated cell lines were found greater than 7 indicating an overall DNA integrity.

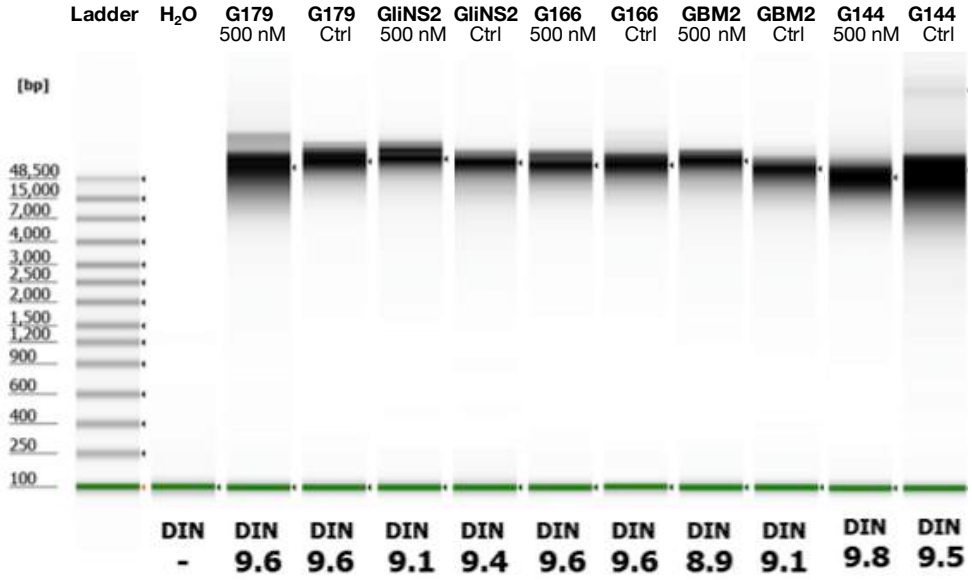

Figure 3.16 Danusertib does not induce any DNA fragmentation in GSC lines. Electrophoretic run of DNA extracted from untreated and 48 hs Danusertib 500 nM treated GSC lines. All the DIN values are >7 indicating DNA integrity.

3.18 AURORA INHIBITION INDUCES AN INCREASE IN SENESCENCE IN SENSITIVE GSCs

Based on previous studies reporting the ability of Aurora inhibitor to induce senescence [337-339], I evaluated the levels of β-galactosidase in two GSC lines with different sensitivity to Danusertib (GBM2 and G166). I observed a significant increase in the percentage of senescent cells in GBM2 cell line, with 79% of these expressing the senescence marker after 48 hs, compared to 0% of matching untreated cells. On the contrary, in G166 cell line Danusertib did not induce any relevant increase of the level of β-galactosidase. (Fig. 3.17 A/B)

3.19 MULTIPLE ROUNDS OF AURORA INHIBITION INDUCE AN INCREASE IN PLOIDY AND SENESCENCE ALSO IN RESISTANT GSCs

Our results reported previously in section 3.9 showed that the cell lines with higher sensitivity for Aurora kinase inhibition, GBM2 and G179, were characterized by a higher ploidy compared to the less sensitive ones. Moreover, in these cell lines Aurora inhibition induced an increase in senescence as shown in Figure 3.17. A straight forward explanation for this result could be the presence of a ploidy threshold that is intolerable even for p53 negative cell lines. A prediction from this hypothesis would be that the resistant cell lines should also undergo senescence after repeated rounds of Aurora inhibition leading to steady increases in ploidy. In order to investigate the correlation between GSCs Danusertib sensitivity and the ploidy level, GBM2 and G166 cell lines were subjected to two rounds of Danusertib exposure. β-galactosidase performed at the desired time points, showed a significant increase of senescent cells also in G166 cell line.

The FISH analysis on interphase nuclei, using probes detecting chromosomes X, Y, 18, 13 and 21, was performed in order to estimate the cell's ploidy as the number of metaphases was extremely low after two rounds of treatments. This assay highlighted that after two round of Danusertib exposure there was a significant increase of the cell's chromosomes content also in the resistant cell line. The number of probes signals per cell detected was comparable in GBM2 and G166 cell lines and was around 12 suggesting that the cells were almost dodecaploid (Fig 3.18).

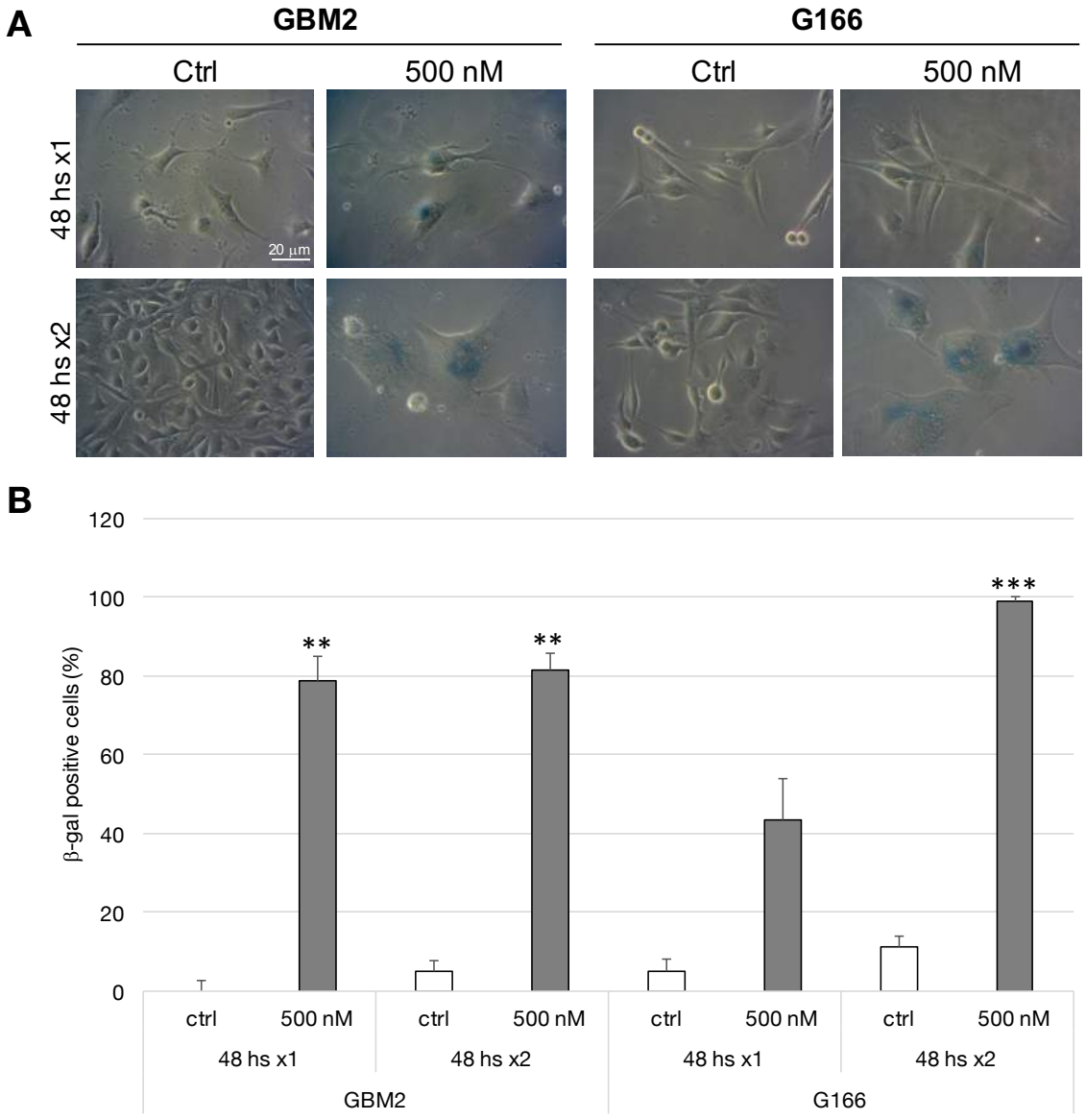

Figure 3.17 Aurora inhibition induces an increase in senescence in GSCs. GBM2 and G166 cell lines were treated with 500 nM Danusertib. Following 48 hs x1 or 48 hs x2 of incubation, they were fixed and stained for β-galactosidase, to evaluate induction of senescence. **A.** Representative images showing β-galactosidase staining (blue) at baseline and after Danusertib treatment. **B.** A graph shows the percentages of senescent cells in the two cell lines. An average of 100 cells/condition/experiment were randomly imaged and scored. Results are representative of two independent experiments. Error bars indicate means ± SEM.

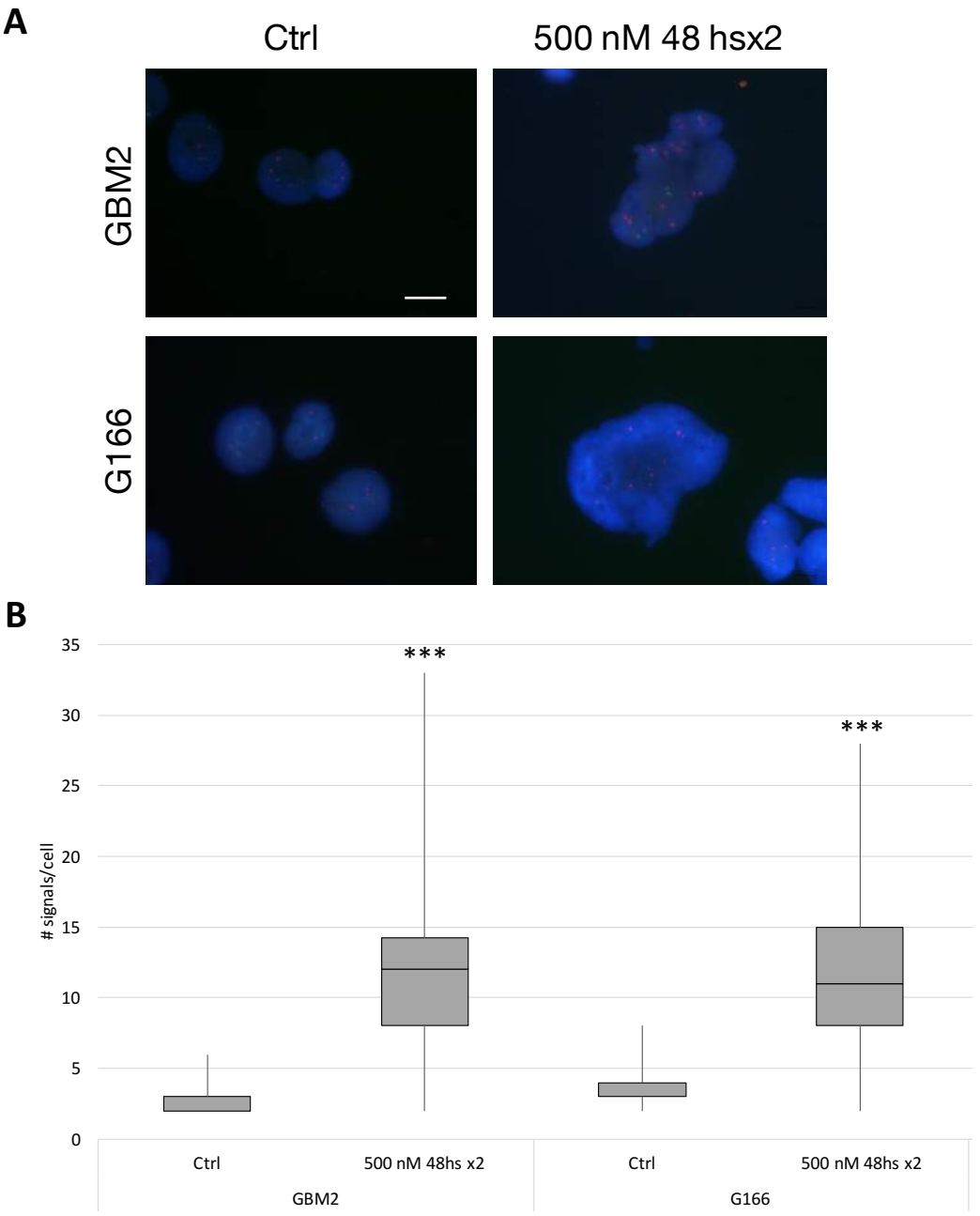

Figure 3.18 Multiple rounds of Danusertib exposure induces an increase in chromosomes content in GBM2 and G166 cell lines. A. Representative images of FISH analysis performed in GBM2 and G166 cell lines after two rounds of 48 hs treatment with Danusertib 500 nM. Red signals correspond to chromosome 21, while green signals indicate chromosome 13. Danusertib exposure induces an increase of the number of signals detected in both the cell lines. Scale bar = 100 μm **B.** Quantification of the number of signals per cell. Results are expressed as mean of two independent experiments. At least 50 cells were analysed in each experiments t- test on raw data: *** p<0,001

Chapter 4

Characterization of GSCs division mode

Chromosomal instability in Glioma Stem Cell lines from Glioblastoma multiforme: implications for new therapeutic strategies

MATERIALS AND METHODS

4.1 MATERIALS

4.1.1 Cell lines

GBM2 cell line was already described in section 3.1.1.

E2 primary glioblastoma cell line was derived from freshly resected glioblastoma patient specimens as described in [340] and was a generous gift of Colin Watts (Cambridge). Protocols for tissue collection were compliant with the UK Human Tissue Act 2004 (HTA Licence ref 12315) and approved by the local regional Ethics Committee (LREC ref 04/Q0108/60). To obtain cancer stem cell enriched populations, E2 cell line was cultured in Neurobasal-A medium supplemented with B-27, epidermal growth factor (20 ng/ml), fibroblast growth factor (20 ng/ml), glutamine and penicillin/streptomycin. E2 glioma stem cells (E2-GSC) were then extensively characterized for their stem cell properties [341].

4.1.2 Solutions and Buffers

- Midi Prep Solution 1: 50 mM glucose, 10 mM EDTA, 25 mM Tris pH8.0
- Midi Prep Solution 2: 1% SDS, 0.2 M NaOH
- Midi Prep Solution 3: 3M KAc, pH to 4.8 with acetic acid
- TE buffer: 10 mM Tris, 1 mM EDTA, pH 8.0 with HCl

4.1.3 Other reagents

- 5-alpha chemically competent *E. Coli*, New England BioLabs
- Accutase, PAA Laboratories UK, L11-007
- B27 supplement, Invitrogen, 17504-044
- DMEM F12, Sigma
- GenElute™ Mammalian Genomic DNA Miniprep kit, Sigma
- Gibson Assembly® kit, New England BioLabs
- Heparin, Sigma, H3393-10KU
- Hu bFGF, Invitrogen, PHG0263
- Hu EGF, Invitrogen, PHG0313
- L-glutamine, Gibco

- Matrigel®, Corning, 354230
- N2 supplement, Invitrogen, 17502-048
- Pen/Strep, Gibco
- Phusion High-fidelity DNA polymerase, New England BioLabs
- QIAprep® Spin Miniprep Kit, Qiagen
- QIAquick® Gel extraction kit, Qiagen
- SOC media, New England BioLabs
- Trypsin 0.05%, Gibco

Table 4.1 List of primers

No	Name	Sequence (5'->3')
1	Nes-Left arm-FW	GATCCCCCGGGCTGCAGGCTGGGGAGATCCCCGAGGGCCCCCA
2	Nes-Left arm-Rv	GGTCTTTTCCATGGTCCTCCCCTGAGGACCAGGACTC
3	Nes-Right arm-FW	GACCATGGGAAAAGACCATCTGCCCGGCACTGG
4	Nes-Right arm-RV	CGATAAGCTTGATATCGCAGGTCACCTGGCCCAGCCTCTCTC
5	Cd133-Left arm-FW	GATCCCCCGGGCTGCAGGCTTTCCTAGGCAGAGGTC
6	Cd133-Left arm-RV	ACGAGGGCACCGGTAGCTAGCAAGATC
7	Cd133-Right arm FW	CTACCGGTGCCCTCGTACTCGGCTCC
8	Cd133-Right arm-RV	CGATAAGCTTGATATCGCCAAACCCTAGTAGCAGATATTTCC
9	mClover-FW	GAGGACGGATCCGGTGCAGGCGCCATGGTGAGCAAGGGCGA
10	mClover-RV	CCGCTTCCCTTGTACAGCTCGTCCATGCCATGTGTAATCCCG
11	T2A-Neo-FW	CTGTACAAGGGAAGCGGAGAGGGCCGCGGCAGCCTGCTG
12	T2A-Neo-RV	GCAGATGGTCTTTTCCTCAGAAGAACTCGTCAAGAAGGCGATAGAAGGC
13	mEmerald-FW	CCGGGCCCATGGTGAGCAAGGGCGAGGAG
14	mEerald-RV	CCGAGTACGAGGGCAGCGCTTCCGCTTCCGCCG
15	Neo-T2A-FW	GAGGATCTTGCTAGCTATGGGATCGGCCATTGAACAAG
16	Neo-T2A-RV	CTCACCATGGGCCCGGGGTTCTCCTC
17	mCherry-FW	TCCTCAGGGGAGGACATGGTGAGCAAGGGCGAGGAGGATA
18	mCherry-RV	CGGCCCTCTTACTTGTACAGCTCGTCCATGCCG
19	T2A-Puro-FW	GTACAAGTAAGAGGGCCGCGGCAGCCTGCTGACCT

20	T2A-Puro-RV	AGATGGTCTTTTCCTCAGGCTCCAGGTTTTCTTGTCATAC
21	Nes-gRNA-FW	GACCGCTTTTCCTAGTCCTCCCCTG
22	Nes-gRNA-RV	AAACCAGGGGAGGATAGGAAAAGC
23	Nes-FW	CAGCATGTGAATGGGGGAGT
24	Nes-RW	GCCTCTCAGCCAGAAACCAT
25	GFP-RV	CTTGTACAGCTCGTCCATGCC

4.2 METHODS

4.2.1 Cell culture conditions

GBM2 expansion was carried out as described in section 3.2.1.
E2 cells were cultured in a proliferation permissive medium composed by DMEM F-12 (Sigma), 2% B-27 supplement (Invitrogen), 1% N2 supplement (Invitrogen), 2 mM L-glutamine (Gibco), 5 ng/µl Heparin (Sigma), 20 ng/ml recombinant human bFGF (Invitrogen) and 20 ng/ml recombinant human EGF (Invitrogen), 20 UI/ml penicillin and 20 µg/ml streptomycin (Gibco).
E2 cells were cultured in adherent culture condition on Matrigel® (Corning) coated surfaces in 5% CO_2/95% O_2 atmosphere. The medium was replaced every 3-5 days in order to remove cell catabolic products and cellular debris and to supply fresh nutrients. Cells were routinely grown to confluence, dissociated using Accutase (PAA Laboratories UK) and then split 1:2 or more depending on cellular concentration.

4.2.2 Cloning of targeting constructs

CrispR/Cas9 mediated GFP N-terminal tagged CD133 (*PROM1* gene) and GFP or RFP C-terminal tagged Nestin (*NES* gene) GBM2 and E2 glioma stem cell lines were assessed.

gRNA cloning into the PSPCas9 (BB) cassette

CD133 and Nestin specific guide RNA sequences, designed using the Benchling (http://benchling.com) platform and obtained from Eurofins Genomics (No.21-22, Table 4.1), were inserted into a CrispR/Cas9 cloning site by means of the following protocol. 1 µl of gRNA forward and gRNA reverse oligos were mixed with 1 µl T4 DNA ligase buffer 10X, 1 µl T4 PNK and 6 µl H_2O. Oligos were phosphorylate and annealed using a thermocycler (Duplex program). 2 µl of the diluted reaction products (1:200) were then mixed with 1 µl PspCas9 (BB, 100 ng), 2 µl 10X FastDigest, 1 µl DTT, 1 µl ATP, 1 µl FastDigest (BpiI), 0.5 µl T7 DNA ligase and 11.5 µl H_2O. The samples were incubated in the thermocycler (Ligation program). A

PlasmidSafe reaction was then performed. 11 µl of the ligation reactions were mixed with 1.5 µl of the PlasmidSafe buffer 10X, 1.5 µl of ATP and 1 µl of the PlasmidSafe exonuclease. Samples were incubated in the thermocycler (Plasmid Safe program).

Donor plasmids cloning in pBS vector

The left and right homology arms of the donor plasmids were designed using specific *in silico* tools (Snapgene, SerialCloner). In between these homology sequences we introduced an in frame insertion of an antibiotic resistance ORF (Neomycin or Puromycin) and mEmerald, mClover (enhanced GFP mutants) or mCherry (an enhanced RFP mutant) linked via a T2A ribosome skipping sequence (Neomycin-T2A- mEmerald-CD133, Nestin-mClover-T2A-Neomycin, Nestin-mCherry-T2A-Puromycin). All the fragments were PCR-amplified using the Phusion High-fidelity DNA polymerase (NEB). Thermocycling conditions were the following: 98°C for 30 s; 30 cycles: 98°C for 5 s, 72°C for 30 s, 72°C 1 min; 72°C 5 minutes; 4°C. PCR products were then run on an electrophoresis gel and gel extracted using the QIAquick® Gel extraction kit (Qiagen). The primers used, designed through the NEBuilder® tool (available online at http://nebuilder.neb.com/) and obtained from Eurofins Genomics, are reported in Table 4.1 (No.1-20).
The sequences were joined together in a pBlueScript (pBS) vector linearized through a EcoRI restriction digest for 1 h at 37°C. Fragments were assembled using the Gibson Assembly® kit (NEB) with a 2:1 ratio of fragment to vector.

4.2.3 Bacteria transformation

50 µl of 5-alpha chemically competent *E. Coli* (NEB, genotype: *fhuA2 Δ(argF-lacZ)U169 phoA glnV44 Φ80 Δ(lacZ)M15 gyrA96 recA1 relA1 endA1 thi-1 hsdR17*), were transformed with CrispR/Cas9 vectors or donor plasmids. Briefly 2 µl of each plasmid DNA were added to bacteria. The mixtures were then placed on ice for 30 minutes, heat shocked at 42°C for exactly 30 seconds and placed again on ice for 5 minutes. 100 µl of room temperature SOC media (NEB) was added into the mixtures. Subsequently bacteria were placed at 37°C for 60 minutes in a revolving incubator and 100 µl of mixture were spread onto ampicillin (1 µg/ml) agar plates and incubated overnight at 37°C.

The day after single colonies were picked and let grow overnight in 5 ml of LB+ampicillin (1 µg/ml) media at 37°C in a revolving incubator. Plasmid DNA were then extracted using the QIAprep® Spin Miniprep Kit (Qiagen). The presence of the expected DNA sequences was confirmed by restriction digestion and sequencing (GATC service).

4.2.4 Plasmid DNA Midi-Prep

A midi-prep protocol was used to purified plasmid DNA from 5-alpha competent *E. Coli* (NEB) grown overnight in 50 ml of LB media with ampicillin (1 µg/ml). Cells were pelleted at 4000 rpm for 20 minutes, and re-suspended in 2.5 ml of Solution 1 on ice. To this, 5 ml of Solution 2 and 2.5 ml of Solution 3 were slowly added. Cells were then spinned at 4000 rpm for 10 minutes and the supernatant was poured off into a fresh tube using tissue paper as a filter to minimize the transfer of white residues. Nucleic acids were precipitated with isopropanol. Pellet was dissolved in 750 µl TE and 1 ml 5M LiCl was used to precipitate RNA. The supernatant was carefully taken off and DNA was precipitated with 2 volumes of EtOH. Samples were incubated on ice for at least 10 minutes and centrifuged at 4000 rpm for 5 minutes. Pellets were left to air-dry. DNA was then dissolved in TE, treated with 12 µg of RNAse and left at 37°C for 30 minutes. DNA was purified using 1 volume of phenol chloroform and precipitated on ice for 30 minutes using 0.1 volumes of 3M NaOAc and 2 volumes of EtOH. Samples were finally spinned down at 13000 for 5 minutes and pellet re-suspended in 100 µl TE. DNA quality and quantity were analysed using a Nanodrop® ND-1000 spectrophotometer (Thermo Scientific).

4.2.5 GSCs transfection

Donor plasmids and CrispR/Cas9 vectors were co-transfected in GBM2 and E2 GSC lines using the Neon® Transfection System (Invitrogen), with an optimized protocol (1400V, 30ms). Transfected cells at 80% confluence in a 6-well were trypsinized with trypsin 0.05% (Gibco), plated in 96-wells in selective media with antibiotic (Neomycin), monitored for single colony formation and expanded upon confluency.

4.2.6 DNA extraction

Genomic DNA from green fluorescent colonies was purified using the GenElute™ Mammalian Genomic DNA Miniprep kit (Sigma) according to the manufacturer's protocol. DNA quality and quantity were analysed using a Nanodrop® ND-1000 spectrophotometer (Thermo Scientific).

4.2.7 Genotyping PCR

In order to verify the correct insertion of the targeting constructs in the loci of interest genomic DNA extracted from green fluorescent clones was PCR-amplified using the Phusion High-fidelity DNA polymerase (NEB) and the primers listed in Table 4.1 (No. 23-28). Thermocycling conditions were the following: 98°C for 30 s; 30 cycles: 98°C for 5 s, 72°C for 30 s, 72°C 1 min; 72°C 5 minutes; 4°C. PCR products were run on agarose gel.

4.2.8 Live cell imaging

Live cell imaging was performed using an Olympus IX71 or IX73 microscope equipped with a CCD camera, temperature controller (37°C) and CO_2 (5%) incubation chamber. GSCs were plated in 2 wells chambered slides (Ibis) coated with Matrigel®. Images of multiple fields per well were collected every 5 min overnight using a dry 20x objective lens. Images were acquired using the MicroManager software and analysed by means of ImageJ software.

RESULTS

In this chapter I will present some preliminary data about the project I took part during the six months I spent in Dr Hochegger's lab (Genome Damage and Stability Center, University of Sussex, Brighton, UK). This study is aimed on setting up CrispR/Cas9 mediated GFP-tagged CD133 (*PROM1* gene) and GFP or RFP-tagged Nestin (*NES* gene) glioma stem cell lines in order to look for signs for asymmetric cell division using live cell imaging.

4.3 *PROM1* AND *NES* TARGETING CONSTRUCTS

N-terminus tagging of *PROM1* was performed in collaboration with Dr. Ann-Kristin Hov.

CrispR-Cas9 gene editing system required two constructs: a targeting construct with homology to the target gene and a plasmid expressing a site-specific single guide RNA (sgRNA) and Cas9 protein from *Streptococcus pyogenes* (SpCas9). The left and right homology arms of the CD133 targeting construct were complementary to *PROM1* 5' UTR and exon 1, respectively. As regards *NES* gene the left and right homology region were complementary to the last exon (exon 4) and the 3'UTR. In between these sequences a neomycin selection marker, a ribosome skipping motif (T2A) and mEmerald (for *PROM1*) or mClover and mCherry (for *NES*) were cloned. Two different *PROM1* sgRNA-SpCas9 plasmids, targeting two positions before exon 1, and one *NES* sgRNA-SpCas9 plasmid, targeting the stop codon, were designed. (Fig. 4.1).

The construction of the donor plasmids was done in two steps by initially amplifying the homology arms, adding an AgeI and a NcoI restriction site to the left arm of *PROM1* and *NES* respectively. These fragments were cloned into a pBlueScript vector, previously linearized by EcoRI. The constructs were then confirmed by restriction digest and Sanger sequencing.

These initial constructs were then linearized with AgeI or NcoI and used as backbone vectors for the cloning of neomycin-T2A-mEmerald, mClover-T2A-Neomycin or mCherry-T2A-Puromycin fragments. The final constructs obtained from clones of transformed 5-alpha chemically competent *E. coli* were checked again by restriction digest and Sanger sequencing (Fig. 4.2). DNA from clones which showed the right construct's sequences were chosen for further applications.

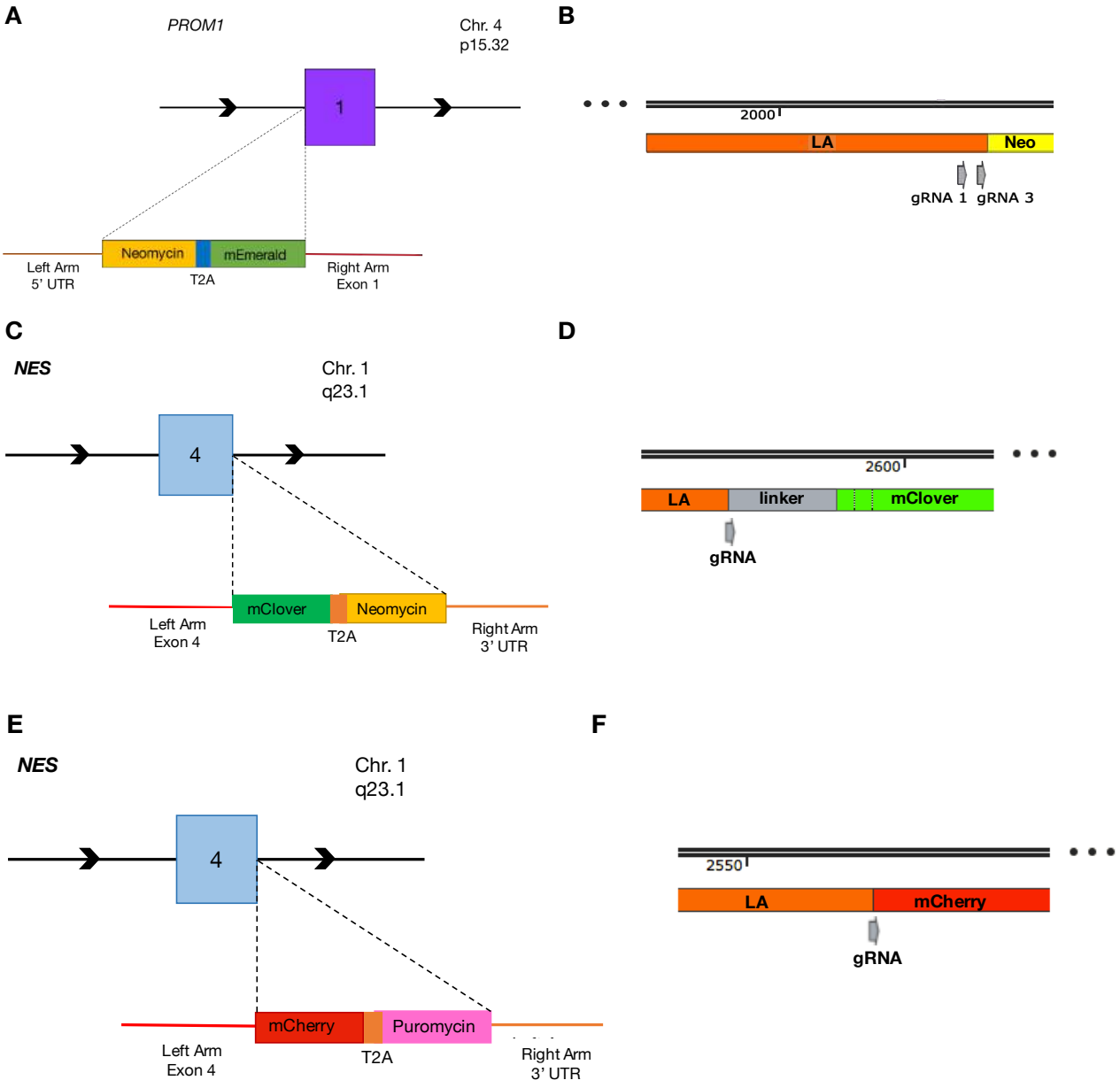

Figure 4.1 *PROM1* and *NES* gene targeting strategy. A. Schematic representation of *PROM1* tagging with a Neomycin resistance cassette, a T2A ribosome skipping motif and mEmerald sequence. **B.** Localization of the two sgRNAs in the 5' UTR of *PROM1*. **C**. Schematic representation of *NES* tagging with a mClover sequence, a T2A ribosome skipping motif and a Neomycin resistance cassette. **D.** Localization of the sgRNAs on the stop codon of *NES*. **E.** Schematic representation of *NES* tagging with a mCherry sequence, a T2A ribosome skipping motif and a Puromycin resistance cassette. F. Localization of the sgRNAs on the stop codon of *NES*.

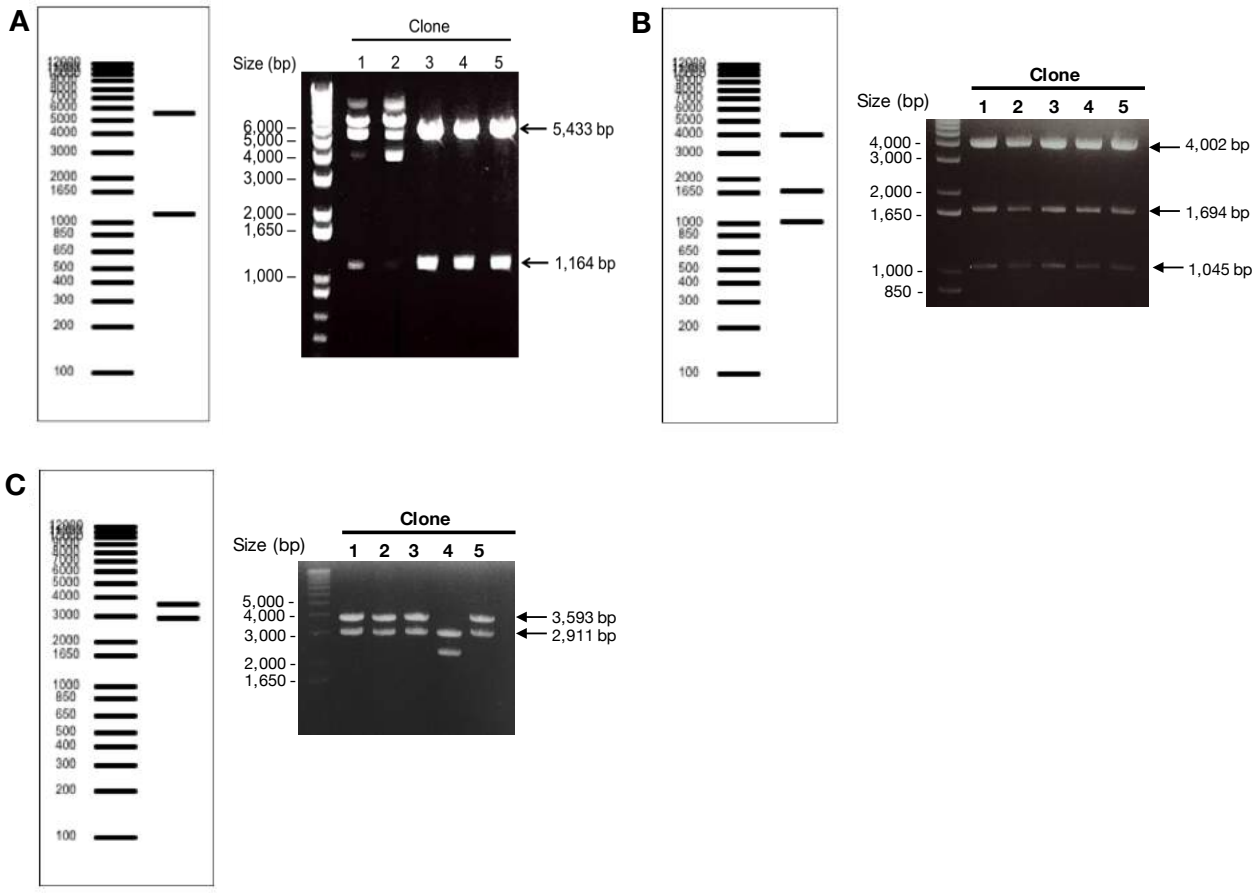

Figure 4.2 Restriction digest of *PROM1* and *NES* gene targeting constructs. A. Predicted digests and electrophoresis gel of CD133 Neomycin-T2A-mEmerald construct isolated from 5 clones of transformed 5-alpha chemically competent *E. Coli*. **B.** Predicted digests and electrophoresis gel of Nestin mClover-T2A-Neomycin construct isolated from 5 clones of transformed 5-alpha chemically competent *E. Coli*. **C.** Predicted digests and electrophoresis gel of Nestin mCherry-T2A-Puromycin construct isolated from 5 clones of transformed 5-alpha chemically competent *E. Coli*.

4.4 Neomycin-T2A-mEmerald AND mClover-T2A-Neomycin INTEGRATION ON *PROM1* AND *NES*

The CD133 and Nestin constructs were transfected with the matching sgRNAs into E2 and GBM2 cell lines using the Neon®Transfection system. Successful transfection was confirmed using a GFP expressing plasmid (Fig. 4.3).

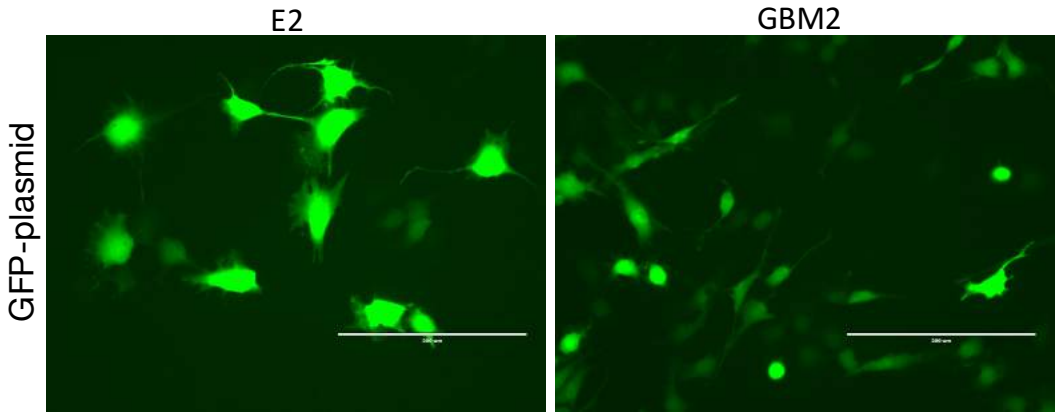

Figure 4.3 E2 and GBM2 transfection control. A GFP expressing plasmid was used. Bar = 200 μm.

Transfected cells were selected for integration of the construct using G418, a derivative of Gentamycin B. Clones began to appear after three to four weeks and some were picked for further analysis.

Clones were then checked under a fluorescence microscope for a GFP signal, and genomic extracts of the ones characterized by the presence of a green signal were purified and PCR genotyped in order to confirm the integration of the tag. The primers used are shown in Figure 4.4 A and 4.5 A. One of the two primers mapped outside of the region of interest in order to confirm the integration at the right *PROM1* and *NES* loci. E2 clone 21 and GBM2 clones 8 and 12 showed the correct integration of CD133 tagging construct (Fig. 4.4 B/C), while E2 clone 4 and GBM2 clone 21 were positive for the Nestin tagging construct (Fig. 4.5 B/C).

To better confirm the GFP tag integration a second genomic PCR was performed on positive clones, using GFP primers (Fig. 4.4 A and 4.5 A). Results are reported in Figure 4.6 and confirmed the correct integration of the tagging constructs in E2 and GBM2 positive clones.

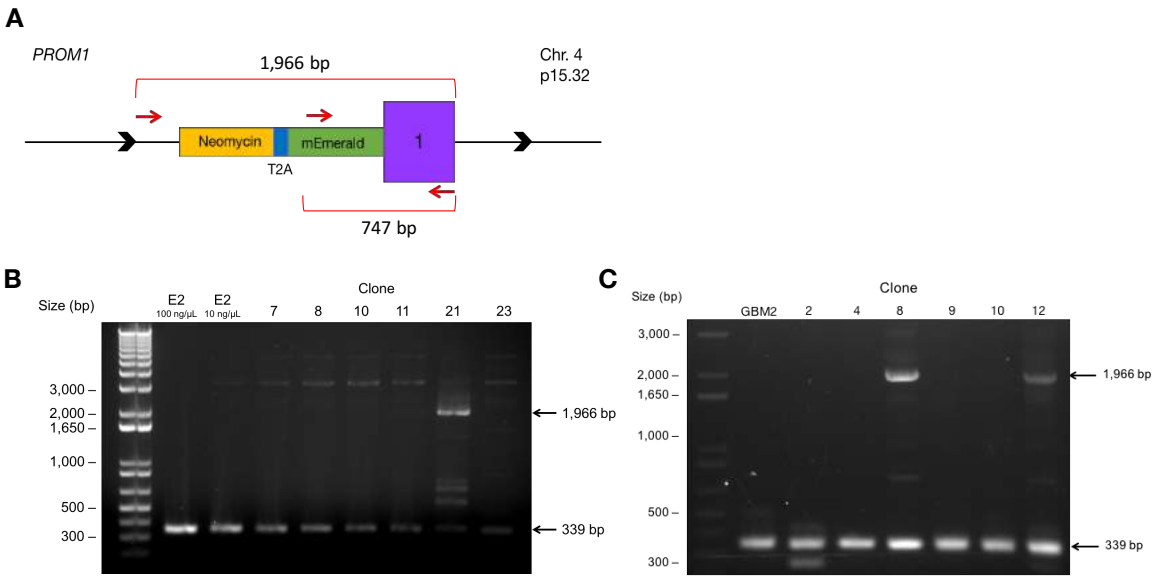

Figure 4.4 PCR genotyping of CD133 GFP-tagged green positive clones. A. Primers designed to test for tag integration on *PROM1*. Two primer pairs were designed using the same reverse primer in exon 1; one forward primer in the 5' UTR and another within the GFP-tag. **B.** PCR reactions of E2 clones using the following primer pair: 5' UTR and exon 1. Arrows indicate the sizes of fragments. The wild type expected size is 339 bp, while the size of the tagged sequence is 1966 bp. **C.** PCR reactions of GBM2 clones using the following primer pair: 5' UTR and exon 1. Arrows indicate the sizes of fragments. The wild type expected size is 339 bp, while the size of the tagged sequence is 1966 bp.

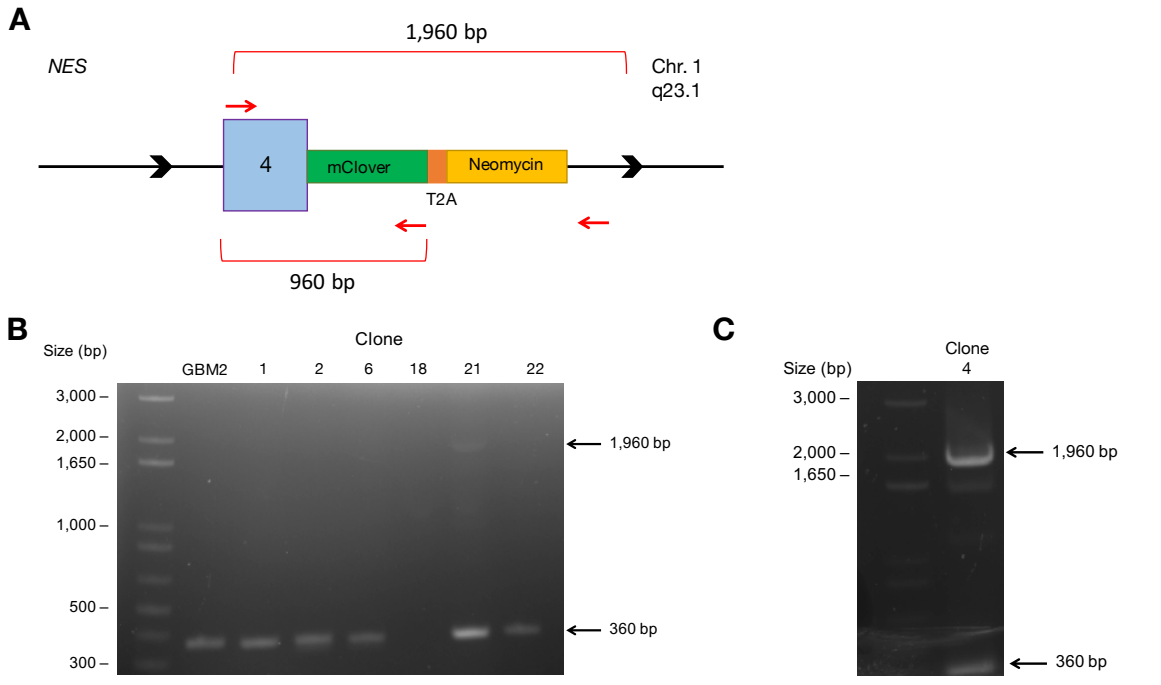

Figure 4.5 PCR genotyping of Nestin GFP-tagged green positive clones. A. Primers designed to test for tag integration on *NES*. Two primer pairs were designed using the same forward primer in exon 4; one reverse primer in the 3' UTR and another within the GFP-tag. **B.** PCR reactions of GBM2 clones using the following primer pair: exon 4 and 3' UTR. Arrows indicate the sizes of fragments. The wild type expected size is 360 bp, while the size of the tagged sequence is 1960 bp. **C.** PCR reactions of E2 clone using the following primer pair: exon 4 and 3' UTR. Arrows indicate the sizes of fragments. The wild type expected size is 360 bp, while the size of the tagged sequence is 1960 bp.

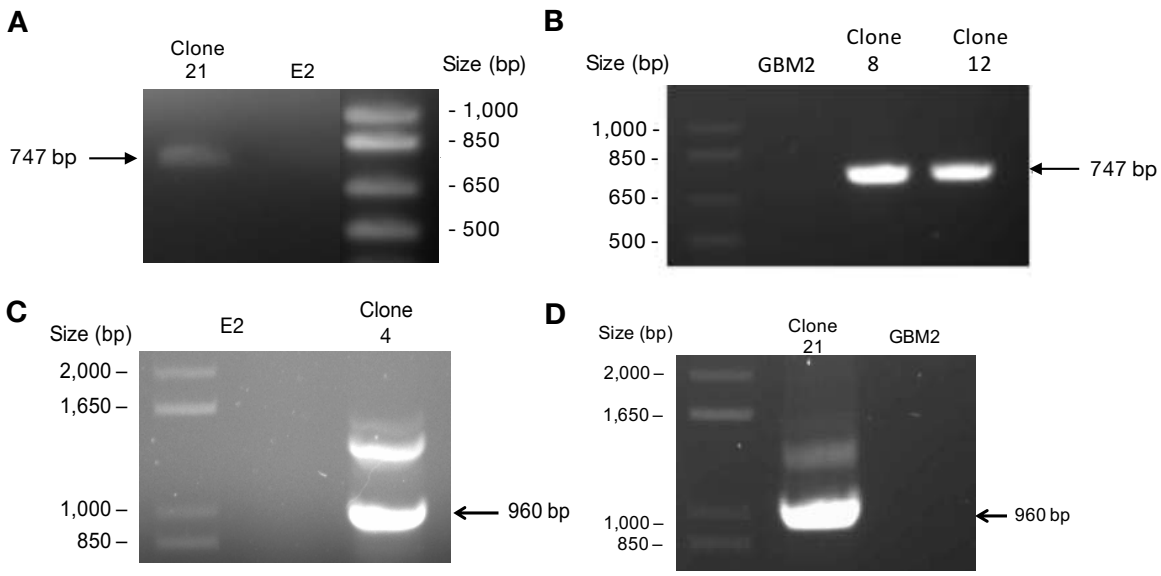

Figure 4.6 PCR genotyping with GFP primers set. A. Genomic PCR of E2 clone 21 and E2 genomic DNA as a negative control using the GFP primer set reported in Fig. 4.4 A. Expected product size was 747 bp. **B.** Genomic PCR of GBM2 clones 8 and 12 and GBM2 genomic DNA as a negative control using the GFP primer set reported in Fig. 4.4 A. Expected product size was 747 bp. **C**. Genomic PCR of E2 clone 4 and E2 genomic DNA as a negative control using the GFP primer set reported in Fig. 4.5 A. Expected product size was 960 bp. **D.** Genomic PCR of GBM2 clone 21 and GBM2 genomic DNA as a negative control using the GFP primer set reported in Fig. 4.5 A. Expected product size was 960 bp.

The expression of the GFP-CD133 fusion protein in E2 and GBM2 CD133-Neomycin-T2A-mEmerald positive clones was also tested by means of Western blot using an anti-GFP antibody.

A weak signal was detected in E2 clone 21 GBM2 clone 8 and GBM2 clone 12, but no signal in wild type E2 and GBM2 cell lines (Fig. 4.7). However, the band detected in E2 clone 21 was around 90 kDa, which is smaller than expected (125 kDa). This could be due to the nature of CD133, as there are multiple isoforms of this protein. Size differences had already been observed in GSCs and reported in literature (43). Western blot analysis of E2 and GBM2 Nestin-mClover-T2A-Neomycin positive clones are still ongoing.

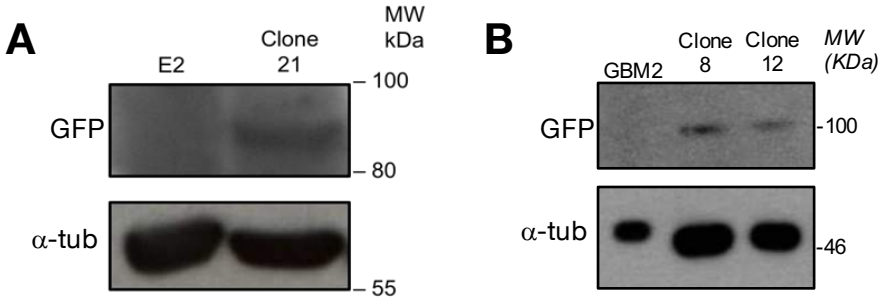

Figure 4.7 GFP-CD133 fusion protein expression analysis in E2 and GBM2 positive clones. **A.** E2 clone 21 weakly expressed GFP-CD133 fusion protein. **B.** A signal was detected in GBM2 clones 8 and 12. No signal was detected in E2 and GBM2 wild type cell lines. α-tubulin was used as a loading control

4.5 CD133 SEGREGATION BETWEEN DAUGHTER CELLS

As an E2 cell line containing a GFP-tagged CD133 has been confirmed, it was used for subsequent studies using fluorescence microscopy. It was previously shown that CD133 segregates asymmetrically during division, promoting asymmetric division of GSCs (21). The GFP-CD133 cell line was observed for 16 hours to trace cell lineages and to observe segregation of CD133. Mitotic cells were assessed using ImageJ to quantify the signal emitted from each daughter cell. Daughters with a 25% to 50% difference were classed under “slight asymmetry” and more than 50% difference was a “severe asymmetry” phenotype. Only one cell was observed to have severe asymmetry (Fig. 4.8).

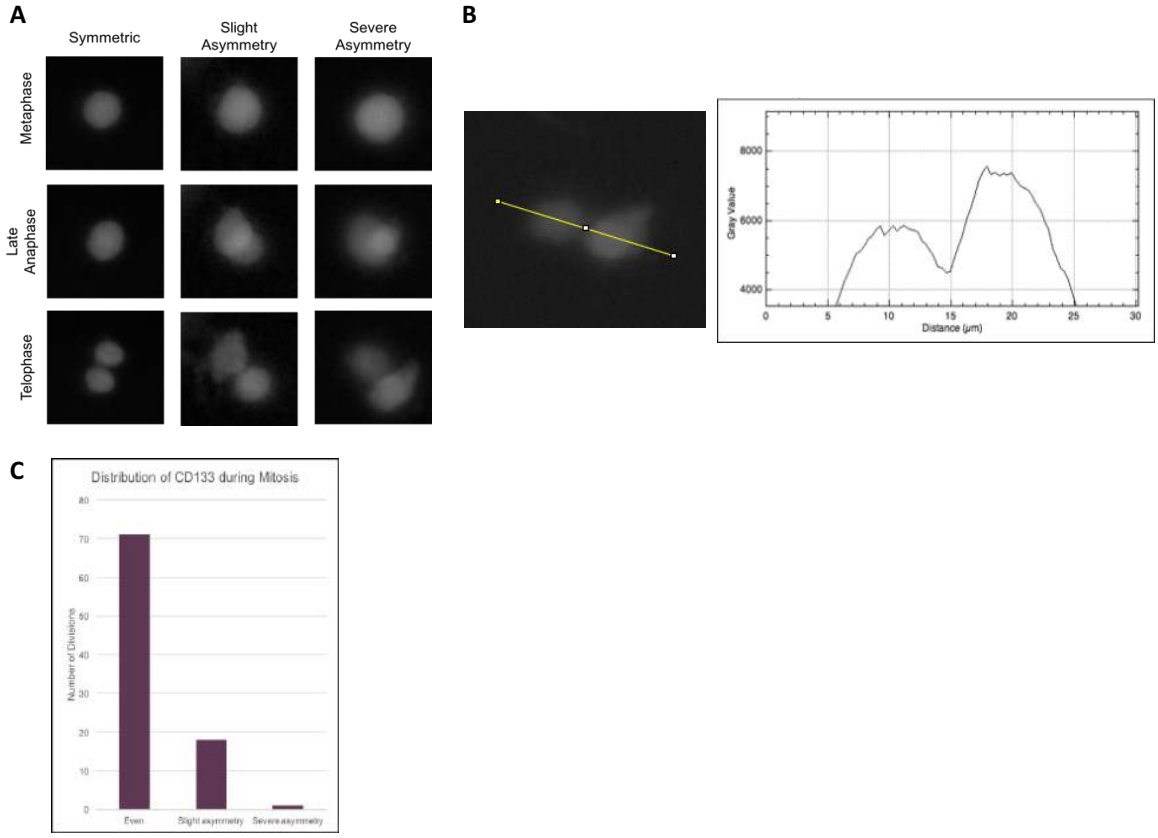

Figure 4.8 Live-cell imaging of GFP-CD133 cells. A. Cells were observed for asymmetric distribution of CD133 during mitosis. Figure shows symmetric, slightly asymmetric and severely asymmetric phenotypes during metaphase, anaphase and telophase/cytokinesis. **B.** Example of ImageJ analysis of dividing cells. Grey values are calculated and plotted against distance (µm). Peaks are compared to establish phenotypes. **C.** Bar graph of mitotic cells and their CD133 segregation phenotypes within a 16 hours movie.

An unexpected observation was the presence of a clustered CD133 signal that is being transferred between cells (Fig. 4.9). The cell sample was a mixed population of tagged and untagged cells, however, this signal is seemingly being passed on to untagged cells as well. Dubreuil et al. (44) observed membrane particles concentrated in CD133 was being released from neuroepithelial cells as a midbody, which may be an explanation of this particular phenotype.

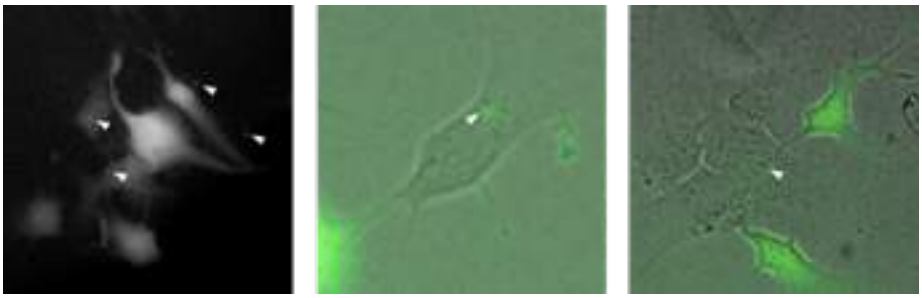

Figure 4.9 Clustered CD133 signal distribution. CD133 signal was found in non-GFP-CD133+ cells and this signal was being passed on from GFP-CD133^{+} cells.

Chapter 5
Discussion and Conclusion

Chromosomal instability in Glioma Stem Cell lines from Glioblastoma multiforme: implications for new therapeutic strategies

Glioblastoma multiforme (GBM) is the most common and aggressive primary brain tumour; the median survival of GBM patients remains about 15 months post-diagnosis, with high risk of recurrence [4]. Recent studies suggested that GBM contains a small subset of tumour cells that display stem-like features [100, 101], named glioma stem cells (GSC) or glioma initiating cells (GICs), that proved to be able to drive cancer growth, resist to chemo and radiotherapy and were responsible for tumour relapse after conventional therapies [95, 100]. Moreover, these GSC subpopulations are highly heterogeneous, hence explaining the difficulty encountered when seeking new therapeutic strategies to deplete them. Due to this high heterogeneous background, in our laboratory we have been studying for several years few GSC lines, characterizing their cytogenomic and epigenomic signature [330]. Previous cytogenetic and molecular cytogenetic analysis showed that a typical feature of GSCs is also the elevated chromosomal instability (CIN): our cell lines are characterized by various numerical and structural aberrations, deletions, amplification and loss of heterozygosity [330]. A variety of alterations have been proposed as being responsible for CIN, including defects in genes involved in the regulation of the mitotic machinery, such as the Aurora Kinases, making them a promising therapeutic target for GSCs eradication [309] [342]. Given that, the effect of Aurora kinases inhibition on GSCs has been investigated and results are reported in chapter 3.

Interestingly it has been demonstrated that GSCs are able to not only recapitulate the pathophysiology of the original tumour from which they were isolated, but also to produce the corresponding diversity of cell populations within the tumour mass in experimental models. Thus, a single GSC is virtually able to both maintain a pool of self-renewing stem cells and produce differential progeny through a combination of asymmetric and symmetric cell division.

In particular, asymmetric division is the key to maintaining a hierarchy within GBM tumors and, for this reason, improved understanding of this phenomenon may lead to the development of preventative treatments or improved therapeutic through the identification of novel targets that are involved in the control of asymmetric cell division.

In 2011 Lathia and colleagues, using fixed cells and fluorescent tagging of CD133 with antibodies, demonstrated that CD133 and Numb could be asymmetrically segregated [257]. In chapter 4 I presented some preliminary data I collected during

the six months I spent in Dr Hochegger's lab (Genome Damage and Stability Center, University of Sussex, Brighton, UK), where I took part in a project aimed on setting up CrispR/Cas9 mediated GFP or RFP-tagged CD133 (*PROM1* gene) and Nestin (*NES* gene) glioma stem cell lines in order to look for signs for asymmetric cell division using live cell imaging.

Effect of Aurora kinases inhibition on GSCs

In chapter 3 of the thesis I showed several data I collected during my PhD program performed in the Medical Genetics laboratory of the University of Milano-Bicocca, concerning the effect of Aurora kinases inhibition on five GSC lines (GBM2, G166, G179, GliNS2 and G144) from GBM. Treatment of GBM should be focused on glioma stem cell subpopulation, as it is considered the real driving force for tumour initiation, progression and relapse, and GSCs lines provide a valuable model for *in vitro* drug-testing.

Several studies demonstrated that CIN can be considered a hallmark of human neoplasms even if the exact mechanisms and contributions of CIN in cancer has been still elusive. A variety of alterations have been proposed as being responsible for CIN, including defects in genes involved in the regulation of the mitotic machinery, such as the Aurora Kinases. Aurora kinases have been shown to be frequently altered in a wide range of tumours. In particular, Aurora A gene has been found to be amplified in human gliomas, while Aurora B overexpression has been correlated with worst prognosis and higher invasiveness in GBM [309, 315].

Starting from this preliminary data I decided to first of all investigate the expression level of Aurora kinases in our GSC lines, using for normalization a foetal neural stem cell line. According to what has been reported in literature, Aurora kinase A and B were upregulated in all the GSC lines, while Aurora kinase C, whose role has been deeply documented in meiosis, was generally downregulated. Interestingly the *AURK* expression levels generally did not correlate with the copy number alterations detected by means of array-CGH, suggesting transcriptional or post-transcriptional mechanisms, such as the increased transcriptional efficacy or the reduced mRNA turnover might play a key role.

Subsequently I analysed the Aurora A and B protein levels in order to evaluate if a variability of Aurk protein expression may be identified in the different GSC lines. The AurkA and B expression levels were similar in four out of five cell lines. Only

GBM2 showed an increased expression of both Aurora kinases compared to the other cell lines.

As accumulating evidence suggests that overexpression of *AURK* induces chemotherapeutic resistance and regulates several key signalling pathways associated with cell proliferation, cell survival, cell migration and invasion, and cell death in various types of cancer cells, I decided to investigate the effect of Danusertib, a small ATP competitive molecule 3-aminopyrazole derivative, with strong activity against all the Aurora kinases, on our GSCs evaluating different parameters. Results showed that response to increasing Danusertib concentrations (5-50-200-500-1000 nM) was heterogeneous among GSC lines. Cell metabolic activity and viability were significantly reduced only in two GSCs out of five (GBM2 and G179), which were indicated as sensitive to Danusertib.

The analysis of cell and nuclear morphology highlighted in these two cell lines the presence of large multinucleated cells and an increase in the number of polymorphic nuclei and micronuclei starting from Danusertib 500 nM. Hence I selected this drug concentration for the subsequent analysis. In order to evaluate if the morphological alterations mirrored variations in the chromosomes content we analysed the cells ploidy by means of chromosome spreads and conventional cytogenetic techniques. Exposure to Danusertib 500 nM for 48 hs induced the appearance of metaphase with higher ploidy in all the GSCs analysed, even if the increase in the cell chromosomes content was more evident in GBM2 and G179 cell lines. These results were further supported by live cell imaging analysis, which showed that in both GBM2 and G166 cell lines, which showed a different sensitivity to Aurora inhibition, Danusertib exposure led to an evident increase in the percentage of non cytokinetic cells.

All these findings confirm previously published data, which demonstrated that Danusertib was able to induce cell cycle inhibition and endoreduplication in different cancer cells. As a matter of fact, several studies highlighted a substantial increase in DNA content with 4N or even >4N cells subpopulations indicating that the dominant phenotype, we also observed in our GSCs, is mainly related to Aurora B inhibition [324].

As an alteration of the cell ploidy was observed in all the GSC lines and, at the same time, Danusertib seemed to present an effective inhibitory action in both sensitive and non-sensitive ones, as demonstrated by the downregulation of Aurora kinases

auto phosphorylation detected by means of immunofluorescence assay, I wondered if the different response to Danusertib, detected also by means of clonogenic assay and mitotic index determination, was due to different mechanisms.

Intriguingly an explanation for cells responding differentially to an Aurora kinase inhibitor has been recently suggested to be depending on the integrity of the p53-p21–dependent post-mitotic checkpoint as assessed in different tumour cell lines [343]. However, several studies analysing whether p53 status influences response to AurkA inhibition, yield conflicting results [344].

Hence, to address the question whether the *TP53* status could be the reason for the different cellular phenotype observed, we examined the *TP53* mutational status in our GSCs, performing a Sanger sequencing of the hot spot mutational region of the gene of interest.

Interestingly all the cell lines carried missense mutations in the DNA-binding region of the protein, except for GliNS2 cell line which was not affected by any mutation in *TP53*. This finding does not support a role of *TP53* status in determining the observed differential sensitivity of GSCs to Aurora inhibition.

Subsequently I determined the cell cycle profile of our GSCs by means of Western blot evaluation of mitotic markers levels and immunofluorescence detection of the percentage of cells in G1, G2, S and M phases, in order to evaluate if the different response to Danusertib could be due to a different cell cycle distribution. Interestingly sensitive and resistant GSCs revealed a completely different cell cycle distribution. Moreover, the discrepancy observed between Western blot and immunofluorescence analysis can suggest the alteration of other mitotic proteins, such as APC/C, which could induce the unusual mitotic markers expression levels.

In order to better characterize the fate of GSCs after Danusertib exposure I evaluated the DNA integrity. I observed that Aurora inhibition did not induce any DNA fragmentation, suggesting that there could be an activation of a caspase-independent cell death or a senescent pathway. Senescence is an irreversible terminal growth arrest that occurs as a result of cellular stress or DNA damage. A wide variety of anticancer agents have been shown to induce accelerated senescence in tumour cells [345, 346]. Senescent cells generally display the enlarged and flattened morphology with increased activity of SA-β-galactosidase. A number of studies (using a variety of different chemotherapeutics in preclinical models) have also shown that senescence induction contributes directly to the

antitumor effect of chemotherapeutics *in vivo* [347, 348]. Two additional studies have directly shown that senescence induction leads to tumour regression [349], with a likely candidate for this regression being the host immune system [350]. In the clinic, existing data linking chemotherapy to senescence is rare; in fact, I could only find one report linking clinical samples to a senescent phenotype [351]. In this report, frozen archival breast tumours from patients receiving neoadjuvant chemotherapies were found to stain positive for SA-β-gal activity (41% compared with 10% on non treated tumours).

Starting from these evidences, I evaluated β-galactosidase levels in GBM2 and G166 cell lines, baseline and after 48 hs of treatment with 500 nM of Danusertib. I observed a significant increase in the percentage of senescent cells in GBM2 cell after drug exposure as judged by increased β-galactosidase staining.

The senescence phenotype in these cell lines is intriguing and reminiscent of published results. Several studies showed that, after treatment with Aurora kinases inhibition, cancer cells displayed a serial of senescent morphological and functional changes such as enlarged and flattened morphology, that we observed also in our cell lines, increased levels of p21 protein and enhanced SA-β-gal staining, suggesting that instead of apoptosis, senescence might be the mainly terminal outcome of Aurk inhibition in some tumour types [352].

Interestingly our results concerning cell ploidy showed also that the cell lines with higher sensitivity for Aurora kinase inhibition, GBM2 and G179, were characterized by a higher ploidy compared to the less sensitive ones. This data reminds previously published studies, which highlighted that increase in polyploidy correlated with increased sensitivity to Aurora inhibition and induction of senescence [341].

A straight forward explanation for this result could be the presence of a ploidy threshold that is intolerable even for p53 negative cell lines. A prediction from this hypothesis would be that the resistant cell lines should also undergo senescence after repeated rounds of Aurora inhibition leading to steady increases in ploidy. Hence, I investigated the correlation between GSCs Danusertib sensitivity and the ploidy level in order to find out if there is a threshold of polyploidization that GSCs have to reach to become sensitive to Aurora kinases inhibitors. G166 cell lines, one of the most resistant cell lines to Aurora kinases inhibition, were subjected to multiple round of Danusertib exposure. At different time point a β-galactosidase assay was performed and ploidy estimated by means of FISH on interphase nuclei.

Intriguingly a promising correlation between ploidy and Aurora kinase inhibitor sensitivity was found, suggesting that the analysis should be extended to a higher number of GSCs derived from GBM patients. This would allow us to investigate if ploidy could be used in the future as a marker to classify patients for a more personalized therapy.

If such a threshold will be confirmed we would like to better investigate the mechanism of p53 independent senescence induction, characterizing the senescent phenotype of GSCs after Danusertib exposure, through the analysis of different markers of senescence and the identification of pathways involved in this process, considering that these cells present also inactivating *TP53* mutations.

Although β-galactosidase assay is currently the standard for detecting senescent cells, several conditions, such as high cell confluence can also stimulate SA-β-Gal activity, leading to many false positives. For this reason, it would be appropriate to evaluate more senescence markers after Danusertib exposure. First of all, p16 and Rb expression levels should be assessed as stress-induced senescence works mainly through the activation of p16, which acts in a telomere length–independent way. Moreover, the formation of senescence-associated heterochromatic foci (SAHF) and Promyelocytic leukemia protein (PML) may be monitored. Finally, it would be useful to detect the expression levels of few soluble signalling factors (interleukins, chemokines, and growth factors) (i.e. IL6, IL8, IL13, bFGF, VEGF), secreted proteases (i.e. MMP-1, -3, -10, -12, -13, -14), and secreted insoluble proteins/extracellular matrix (ECM) components (i.e. fibronectin, collagen, laminin, nitric oxide), which constitute the senescence-associated secretory phenotype (SASP).

Intriguingly recent studies have also shed light on the correlation between autophagy and the mitotic senescence transition. Autophagy is a genetically regulated program responsible for the turnover of cellular proteins and damaged or superfluous organelles. This evolutionarily conserved process is characterized by the formation of double membrane cytosolic vesicle, called autophagosomes, which sequester cytoplasmic content and deliver it to lysosomes. Previous studies demonstrated that an increase in misfolded proteins caused by aneuploidy/polyploidy-induced proteomic stress could be at the origin of proteotoxic stress, leading to the activation of an autophagic process. Hence, autophagy is meant to be a new effector mechanism of senescence, important for the rapid

protein remodelling required to make the efficient transition from a proliferative to a senescent state [353]. Therefore, in the future, it would be interesting to investigate the expression levels of autophagic markers, such as LC3, which localizes to the membranes of autophagosomes, in order to investigate if the autophagy mediates the senescent phenotype induced by Danusertib exposure.

Characterization of GSCs division mode

In chapter 4 of the thesis I presented some preliminary data about the setting up of CrispR/Cas9 mediated GFP-tagged CD133 (*PROM1* gene) and Nestin (*NES* gene), two GSCs markers, glioma stem cell lines in order to look for signs for asymmetric cell division using live cell imaging. As asymmetric division has been demonstrated to be one of the key factor involved in maintaining a hierarchy within GBM tumours and GSCs population is thought to be the cause for reoccurrence and treatment resistance, it would be important to understand how and when these cells divide asymmetrically. Previous studies have already demonstrated that a combination of asymmetric and symmetric cellular divisions allows GSCs to both expand the tumour mass and produce differential progeny. In particular evidence of this was presented in an in vitro study by Lathia et al. who used single cell lineage tracing analysis of GSCs isolated from human surgical glioma specimens, in order to determine the mode of GSCs division. This study revealed that GSCs predominantly perform symmetric cell divisions under expansion conditions, functioning to build up the bulk of the tumour, whilst completing principally asymmetric cell divisions under growth factor deficient conditions [257]. In this latter case CD133 was asymmetrically segregated between the two daughter cells, as determined by mitotic paired cell analysis. However, all these previous experiments were performed using fixed cells and fluorescent tagging of CD133 with antibodies. This method might not be the most reliable one, as there have been numerous concerns about CD133 antibodies and epitope expression. Hence, we decided to first of all set up GFP-tagged CD133 (*PROM1* gene) GSC lines and use live-cell imaging for lineage studies in order to observe this marker's distribution and progression in real time. Subsequently we also decided to set up GFP and RFP-tagged Nestin GSC lines in order to study in real time the distribution of another typical stemness marker. The use of different fluorescent protein to tag *PROM1* and *NES* genes will

allowed us to co-transfect the GSCs with different gene constructs and study, at the same time, the distribution of different markers in mitotic cells.

In order to obtain a GFP or RFP Knock in at the *PROM1* or *NES* loci we used CrispR/Cas9 mediated genome engineering. A number of genome editing technologies have emerged in recent years, including zinc-finger nucleases (ZFNs), transcription activator-like effector nucleases (TALENs) and the RNA-guided CrispR/Cas nuclease system. The first two technologies use a strategy of tethering endonuclease catalytic domains to modular DNA binding proteins for inducing targeted DNA double strand breaks (DSBs) at specific genomic loci.[354].

By contrast the prokaryotic Clustered, regularly interspaced, short palindromic Repeats (CrispR) and the CrispR-associated system (Cas) is a very attractive alternative since it is the only genome engineering tool described so far that relies on Watson-Crick base pairing rather than the potentially less specific protein-DNA interaction [355]. The CrispR/Cas system is derived from bacteria and archaea, where it is used as an innate immune strategy to inactivate foreign intruding nucleic acids [356]. The CrispR locus consists of short palindromic repeats and short interspersed sequences of foreign DNA. Upon transcription, they serve as guide RNA (gRNA) to identify foreign DNA and target it for inactivation by nuclease-mediated cleavage. The CrispR/Cas9 type II system of *Streptococcus pyogenes* has been optimized and successfully used in vertebrate cells to edit genomes [357]. Similarly to ZFNs and TALENs, Cas9 promotes genome editing by stimulating a DSB at a target genomic locus. The DSBs activates repair through error-prone non homologous end joining (NHEJ) or homology-directed repair (HDR). In the absence of a template, NHEJ is activated, resulting in insertions and/or deletions (indels) that disrupt the target loci. In the presence of a donor template with homology to the targeted locus, the HDR pathway operates, allowing for precise mutations or gene knock in to be made. However, Cas9 offers several potential advantages over ZFNs and TALENs, including the ease of customization, higher targeting efficiency and the ability to facilitate multiplex genome editing [358].

In particular, in our study we easily designed a donor plasmid, with two homology arms on each side around 1kb, flanking the desired target sequences (*PROM1* N-term or *NES* C-term) and an all-in-one vector system expressing Cas9 and the gRNA, selected using specific web-based tools in order to improve off-target

specificity. The vectors were used to successfully transfect and gene target GSC lines, as highlighted by genomic PCR and Western blot analysis.

Interestingly live cell imaging analysis of GFP-tagged *PROM1* E2 cell line revealed that CD133 was expressed in each daughter cell and only slight asymmetric distribution was observed. An unexpected observation was the appearance of small particles expressing CD133 that were being passed on from cell to cell, including cells that were not expressing GFP-CD133. We speculated that these particles could be midbodies. The midbody is a singular organelle formed between daughter cells during cytokinesis and required for their final separation. Midbodies persist in cells long after division as midbody derivatives (MB^ds). Interestingly Kuo et al. showed that MB^ds were inherited asymmetrically by the daughter cell with the older centrosome. They selectively accumulated in stem cells, induced pluripotent stem cells and potential cancer 'stem cells' *in vivo* and *in vitro*, by evading autophagosome encapsulation. In neuroepithelial cells, midbodies were also found to be enriched in CD133. On the contrary differentiating cells and normal dividing cells did not accumulate MB^ds and possessed high autophagic activity. MB^d enrichment enhanced reprogramming to induced pluripotent stem cells and increased the *in vitro* tumorigenicity of cancer cells. These results indicate unexpected roles for MB^ds in stem cells and cancer stem cells, suggesting that they might contribute to the cell fate determining. However, more investigations are certainly required [359].

For the live cell analysis cells were always kept in a stemness promoting media. It would be interesting to trace these cell using also different culture conditions, which might mimic the extracellular environment which can be found *in vivo*. In particular, the role of a perinecrotic and hypoxic niche has been well studied in the GBM development. Astrocytomas, in particularly GBM, commonly contain areas within the centre of the tumour that are hypoxic due to the inadequate expansion of blood vessels for the nutritional needs of the neoplastic mass. It is thought that these hypoxic regions enrich the tumour for GSCs, in a similar manner to the normal brain, which under hypoxic conditions is enriched for neural stem cells. This is supported by the fact that GSCs have been found to be most prevalent within the centre or inner core of GBM tumour masses, where hypoxic environments are commonly found. Moreover, CD133 expression increases when GBM cells are cultured in 7% oxygen, compared with 20% oxygen [360].

As the single CD133 and Nestin CrispR-Cas9 gene targeting method seemed to be efficient in GSCs, a multiplex genome editing co-transfecting different stemness and differentiation markers may be performed. Among these Numb and GFAP are noteworthy.

Previous data suggested that normal Numb function and distribution is required for asymmetric cell division of GSCs, which may inhibit excessive proliferation of this population, but may also contribute to treatment resistance and tumour propagation in astrocytomas [360].

Another category of protein, which has been given little attention in the asymmetric division process, is intermediate filaments. Interestingly using immunofluorescence (IF) and videomicroscopy, Guichet et al. demonstrated that GFAP can be asymmetrically distributed during division. Similar observations were made in non tumoral neural stem cell cultures. This unequal repartition of GFAP indicate that it possibly plays a role in the asymmetric division process and cell fate regulation [361].

Finally Knock-in reporter cell lines would be a useful approach not only for *in vitro* 2D live cell imaging but also for 3D model, which will allow to evaluate the invasive and proliferative behaviour of GSCs in a structure that resemble more closely the original tumoral niche, and *in vivo* studies.

In vivo fluorescence-based imaging system, could be used to detect the distribution of stemness/differentiation markers tagged GSCs and a broad range of disease-related biomarkers, such as tumour volume, vascularity, hypoxia and MMP (metalloproteinase) activity.

Conclusion

Glioblastoma multiforme is one of the most fatal and least successfully treated solid tumours despite aggressive treatments. This research project aimed to address new therapeutic strategies GSC-targeted investigating two main aspects of this research area: the first one was to better characterize the effect of a pan Aurora kinases inhibitor (Danusertib) in GSCs; the second one was aimed at studying the mechanisms by which GSC are able to both maintain a pool of self-renewing and highly invasive stem cells and produce differential progeny.

As regards the first aim of the project, the study of the efficacy of the Aurora kinases inhibitor Danusertib in GSCs could identify new therapeutic targets.

The clinical potential for Aurora kinases inhibitors has recently been highlighted. In particular, in phase I and II studies, Danusertib was generally well tolerated, neutropenia being one of the most commonly observed hematologic toxicities. Future clinical investigation should focus on identifying patient subsets who might benefit most from treatment. Factors that could determine sensitivity could include the kinase selectivity profile of the drug, the proliferation rate of the tumour (that is, the number of mitotic cells exposed to Aurora kinase inhibition), the complexity of the genotype of the tumour and the ploidy status. In this respect, the correlation between GSC ploidy status and Aurora kinases inhibitor sensitivity we observed, may play an important role in the finding of new markers which enable to classify patients for a more personalized therapy. The combination with existing DNA damaging agents should also be a priority for future trials as it is likely that the optimal use of Aurora kinase inhibitors will be in combination with cytotoxic agents already in use. Finally, the characterization of the senescent/autophagic phenotype of GSCs after Danusertib exposure will shed light on the pathways involved in this process.

As regard the second aim, the evaluation of GSC proliferation and invasive behaviour will increase our understanding of the biology of this aggressive brain tumour, allowing the identification of new potential therapeutic targets and the design of ever more efficacious anticancer treatments. The use in the future of different culture models (2D, 3D an *in vivo* xenograft) will provide tools to analyse intrinsic cellular characteristics as well as those induced by microenvironmental factors. The comparison between 3D culture system and *in vivo* models might also allow us to evaluate the possibility of replacing animals for a portion of the pre-clinical investigational studies.

Chapter 6
Supplementals

Chromosomal instability in Glioma Stem Cell lines from Glioblastoma multiforme: implications for new therapeutic strategies

Table S1 MTT Statistical analysis. p-values (t-test) of the effects of Danusertib on cell metabolic activity (MTT assay). p-values are referred to the specific treatment compared to the respective untreated cells

Dose	5 nM			50 nM			200 nM			500 nM			1000 nM			5000 nM		
Time (hs)	24	48	72	24	48	72	24	48	72	24	48	72	24	48	72	24	48	72
GBM2	0,001	0,001	0,001	0,001	0,001	0,001	0,001	0,001	0,001	0,001	0,001	0,001	0,001	0,001	0,001	0,001	0,001	0,001
G179	ns	ns	0,001	0,05	0,001	0,001	0,001	0,001	0,001	0,001	0,001	0,001	0,001	0,001	0,001	0,001	0,001	0,001
G166	0,05	0,05	0,001	0,05	0,01	0,001	0,001	0,01	0,01	0,001	ns	0,001	0,01	ns	0,001	0,001	0,001	0,001
GliNS2	ns	ns	0,01	ns	0,01	0,001	ns	0,001	0,001	ns	0,001	0,001	ns	0,001	0,001	0,001	0,001	0,001
G144	ns	0,001	ns	ns	0,001	0,001	ns	0,001	0,001	0,05	0,001	0,001	0,05	0,001	0,001	ns	0,001	0,001

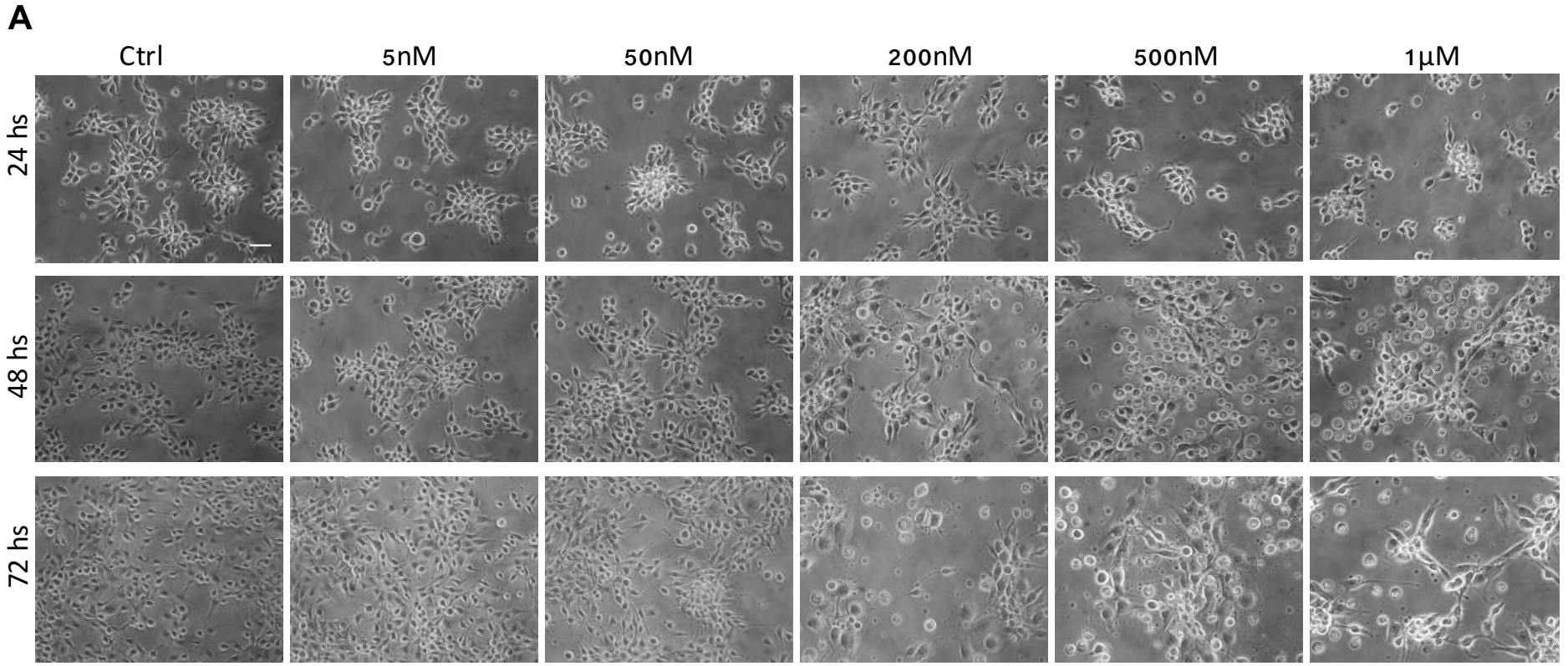
A
Ctrl
5nM
50nM
200nM
500nM
1µM
24 hs
48 hs
72 hs

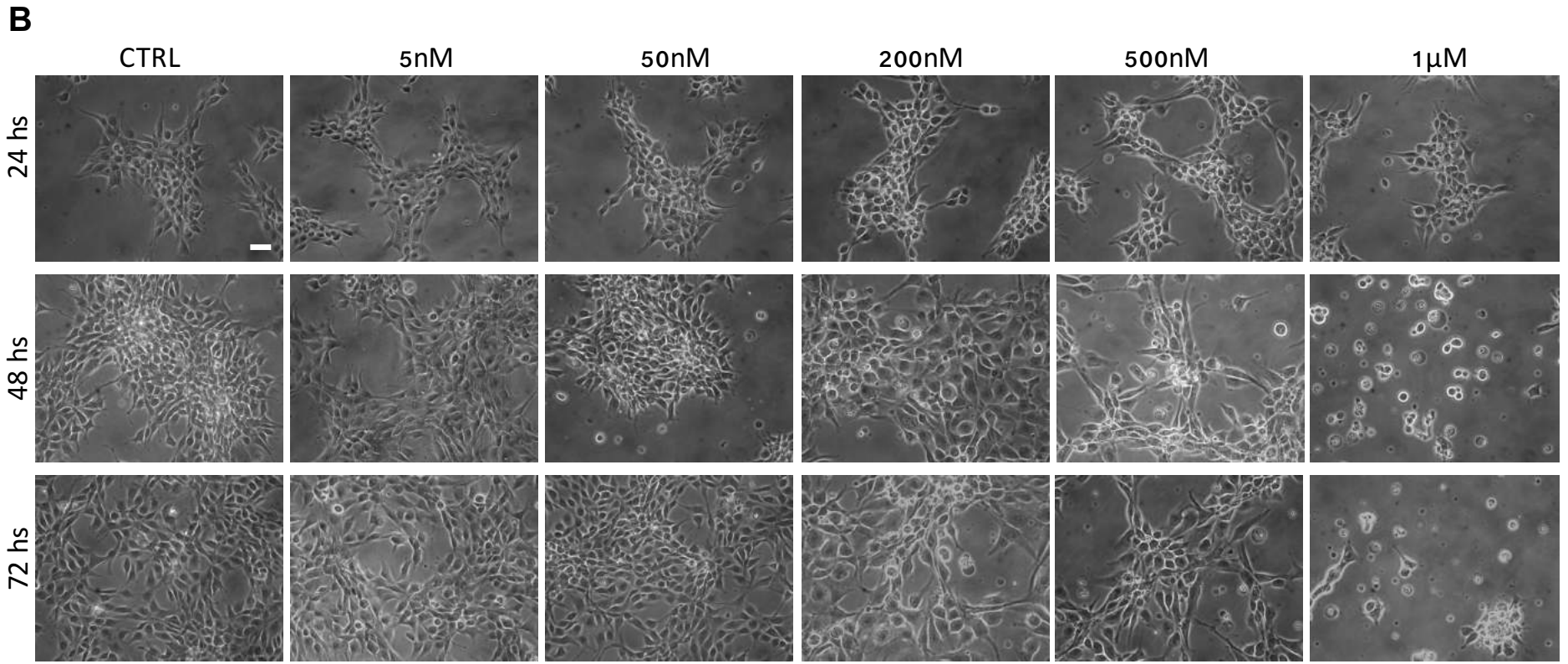
B
CTRL
5nM
50nM
200nM
500nM
1µM
24 hs
48 hs
72 hs

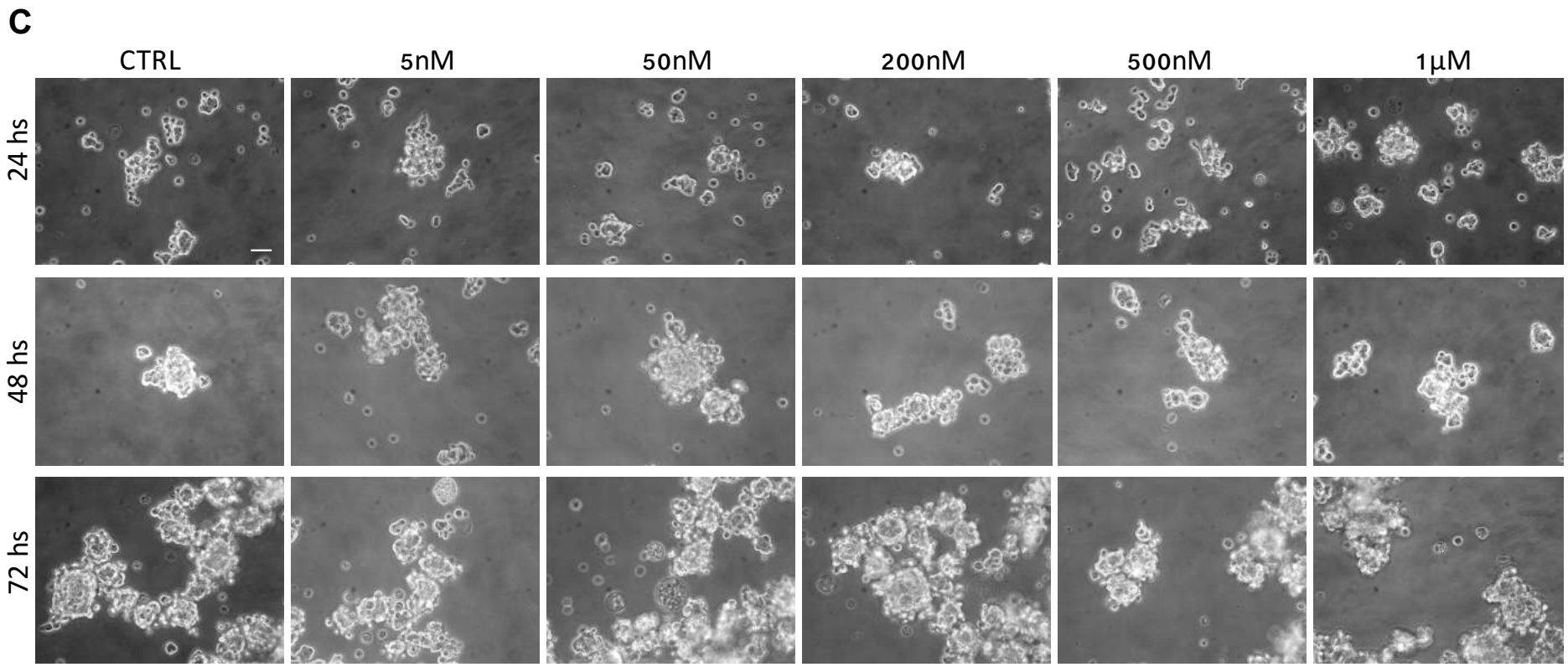
C
CTRL
5nM
50nM
200nM
500nM
1µM
24 hs
48 hs
72 hs

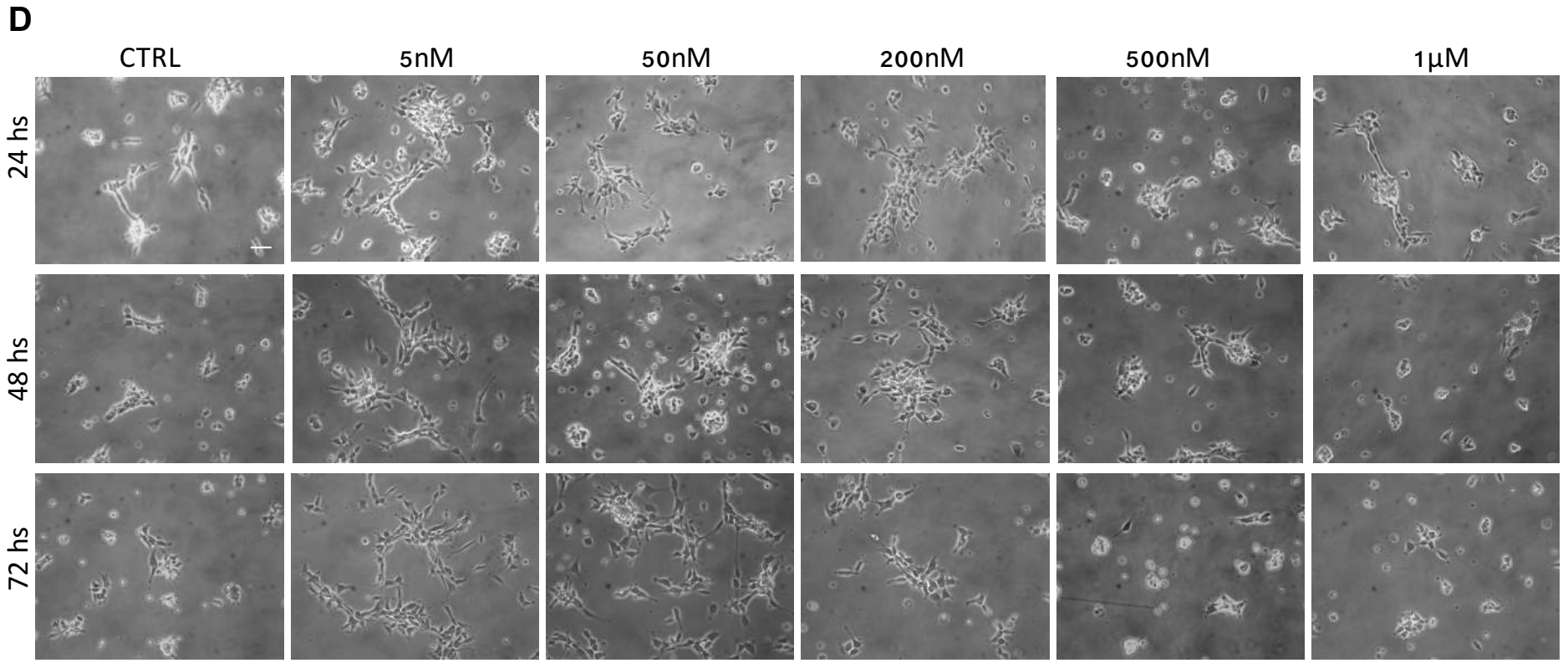
D
CTRL
5nM
50nM
200nM
500nM
1µM
24 hs
48 hs
72 hs

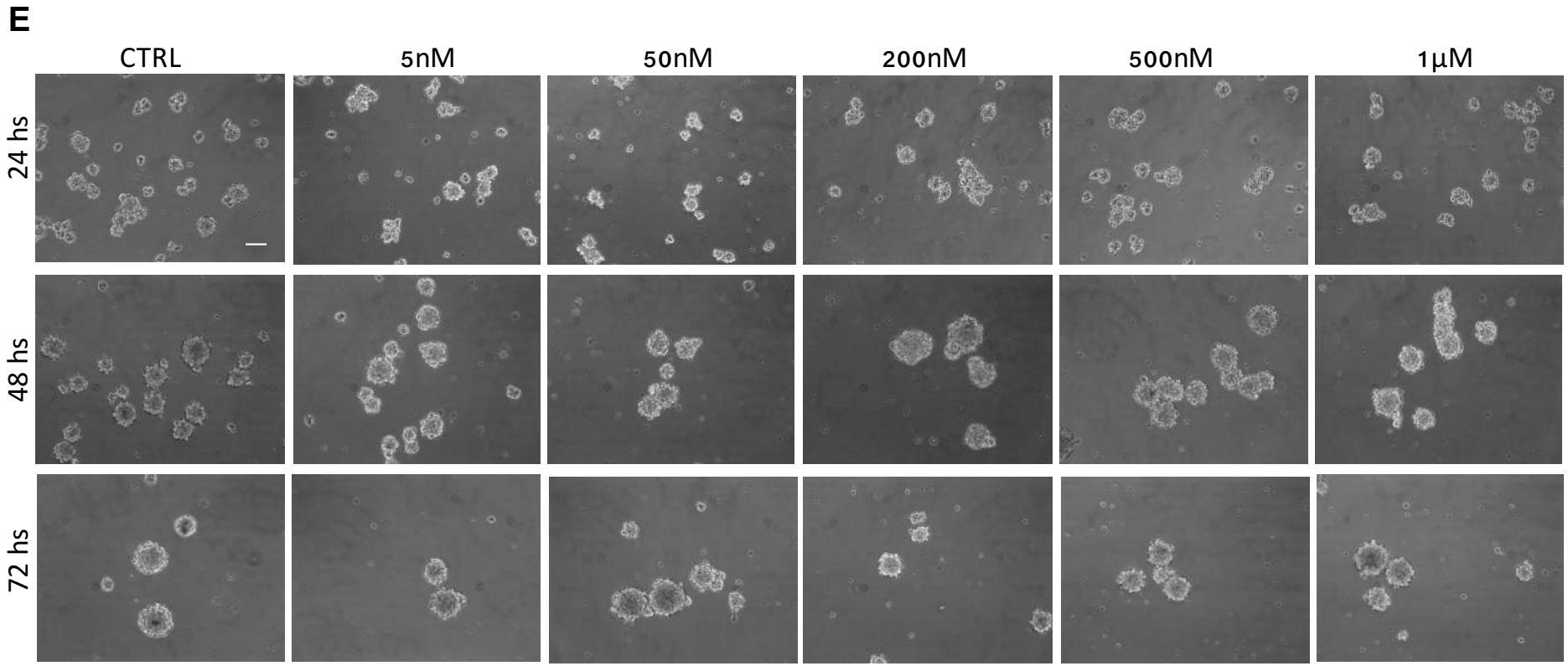

Figure S1 Morphological analysis after Danusertib treatment. Cell morphology was evaluated after treatment with different Danusertib concentrations (5-50-200-500-1000 nM) for 24, 48 and 72 hs. **A.** GBM7 **B.** G166 **C.** G179 **D.** GliNS2 **E.** G144 cell lines. Scale bar = 100 μm

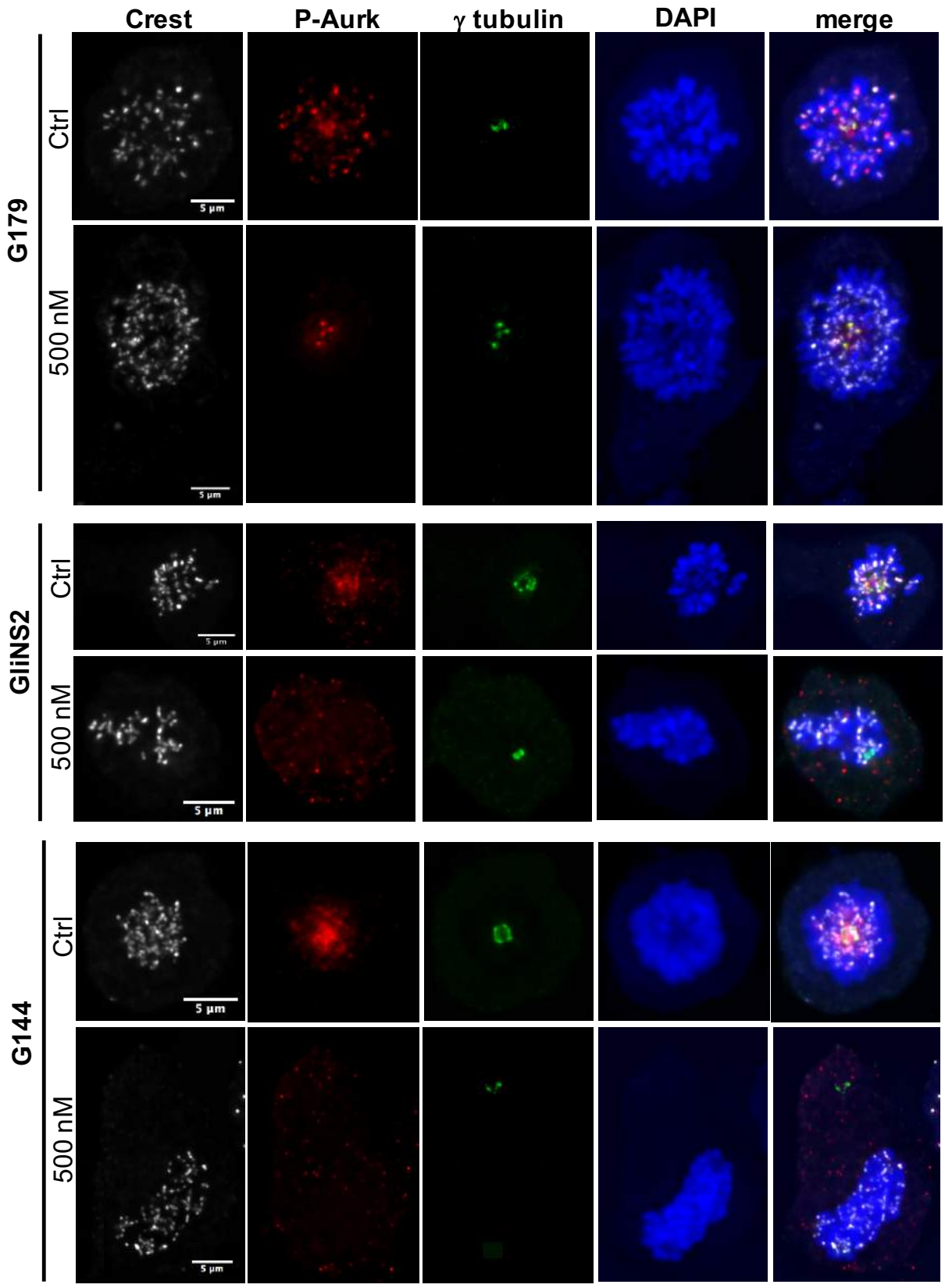

Figure S2 Danusertib induces a reduction of phosphorylated Aurora kinases in GSCs. Representative images of GSCs lines (G179, GliNS2 and G144) untreated or treated with Danusertib 500 nM for 48 hs, synchronized with STLC and stained for Crest (white), phospho-Aurora kinases (red), γ tubulin (green) and DAPI (blue)

REFERENCES

1. Buckner JC, Brown PD, O'Neill BP, Meyer FB, Wetmore CJ, Uhm JH: Central nervous system tumors. Mayo Clin Proc 2007, 82(10):1271-1286.
2. Gu J, Liu Y, Kyritsis AP, Bondy ML: Molecular epidemiology of primary brain tumors. Neurotherapeutics 2009, 6(3):427-435.
3. Ohgaki H, Kleihues P: Epidemiology and etiology of gliomas. Acta Neuropathol 2005, 109(1):93-108.
4. Wen PY, Kesari S: Malignant gliomas in adults. N Engl J Med 2008, 359(5):492-507.
5. Louis DN, Ohgaki H, Wiestler OD, Cavenee WK, Burger PC, Jouvet A, Scheithauer BW, Kleihues P: The 2007 WHO classification of tumours of the central nervous system. Acta Neuropathol 2007, 114(2):97-109.
6. Furnari FB, Fenton T, Bachoo RM, Mukasa A, Stommel JM, Stegh A, Hahn WC, Ligon KL, Louis DN, Brennan C et al: Malignant astrocytic glioma: genetics, biology, and paths to treatment. Genes Dev 2007, 21(21):2683-2710.
7. Louis DN, Perry A, Reifenberger G, von Deimling A, Figarella-Branger D, Cavenee WK, Ohgaki H, Wiestler OD, Kleihues P, Ellison DW: The 2016 World Health Organization Classification of Tumors of the Central Nervous System: a summary. Acta Neuropathol 2016, 131(6):803-820.
8. Stupp R, Mason WP, van den Bent MJ, Weller M, Fisher B, Taphoorn MJ, Belanger K, Brandes AA, Marosi C, Bogdahn U et al: Radiotherapy plus concomitant and adjuvant temozolomide for glioblastoma. N Engl J Med 2005, 352(10):987-996.
9. Zhang X, Zhang W, Cao WD, Cheng G, Zhang YQ: Glioblastoma multiforme: Molecular characterization and current treatment strategy (Review). Exp Ther Med 2012, 3(1):9-14.
10. Fisher T, Galanti G, Lavie G, Jacob-Hirsch J, Kventsel I, Zeligson S, Winkler R, Simon AJ, Amariglio N, Rechavi G et al: Mechanisms operative in the antitumor activity of temozolomide in glioblastoma multiforme. Cancer J 2007, 13(5):335-344.
11. Iacob G, Dinca EB: Current data and strategy in glioblastoma multiforme. J Med Life 2009, 2(4):386-393.
12. Preusser M, Haberler C, Hainfellner JA: Malignant glioma: neuropathology and neurobiology. Wien Med Wochenschr 2006, 156(11-12):332-337.
13. Nakada M, Nakada S, Demuth T, Tran NL, Hoelzinger DB, Berens ME: Molecular targets of glioma invasion. Cell Mol Life Sci 2007, 64(4):458-478.
14. Behin A, Hoang-Xuan K, Carpentier AF, Delattre JY: Primary brain tumours in adults. Lancet 2003, 361(9354):323-331.
15. Ohgaki H, Kleihues P: The definition of primary and secondary glioblastoma. Clin Cancer Res 2013, 19(4):764-772.
16. Jiao Y, Killela PJ, Reitman ZJ, Rasheed AB, Heaphy CM, de Wilde RF, Rodriguez FJ, Rosemberg S, Oba-Shinjo SM, Nagahashi Marie SK et al:

Frequent ATRX, CIC, FUBP1 and IDH1 mutations refine the classification of malignant gliomas. Oncotarget 2012, 3(7):709-722.
17. Noushmehr H, Weisenberger DJ, Diefes K, Phillips HS, Pujara K, Berman BP, Pan F, Pelloski CE, Sulman EP, Bhat KP et al: Identification of a CpG island methylator phenotype that defines a distinct subgroup of glioma. Cancer Cell 2010, 17(5):510-522.
18. Verhaak RG, Hoadley KA, Purdom E, Wang V, Qi Y, Wilkerson MD, Miller CR, Ding L, Golub T, Mesirov JP et al: Integrated genomic analysis identifies clinically relevant subtypes of glioblastoma characterized by abnormalities in PDGFRA, IDH1, EGFR, and NF1. Cancer Cell 2010, 17(1):98-110.
19. Network CGAR: Comprehensive genomic characterization defines human glioblastoma genes and core pathways. Nature 2008, 455(7216):1061-1068.
20. Zhu Y, Parada LF: The molecular and genetic basis of neurological tumours. Nat Rev Cancer 2002, 2(8):616-626.
21. Ueki K, Ono Y, Henson JW, Efird JT, von Deimling A, Louis DN: CDKN2/p16 or RB alterations occur in the majority of glioblastomas and are inversely correlated. Cancer Res 1996, 56(1):150-153.
22. Ichimura K, Schmidt EE, Goike HM, Collins VP: Human glioblastomas with no alterations of the CDKN2A (p16INK4A, MTS1) and CDK4 genes have frequent mutations of the retinoblastoma gene. Oncogene 1996, 13(5):1065-1072.
23. Schmidt EE, Ichimura K, Reifenberger G, Collins VP: CDKN2 (p16/MTS1) gene deletion or CDK4 amplification occurs in the majority of glioblastomas. Cancer Res 1994, 54(24):6321-6324.
24. Costello JF, Plass C, Arap W, Chapman VM, Held WA, Berger MS, Su Huang HJ, Cavenee WK: Cyclin-dependent kinase 6 (CDK6) amplification in human gliomas identified using two-dimensional separation of genomic DNA. Cancer Res 1997, 57(7):1250-1254.
25. Reifenberger G, Reifenberger J, Ichimura K, Meltzer PS, Collins VP: Amplification of multiple genes from chromosomal region 12q13-14 in human malignant gliomas: preliminary mapping of the amplicons shows preferential involvement of CDK4, SAS, and MDM2. Cancer Res 1994, 54(16):4299-4303.
26. Riemenschneider MJ, Büschges R, Wolter M, Reifenberger J, Boström J, Kraus JA, Schlegel U, Reifenberger G: Amplification and overexpression of the MDM4 (MDMX) gene from 1q32 in a subset of malignant gliomas without TP53 mutation or MDM2 amplification. Cancer Res 1999, 59(24):6091-6096.
27. Molofsky AV, Slutsky SG, Joseph NM, He S, Pardal R, Krishnamurthy J, Sharpless NE, Morrison SJ: Increasing p16INK4a expression decreases forebrain progenitors and neurogenesis during ageing. Nature 2006, 443(7110):448-452.
28. Jen J, Harper JW, Bigner SH, Bigner DD, Papadopoulos N, Markowitz S, Willson JK, Kinzler KW, Vogelstein B: Deletion of p16 and p15 genes in brain tumors. Cancer Res 1994, 54(24):6353-6358.

29. Libermann TA, Nusbaum HR, Razon N, Kris R, Lax I, Soreq H, Whittle N, Waterfield MD, Ullrich A, Schlessinger J: Amplification, enhanced expression and possible rearrangement of EGF receptor gene in primary human brain tumours of glial origin. Nature 1985, 313(5998):144-147.
30. Ichimura K, Narita Y, Hawkins CE: Diffusely infiltrating astrocytomas: pathology, molecular mechanisms and markers. Acta Neuropathol 2015, 129(6):789-808.
31. Chaffanet M, Chauvin C, Lainé M, Berger F, Chédin M, Rost N, Nissou MF, Benabid AL: EGF receptor amplification and expression in human brain tumours. Eur J Cancer 1992, 28(1):11-17.
32. Schwechheimer K, Huang S, Cavenee WK: EGFR gene amplification--rearrangement in human glioblastomas. Int J Cancer 1995, 62(2):145-148.
33. Frederick L, Wang XY, Eley G, James CD: Diversity and frequency of epidermal growth factor receptor mutations in human glioblastomas. Cancer Res 2000, 60(5):1383-1387.
34. Nagane M, Coufal F, Lin H, Bögler O, Cavenee WK, Huang HJ: A common mutant epidermal growth factor receptor confers enhanced tumorigenicity on human glioblastoma cells by increasing proliferation and reducing apoptosis. Cancer Res 1996, 56(21):5079-5086.
35. Phillips JJ, Aranda D, Ellison DW, Judkins AR, Croul SE, Brat DJ, Ligon KL, Horbinski C, Venneti S, Zadeh G et al: PDGFRA amplification is common in pediatric and adult high-grade astrocytomas and identifies a poor prognostic group in IDH1 mutant glioblastoma. Brain Pathol 2013, 23(5):565-573.
36. Westermark B: Platelet-derived growth factor in glioblastoma-driver or biomarker? Ups J Med Sci 2014, 119(4):298-305.
37. Hermanson M, Funa K, Hartman M, Claesson-Welsh L, Heldin CH, Westermark B, Nistér M: Platelet-derived growth factor and its receptors in human glioma tissue: expression of messenger RNA and protein suggests the presence of autocrine and paracrine loops. Cancer Res 1992, 52(11):3213-3219.
38. Shen WH, Balajee AS, Wang J, Wu H, Eng C, Pandolfi PP, Yin Y: Essential role for nuclear PTEN in maintaining chromosomal integrity. Cell 2007, 128(1):157-170.
39. Wechsler DS, Shelly CA, Petroff CA, Dang CV: MXI1, a putative tumor suppressor gene, suppresses growth of human glioblastoma cells. Cancer Res 1997, 57(21):4905-4912.
40. Mollenhauer J, Wiemann S, Scheurlen W, Korn B, Hayashi Y, Wilgenbus KK, von Deimling A, Poustka A: DMBT1, a new member of the SRCR superfamily, on chromosome 10q25.3-26.1 is deleted in malignant brain tumours. Nat Genet 1997, 17(1):32-39.
41. Sottoriva A, Spiteri I, Piccirillo SG, Touloumis A, Collins VP, Marioni JC, Curtis C, Watts C, Tavaré S: Intratumor heterogeneity in human glioblastoma reflects cancer evolutionary dynamics. Proc Natl Acad Sci U S A 2013, 110(10):4009-4014.

42. Sottoriva A, Spiteri I, Shibata D, Curtis C, Tavaré S: Single-molecule genomic data delineate patient-specific tumor profiles and cancer stem cell organization. Cancer Res 2013, 73(1):41-49.
43. Phillips HS, Kharbanda S, Chen R, Forrest WF, Soriano RH, Wu TD, Misra A, Nigro JM, Colman H, Soroceanu L et al: Molecular subclasses of high-grade glioma predict prognosis, delineate a pattern of disease progression, and resemble stages in neurogenesis. Cancer Cell 2006, 9(3):157-173.
44. Thiery JP: Epithelial-mesenchymal transitions in tumour progression. Nat Rev Cancer 2002, 2(6):442-454.
45. Smith JS, Perry A, Borell TJ, Lee HK, O'Fallon J, Hosek SM, Kimmel D, Yates A, Burger PC, Scheithauer BW et al: Alterations of chromosome arms 1p and 19q as predictors of survival in oligodendrogliomas, astrocytomas, and mixed oligoastrocytomas. J Clin Oncol 2000, 18(3):636-645.
46. Labussière M, Idbaih A, Wang XW, Marie Y, Boisselier B, Falet C, Paris S, Laffaire J, Carpentier C, Crinière E et al: All the 1p19q codeleted gliomas are mutated on IDH1 or IDH2. Neurology 2010, 74(23):1886-1890.
47. Bettegowda C, Agrawal N, Jiao Y, Sausen M, Wood LD, Hruban RH, Rodriguez FJ, Cahill DP, McLendon R, Riggins G et al: Mutations in CIC and FUBP1 contribute to human oligodendroglioma. Science 2011, 333(6048):1453-1455.
48. Liu XY, Gerges N, Korshunov A, Sabha N, Khuong-Quang DA, Fontebasso AM, Fleming A, Hadjadj D, Schwartzentruber J, Majewski J et al: Frequent ATRX mutations and loss of expression in adult diffuse astrocytic tumors carrying IDH1/IDH2 and TP53 mutations. Acta Neuropathol 2012, 124(5):615-625.
49. Kannan K, Inagaki A, Silber J, Gorovets D, Zhang J, Kastenhuber ER, Heguy A, Petrini JH, Chan TA, Huse JT: Whole-exome sequencing identifies ATRX mutation as a key molecular determinant in lower-grade glioma. Oncotarget 2012, 3(10):1194-1203.
50. Parsons DW, Jones S, Zhang X, Lin JC, Leary RJ, Angenendt P, Mankoo P, Carter H, Siu IM, Gallia GL et al: An integrated genomic analysis of human glioblastoma multiforme. Science 2008, 321(5897):1807-1812.
51. Hartmann C, Hentschel B, Wick W, Capper D, Felsberg J, Simon M, Westphal M, Schackert G, Meyermann R, Pietsch T et al: Patients with IDH1 wild type anaplastic astrocytomas exhibit worse prognosis than IDH1-mutated glioblastomas, and IDH1 mutation status accounts for the unfavorable prognostic effect of higher age: implications for classification of gliomas. Acta Neuropathol 2010, 120(6):707-718.
52. Yan H, Parsons DW, Jin G, McLendon R, Rasheed BA, Yuan W, Kos I, Batinic-Haberle I, Jones S, Riggins GJ et al: IDH1 and IDH2 mutations in gliomas. N Engl J Med 2009, 360(8):765-773.
53. Mur P, Mollejo M, Ruano Y, de Lope Á, Fiaño C, García JF, Castresana JS, Hernández-Laín A, Rey JA, Meléndez B: Codeletion of 1p and 19q determines distinct gene methylation and expression profiles in IDH-mutated oligodendroglial tumors. Acta Neuropathol 2013, 126(2):277-289.

54. Esteller M, Garcia-Foncillas J, Andion E, Goodman SN, Hidalgo OF, Vanaclocha V, Baylin SB, Herman JG: Inactivation of the DNA-repair gene MGMT and the clinical response of gliomas to alkylating agents. N Engl J Med 2000, 343(19):1350-1354.
55. Hegi ME, Diserens AC, Gorlia T, Hamou MF, de Tribolet N, Weller M, Kros JM, Hainfellner JA, Mason W, Mariani L et al: MGMT gene silencing and benefit from temozolomide in glioblastoma. N Engl J Med 2005, 352(10):997-1003.
56. Chen Y, Hu F, Zhou Y, Chen W, Shao H, Zhang Y: MGMT promoter methylation and glioblastoma prognosis: a systematic review and meta-analysis. Arch Med Res 2013, 44(4):281-290.
57. Sadones J, Michotte A, Veld P, Chaskis C, Sciot R, Menten J, Joossens EJ, Strauven T, D'Hondt LA, Sartenaer D et al: MGMT promoter hypermethylation correlates with a survival benefit from temozolomide in patients with recurrent anaplastic astrocytoma but not glioblastoma. Eur J Cancer 2009, 45(1):146-153.
58. van den Bent MJ, Gravendeel LA, Gorlia T, Kros JM, Lapre L, Wesseling P, Teepen JL, Idbaih A, Sanson M, Smitt PA et al: A hypermethylated phenotype is a better predictor of survival than MGMT methylation in anaplastic oligodendroglial brain tumors: a report from EORTC study 26951. Clin Cancer Res 2011, 17(22):7148-7155.
59. Killela PJ, Reitman ZJ, Jiao Y, Bettegowda C, Agrawal N, Diaz LA, Friedman AH, Friedman H, Gallia GL, Giovanella BC et al: TERT promoter mutations occur frequently in gliomas and a subset of tumors derived from cells with low rates of self-renewal. Proc Natl Acad Sci U S A 2013, 110(15):6021-6026.
60. Arita H, Narita Y, Fukushima S, Tateishi K, Matsushita Y, Yoshida A, Miyakita Y, Ohno M, Collins VP, Kawahara N et al: Upregulating mutations in the TERT promoter commonly occur in adult malignant gliomas and are strongly associated with total 1p19q loss. Acta Neuropathol 2013, 126(2):267-276.
61. Wiestler B, Capper D, Holland-Letz T, Korshunov A, von Deimling A, Pfister SM, Platten M, Weller M, Wick W: ATRX loss refines the classification of anaplastic gliomas and identifies a subgroup of IDH mutant astrocytic tumors with better prognosis. Acta Neuropathol 2013, 126(3):443-451.
62. Gorlia T, van den Bent MJ, Hegi ME, Mirimanoff RO, Weller M, Cairncross JG, Eisenhauer E, Belanger K, Brandes AA, Allgeier A et al: Nomograms for predicting survival of patients with newly diagnosed glioblastoma: prognostic factor analysis of EORTC and NCIC trial 26981-22981/CE.3. Lancet Oncol 2008, 9(1):29-38.
63. Laws ER, Parney IF, Huang W, Anderson F, Morris AM, Asher A, Lillehei KO, Bernstein M, Brem H, Sloan A et al: Survival following surgery and prognostic factors for recently diagnosed malignant glioma: data from the Glioma Outcomes Project. J Neurosurg 2003, 99(3):467-473.
64. Wilson TA, Karajannis MA, Harter DH: Glioblastoma multiforme: State of the art and future therapeutics. Surg Neurol Int 2014, 5:64.

65. Preusser M, de Ribaupierre S, Wöhrer A, Erridge SC, Hegi M, Weller M, Stupp R: Current concepts and management of glioblastoma. Ann Neurol 2011, 70(1):9-21.
66. Stupp R, Hegi ME, Mason WP, van den Bent MJ, Taphoorn MJ, Janzer RC, Ludwin SK, Allgeier A, Fisher B, Belanger K et al: Effects of radiotherapy with concomitant and adjuvant temozolomide versus radiotherapy alone on survival in glioblastoma in a randomised phase III study: 5-year analysis of the EORTC-NCIC trial. Lancet Oncol 2009, 10(5):459-466.
67. Laperriere N, Weller M, Stupp R, Perry JR, Brandes AA, Wick W, van den Bent MJ: Optimal management of elderly patients with glioblastoma. Cancer Treat Rev 2013, 39(4):350-357.
68. Marina O, Suh JH, Reddy CA, Barnett GH, Vogelbaum MA, Peereboom DM, Stevens GH, Elinzano H, Chao ST: Treatment outcomes for patients with glioblastoma multiforme and a low Karnofsky Performance Scale score on presentation to a tertiary care institution. Clinical article. J Neurosurg 2011, 115(2):220-229.
69. Chaichana KL, Martinez-Gutierrez JC, De la Garza-Ramos R, Weingart JD, Olivi A, Gallia GL, Lim M, Brem H, Quinones-Hinojosa A: Factors associated with survival for patients with glioblastoma with poor pre-operative functional status. J Clin Neurosci 2013, 20(6):818-823.
70. Liu G, Yuan X, Zeng Z, Tunici P, Ng H, Abdulkadir IR, Lu L, Irvin D, Black KL, Yu JS: Analysis of gene expression and chemoresistance of CD133+ cancer stem cells in glioblastoma. Mol Cancer 2006, 5:67.
71. Duntze J, Litré CF, Eap C, Théret E, Debreuve A, Jovenin N, Lechapt-Zalcman E, Metellus P, Colin P, Guillamo JS et al: Implanted carmustine wafers followed by concomitant radiochemotherapy to treat newly diagnosed malignant gliomas: prospective, observational, multicenter study on 92 cases. Ann Surg Oncol 2013, 20(6):2065-2072.
72. Gutenberg A, Lumenta CB, Braunsdorf WE, Sabel M, Mehdorn HM, Westphal M, Giese A: The combination of carmustine wafers and temozolomide for the treatment of malignant gliomas. A comprehensive review of the rationale and clinical experience. J Neurooncol 2013, 113(2):163-174.
73. Chinot OL, Wick W, Mason W, Henriksson R, Saran F, Nishikawa R, Carpentier AF, Hoang-Xuan K, Kavan P, Cernea D et al: Bevacizumab plus radiotherapy-temozolomide for newly diagnosed glioblastoma. N Engl J Med 2014, 370(8):709-722.
74. Plate KH, Breier G, Weich HA, Mennel HD, Risau W: Vascular endothelial growth factor and glioma angiogenesis: coordinate induction of VEGF receptors, distribution of VEGF protein and possible in vivo regulatory mechanisms. Int J Cancer 1994, 59(4):520-529.
75. Brem S, Cotran R, Folkman J: Tumor angiogenesis: a quantitative method for histologic grading. J Natl Cancer Inst 1972, 48(2):347-356.
76. Vredenburgh JJ, Desjardins A, Herndon JE, Marcello J, Reardon DA, Quinn JA, Rich JN, Sathornsumetee S, Gururangan S, Sampson J et al:

Bevacizumab plus irinotecan in recurrent glioblastoma multiforme. J Clin Oncol 2007, 25(30):4722-4729.
77. Friedman HS, Prados MD, Wen PY, Mikkelsen T, Schiff D, Abrey LE, Yung WK, Paleologos N, Nicholas MK, Jensen R et al: Bevacizumab alone and in combination with irinotecan in recurrent glioblastoma. J Clin Oncol 2009, 27(28):4733-4740.
78. Chamberlain MC: Bevacizumab for the treatment of recurrent glioblastoma. Clin Med Insights Oncol 2011, 5:117-129.
79. Fonkem E, Wong ET: NovoTTF-100A: a new treatment modality for recurrent glioblastoma. Expert Rev Neurother 2012, 12(8):895-899.
80. Kirson ED, Dbalý V, Tovarys F, Vymazal J, Soustiel JF, Itzhaki A, Mordechovich D, Steinberg-Shapira S, Gurvich Z, Schneiderman R et al: Alternating electric fields arrest cell proliferation in animal tumor models and human brain tumors. Proc Natl Acad Sci U S A 2007, 104(24):10152-10157.
81. Kirson ED, Gurvich Z, Schneiderman R, Dekel E, Itzhaki A, Wasserman Y, Schatzberger R, Palti Y: Disruption of cancer cell replication by alternating electric fields. Cancer Res 2004, 64(9):3288-3295.
82. Stupp R, Wong ET, Kanner AA, Steinberg D, Engelhard H, Heidecke V, Kirson ED, Taillibert S, Liebermann F, Dbalý V et al: NovoTTF-100A versus physician's choice chemotherapy in recurrent glioblastoma: a randomised phase III trial of a novel treatment modality. Eur J Cancer 2012, 48(14):2192-2202.
83. Steinbach JP, Blaicher HP, Herrlinger U, Wick W, Nägele T, Meyermann R, Tatagiba M, Bamberg M, Dichgans J, Karnath HO et al: Surviving glioblastoma for more than 5 years: the patient's perspective. Neurology 2006, 66(2):239-242.
84. Bramwell B: The Process of Compensation and some of its Bearings on Prognosis and Treatment. Br Med J 1888, 1(1426):889-894.
85. Dick JE: Stem cell concepts renew cancer research. Blood 2008, 112(13):4793-4807.
86. Bradshaw A, Wickremsekera A, Tan ST, Peng L, Davis PF, Itinteang T: Cancer Stem Cell Hierarchy in Glioblastoma Multiforme. Front Surg 2016, 3:21.
87. Dick JE: Looking ahead in cancer stem cell research. Nat Biotechnol 2009, 27(1):44-46.
88. Pardal R, Clarke MF, Morrison SJ: Applying the principles of stem-cell biology to cancer. Nat Rev Cancer 2003, 3(12):895-902.
89. Zaidi HA, Kosztowski T, DiMeco F, Quiñones-Hinojosa A: Origins and clinical implications of the brain tumor stem cell hypothesis. J Neurooncol 2009, 93(1):49-60.
90. Brunschwig A, Southam CM, Levin AG: Host resistance to cancer. Clinical experiments by homotransplants, autotransplants and admixture of autologous leucocytes. Ann Surg 1965, 162(3):416-425.

91. BRUCE WR, VAN DER GAAG H: A QUANTITATIVE ASSAY FOR THE NUMBER OF MURINE LYMPHOMA CELLS CAPABLE OF PROLIFERATION IN VIVO. Nature 1963, 199:79-80.
92. Druker BJ: Chronic myeloid leukemia. Sceptical scientists. Lancet 2001, 358 Suppl:S11.
93. Chen Y, Li S: Molecular signatures of chronic myeloid leukemia stem cells. Biomark Res 2013, 1(1):21.
94. Al-Hajj M, Wicha MS, Benito-Hernandez A, Morrison SJ, Clarke MF: Prospective identification of tumorigenic breast cancer cells. Proc Natl Acad Sci U S A 2003, 100(7):3983-3988.
95. Ignatova TN, Kukekov VG, Laywell ED, Suslov ON, Vrionis FD, Steindler DA: Human cortical glial tumors contain neural stem-like cells expressing astroglial and neuronal markers in vitro. Glia 2002, 39(3):193-206.
96. Collins AT, Berry PA, Hyde C, Stower MJ, Maitland NJ: Prospective identification of tumorigenic prostate cancer stem cells. Cancer Res 2005, 65(23):10946-10951.
97. Ho MM, Ng AV, Lam S, Hung JY: Side population in human lung cancer cell lines and tumors is enriched with stem-like cancer cells. Cancer Res 2007, 67(10):4827-4833.
98. Ma S, Chan KW, Guan XY: In search of liver cancer stem cells. Stem Cell Rev 2008, 4(3):179-192.
99. O'Brien CA, Pollett A, Gallinger S, Dick JE: A human colon cancer cell capable of initiating tumour growth in immunodeficient mice. Nature 2007, 445(7123):106-110.
100. Singh SK, Hawkins C, Clarke ID, Squire JA, Bayani J, Hide T, Henkelman RM, Cusimano MD, Dirks PB: Identification of human brain tumour initiating cells. Nature 2004, 432(7015):396-401.
101. Vescovi AL, Galli R, Reynolds BA: Brain tumour stem cells. Nat Rev Cancer 2006, 6(6):425-436.
102. Hemmati HD, Nakano I, Lazareff JA, Masterman-Smith M, Geschwind DH, Bronner-Fraser M, Kornblum HI: Cancerous stem cells can arise from pediatric brain tumors. Proc Natl Acad Sci U S A 2003, 100(25):15178-15183.
103. Suvà ML, Rheinbay E, Gillespie SM, Patel AP, Wakimoto H, Rabkin SD, Riggi N, Chi AS, Cahill DP, Nahed BV et al: Reconstructing and reprogramming the tumor-propagating potential of glioblastoma stem-like cells. Cell 2014, 157(3):580-594.
104. Ben-Porath I, Thomson MW, Carey VJ, Ge R, Bell GW, Regev A, Weinberg RA: An embryonic stem cell-like gene expression signature in poorly differentiated aggressive human tumors. Nat Genet 2008, 40(5):499-507.
105. Ligon KL, Huillard E, Mehta S, Kesari S, Liu H, Alberta JA, Bachoo RM, Kane M, Louis DN, Depinho RA et al: Olig2-regulated lineage-restricted pathway controls replication competence in neural stem cells and malignant glioma. Neuron 2007, 53(4):503-517.

106. Kim J, Woo AJ, Chu J, Snow JW, Fujiwara Y, Kim CG, Cantor AB, Orkin SH: A Myc network accounts for similarities between embryonic stem and cancer cell transcription programs. Cell 2010, 143(2):313-324.
107. Tunici P, Bissola L, Lualdi E, Pollo B, Cajola L, Broggi G, Sozzi G, Finocchiaro G: Genetic alterations and in vivo tumorigenicity of neurospheres derived from an adult glioblastoma. Mol Cancer 2004, 3:25.
108. Anido J, Sáez-Borderías A, Gonzàlez-Juncà A, Rodón L, Folch G, Carmona MA, Prieto-Sánchez RM, Barba I, Martínez-Sáez E, Prudkin L et al: TGF-β Receptor Inhibitors Target the CD44(high)/Id1(high) Glioma-Initiating Cell Population in Human Glioblastoma. Cancer Cell 2010, 18(6):655-668.
109. Wegner M: From head to toes: the multiple facets of Sox proteins. Nucleic Acids Res 1999, 27(6):1409-1420.
110. Dong C, Wilhelm D, Koopman P: Sox genes and cancer. Cytogenet Genome Res 2004, 105(2-4):442-447.
111. Saigusa S, Tanaka K, Toiyama Y, Yokoe T, Okugawa Y, Ioue Y, Miki C, Kusunoki M: Correlation of CD133, OCT4, and SOX2 in rectal cancer and their association with distant recurrence after chemoradiotherapy. Ann Surg Oncol 2009, 16(12):3488-3498.
112. Chen Y, Shi L, Zhang L, Li R, Liang J, Yu W, Sun L, Yang X, Wang Y, Zhang Y et al: The molecular mechanism governing the oncogenic potential of SOX2 in breast cancer. J Biol Chem 2008, 283(26):17969-17978.
113. Rudin CM, Durinck S, Stawiski EW, Poirier JT, Modrusan Z, Shames DS, Bergbower EA, Guan Y, Shin J, Guillory J et al: Comprehensive genomic analysis identifies SOX2 as a frequently amplified gene in small-cell lung cancer. Nat Genet 2012, 44(10):1111-1116.
114. Schmitz M, Temme A, Senner V, Ebner R, Schwind S, Stevanovic S, Wehner R, Schackert G, Schackert HK, Fussel M et al: Identification of SOX2 as a novel glioma-associated antigen and potential target for T cell-based immunotherapy. Br J Cancer 2007, 96(8):1293-1301.
115. Guo Y, Liu S, Wang P, Zhao S, Wang F, Bing L, Zhang Y, Ling EA, Gao J, Hao A: Expression profile of embryonic stem cell-associated genes Oct4, Sox2 and Nanog in human gliomas. Histopathology 2011, 59(4):763-775.
116. Gangemi RM, Griffero F, Marubbi D, Perera M, Capra MC, Malatesta P, Ravetti GL, Zona GL, Daga A, Corte G: SOX2 silencing in glioblastoma tumor-initiating cells causes stop of proliferation and loss of tumorigenicity. Stem Cells 2009, 27(1):40-48.
117. Chiou SH, Wang ML, Chou YT, Chen CJ, Hong CF, Hsieh WJ, Chang HT, Chen YS, Lin TW, Hsu HS et al: Coexpression of Oct4 and Nanog enhances malignancy in lung adenocarcinoma by inducing cancer stem cell-like properties and epithelial-mesenchymal transdifferentiation. Cancer Res 2010, 70(24):10433-10444.
118. Chiou SH, Yu CC, Huang CY, Lin SC, Liu CJ, Tsai TH, Chou SH, Chien CS, Ku HH, Lo JF: Positive correlations of Oct-4 and Nanog in oral cancer stem-like cells and high-grade oral squamous cell carcinoma. Clin Cancer Res 2008, 14(13):4085-4095.

119. Bourguignon LY, Peyrollier K, Xia W, Gilad E: Hyaluronan-CD44 interaction activates stem cell marker Nanog, Stat-3-mediated MDR1 gene expression, and ankyrin-regulated multidrug efflux in breast and ovarian tumor cells. J Biol Chem 2008, 283(25):17635-17651.
120. Bourguignon LY, Spevak CC, Wong G, Xia W, Gilad E: Hyaluronan-CD44 interaction with protein kinase C(epsilon) promotes oncogenic signaling by the stem cell marker Nanog and the Production of microRNA-21, leading to down-regulation of the tumor suppressor protein PDCD4, anti-apoptosis, and chemotherapy resistance in breast tumor cells. J Biol Chem 2009, 284(39):26533-26546.
121. Jeter CR, Liu B, Liu X, Chen X, Liu C, Calhoun-Davis T, Repass J, Zaehres H, Shen JJ, Tang DG: NANOG promotes cancer stem cell characteristics and prostate cancer resistance to androgen deprivation. Oncogene 2011, 30(36):3833-3845.
122. Clement V, Sanchez P, de Tribolet N, Radovanovic I, Ruiz i Altaba A: HEDGEHOG-GLI1 signaling regulates human glioma growth, cancer stem cell self-renewal, and tumorigenicity. Curr Biol 2007, 17(2):165-172.
123. Zbinden M, Duquet A, Lorente-Trigos A, Ngwabyt SN, Borges I, Ruiz i Altaba A: NANOG regulates glioma stem cells and is essential in vivo acting in a cross-functional network with GLI1 and p53. EMBO J 2010, 29(15):2659-2674.
124. Niu CS, Yang Y, Cheng CD: MiR-134 regulates the proliferation and invasion of glioblastoma cells by reducing Nanog expression. Int J Oncol 2013, 42(5):1533-1540.
125. Boyer LA, Lee TI, Cole MF, Johnstone SE, Levine SS, Zucker JP, Guenther MG, Kumar RM, Murray HL, Jenner RG et al: Core transcriptional regulatory circuitry in human embryonic stem cells. Cell 2005, 122(6):947-956.
126. Li W, Wei W, Zhu S, Zhu J, Shi Y, Lin T, Hao E, Hayek A, Deng H, Ding S: Generation of rat and human induced pluripotent stem cells by combining genetic reprogramming and chemical inhibitors. Cell Stem Cell 2009, 4(1):16-19.
127. Du Z, Jia D, Liu S, Wang F, Li G, Zhang Y, Cao X, Ling EA, Hao A: Oct4 is expressed in human gliomas and promotes colony formation in glioma cells. Glia 2009, 57(7):724-733.
128. Klein WM, Wu BP, Zhao S, Wu H, Klein-Szanto AJ, Tahan SR: Increased expression of stem cell markers in malignant melanoma. Mod Pathol 2007, 20(1):102-107.
129. Gu G, Yuan J, Wills M, Kasper S: Prostate cancer cells with stem cell characteristics reconstitute the original human tumor in vivo. Cancer Res 2007, 67(10):4807-4815.
130. Su HT, Weng CC, Hsiao PJ, Chen LH, Kuo TL, Chen YW, Kuo KK, Cheng KH: Stem cell marker nestin is critical for TGF-β1-mediated tumor progression in pancreatic cancer. Mol Cancer Res 2013, 11(7):768-779.

131. Yuan X, Curtin J, Xiong Y, Liu G, Waschsmann-Hogiu S, Farkas DL, Black KL, Yu JS: Isolation of cancer stem cells from adult glioblastoma multiforme. Oncogene 2004, 23(58):9392-9400.
132. Hatanpaa KJ, Hu T, Vemireddy V, Foong C, Raisanen JM, Oliver D, Hiemenz MC, Burns DK, White CL, Whitworth LA et al: High expression of the stem cell marker nestin is an adverse prognostic factor in WHO grade II-III astrocytomas and oligoastrocytomas. J Neurooncol 2014, 117(1):183-189.
133. Zhang M, Song T, Yang L, Chen R, Wu L, Yang Z, Fang J: Nestin and CD133: valuable stem cell-specific markers for determining clinical outcome of glioma patients. J Exp Clin Cancer Res 2008, 27:85.
134. Kemper K, Sprick MR, de Bree M, Scopelliti A, Vermeulen L, Hoek M, Zeilstra J, Pals ST, Mehmet H, Stassi G et al: The AC133 epitope, but not the CD133 protein, is lost upon cancer stem cell differentiation. Cancer Res 2010, 70(2):719-729.
135. Gambelli F, Sasdelli F, Manini I, Gambarana C, Oliveri G, Miracco C, Sorrentino V: Identification of cancer stem cells from human glioblastomas: growth and differentiation capabilities and CD133/prominin-1 expression. Cell Biol Int 2012, 36(1):29-38.
136. Beier D, Hau P, Proescholdt M, Lohmeier A, Wischhusen J, Oefner PJ, Aigner L, Brawanski A, Bogdahn U, Beier CP: CD133(+) and CD133(-) glioblastoma-derived cancer stem cells show differential growth characteristics and molecular profiles. Cancer Res 2007, 67(9):4010-4015.
137. Joo KM, Kim SY, Jin X, Song SY, Kong DS, Lee JI, Jeon JW, Kim MH, Kang BG, Jung Y et al: Clinical and biological implications of CD133-positive and CD133-negative cells in glioblastomas. Lab Invest 2008, 88(8):808-815.
138. Yang T, Rycaj K: Targeted therapy against cancer stem cells. Oncol Lett 2015, 10(1):27-33.
139. Chen R, Nishimura MC, Bumbaca SM, Kharbanda S, Forrest WF, Kasman IM, Greve JM, Soriano RH, Gilmour LL, Rivers CS et al: A hierarchy of self-renewing tumor-initiating cell types in glioblastoma. Cancer Cell 2010, 17(4):362-375.
140. Brescia P, Ortensi B, Fornasari L, Levi D, Broggi G, Pelicci G: CD133 is essential for glioblastoma stem cell maintenance. Stem Cells 2013, 31(5):857-869.
141. Sun Y, Kong W, Falk A, Hu J, Zhou L, Pollard S, Smith A: CD133 (Prominin) negative human neural stem cells are clonogenic and tripotent. PLoS One 2009, 4(5):e5498.
142. Wu B, Sun C, Feng F, Ge M, Xia L: Do relevant markers of cancer stem cells CD133 and Nestin indicate a poor prognosis in glioma patients? A systematic review and meta-analysis. J Exp Clin Cancer Res 2015, 34:44.
143. Lathia JD, Gallagher J, Heddleston JM, Wang J, Eyler CE, Macswords J, Wu Q, Vasanji A, McLendon RE, Hjelmeland AB et al: Integrin alpha 6 regulates glioblastoma stem cells. Cell Stem Cell 2010, 6(5):421-432.

144. Son MJ, Woolard K, Nam DH, Lee J, Fine HA: SSEA-1 is an enrichment marker for tumor-initiating cells in human glioblastoma. Cell Stem Cell 2009, 4(5):440-452.
145. Bao S, Wu Q, Li Z, Sathornsumetee S, Wang H, McLendon RE, Hjelmeland AB, Rich JN: Targeting cancer stem cells through L1CAM suppresses glioma growth. Cancer Res 2008, 68(15):6043-6048.
146. Ogden AT, Waziri AE, Lochhead RA, Fusco D, Lopez K, Ellis JA, Kang J, Assanah M, McKhann GM, Sisti MB et al: Identification of A2B5+CD133-tumor-initiating cells in adult human gliomas. Neurosurgery 2008, 62(2):505-514; discussion 514-505.
147. Sneath RJ, Mangham DC: The normal structure and function of CD44 and its role in neoplasia. Mol Pathol 1998, 51(4):191-200.
148. Breyer R, Hussein S, Radu DL, Pütz KM, Gunia S, Hecker H, Samii M, Walter GF, Stan AC: Disruption of intracerebral progression of C6 rat glioblastoma by in vivo treatment with anti-CD44 monoclonal antibody. J Neurosurg 2000, 92(1):140-149.
149. Kamiguchi H, Hlavin ML, Lemmon V: Role of L1 in neural development: what the knockouts tell us. Mol Cell Neurosci 1998, 12(1-2):48-55.
150. Held-Feindt J, Schmelz S, Hattermann K, Mentlein R, Mehdorn HM, Sebens S: The neural adhesion molecule L1CAM confers chemoresistance in human glioblastomas. Neurochem Int 2012, 61(7):1183-1191.
151. Hu J, Ho AL, Yuan L, Hu B, Hua S, Hwang SS, Zhang J, Hu T, Zheng H, Gan B et al: From the Cover: Neutralization of terminal differentiation in gliomagenesis. Proc Natl Acad Sci U S A 2013, 110(36):14520-14527.
152. Artavanis-Tsakonas S, Rand MD, Lake RJ: Notch signaling: cell fate control and signal integration in development. Science 1999, 284(5415):770-776.
153. Kanamori M, Kawaguchi T, Nigro JM, Feuerstein BG, Berger MS, Miele L, Pieper RO: Contribution of Notch signaling activation to human glioblastoma multiforme. J Neurosurg 2007, 106(3):417-427.
154. Purow BW, Haque RM, Noel MW, Su Q, Burdick MJ, Lee J, Sundaresan T, Pastorino S, Park JK, Mikolaenko I et al: Expression of Notch-1 and its ligands, Delta-like-1 and Jagged-1, is critical for glioma cell survival and proliferation. Cancer Res 2005, 65(6):2353-2363.
155. Pistollato F, Chen HL, Rood BR, Zhang HZ, D'Avella D, Denaro L, Gardiman M, te Kronnie G, Schwartz PH, Favaro E et al: Hypoxia and HIF1alpha repress the differentiative effects of BMPs in high-grade glioma. Stem Cells 2009, 27(1):7-17.
156. Kasai M, Satoh K, Akiyama T: Wnt signaling regulates the sequential onset of neurogenesis and gliogenesis via induction of BMPs. Genes Cells 2005, 10(8):777-783.
157. Piccirillo SG, Reynolds BA, Zanetti N, Lamorte G, Binda E, Broggi G, Brem H, Olivi A, Dimeco F, Vescovi AL: Bone morphogenetic proteins inhibit the tumorigenic potential of human brain tumour-initiating cells. Nature 2006, 444(7120):761-765.

158. Persano L, Pistollato F, Rampazzo E, Della Puppa A, Abbadi S, Frasson C, Volpin F, Indraccolo S, Scienza R, Basso G: BMP2 sensitizes glioblastoma stem-like cells to Temozolomide by affecting HIF-1α stability and MGMT expression. Cell Death Dis 2012, 3:e412.
159. Yan K, Wu Q, Yan DH, Lee CH, Rahim N, Tritschler I, DeVecchio J, Kalady MF, Hjelmeland AB, Rich JN: Glioma cancer stem cells secrete Gremlin1 to promote their maintenance within the tumor hierarchy. Genes Dev 2014, 28(10):1085-1100.
160. Pei Y, Brun SN, Markant SL, Lento W, Gibson P, Taketo MM, Giovannini M, Gilbertson RJ, Wechsler-Reya RJ: WNT signaling increases proliferation and impairs differentiation of stem cells in the developing cerebellum. Development 2012, 139(10):1724-1733.
161. Grigoryan T, Wend P, Klaus A, Birchmeier W: Deciphering the function of canonical Wnt signals in development and disease: conditional loss- and gain-of-function mutations of beta-catenin in mice. Genes Dev 2008, 22(17):2308-2341.
162. Munji RN, Choe Y, Li G, Siegenthaler JA, Pleasure SJ: Wnt signaling regulates neuronal differentiation of cortical intermediate progenitors. J Neurosci 2011, 31(5):1676-1687.
163. Zhang N, Wei P, Gong A, Chiu WT, Lee HT, Colman H, Huang H, Xue J, Liu M, Wang Y et al: FoxM1 promotes β-catenin nuclear localization and controls Wnt target-gene expression and glioma tumorigenesis. Cancer Cell 2011, 20(4):427-442.
164. Zheng H, Ying H, Wiedemeyer R, Yan H, Quayle SN, Ivanova EV, Paik JH, Zhang H, Xiao Y, Perry SR et al: PLAGL2 regulates Wnt signaling to impede differentiation in neural stem cells and gliomas. Cancer Cell 2010, 17(5):497-509.
165. Ayuso-Sacido A, Moliterno JA, Kratovac S, Kapoor GS, O'Rourke DM, Holland EC, García-Verdugo JM, Roy NS, Boockvar JA: Activated EGFR signaling increases proliferation, survival, and migration and blocks neuronal differentiation in post-natal neural stem cells. J Neurooncol 2010, 97(3):323-337.
166. Lillien L, Raphael H: BMP and FGF regulate the development of EGF-responsive neural progenitor cells. Development 2000, 127(22):4993-5005.
167. Yang W, Xia Y, Ji H, Zheng Y, Liang J, Huang W, Gao X, Aldape K, Lu Z: Nuclear PKM2 regulates β-catenin transactivation upon EGFR activation. Nature 2011, 480(7375):118-122.
168. Nicholas MK, Lukas RV, Jafri NF, Faoro L, Salgia R: Epidermal growth factor receptor - mediated signal transduction in the development and therapy of gliomas. Clin Cancer Res 2006, 12(24):7261-7270.
169. Agarwala S, Sanders TA, Ragsdale CW: Sonic hedgehog control of size and shape in midbrain pattern formation. Science 2001, 291(5511):2147-2150.
170. Balordi F, Fishell G: Hedgehog signaling in the subventricular zone is required for both the maintenance of stem cells and the migration of newborn neurons. J Neurosci 2007, 27(22):5936-5947.

171. Hardee ME, Zagzag D: Mechanisms of glioma-associated neovascularization. Am J Pathol 2012, 181(4):1126-1141.
172. Jhaveri N, Chen TC, Hofman FM: Tumor vasculature and glioma stem cells: Contributions to glioma progression. Cancer Lett 2016, 380(2):545-551.
173. Calabrese C, Poppleton H, Kocak M, Hogg TL, Fuller C, Hamner B, Oh EY, Gaber MW, Finklestein D, Allen M et al: A perivascular niche for brain tumor stem cells. Cancer Cell 2007, 11(1):69-82.
174. Huang Z, Cheng L, Guryanova OA, Wu Q, Bao S: Cancer stem cells in glioblastoma--molecular signaling and therapeutic targeting. Protein Cell 2010, 1(7):638-655.
175. Charles NA, Holland EC, Gilbertson R, Glass R, Kettenmann H: The brain tumor microenvironment. Glia 2012, 60(3):502-514.
176. Christensen K, Schrøder HD, Kristensen BW: CD133+ niches and single cells in glioblastoma have different phenotypes. J Neurooncol 2011, 104(1):129-143.
177. Jain RK, di Tomaso E, Duda DG, Loeffler JS, Sorensen AG, Batchelor TT: Angiogenesis in brain tumours. Nat Rev Neurosci 2007, 8(8):610-622.
178. Thirant C, Galan-Moya EM, Dubois LG, Pinte S, Chafey P, Broussard C, Varlet P, Devaux B, Soncin F, Gavard J et al: Differential proteomic analysis of human glioblastoma and neural stem cells reveals HDGF as a novel angiogenic secreted factor. Stem Cells 2012, 30(5):845-853.
179. Ricci-Vitiani L, Pallini R, Biffoni M, Todaro M, Invernici G, Cenci T, Maira G, Parati EA, Stassi G, Larocca LM et al: Tumour vascularization via endothelial differentiation of glioblastoma stem-like cells. Nature 2010, 468(7325):824-828.
180. Wang R, Chadalavada K, Wilshire J, Kowalik U, Hovinga KE, Geber A, Fligelman B, Leversha M, Brennan C, Tabar V: Glioblastoma stem-like cells give rise to tumour endothelium. Nature 2010, 468(7325):829-833.
181. Soda Y, Marumoto T, Friedmann-Morvinski D, Soda M, Liu F, Michiue H, Pastorino S, Yang M, Hoffman RM, Kesari S et al: Transdifferentiation of glioblastoma cells into vascular endothelial cells. Proc Natl Acad Sci U S A 2011, 108(11):4274-4280.
182. Cheng L, Huang Z, Zhou W, Wu Q, Donnola S, Liu JK, Fang X, Sloan AE, Mao Y, Lathia JD et al: Glioblastoma stem cells generate vascular pericytes to support vessel function and tumor growth. Cell 2013, 153(1):139-152.
183. Zhu TS, Costello MA, Talsma CE, Flack CG, Crowley JG, Hamm LL, He X, Hervey-Jumper SL, Heth JA, Muraszko KM et al: Endothelial cells create a stem cell niche in glioblastoma by providing NOTCH ligands that nurture self-renewal of cancer stem-like cells. Cancer Res 2011, 71(18):6061-6072.
184. Liu ZJ, Shirakawa T, Li Y, Soma A, Oka M, Dotto GP, Fairman RM, Velazquez OC, Herlyn M: Regulation of Notch1 and Dll4 by vascular endothelial growth factor in arterial endothelial cells: implications for modulating arteriogenesis and angiogenesis. Mol Cell Biol 2003, 23(1):14-25.

185. Lathia JD, Li M, Hall PE, Gallagher J, Hale JS, Wu Q, Venere M, Levy E, Rani MR, Huang P et al: Laminin alpha 2 enables glioblastoma stem cell growth. Ann Neurol 2012, 72(5):766-778.
186. Zheng X, Xie Q, Li S, Zhang W: CXCR4-positive subset of glioma is enriched for cancer stem cells. Oncol Res 2011, 19(12):555-561.
187. Würth R, Bajetto A, Harrison JK, Barbieri F, Florio T: CXCL12 modulation of CXCR4 and CXCR7 activity in human glioblastoma stem-like cells and regulation of the tumor microenvironment. Front Cell Neurosci 2014, 8:144.
188. Infanger DW, Cho Y, Lopez BS, Mohanan S, Liu SC, Gursel D, Boockvar JA, Fischbach C: Glioblastoma stem cells are regulated by interleukin-8 signaling in a tumoral perivascular niche. Cancer Res 2013, 73(23):7079-7089.
189. Dey N, De P, Brian LJ: Evading anti-angiogenic therapy: resistance to anti-angiogenic therapy in solid tumors. Am J Transl Res 2015, 7(10):1675-1698.
190. Heddleston JM, Li Z, McLendon RE, Hjelmeland AB, Rich JN: The hypoxic microenvironment maintains glioblastoma stem cells and promotes reprogramming towards a cancer stem cell phenotype. Cell Cycle 2009, 8(20):3274-3284.
191. Keith B, Johnson RS, Simon MC: HIF1α and HIF2α: sibling rivalry in hypoxic tumour growth and progression. Nat Rev Cancer 2011, 12(1):9-22.
192. Li Z, Bao S, Wu Q, Wang H, Eyler C, Sathornsumetee S, Shi Q, Cao Y, Lathia J, McLendon RE et al: Hypoxia-inducible factors regulate tumorigenic capacity of glioma stem cells. Cancer Cell 2009, 15(6):501-513.
193. Yang L, Lin C, Wang L, Guo H, Wang X: Hypoxia and hypoxia-inducible factors in glioblastoma multiforme progression and therapeutic implications. Exp Cell Res 2012, 318(19):2417-2426.
194. Covello KL, Kehler J, Yu H, Gordan JD, Arsham AM, Hu CJ, Labosky PA, Simon MC, Keith B: HIF-2alpha regulates Oct-4: effects of hypoxia on stem cell function, embryonic development, and tumor growth. Genes Dev 2006, 20(5):557-570.
195. Gordan JD, Bertout JA, Hu CJ, Diehl JA, Simon MC: HIF-2alpha promotes hypoxic cell proliferation by enhancing c-myc transcriptional activity. Cancer Cell 2007, 11(4):335-347.
196. Vlashi E, Lagadec C, Vergnes L, Matsutani T, Masui K, Poulou M, Popescu R, Della Donna L, Evers P, Dekmezian C et al: Metabolic state of glioma stem cells and nontumorigenic cells. Proc Natl Acad Sci U S A 2011, 108(38):16062-16067.
197. Kathagen A, Schulte A, Balcke G, Phillips HS, Martens T, Matschke J, Günther HS, Soriano R, Modrusan Z, Sandmann T et al: Hypoxia and oxygenation induce a metabolic switch between pentose phosphate pathway and glycolysis in glioma stem-like cells. Acta Neuropathol 2013, 126(5):763-780.
198. Flavahan WA, Wu Q, Hitomi M, Rahim N, Kim Y, Sloan AE, Weil RJ, Nakano I, Sarkaria JN, Stringer BW et al: Brain tumor initiating cells adapt to restricted nutrition through preferential glucose uptake. Nat Neurosci 2013, 16(10):1373-1382.

199. Eyler CE, Wu Q, Yan K, MacSwords JM, Chandler-Militello D, Misuraca KL, Lathia JD, Forrester MT, Lee J, Stamler JS et al: Glioma stem cell proliferation and tumor growth are promoted by nitric oxide synthase-2. Cell 2011, 146(1):53-66.
200. Lu C, Ward PS, Kapoor GS, Rohle D, Turcan S, Abdel-Wahab O, Edwards CR, Khanin R, Figueroa ME, Melnick A et al: IDH mutation impairs histone demethylation and results in a block to cell differentiation. Nature 2012, 483(7390):474-478.
201. Grivennikov SI, Greten FR, Karin M: Immunity, inflammation, and cancer. Cell 2010, 140(6):883-899.
202. Filatova A, Acker T, Garvalov BK: The cancer stem cell niche(s): the crosstalk between glioma stem cells and their microenvironment. Biochim Biophys Acta 2013, 1830(2):2496-2508.
203. Parney IF, Waldron JS, Parsa AT: Flow cytometry and in vitro analysis of human glioma-associated macrophages. Laboratory investigation. J Neurosurg 2009, 110(3):572-582.
204. Watters JJ, Schartner JM, Badie B: Microglia function in brain tumors. J Neurosci Res 2005, 81(3):447-455.
205. Roggendorf W, Strupp S, Paulus W: Distribution and characterization of microglia/macrophages in human brain tumors. Acta Neuropathol 1996, 92(3):288-293.
206. Yi L, Xiao H, Xu M, Ye X, Hu J, Li F, Li M, Luo C, Yu S, Bian X et al: Glioma-initiating cells: a predominant role in microglia/macrophages tropism to glioma. J Neuroimmunol 2011, 232(1-2):75-82.
207. Wang SC, Hong JH, Hsueh C, Chiang CS: Tumor-secreted SDF-1 promotes glioma invasiveness and TAM tropism toward hypoxia in a murine astrocytoma model. Lab Invest 2012, 92(1):151-162.
208. Tafani M, Di Vito M, Frati A, Pellegrini L, De Santis E, Sette G, Eramo A, Sale P, Mari E, Santoro A et al: Pro-inflammatory gene expression in solid glioblastoma microenvironment and in hypoxic stem cells from human glioblastoma. J Neuroinflammation 2011, 8:32.
209. Gabrusiewicz K, Ellert-Miklaszewska A, Lipko M, Sielska M, Frankowska M, Kaminska B: Characteristics of the alternative phenotype of microglia/macrophages and its modulation in experimental gliomas. PLoS One 2011, 6(8):e23902.
210. Wu A, Wei J, Kong LY, Wang Y, Priebe W, Qiao W, Sawaya R, Heimberger AB: Glioma cancer stem cells induce immunosuppressive macrophages/microglia. Neuro Oncol 2010, 12(11):1113-1125.
211. Hanahan D, Weinberg RA: Hallmarks of cancer: the next generation. Cell 2011, 144(5):646-674.
212. Platten M, Wick W, Weller M: Malignant glioma biology: role for TGF-beta in growth, motility, angiogenesis, and immune escape. Microsc Res Tech 2001, 52(4):401-410.
213. Fecci PE, Mitchell DA, Whitesides JF, Xie W, Friedman AH, Archer GE, Herndon JE, Bigner DD, Dranoff G, Sampson JH: Increased regulatory T-cell

fraction amidst a diminished CD4 compartment explains cellular immune defects in patients with malignant glioma. Cancer Res 2006, 66(6):3294-3302.
214. Di Tomaso T, Mazzoleni S, Wang E, Sovena G, Clavenna D, Franzin A, Mortini P, Ferrone S, Doglioni C, Marincola FM et al: Immunobiological characterization of cancer stem cells isolated from glioblastoma patients. Clin Cancer Res 2010, 16(3):800-813.
215. Wei J, Barr J, Kong LY, Wang Y, Wu A, Sharma AK, Gumin J, Henry V, Colman H, Sawaya R et al: Glioma-associated cancer-initiating cells induce immunosuppression. Clin Cancer Res 2010, 16(2):461-473.
216. Reardon DA, Freeman G, Wu C, Chiocca EA, Wucherpfennig KW, Wen PY, Fritsch EF, Curry WT, Sampson JH, Dranoff G: Immunotherapy advances for glioblastoma. Neuro Oncol 2014, 16(11):1441-1458.
217. Clarke MF, Dick JE, Dirks PB, Eaves CJ, Jamieson CH, Jones DL, Visvader J, Weissman IL, Wahl GM: Cancer stem cells--perspectives on current status and future directions: AACR Workshop on cancer stem cells. Cancer Res 2006, 66(19):9339-9344.
218. Bao S, Wu Q, McLendon RE, Hao Y, Shi Q, Hjelmeland AB, Dewhirst MW, Bigner DD, Rich JN: Glioma stem cells promote radioresistance by preferential activation of the DNA damage response. Nature 2006, 444(7120):756-760.
219. Ishikawa F, Yoshida S, Saito Y, Hijikata A, Kitamura H, Tanaka S, Nakamura R, Tanaka T, Tomiyama H, Saito N et al: Chemotherapy-resistant human AML stem cells home to and engraft within the bone-marrow endosteal region. Nat Biotechnol 2007, 25(11):1315-1321.
220. Hegi ME, Liu L, Herman JG, Stupp R, Wick W, Weller M, Mehta MP, Gilbert MR: Correlation of O6-methylguanine methyltransferase (MGMT) promoter methylation with clinical outcomes in glioblastoma and clinical strategies to modulate MGMT activity. J Clin Oncol 2008, 26(25):4189-4199.
221. Eramo A, Ricci-Vitiani L, Zeuner A, Pallini R, Lotti F, Sette G, Pilozzi E, Larocca LM, Peschle C, De Maria R: Chemotherapy resistance of glioblastoma stem cells. Cell Death Differ 2006, 13(7):1238-1241.
222. Bleau AM, Hambardzumyan D, Ozawa T, Fomchenko EI, Huse JT, Brennan CW, Holland EC: PTEN/PI3K/Akt pathway regulates the side population phenotype and ABCG2 activity in glioma tumor stem-like cells. Cell Stem Cell 2009, 4(3):226-235.
223. Shi L, Zhang S, Feng K, Wu F, Wan Y, Wang Z, Zhang J, Wang Y, Yan W, Fu Z et al: MicroRNA-125b-2 confers human glioblastoma stem cells resistance to temozolomide through the mitochondrial pathway of apoptosis. Int J Oncol 2012, 40(1):119-129.
224. Capper D, Gaiser T, Hartmann C, Habel A, Mueller W, Herold-Mende C, von Deimling A, Siegelin MD: Stem-cell-like glioma cells are resistant to TRAIL/Apo2L and exhibit down-regulation of caspase-8 by promoter methylation. Acta Neuropathol 2009, 117(4):445-456.

225. Ashley DM, Riffkin CD, Muscat AM, Knight MJ, Kaye AH, Novak U, Hawkins CJ: Caspase 8 is absent or low in many ex vivo gliomas. Cancer 2005, 104(7):1487-1496.
226. Yamada K, Tso J, Ye F, Choe J, Liu Y, Liau LM, Tso CL: Essential gene pathways for glioblastoma stem cells: clinical implications for prevention of tumor recurrence. Cancers (Basel) 2011, 3(2):1975-1995.
227. Gómez-López S, Lerner RG, Petritsch C: Asymmetric cell division of stem and progenitor cells during homeostasis and cancer. Cell Mol Life Sci 2014, 71(4):575-597.
228. Wang H, Chia W: Drosophila neural progenitor polarity and asymmetric division. Biol Cell 2005, 97(1):63-74.
229. Neumüller RA, Knoblich JA: Dividing cellular asymmetry: asymmetric cell division and its implications for stem cells and cancer. Genes Dev 2009, 23(23):2675-2699.
230. Schaefer M, Shevchenko A, Knoblich JA: A protein complex containing Inscuteable and the Galpha-binding protein Pins orients asymmetric cell divisions in Drosophila. Curr Biol 2000, 10(7):353-362.
231. Atwood SX, Chabu C, Penkert RR, Doe CQ, Prehoda KE: Cdc42 acts downstream of Bazooka to regulate neuroblast polarity through Par-6 aPKC. J Cell Sci 2007, 120(Pt 18):3200-3206.
232. Peterson FC, Penkert RR, Volkman BF, Prehoda KE: Cdc42 regulates the Par-6 PDZ domain through an allosteric CRIB-PDZ transition. Mol Cell 2004, 13(5):665-676.
233. Kraut R, Chia W, Jan LY, Jan YN, Knoblich JA: Role of inscuteable in orienting asymmetric cell divisions in Drosophila. Nature 1996, 383(6595):50-55.
234. Petritsch C, Tavosanis G, Turck CW, Jan LY, Jan YN: The Drosophila myosin VI Jaguar is required for basal protein targeting and correct spindle orientation in mitotic neuroblasts. Dev Cell 2003, 4(2):273-281.
235. Betschinger J, Mechtler K, Knoblich JA: The Par complex directs asymmetric cell division by phosphorylating the cytoskeletal protein Lgl. Nature 2003, 422(6929):326-330.
236. Smith CA, Lau KM, Rahmani Z, Dho SE, Brothers G, She YM, Berry DM, Bonneil E, Thibault P, Schweisguth F et al: aPKC-mediated phosphorylation regulates asymmetric membrane localization of the cell fate determinant Numb. EMBO J 2007, 26(2):468-480.
237. Lu B, Rothenberg M, Jan LY, Jan YN: Partner of Numb colocalizes with Numb during mitosis and directs Numb asymmetric localization in Drosophila neural and muscle progenitors. Cell 1998, 95(2):225-235.
238. Wang H, Somers GW, Bashirullah A, Heberlein U, Yu F, Chia W: Aurora-A acts as a tumor suppressor and regulates self-renewal of Drosophila neuroblasts. Genes Dev 2006, 20(24):3453-3463.
239. Pece S, Confalonieri S, R Romano P, Di Fiore PP: NUMB-ing down cancer by more than just a NOTCH. Biochim Biophys Acta 2011, 1815(1):26-43.

240. Atwood SX, Prehoda KE: aPKC phosphorylates Miranda to polarize fate determinants during neuroblast asymmetric cell division. Curr Biol 2009, 19(9):723-729.
241. Ikeshima-Kataoka H, Skeath JB, Nabeshima Y, Doe CQ, Matsuzaki F: Miranda directs Prospero to a daughter cell during Drosophila asymmetric divisions. Nature 1997, 390(6660):625-629.
242. Matsuzaki F, Ohshiro T, Ikeshima-Kataoka H, Izumi H: miranda localizes staufen and prospero asymmetrically in mitotic neuroblasts and epithelial cells in early Drosophila embryogenesis. Development 1998, 125(20):4089-4098.
243. Betschinger J, Mechtler K, Knoblich JA: Asymmetric segregation of the tumor suppressor brat regulates self-renewal in Drosophila neural stem cells. Cell 2006, 124(6):1241-1253.
244. Doe CQ, Chu-LaGraff Q, Wright DM, Scott MP: The prospero gene specifies cell fates in the Drosophila central nervous system. Cell 1991, 65(3):451-464.
245. Dewey EB, Taylor DT, Johnston CA: Cell Fate Decision Making through Oriented Cell Division. J Dev Biol 2015, 3(4):129-157.
246. Qian X, Goderie SK, Shen Q, Stern JH, Temple S: Intrinsic programs of patterned cell lineages in isolated vertebrate CNS ventricular zone cells. Development 1998, 125(16):3143-3152.
247. Aaku-Saraste E, Hellwig A, Huttner WB: Loss of occludin and functional tight junctions, but not ZO-1, during neural tube closure--remodeling of the neuroepithelium prior to neurogenesis. Dev Biol 1996, 180(2):664-679.
248. Zhadanov AB, Provance DW, Speer CA, Coffin JD, Goss D, Blixt JA, Reichert CM, Mercer JA: Absence of the tight junctional protein AF-6 disrupts epithelial cell-cell junctions and cell polarity during mouse development. Curr Biol 1999, 9(16):880-888.
249. Noctor SC, Martínez-Cerdeño V, Kriegstein AR: Distinct behaviors of neural stem and progenitor cells underlie cortical neurogenesis. J Comp Neurol 2008, 508(1):28-44.
250. Miyata T, Kawaguchi A, Saito K, Kawano M, Muto T, Ogawa M: Asymmetric production of surface-dividing and non-surface-dividing cortical progenitor cells. Development 2004, 131(13):3133-3145.
251. Gal JS, Morozov YM, Ayoub AE, Chatterjee M, Rakic P, Haydar TF: Molecular and morphological heterogeneity of neural precursors in the mouse neocortical proliferative zones. J Neurosci 2006, 26(3):1045-1056.
252. Wang X, Tsai JW, LaMonica B, Kriegstein AR: A new subtype of progenitor cell in the mouse embryonic neocortex. Nat Neurosci 2011, 14(5):555-561.
253. Bultje RS, Castaneda-Castellanos DR, Jan LY, Jan YN, Kriegstein AR, Shi SH: Mammalian Par3 regulates progenitor cell asymmetric division via notch signaling in the developing neocortex. Neuron 2009, 63(2):189-202.
254. Gaiano N, Nye JS, Fishell G: Radial glial identity is promoted by Notch1 signaling in the murine forebrain. Neuron 2000, 26(2):395-404.
255. Kosodo Y, Röper K, Haubensak W, Marzesco AM, Corbeil D, Huttner WB: Asymmetric distribution of the apical plasma membrane during neurogenic

divisions of mammalian neuroepithelial cells. EMBO J 2004, 23(11):2314-2324.
256. Doe CQ: Neural stem cells: balancing self-renewal with differentiation. Development 2008, 135(9):1575-1587.
257. Lathia JD, Hitomi M, Gallagher J, Gadani SP, Adkins J, Vasanji A, Liu L, Eyler CE, Heddleston JM, Wu Q et al: Distribution of CD133 reveals glioma stem cells self-renew through symmetric and asymmetric cell divisions. Cell Death Dis 2011, 2:e200.
258. McGranahan N, Burrell RA, Endesfelder D, Novelli MR, Swanton C: Cancer chromosomal instability: therapeutic and diagnostic challenges. EMBO Rep 2012, 13(6):528-538.
259. Geigl JB, Obenauf AC, Schwarzbraun T, Speicher MR: Defining 'chromosomal instability'. Trends Genet 2008, 24(2):64-69.
260. Oda S, Zhao Y, Maehara Y: Microsatellite instability in gastrointestinal tract cancers: a brief update. Surg Today 2005, 35(12):1005-1015.
261. Buecher B, Cacheux W, Rouleau E, Dieumegard B, Mitry E, Lièvre A: Role of microsatellite instability in the management of colorectal cancers. Dig Liver Dis 2013, 45(6):441-449.
262. Thompson SL, Bakhoum SF, Compton DA: Mechanisms of chromosomal instability. Curr Biol 2010, 20(6):R285-295.
263. Natarajan AT, Palitti F: DNA repair and chromosomal alterations. Mutat Res 2008, 657(1):3-7.
264. Speicher MR, Carter NP: The new cytogenetics: blurring the boundaries with molecular biology. Nat Rev Genet 2005, 6(10):782-792.
265. Fiegler H, Geigl JB, Langer S, Rigler D, Porter K, Unger K, Carter NP, Speicher MR: High resolution array-CGH analysis of single cells. Nucleic Acids Res 2007, 35(3):e15.
266. Hiddemann W, Schumann J, Andreef M, Barlogie B, Herman CJ, Leif RC, Mayall BH, Murphy RF, Sandberg AA: Convention on nomenclature for DNA cytometry. Committee on Nomenclature, Society for Analytical Cytology. Cancer Genet Cytogenet 1984, 13(2):181-183.
267. Greenman CD, Bignell G, Butler A, Edkins S, Hinton J, Beare D, Swamy S, Santarius T, Chen L, Widaa S et al: PICNIC: an algorithm to predict absolute allelic copy number variation with microarray cancer data. Biostatistics 2010, 11(1):164-175.
268. Colella S, Yau C, Taylor JM, Mirza G, Butler H, Clouston P, Bassett AS, Seller A, Holmes CC, Ragoussis J: QuantiSNP: an Objective Bayes Hidden-Markov Model to detect and accurately map copy number variation using SNP genotyping data. Nucleic Acids Res 2007, 35(6):2013-2025.
269. Vogelstein B, Kinzler KW: Digital PCR. Proc Natl Acad Sci U S A 1999, 96(16):9236-9241.
270. Shih IM, Zhou W, Goodman SN, Lengauer C, Kinzler KW, Vogelstein B: Evidence that genetic instability occurs at an early stage of colorectal tumorigenesis. Cancer Res 2001, 61(3):818-822.

271. Meyer R, Fofanov V, Panigrahi A, Merchant F, Zhang N, Pati D: Overexpression and mislocalization of the chromosomal segregation protein separase in multiple human cancers. Clin Cancer Res 2009, 15(8):2703-2710.
272. Cimini D: Merotelic kinetochore orientation, aneuploidy, and cancer. Biochim Biophys Acta 2008, 1786(1):32-40.
273. DeLuca JG, Gall WE, Ciferri C, Cimini D, Musacchio A, Salmon ED: Kinetochore microtubule dynamics and attachment stability are regulated by Hec1. Cell 2006, 127(5):969-982.
274. Cosenza MR, Krämer A: Centrosome amplification, chromosomal instability and cancer: mechanistic, clinical and therapeutic issues. Chromosome Res 2016, 24(1):105-126.
275. Holland AJ, Cleveland DW: Boveri revisited: chromosomal instability, aneuploidy and tumorigenesis. Nat Rev Mol Cell Biol 2009, 10(7):478-487.
276. Tanaka K, Hirota T: Chromosome segregation machinery and cancer. Cancer Sci 2009, 100(7):1158-1165.
277. Cimini D, Wan X, Hirel CB, Salmon ED: Aurora kinase promotes turnover of kinetochore microtubules to reduce chromosome segregation errors. Curr Biol 2006, 16(17):1711-1718.
278. Gregan J, Polakova S, Zhang L, Tolić-Nørrelykke IM, Cimini D: Merotelic kinetochore attachment: causes and effects. Trends Cell Biol 2011, 21(6):374-381.
279. Cimini D, Cameron LA, Salmon ED: Anaphase spindle mechanics prevent mis-segregation of merotelically oriented chromosomes. Curr Biol 2004, 14(23):2149-2155.
280. London N, Biggins S: Signalling dynamics in the spindle checkpoint response. Nat Rev Mol Cell Biol 2014, 15(11):736-747.
281. Chan JY: A clinical overview of centrosome amplification in human cancers. Int J Biol Sci 2011, 7(8):1122-1144.
282. Quintyne NJ, Reing JE, Hoffelder DR, Gollin SM, Saunders WS: Spindle multipolarity is prevented by centrosomal clustering. Science 2005, 307(5706):127-129.
283. Leber B, Maier B, Fuchs F, Chi J, Riffel P, Anderhub S, Wagner L, Ho AD, Salisbury JL, Boutros M et al: Proteins required for centrosome clustering in cancer cells. Sci Transl Med 2010, 2(33):33ra38.
284. Nasmyth K: Cohesin: a catenase with separate entry and exit gates? Nat Cell Biol 2011, 13(10):1170-1177.
285. Mannini L, Musio A: The dark side of cohesin: the carcinogenic point of view. Mutat Res 2011, 728(3):81-87.
286. Musacchio A: The Molecular Biology of Spindle Assembly Checkpoint Signaling Dynamics. Curr Biol 2015, 25(20):R1002-1018.
287. Haering CH, Farcas AM, Arumugam P, Metson J, Nasmyth K: The cohesin ring concatenates sister DNA molecules. Nature 2008, 454(7202):297-301.

288. Foley EA, Kapoor TM: Microtubule attachment and spindle assembly checkpoint signalling at the kinetochore. Nat Rev Mol Cell Biol 2013, 14(1):25-37.
289. Shannon KB, Canman JC, Salmon ED: Mad2 and BubR1 function in a single checkpoint pathway that responds to a loss of tension. Mol Biol Cell 2002, 13(10):3706-3719.
290. Musacchio A, Salmon ED: The spindle-assembly checkpoint in space and time. Nat Rev Mol Cell Biol 2007, 8(5):379-393.
291. Schvartzman JM, Sotillo R, Benezra R: Mitotic chromosomal instability and cancer: mouse modelling of the human disease. Nat Rev Cancer 2010, 10(2):102-115.
292. Hanks S, Coleman K, Reid S, Plaja A, Firth H, Fitzpatrick D, Kidd A, Méhes K, Nash R, Robin N et al: Constitutional aneuploidy and cancer predisposition caused by biallelic mutations in BUB1B. Nat Genet 2004, 36(11):1159-1161.
293. Liu D, Davydenko O, Lampson MA: Polo-like kinase-1 regulates kinetochore-microtubule dynamics and spindle checkpoint silencing. J Cell Biol 2012, 198(4):491-499.
294. Santaguida S, Amon A: Short- and long-term effects of chromosome mis-segregation and aneuploidy. Nat Rev Mol Cell Biol 2015, 16(8):473-485.
295. Högstedt B, Mitelman F: The interrelations of micronuclei, chromosomal instability, and mutational activity in acute non-lymphocytic leukemia--a hypothesis. Hereditas 1981, 95(1):165-167.
296. McClelland SE, Burrell RA, Swanton C: Chromosomal instability: a composite phenotype that influences sensitivity to chemotherapy. Cell Cycle 2009, 8(20):3262-3266.
297. Carter SL, Eklund AC, Kohane IS, Harris LN, Szallasi Z: A signature of chromosomal instability inferred from gene expression profiles predicts clinical outcome in multiple human cancers. Nat Genet 2006, 38(9):1043-1048.
298. Perucho M, Goldfarb M, Shimizu K, Lama C, Fogh J, Wigler M: Human-tumor-derived cell lines contain common and different transforming genes. Cell 1981, 27(3 Pt 2):467-476.
299. Land H, Parada LF, Weinberg RA: Cellular oncogenes and multistep carcinogenesis. Science 1983, 222(4625):771-778.
300. Vader G, Lens SM: The Aurora kinase family in cell division and cancer. Biochim Biophys Acta 2008, 1786(1):60-72.
301. Pei L, Melmed S: Isolation and characterization of a pituitary tumor-transforming gene (PTTG). Mol Endocrinol 1997, 11(4):433-441.
302. Janssen A, Medema RH: Genetic instability: tipping the balance. Oncogene 2013, 32(38):4459-4470.
303. Carmena M, Earnshaw WC: The cellular geography of aurora kinases. Nat Rev Mol Cell Biol 2003, 4(11):842-854.
304. Bolanos-Garcia VM: Aurora kinases. Int J Biochem Cell Biol 2005, 37(8):1572-1577.

305. Andrews PD, Knatko E, Moore WJ, Swedlow JR: Mitotic mechanics: the auroras come into view. Curr Opin Cell Biol 2003, 15(6):672-683.
306. Bar-Shira A, Pinthus JH, Rozovsky U, Goldstein M, Sellers WR, Yaron Y, Eshhar Z, Orr-Urtreger A: Multiple genes in human 20q13 chromosomal region are involved in an advanced prostate cancer xenograft. Cancer Res 2002, 62(23):6803-6807.
307. Andrews PD: Aurora kinases: shining lights on the therapeutic horizon? Oncogene 2005, 24(32):5005-5015.
308. Reichardt W, Jung V, Brunner C, Klein A, Wemmert S, Romeike BF, Zang KD, Urbschat S: The putative serine/threonine kinase gene STK15 on chromosome 20q13.2 is amplified in human gliomas. Oncol Rep 2003, 10(5):1275-1279.
309. Zhou H, Kuang J, Zhong L, Kuo WL, Gray JW, Sahin A, Brinkley BR, Sen S: Tumour amplified kinase STK15/BTAK induces centrosome amplification, aneuploidy and transformation. Nat Genet 1998, 20(2):189-193.
310. Tchatchou S, Wirtenberger M, Hemminki K, Sutter C, Meindl A, Wappenschmidt B, Kiechle M, Bugert P, Schmutzler RK, Bartram CR et al: Aurora kinases A and B and familial breast cancer risk. Cancer Lett 2007, 247(2):266-272.
311. Meraldi P, Honda R, Nigg EA: Aurora kinases link chromosome segregation and cell division to cancer susceptibility. Curr Opin Genet Dev 2004, 14(1):29-36.
312. Hochegger H, Hégarat N, Pereira-Leal JB: Aurora at the pole and equator: overlapping functions of Aurora kinases in the mitotic spindle. Open Biol 2013, 3(3):120185.
313. Katayama H, Ota T, Jisaki F, Ueda Y, Tanaka T, Odashima S, Suzuki F, Terada Y, Tatsuka M: Mitotic kinase expression and colorectal cancer progression. J Natl Cancer Inst 1999, 91(13):1160-1162.
314. Sorrentino R, Libertini S, Pallante PL, Troncone G, Palombini L, Bavetsias V, Spalletti-Cernia D, Laccetti P, Linardopoulos S, Chieffi P et al: Aurora B overexpression associates with the thyroid carcinoma undifferentiated phenotype and is required for thyroid carcinoma cell proliferation. J Clin Endocrinol Metab 2005, 90(2):928-935.
315. Zeng WF, Navaratne K, Prayson RA, Weil RJ: Aurora B expression correlates with aggressive behaviour in glioblastoma multiforme. J Clin Pathol 2007, 60(2):218-221.
316. Quartuccio SM, Schindler K: Functions of Aurora kinase C in meiosis and cancer. Front Cell Dev Biol 2015, 3:50.
317. Weaver BA, Silk AD, Montagna C, Verdier-Pinard P, Cleveland DW: Aneuploidy acts both oncogenically and as a tumor suppressor. Cancer Cell 2007, 11(1):25-36.
318. Baker DJ, Jin F, Jeganathan KB, van Deursen JM: Whole chromosome instability caused by Bub1 insufficiency drives tumorigenesis through tumor suppressor gene loss of heterozygosity. Cancer Cell 2009, 16(6):475-486.

319. Tanaka K, Hirota T: Chromosomal instability: A common feature and a therapeutic target of cancer. Biochim Biophys Acta 2016, 1866(1):64-75.
320. Pollard JR, Mortimore M: Discovery and development of aurora kinase inhibitors as anticancer agents. J Med Chem 2009, 52(9):2629-2651.
321. Kollareddy M, Zheleva D, Dzubak P, Brahmkshatriya PS, Lepsik M, Hajduch M: Aurora kinase inhibitors: progress towards the clinic. Invest New Drugs 2012, 30(6):2411-2432.
322. Fancelli D, Berta D, Bindi S, Cameron A, Cappella P, Carpinelli P, Catana C, Forte B, Giordano P, Giorgini ML et al: Potent and selective Aurora inhibitors identified by the expansion of a novel scaffold for protein kinase inhibition. J Med Chem 2005, 48(8):3080-3084.
323. Meulenbeld HJ, Mathijssen RH, Verweij J, de Wit R, de Jonge MJ: Danusertib, an aurora kinase inhibitor. Expert Opin Investig Drugs 2012, 21(3):383-393.
324. Carpinelli P, Ceruti R, Giorgini ML, Cappella P, Gianellini L, Croci V, Degrassi A, Texido G, Rocchetti M, Vianello P et al: PHA-739358, a potent inhibitor of Aurora kinases with a selective target inhibition profile relevant to cancer. Mol Cancer Ther 2007, 6(12 Pt 1):3158-3168.
325. Carpinelli P, Moll J: Aurora kinases and their inhibitors: more than one target and one drug. Adv Exp Med Biol 2008, 610:54-73.
326. Fancelli D, Moll J, Varasi M, Bravo R, Artico R, Berta D, Bindi S, Cameron A, Candiani I, Cappella P et al: 1,4,5,6-tetrahydropyrrolo[3,4-c]pyrazoles: identification of a potent Aurora kinase inhibitor with a favorable antitumor kinase inhibition profile. J Med Chem 2006, 49(24):7247-7251.
327. Lee EC, Frolov A, Li R, Ayala G, Greenberg NM: Targeting Aurora kinases for the treatment of prostate cancer. Cancer Res 2006, 66(10):4996-5002.
328. Benten D, Keller G, Quaas A, Schrader J, Gontarewicz A, Balabanov S, Braig M, Wege H, Moll J, Lohse AW et al: Aurora kinase inhibitor PHA-739358 suppresses growth of hepatocellular carcinoma in vitro and in a xenograft mouse model. Neoplasia 2009, 11(9):934-944.
329. Steeghs N, Mathijssen RH, Wessels JA, de Graan AJ, van der Straaten T, Mariani M, Laffranchi B, Comis S, de Jonge MJ, Gelderblom H et al: Influence of pharmacogenetic variability on the pharmacokinetics and toxicity of the aurora kinase inhibitor danusertib. Invest New Drugs 2011, 29(5):953-962.
330. Baronchelli S, Bentivegna A, Redaelli S, Riva G, Butta V, Paoletta L, Isimbaldi G, Miozzo M, Tabano S, Daga A et al: Delineating the cytogenomic and epigenomic landscapes of glioma stem cell lines. PLoS One 2013, 8(2):e57462.
331. Pollard SM, Yoshikawa K, Clarke ID, Danovi D, Stricker S, Russell R, Bayani J, Head R, Lee M, Bernstein M et al: Glioma stem cell lines expanded in adherent culture have tumor-specific phenotypes and are suitable for chemical and genetic screens. Cell Stem Cell 2009, 4(6):568-580.
332. Griffero F, Daga A, Marubbi D, Capra MC, Melotti A, Pattarozzi A, Gatti M, Bajetto A, Porcile C, Barbieri F et al: Different response of human glioma

tumor-initiating cells to epidermal growth factor receptor kinase inhibitors. J Biol Chem 2009, 284(11):7138-7148.
333. Kalous O, Conklin D, Desai AJ, Dering J, Goldstein J, Ginther C, Anderson L, Lu M, Kolarova T, Eckardt MA et al: AMG 900, pan-Aurora kinase inhibitor, preferentially inhibits the proliferation of breast cancer cell lines with dysfunctional p53. Breast Cancer Res Treat 2013, 141(3):397-408.
334. Ikezoe T, Yang J, Nishioka C, Yokoyama A: p53 is critical for the Aurora B kinase inhibitor-mediated apoptosis in acute myelogenous leukemia cells. Int J Hematol 2010, 91(1):69-77.
335. Greenblatt MS, Bennett WP, Hollstein M, Harris CC: Mutations in the p53 tumor suppressor gene: clues to cancer etiology and molecular pathogenesis. Cancer Res 1994, 54(18):4855-4878.
336. Freed-Pastor WA, Prives C: Mutant p53: one name, many proteins. Genes Dev 2012, 26(12):1268-1286.
337. Görgün G, Calabrese E, Hideshima T, Ecsedy J, Perrone G, Mani M, Ikeda H, Bianchi G, Hu Y, Cirstea D et al: A novel Aurora-A kinase inhibitor MLN8237 induces cytotoxicity and cell-cycle arrest in multiple myeloma. Blood 2010, 115(25):5202-5213.
338. Huck JJ, Zhang M, McDonald A, Bowman D, Hoar KM, Stringer B, Ecsedy J, Manfredi MG, Hyer ML: MLN8054, an inhibitor of Aurora A kinase, induces senescence in human tumor cells both in vitro and in vivo. Mol Cancer Res 2010, 8(3):373-384.
339. Liu Y, Hawkins OE, Su Y, Vilgelm AE, Sobolik T, Thu YM, Kantrow S, Splittgerber RC, Short S, Amiri KI et al: Targeting aurora kinases limits tumour growth through DNA damage-mediated senescence and blockade of NF-κB impairs this drug-induced senescence. EMBO Mol Med 2013, 5(1):149-166.
340. Fael Al-Mayhani TM, Ball SL, Zhao JW, Fawcett J, Ichimura K, Collins PV, Watts C: An efficient method for derivation and propagation of glioblastoma cell lines that conserves the molecular profile of their original tumours. J Neurosci Methods 2009, 176(2):192-199.
341. Mannino M, Gomez-Roman N, Hochegger H, Chalmers AJ: Differential sensitivity of Glioma stem cells to Aurora kinase A inhibitors: implications for stem cell mitosis and centrosome dynamics. Stem Cell Res 2014, 13(1):135-143.
342. Lehman NL, O'Donnell JP, Whiteley LJ, Stapp RT, Lehman TD, Roszka KM, Schultz LR, Williams CJ, Mikkelsen T, Brown SL et al: Aurora A is differentially expressed in gliomas, is associated with patient survival in glioblastoma and is a potential chemotherapeutic target in gliomas. Cell Cycle 2012, 11(3):489-502.
343. Gizatullin F, Yao Y, Kung V, Harding MW, Loda M, Shapiro GI: The Aurora kinase inhibitor VX-680 induces endoreduplication and apoptosis preferentially in cells with compromised p53-dependent postmitotic checkpoint function. Cancer Res 2006, 66(15):7668-7677.

344. Nair JS, Ho AL, Tse AN, Coward J, Cheema H, Ambrosini G, Keen N, Schwartz GK: Aurora B kinase regulates the postmitotic endoreduplication checkpoint via phosphorylation of the retinoblastoma protein at serine 780. Mol Biol Cell 2009, 20(8):2218-2228.
345. Roninson IB: Tumor cell senescence in cancer treatment. Cancer Res 2003, 63(11):2705-2715.
346. Chang BD, Broude EV, Dokmanovic M, Zhu H, Ruth A, Xuan Y, Kandel ES, Lausch E, Christov K, Roninson IB: A senescence-like phenotype distinguishes tumor cells that undergo terminal proliferation arrest after exposure to anticancer agents. Cancer Res 1999, 59(15):3761-3767.
347. Schmitt CA, Fridman JS, Yang M, Lee S, Baranov E, Hoffman RM, Lowe SW: A senescence program controlled by p53 and p16INK4a contributes to the outcome of cancer therapy. Cell 2002, 109(3):335-346.
348. Roninson IB, Broude EV, Chang BD: If not apoptosis, then what? Treatment-induced senescence and mitotic catastrophe in tumor cells. Drug Resist Updat 2001, 4(5):303-313.
349. Ventura A, Kirsch DG, McLaughlin ME, Tuveson DA, Grimm J, Lintault L, Newman J, Reczek EE, Weissleder R, Jacks T: Restoration of p53 function leads to tumour regression in vivo. Nature 2007, 445(7128):661-665.
350. Xue W, Zender L, Miething C, Dickins RA, Hernando E, Krizhanovsky V, Cordon-Cardo C, Lowe SW: Senescence and tumour clearance is triggered by p53 restoration in murine liver carcinomas. Nature 2007, 445(7128):656-660.
351. te Poele RH, Okorokov AL, Jardine L, Cummings J, Joel SP: DNA damage is able to induce senescence in tumor cells in vitro and in vivo. Cancer Res 2002, 62(6):1876-1883.
352. Wang LX, Wang JD, Chen JJ, Long B, Liu LL, Tu XX, Luo Y, Hu Y, Lin DJ, Lu G et al: Aurora A Kinase Inhibitor AKI603 Induces Cellular Senescence in Chronic Myeloid Leukemia Cells Harboring T315I Mutation. Sci Rep 2016, 6:35533.
353. Young AR, Narita M, Ferreira M, Kirschner K, Sadaie M, Darot JF, Tavaré S, Arakawa S, Shimizu S, Watt FM: Autophagy mediates the mitotic senescence transition. Genes Dev 2009, 23(7):798-803.
354. Ran FA, Hsu PD, Wright J, Agarwala V, Scott DA, Zhang F: Genome engineering using the CRISPR-Cas9 system. Nat Protoc 2013, 8(11):2281-2308.
355. Gaj T, Gersbach CA, Barbas CF: ZFN, TALEN, and CRISPR/Cas-based methods for genome engineering. Trends Biotechnol 2013, 31(7):397-405.
356. Wiedenheft B, Sternberg SH, Doudna JA: RNA-guided genetic silencing systems in bacteria and archaea. Nature 2012, 482(7385):331-338.
357. Cho SW, Kim S, Kim JM, Kim JS: Targeted genome engineering in human cells with the Cas9 RNA-guided endonuclease. Nat Biotechnol 2013, 31(3):230-232.
358. Ma Y, Zhang L, Huang X: Genome modification by CRISPR/Cas9. FEBS J 2014, 281(23):5186-5193.

359. Kuo TC, Chen CT, Baron D, Onder TT, Loewer S, Almeida S, Weismann CM, Xu P, Houghton JM, Gao FB et al: Midbody accumulation through evasion of autophagy contributes to cellular reprogramming and tumorigenicity. Nat Cell Biol 2011, 13(10):1214-1223.
360. Lewis KM, Petritsch C: ASYMMETRIC CELL DIVISION: IMPLICATIONS FOR GLIOMA DEVELOPMENT AND TREATMENT. Transl Neurosci 2013, 4(4):484-503.
361. Guichet PO, Guelfi S, Ripoll C, Teigell M, Sabourin JC, Bauchet L, Rigau V, Rothhut B, Hugnot JP: Asymmetric Distribution of GFAP in Glioma Multipotent Cells. PLoS One 2016, 11(3):e0151274.